THE ROLE OF NADPH OXIDASE AND NEUTROPHIL EXTRACELLULAR TRAPS IN THE PATHOGENESIS OF SYSTEMIC LUPUS ERYTHEMATOSUS

by

Rachael A. Gordon

Bachelor of Arts, University of Pennsylvania, 2008

Submitted to the Graduate Faculty of

The School of Medicine in partial fulfillment

of the requirements for the degree of

Doctor of Philosophy in Immunology and Microbiology

University of Pittsburgh

2017

UNIVERSITY OF PITTSBURGH

SCHOOL OF MEDICINE

This dissertation was presented

by

Rachael A. Gordon

It was defended on

December 8, 2017

and approved by

Michael T. Lotze, MD, Professor and Vice Chair, Department of Surgery

Patrick J. Pagano, PhD, Professor and Vice Chair, Department of Pharmacology and Chemical Biology

Jon D. Piganelli, PhD, Associate Professor, Department of Surgery

Simon Watkins, PhD, Distinguished Professor and Vice Chair, Department of Cell Biology

Dissertation Advisor: Mark J. Shlomchik, MD, PhD, Endowed Professor and Chair, Department of Immunology

THE ROLE OF NADPH OXIDASE AND NEUTROPHIL EXTRACELLULAR TRAPS IN THE PATHOGENSIS OF SYSTEMIC LUPUS ERYTHEMATOSUS

Rachael A. Gordon, B.A.

University of Pittsburgh, 2017

Systemic lupus erythematosus (SLE) is a multisystem autoimmune disease characterized by loss of tolerance to nuclear antigens and tissue destruction. While the sources of autoantigens in SLE are unknown, release of contents from dying cells and/or inadequate clearance of resulting debris are likely possibilities.

Prior reports suggest that neutrophil extracellular traps (NETs) and its associated death pathway, NETosis, are sources of autoantigen in SLE. However, we showed that inhibition of NETs by targeting the NADPH oxidase complex, via *Cybb*-deletion, exacerbated disease in the MRL.Fas^{lpr} model of SLE. To clarify the contribution of NETs in SLE pathogenesis, we employed a genetic approach to delete peptidyl arginine deiminase IV (*Padi4*) and neutrophil elastase (*Elane*), two distal mediators of NET formation, in MRL.Fas^{lpr} mice. Both *Padi4* and *Elane* deficiency did alter disease course, directly challenging the concept that NETs promote autoimmunity.

Therefore, it remains unknown how NADPH oxidase regulates autoimmunity. NADPH oxidase can constrain inflammation by neutrophil, macrophage, and lymphocyte dependent mechanisms. To identify the cell lineage in which *Cybb* deficiency drives SLE, we employed bone marrow chimera and conditional knockout approaches to delete *Cybb* in the myeloid compartment of MRL.Fas^{lpr} mice. Myeloid *Cybb* deficiency is sufficient to worsen glomerular and interstitial nephritis, suggesting that *Cybb* is protective in SLE due to a fundamental regulatory activity of *Cybb* within the myeloid compartment.

NADPH oxidase is a critical mediator of LC3-associated phagocytosis (LAP), which is important for the clearance of dead cells by macrophages. As Cybb modulates SLE pathogenesis by its function in myeloid cells, we assessed LAP in lupus. To test the hypothesis that exacerbated SLE in *Cybb*-deficient mice is due to defective LAP, we genetically deleted another critical LAP mediator, *Rubicon*, in *Cybb*-sufficient and *Cybb*-deficient SLE prone mice. Unexpectedly, *Rubicon* deficiency increased the lifespan and ameliorated renal disease in *Cybb*-deficient MRL.Fas^{lpr} mice. Strikingly, *Rubicon* deficiency reduced the autoantibody responses to RNA associated autoantigens. These data suggest that a defect in LAP is not a major driver of SLE and highlights RUBICON as a novel mediator of lupus pathogenesis. The mechanism by which myeloid Cybb regulates SLE remains enigmatic and requires further investigation.

TABLE OF CONTENTS

LIST OF TABLES

LIST OF FIGURES

PREFACE

First and foremost, I thank Mark Shlomchik for providing me with the opportunity to complete my thesis work in his laboratory. Mark is an outstanding mentor and he fosters a collaborative environment in his lab, facilitating the exchange of ideas and expertise among the group. I am forever grateful for his advice, encouragement, and resources. Jeremy Tilstra is my collaborator on nearly every project in the lab. Jeremy's guidance and support has been instrumental throughout the duration of my PhD. Kevin Nickerson provided intellectual and technical guidance. A special thank you to Allison Campbell who started this line of investigation as an MD-PhD student in the Shlomchik lab.

I would also like to thank my committee: Michael Lotze, Patrick Pagano, Jon Piganelli, and Simon Watkins for their scientific input and mentorship that was critical towards guiding my project. My thesis work would have been impossible without the help and support of the University of Pittsburgh Transgenic Core and the Innovative Technologies Core. Sebastien Gingras and Chunming Bi were instrumental in helping me to generate novel mouse models critical for completion of this thesis work.

I received superb technical assistance from Tony Marinov, Brady Mareburger, and Kassandra Baron. We could not accomplish large, complex *in vivo* experiments without a stellar technical team.

I would like to thank my mother, Judy Gordon, and my life partner, Evan Davis, for their unconditional love and support throughout this journey. Additionally, Evan developed a CRISPR-Cas9 tool to identify sgRNAs and associated off target sequences.

I dedicate this dissertation to my father, Leonard Gordon (1945-2016). He fostered my intellectual curiosity and love for scientific discovery.

1.0 INTRODUCTION

Systemic Lupus Erythematosus (SLE) is a multisystem autoimmune disease featuring renal, dermatological, musculoskeletal, hematological, cardiac, pulmonary, and neurological manifestations (1). Predominantly targeting women of childbearing age, the estimated incidence and prevalence of SLE of lupus in the United States is 5.1 and 52.2 per 100,000 people respectively (2). The direct annual costs to SLE patients range from $29,034-$62,651 for those with nephritis to $12,273-$16,575 for those without renal manifestations of SLE impacting their quality of life (3). SLE is treated with broad immunosuppressive agents, autophagosome-lysosome fusion inhibitors, and biologics targeting B cells. Belimumab (Benlysta), a monoclonal antibody that targets B cell activating factor (BAFF), was the first drug to be FDA approved for the treatment of patients with SLE in nearly 50 years (2). More recently, monoclonal antibodies targeting type I interferons (IFN) and their corresponding receptor are in clinical trials and show promising therapeutic benefit (4, 5). Despite these advances, current therapeutics are not curative and are riddled with adverse effects, contributing to the morbidity and mortality of this patient population. Understanding the underlying immunological mechanisms that mediate SLE pathogenesis will provide insight into how the immune system constrains the response to self and uncover targets for therapeutic development that address the unmet needs of this patient population.

1.1 NUCLEIC ACID SENSING IN SLE

SLE is characterized by the formation of autoantibodies to nucleic acids and the proteins to which these nucleic acids associate. Loss of tolerance to self results in immune activation and tissue destruction. Innate immune sensing of self nucleic acids and nucleoproteins is implicated in the initiation and progression of SLE. Endosomal Toll-Like Receptors (TLRs) or cytoplasmic DNA and RNA sensors can detect foreign nucleic acids from invading pathogens but also have the capability to recognize self DNA and RNA. The mechanism by which exogenous nucleic acids enter immune cells is unclear but may involve the MHC class III molecule, RAGE.

1.1.1 TLRs and SLE

The endosomal TLRs, TLR7 and TLR9, are important in the pathogenesis of SLE. Indeed, polymorphisms in TLRs and their signaling adaptors are associated with SLE. While TLR9 canonically recognizes bacterial CpG DNA and TLR7 detects viral ssRNA, endosomal TLRs can be activated by endogenous ligands (Figure 1) (1). The development of autoantibodies in lupus is dependent on endosomal TLRs, with TLR9 and TLR7 requisite for the generation of antibodies to DNA and RNA associated autoantigens respectively (2, 3). The function of individual autoantibody subsets in SLE remains elusive. While nucleic acid sensing is critical for autoantibody formation, the global role of TLR7 and TLR9 in disease pathogenesis is diametrically opposed; *Tlr7* deficiency ameliorates disease while *Tlr9* deficiency exacerbates disease in multiple murine models of systemic autoimmunity (3-10). Mirroring these observations, overexpression of *Tlr7* worsens clinical and immunological manifestations of SLE in the *Tlr7* transgenic system and in the *Yaa* model of murine lupus where a portion of the Y

chromosome harboring *Tlr7* is duplicated (5, 6). *Tlr7*$^{-/y}$*Tlr9*$^{-/-}$ MRL.Fas^{lpr} SLE prone mice are protected from the clinical manifestations of lupus and lack autoantibodies to DNA and RNA related antigens (2). MYD88 is a critical signaling adaptor for both TLR7 and TLR9. Concordantly, genetic deletion of *Myd88* phenocopies *Tlr7*$^{-/-}$*Tlr9*$^{-/-}$ SLE susceptible mice (2). These findings implicate TLRs, and not other receptors that use MYD88, as the major regulators of SLE pathogenesis. The role of TLRs in the clinical manifestations of lupus is likely cell specific. While *Myd88* deficiency in B cells ameliorates renal disease and autoantibody production, *Myd88* deletion in dendritic cells (DCs) abrogates dermatitis without impacting other manifestations of lupus (11). The cell specific function of the endosomal TLRs in SLE remains enigmatic and requires further investigation.

1.1.2 Cytosolic DNA sensors and SLE

The function of cytoplasmic DNA and RNA sensors in SLE is less well characterized. The detection of cytosolic RNA is attributed to three helicases that serve as RNA sensors including retinoic acid-inducible gene (RIG-I), melanoma differentiation-associated gene 5 (MDA5), and laboratory of genetics and physiology 2 (LGP2) (12-14) (Figure 1). While RIG-I recognizes viral single stranded RNA (ssRNA), double stranded RNA (dsRNA) with 5' triphosphates or diphosphates and short dsRNA, MDA5 detects long blunt dsRNAs (15-18). LGP2 facilitates recognition of RNA viruses by RIG-I and MDA5 but does not contain a caspase activation and recruitment domain (CARD) requisite for downstream signaling (14, 19). RIG-I and MDA5 signal via the mitochondrial anchored adaptor mitochondrial antiviral signaling protein (MAVS) resulting in the activation of tank binding kinase 1 (TBK1) (20). TBK1 induces nuclear factor kappa-light-chain-enhancer of activated B cells (NFκB) dependent proinflammatory cytokine

production and phosphorylates interferon regulatory factor (IRF) 3 and IRF7 allowing for their hetero- and homo-dimerization and translocation to the nucleus where IRFs serve as transcription factors to mediate IFN transcription (21-23). Stimulator of interferon genes (STING) is required for optimal type I IFN production by RIG-I but not MDA5 (24). Recently, mitochondrial reactive oxygen species (ROS) were implicated in MAVS oligomerization and subsequent type I IFN production in SLE patients (25). A gain of function polymorphism in *MDA5* (A946T) is associated with SLE (26-29). Moreover, *IRF3* promoter polymorphisms that result in reduced *IRF3* expression are reported to confer protection from SLE (30). However, in the MRL.Fas^{lpr} mouse model of SLE, *Irf3* deficiency does not alter manifestations of autoimmunity (31).

Cytosolic sensing of DNA can occur through a variety of different receptors and downstream signaling mechanisms (Figure 1). Strikingly, cytosolic DNA sensors do not mandate a specific DNA sequence nor are impacted by DNA methylation status that is unique to pathogens. Therefore, cytosolic DNA sensors have the capacity to respond to self DNA. DNA-dependent activator of IRFs (DIA) was one of the first receptors suggested to recognize cytosolic DNA (32). However, DIA-deficient mice were still able to generate type I IFNs in response to cytosolic DNA suggesting the existence of additional cytosolic DNA sensors (33). More recently, guanosine monophosphate adenosine monophosphate synthase (cGAS), IFN inducible protein 16 (IFI16), and the DExD/H family of helicase DDX41 have been recognized as cytosolic DNA sensors that converge on the STING pathway as a central hub (24, 34-36). DNA-dependent RNA polymerase III can sense and transcribe AT-rich dsDNA and the resulting dsRNA product initiates the RIG-I pathway (37, 38).

There are several lines of evidence that link cytosolic DNA sensing to systemic autoimmunity. DNase II and III (3′ repair exonuclease 1, Trex1) are important for the

degradation of endogenous DNA (39) (40). Loss of function polymorphisms in *DNASE II* and *TREX1* are associated with SLE (41-43). Mice and humans with *DNASE II* and *TREX1* deficiency are not able to degrade endogenous DNA, resulting in a rampant type I IFN response and autoinflammation (39-42). Patients with Aicardi Goutières syndrome, characterized by loss of function mutations in *TREX1*, develop severe neurological impairment and debilitating SLE-like autoimmunity (42). In mice, the inflammatory syndrome observed in the setting of *Trex1* deficiency is STING dependent. *DNase II*$^{-/-}$ mice that are crossed to the interferon-α/β receptor (IFNAR) knockout allele to prevent embryonic lethality caused by type I IFN induced anemia, develop inflammatory arthritis that is both dependent on STING and the absent in melanoma 2 (AIM2) inflammasome (44, 45). Similarly, gain of function mutations in *TMEM173*, the gene that codes for STING, can result in autoinflammation. Patients with STING-associated vasculopathy with onset in infancy (SAVI) exhibit increased IFNβ production and rampant inflammation that results in tissue damage (46, 47). Discordant with these observations, STING-deficient MRL.Fas^{lpr} mice develop markedly accelerated SLE, manifesting in decreased survival, worsened renal disease, and higher titers of autoantibodies. In this setting, STING controls the expression of critical innate signaling regulators (31). The multiple facets of STING in systemic autoimmunity require further exploration.

The inflammasome is also implicated in cytosolic DNA sensing as AIM2 is activated by cytosolic DNA (48-50). Upon DNA sensing, AIM2 complexes with apoptosis-associated speck-like protein containing a CARD (ASC) to form the AIM2 inflammasome. Inflammasome activation triggers caspase-1 dependent proteolytic processing of the inflammatory cytokine Interleukin (IL)-1β into its active form (49, 50). Moreover, the AIM2 inflammasome initiates pyroptosis, an inflammatory form of programmed cell death, in macrophages (51). Indeed, AIM2

is found within SLE susceptibility loci and AIM2 expression (52) is elevated in macrophages from male SLE patients (53). However, our group genetically deleted *Asc*, a central adaptor for most inflammasomes complexes, including AIM2, and found no effect on disease in MRL.Fas^{lpr} mice (54). It is possible that inflammasomes that function independent of ASC are important for SLE pathogenesis but these data preclude a role for AIM2 in the MRL model of SLE.

1.2 THE SOURCE OF AUTOANTIGEN IN SLE

While sensing of self nucleic acids and nucleoproteins is critical for SLE pathogenesis, the source of these autoantigens is still unknown. One possibility is that dying cells could be this source. The mechanism by which a cell dies may have critical implications on the host response to resulting debris by revealing ligands to nucleic acid sensors and/or altering the environment in which these endogenous ligands are detected. Apoptosis is a non-immunogenic caspase dependent programmed cell death pathway whereby the proteolytic cascade leads to cleavage of cellular proteins and DNA (55). Successful apoptosis produces fewer damage associated molecular patterns (DAMPs) and induces production of the immunoregulatory cytokines IL-10 and Transforming Growth Factor β (TGFβ) from phagocytic macrophages (55). Subsequent release of "eat me" and "find me" signals, such as calreticulin and phosphatidylserine (PS), leads to clearance of cell corpses by macrophages (56). The role of dead cell clearance and associated production of immunoregulatory cytokines in SLE is the subject of chapters 3 and 4. Impaired clearance of apoptotic cells can promote secondary necrosis (55, 57). Necrosis or programmed necroptosis is an immunogenic form of cell death characterized by cytoplasmic swelling, membrane rupture, and organelle degradation. Receptor-interacting protein (RIP) Kinases and

the terminal effector MLKL mediate the formation of the necrosome composed of Caspase 8, RIP1, and RIP3 (55, 58, 59). Necroptosis has been associated with kidney transplant rejection (60). Pyroptosis is another form of catastrophic cell death that results from caspase 1 dependent pore formation and rapid plasma membrane lysis, releasing cellular contents, IL-1β, and IL-18 (51, 55). Ferroptosis is a more recently defined mechanism associated with iron dependent oxidation of polyunsaturated fatty acids (PUFA) and resultant cell death (61).

In 2004, Brinkmann and colleagues first described a process whereby neutrophils can release DNA coated with antimicrobial peptides and proteases into the extracellular space forming structures that we now refer to as neutrophil extracellular traps (NETs) (62). Neutrophil death resulting from NET generation is termed suicidal NETosis. NET formation is generally dependent on Nicotinamide adenine dinucleotide phosphate (NADPH) oxidase generated ROS (63, 64). Peptidyl arginine deiminase 4 (PADI4), an enzyme which citrullinates histones requisite for chromatin decondensation (65, 66), is an important conserved mediator for NET formation. Though reports suggest that NETs are a source of antigenic nucleic acids in SLE (67-74), we and others have recently shown that inhibition of classical NETs by genetically deleting critical components of the NADPH oxidase complex, including Cytochrome b-245, β polypeptide (*Cybb*), exacerbates multiple manifestations of SLE in several murine models (75-77). The role of critical distal NET mediators, such as *Padi4* and neutrophils elastase (*Elane*), in SLE is the topic of chapter 2. The mechanism by which NADPH oxidase deficiency drives SLE pathogenesis will be addressed in chapters 3 and 4.

1.3 THE MRL.FAS^{LPR} MODEL OF SLE

To study the causative impact of a gene or biological process in a disease setting, it is important to have a model system that can be both genetically manipulated and recapitulates pathology observed in patients. The MRL.Fas^{lpr} model of SLE is a leading system for the study of lupus since it has the advantage of being driven by multiple genes of the MRL background coupled with spontaneous onset, as in the case of human SLE (78). Fas-deficiency accelerates the disease but is not required for it, nor does it generally impact outcomes of genetic or therapeutic manipulations (78). MRL.Fas^{lpr} mice typically develop clinical features of SLE and lymphoproliferation by 16-weeks of age. Notably, the MRL model recapitulates nearly all American College of Rheumatology diagnostic criteria (75, 79) and is both type I/type II IFN-dependent (80, 81). On multiple occasions, observations first obtained with MRL.Fas^{lpr} were later confirmed in Fas-sufficient MRL mice. Therefore, we used MRL.Fas^{lpr} mouse model of SLE in the studies that we present here as this strain allows for a comprehensive analysis of multiple relevant disease parameters.

1.4 SPECIFIC AIMS

The source of autoantigen remains an important and unresolved question in the study of SLE with major implications in our understanding of autoimmune pathogenesis and strategies towards therapeutic intervention. While the sources of autoantigens in SLE are not known, two leading possibilities include (1) the release of antigenic contents from dying cells and/or (2) subsequent failure to adequately dispose of resulting debris by macrophages.

While exacerbated SLE in the context of NADPH oxidase deficiency challenges the idea that NETs promote lupus, it is conceivable that global regulatory properties of NADPH oxidase and NADPH oxidase independent NETs confound these findings. Indeed, there are multiple reported means by which NADPH oxidase can inhibit inflammation (82, 83), including neutrophil (84, 85), macrophage (86), and lymphocyte (87, 88) dependent mechanisms. Recently, NADPH oxidase function was found to be required for LC3-associated phagocytosis (LAP) (89). LAP has been linked to the concurrent production of suppressive rather than pro-inflammatory cytokines and mice incapable of performing LAP develop autoimmunity (90). This line of investigation will be further addressed in chapters 3 and 4.

The overarching hypotheses of this thesis are: (1) NETs are not the primary source of autoantigen in SLE and (2) NADPH oxidase exerts a fundamental regulatory activity in the myeloid compartment by modulating neutrophil death and or dead cell clearance by macrophages. These hypotheses will be addressed in the following specific aims:

Specific aim 1: Evaluating the role of NETs in SLE by knocking out *Padi4* or *Elane* in lupus prone mice.

Specific aim 2: Investigating the cell specific role of NADPH oxidase in the pathogenesis of SLE by employing chimera and conditional knockout approaches in a mouse model of lupus.

Specific aim 3: Assess the contribution of LAP by genetically deleting *Cybb*, *Rubicon*, and myeloid *IL-10* in the MRL.Fas^{lpr} mouse model of SLE.

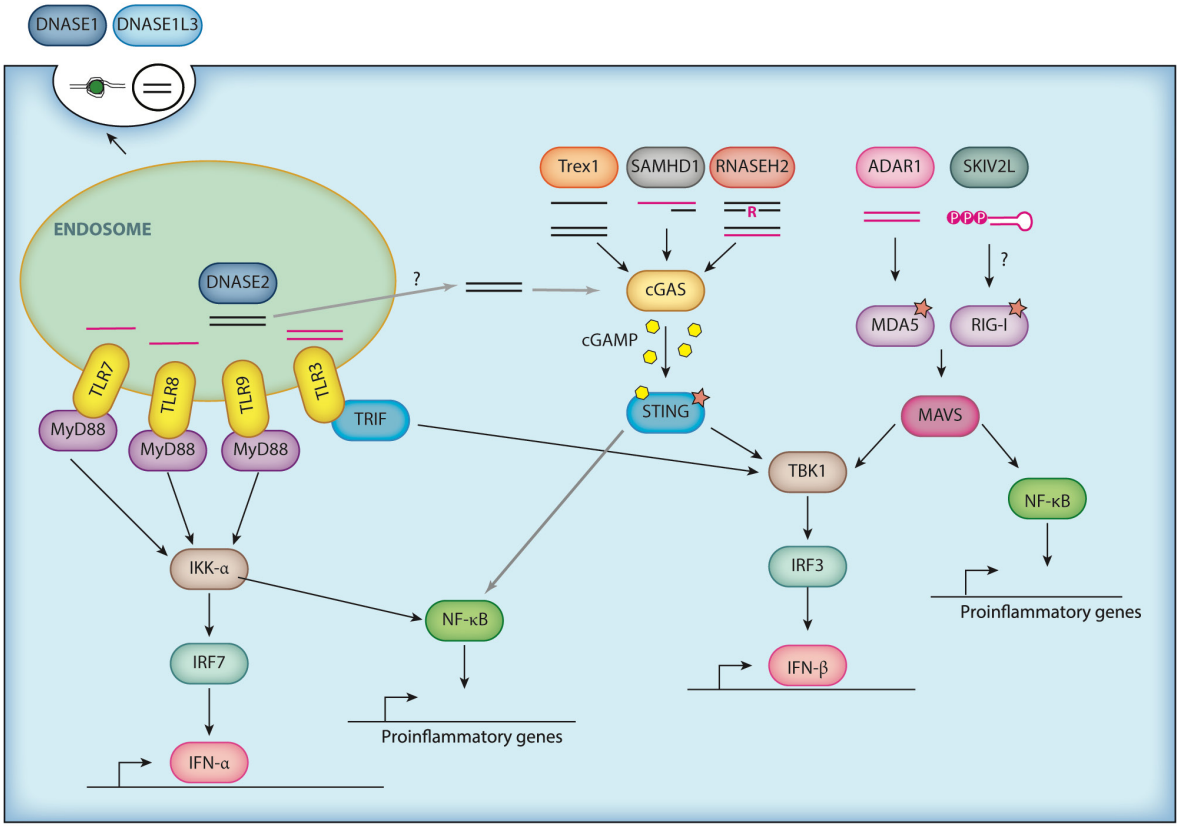

Figure 1. Endosomal Toll-like receptors and sensors of cytosolic nucleic acids.
Adapted from: Crowl JT, Gray EE, Pestal K, Volkman HE, and Stetson DB. Intracellular Nucleic Acid Detection in Autoimmunity. Annual Review of Immunology. 2017;35(1):313-36.

2.0 NEUTROPHIL EXTRACELLULAR TRAPS AND SLE: EVALUATING THE ROLE OF PEPTIDYL ARGININE DEIMINASE 4 AND NEUTROPHIL ELASTASE IN THE PATHOGENESIS OF LUPUS

Adapted from: Gordon RA, et al. Lupus and proliferative nephritis are PAD4 independent in murine models. *JCI Insight.* 2017;2(10)

2.1 INTRODUCTION

SLE is a systemic autoimmune disease characterized by the formation of autoantibodies to nucleic acids and the proteins to which these nucleic acids associate. Loss of tolerance to self results in immune activation and tissue destruction. While the sources of autoantigens in SLE are not known, the liberation of antigenic contents from dying is considered a likely culprit.

2.1.1 Neutrophil extracellular traps

NETs are extruded DNA structures coated with granular and cytoplasmic contents that are released into the extracellular environment. It is conceivable and compelling that NETs could be a source of autoantigen in SLE and a downstream mediator of end-organ damage. At least one billion neutrophils die per kilogram of body weight each day, underscoring the neutrophil as a

potential antigen source (91). Early studies proposed that NETs are composed of decondensed nuclear DNA and that the neutrophil dies upon NET release (64). More recently, nuclear DNA externalization without concomitant cell lysis (92) and extrusion of mitochondrial DNA (93-95) have been described. Classical NET formation in humans and mice is dependent on NADPH oxidase-generated reactive oxygen species (ROS) (63, 64), though rapid NADPH oxidase-independent NET formation has been reported (92, 96).

2.1.2 Peptidyl arginine deiminase 4 and NETs

Peptidyl arginine deiminases (PADI) are a family of calcium dependent enzymes that catalyze the conversion of arginine to citrulline (97). There are 5 PADI members in mouse and humans, PADI1-4 and PADI6, each with differential tissue distribution and cellular localization (97). PADI4 is predominantly expressed in granulocytes and resides in the nucleus where it can deaminate histones (98). The physiological functions of PADIs are not well characterized. PADI4 dependent histone citrullination is associated with transcriptional regulation (99, 100). Antibodies towards citrullinated peptides are associated with systemic autoimmune diseases including rheumatoid arthritis and SLE (101-103). Importantly, PADI4-dependent histone citrulluation facilitates chromatin decondensation a conserved step in NET formation (65, 66, 104-107). PADI4 is critical for the generation of NETs (65, 66, 104-107). Neutrophils from *Padi4*-deficient mice fail to make NETs (65, 66) and pharmacological inhibition of PADI4 with potent and specific PADI4 inhibitors, GSK199 and GSK484, reduced NET formation in mouse and human neutrophils (106).

2.1.3 Neutrophil Elastase and NETs

Neutrophil elastase (ELANE) is a serine protease representing 5% of the total protein content in NETs, second to histones (108, 109). Many groups report that ELANE is not only a structural component of the NET but crucial for their formation in mice and humans (107, 110-113). Upon activation, ELANE is released from the azurophilic granules and translocates to the nucleus in a NADPH-oxidase and myeloperoxidase (MPO)- dependent manner (111, 112). Production of H_2O_2 allows for disassociation of ELANE from a membrane bound complex into the cytosol (111, 112). During this process, ELANE binds F-actin in the cytoplasm and degrades it to translocate to the nucleus (111). In the nucleus, ELANE initially degrades H1 followed by H4 histones, the latter of which is associated with decondensation of nuclear DNA (111, 112). Recently, neutrophils derived from a patient with a novel loss of function polymorphism (G210R) in exon 5 of *ELANE* were shown to exhibit defective NET formation (110). Interestingly, this mutation did not confer congenital neutropenia but the patient did exhibit inflammatory arthritis and recurrent parvovirus infections (110).

Several lines of indirect evidence link ELANE as an important mediator of NET formation. Protease inhibitors can prevent NET formation, including the ELANE inhibitors, secretory leukocyte protease inhibitor (SLPI) and Serpin Family B Member 1 (SERPIN1b) (114, 115). Neutrophils from *Slpi*-deficient mice are more efficient at generating NETs both *in vitro* and in the context of a murine psoriasis model *in vivo* (115). *Serpin1b*-deficient neutrophils have a greater propensity to form NADPH oxidase-dependent and -independent NETs in response to various stimuli *in vitro* (114). Moreover, NET generation of serpin1-deficient neutrophils is increased in the setting of *Pseudomonas aeruginosa* lung infection (114). Papillon-Lefèvre syndrome (PLS) is characterized by mutations that inactivate cysteine protease Cathepsin C

(CTSC) which processes a variety of serine proteases into an active state, including ELANE (116). Neutrophils from PLS patients undergo reduced NET formation (116, 117).

2.1.4 NETs and SLE

Several lines of evidence suggest that NETs may be a primary and non-redundant source of self-antigen in SLE. NET-like structures are found in the skin and kidneys of SLE patients and SLE prone mice (67-70), while NET degradation is impaired in a minor subset of individuals with lupus (71, 72). Abnormal low density granulocyte (LDGs) populations identified in a peripheral blood mononuclear cell (PBMC) fractions isolated from SLE cohorts have an increased propensity to form NETs *in vitro*, potentially enhancing exposure to autoantigens and immunostimulatory molecules (67, 73). Neutrophils from SLE patients can activate plasmacytoid dendritic cells (pDC) to produce type I IFN upon culture *in vitro*, a phenomenon attributed specifically to NET formation (68, 74). Concordantly, anti-ribonuclear protein (RNP) antibodies, which are present in a subgroup of SLE patients, can induce *in vitro* NETs from SLE but not normal neutrophils, in a process dependent on FcγRIIA, ROS, and TLR7 (68). Activating Fcγ receptors (FcγRs) are critical for the pathogenesis of SLE nephritis (118), and neutrophil FcγRs promote renal injury (119) leading to the possibility that FcγR mediated NET formation contributes to end organ injury. More recently, two groups reported that anti-RNP antibodies and immune complexes (IC) can induce the externalization of immunostimulatory oxidized mitochondrial DNA (94, 95). While SLE LDGs release oxidized mitochondrial DNA (95) and anti-oxidized mitochondrial DNA autoantibodies (94) are elevated in pediatric SLE patients, the mechanism by which oxidized mitochondrial DNA is released in the context of SLE, its relationship to NET-like structures, and its role in disease pathogenesis remains controversial.

While the above data tend to associate NETs with SLE pathogenesis, this concept is challenged by murine studies in which classical NETs were abolished by genetically deleting *Cybb*, an essential component of the NADPH oxidase complex, in the context of a lupus-prone genetic background (75). In these mice, not only was lupus still present but *Cybb*-deficiency exacerbated multiple manifestations of lupus and immune activation, including kidney disease. These results parallel prior observations in male chronic granulomatous disease (CGD) patients who carry an X-linked mutation in *CYBB* (120), as well as their carrier mothers (121, 122). These individuals have higher, not lower, incidences of spontaneous autoimmunity. Furthermore, alleles of other components of the NADPH oxidase complex, neutrophil cytosolic factor (*NCF*) 1 and 2, that are thought to be less functional, are positively associated with lupus across multiple ethnic groups (123-125). Although these studies argue against the hypothesis that NETs drive lupus, it remains possible that other immune dysregulatory effects of global *Cybb*-deficiency dominantly override the requirement for NADPH oxidase driven NETs in this case. In addition, as there have been reports that various stimuli induce distinct types of NETs, it is possible that CYBB-independent NET formation could drive SLE.

To address this pivotal controversy, it is important to evaluate independent approaches to block NET generation in the setting of SLE. PADI4 and ELANE are natural targets since neutrophils from *Padi4*- and *Elane*-deficient mice fail to make NETs (65, 66). We chose to eliminate *Padi4* and *Elane* in the MRL.Fas^{lpr} strain as it has been tested in both the context of *Cybb*-deficiency and PAD pharmacological inhibition (69, 70, 75), thus allowing for direct comparison of results. Importantly, inhibitors targeting the NET pathway will enter clinical trials, underscoring the need for a better understanding of their targets in NET formation and the *in vivo* consequences of their use.

Here, we show that abrogation of *Padi4* and *Elane* by a genetic approach did not have any impact on clinical or immunological parameters of SLE in MRL.Fas^{lpr}. Taken together with earlier work (75), these findings challenge the concept that NETs, to the degree that NET generation relies on PADI4 (65, 66, 104-107, 126), ELANE (107, 110-113), or CYBB (63, 64, 127-129), critically drives lupus and nephritis.

2.2 SYSTEMIC LUPUS ERYTHEMATOSUS IS INDEPENDENT OF PADI4 IN THE MRL.*FAS*^{LPR} MURINE MODEL

To assess the role of Padi4-deficiency in SLE, we backcrossed the *Padi4*$^{-/-}$ allele onto the MRL.Fas^{lpr} background for 9 generations. Heterozygous mice were then intercrossed to produce an experimental cohort. SLE pathology was analyzed at 17 weeks of age.

2.2.1 *Padi4*-deficiency did not affect nephritis or dermatitis

No differences in urine protein were detected in the fully backcrossed cohort (Figure 2A). *Padi4*-deficiency had no impact on dermatitis (Figure 2B). No statistically significant differences in glomerulonephritis or interstitial nephritis were detected among the different *Padi4* genotypes in either cohort (Figure 2C and D). Similarly, *Padi4* genotype did not impact splenomegaly and lymphadenopathy (Figure 2E and F).

2.2.2 *Padi4*-genotype had no impact on loss of tolerance or the anti-self responses

Padi4-genotype did not generally alter the autoantibody response or Ig titers. We did not detect any change in anti-RNA antibody (Figure 3A), anti-Sm antibody (Figure 3B), anti-nucleosome antibody (Figure 3C), rheumatoid factor (RF) (Figure 3D), or total IgM (Figure 3E) and total IgG titers (Figure 3F) in the context of *Padi4*-deficiency. Concordant with these data, there were no statistically significant differences in total kappa Ig antibody forming cell (AFC) ELISpots (Figure 4A). Similar AFC ELISpot results were obtained for the IgG1, IgG2a, and IgM isotypes (Figure 4-D). Furthermore, *Padi4*-genotype did not affect the percentage of $CD19^{+}$ B cells (Figure 4E) or $CD19^{low\text{-}int}$ $CD44^{+}$ $CD138^{+}$ intracellular κ^{high} AFCs (Figure 4F).

2.2.3 *Padi4*-deficiency did not change the myeloid compartment

Padi4-genotype had only a minor impact on the myeloid compartment in MRL.Fas^{lpr} mice. The percentages of $CD11b^{+}Ly6G^{+}$ bone marrow (BM) neutrophils (Figure 5A) and $CD11b^{+}F4/80^{+}Gr1^{low\text{-}int}$ BM macrophages (Figure 5B) were not statistically different among the groups. Female *Padi4*$^{-/-}$ mice had a greater percentage of splenic neutrophils compared to their heterozygous counterparts (Figure 5C). Additionally, no change in $CD11b^{+}F4/80^{+}Gr1^{low\text{-}int}$ macrophages were identified across *Padi4* genotype (Figure 5D). No differences in the percentage of $CD19^{-}CD11c^{+}MHCII^{+}$ conventional DCs (cDCs) (Figure 6A and B) and $CD19^{-}$ $BST2^{+}$ $SiglecH^{+}$ pDCs (Figure 6A and C) were identified among the groups.

2.2.4 *Padi4*-deficiency did not alter the lymphoid compartment

Padi4-deficiency did not substantially impact the lymphoid compartment. All genotypes exhibited indistinguishable total percentages of TCRβ$^+$ T cells (Figure 7A and B). The percentages of CD4$^+$ T cells and CD4$^+$CD44$^+$CD62L$^-$ activated T cells were also similar amongst wild-type, *Padi4*-deficient, and heterozygous mice (Figure 7A and C). Similar results were obtained for naive and activated CD8$^+$ T cells (Figure 7A and D).

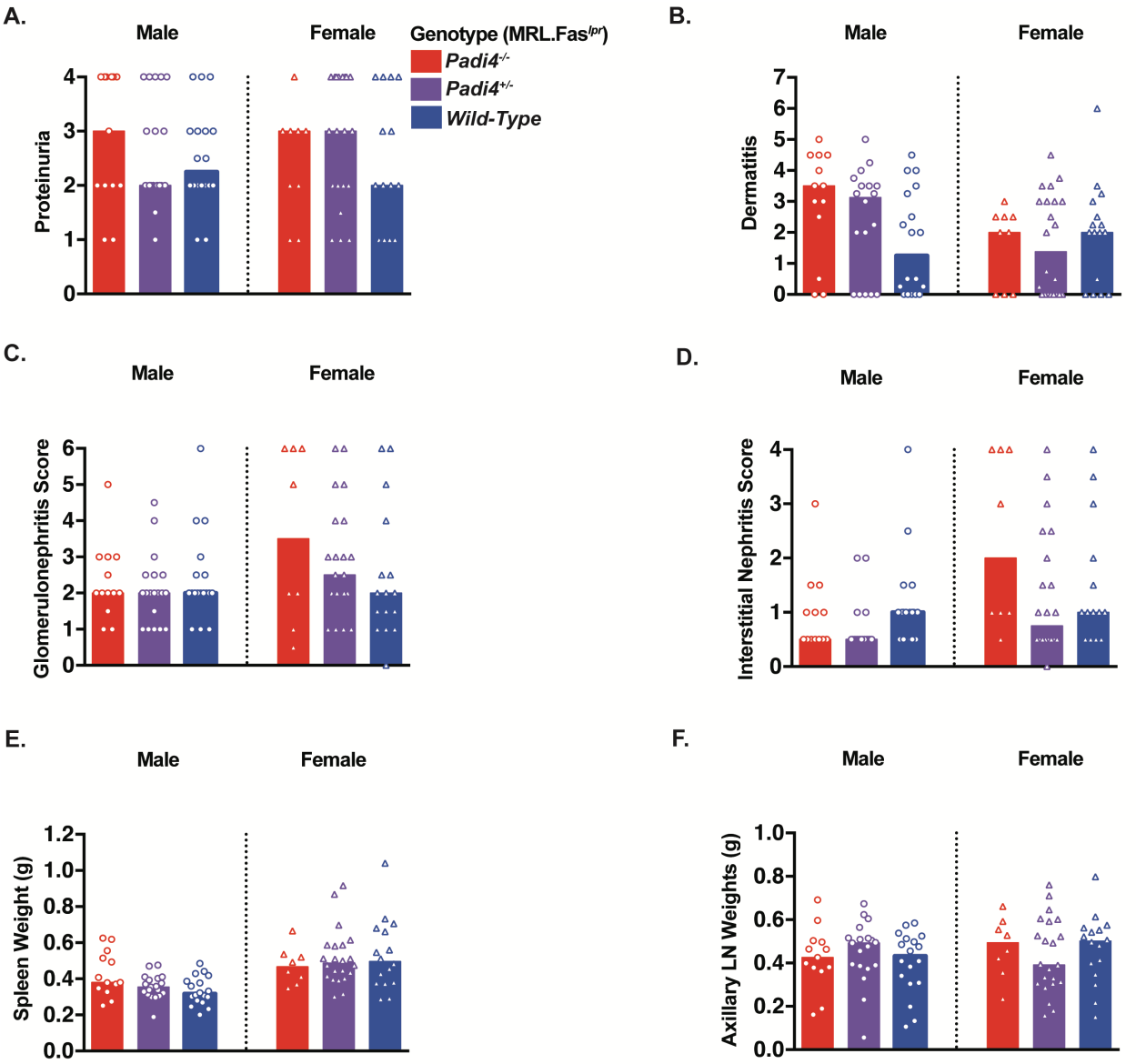

Figure 2. *Padi4*-genotype did not impact lupus nephritis, dermatitis, or lymphadenopathy/splenomegaly. **(A)** Proteinuria. **(B)** Dermatitis scores. **(C)** Glomerulonephritis scores. **(D)** Interstitial nephritis scores. **(E)** Spleen weight. **(F)** Axillary lymph node weights. Scores and weights are represented as a function of *Padi4*-genotype and gender at 17 weeks of age. Bars represent the median and each dot represents and individual mouse. A Kruskal-Wallis test with post-hoc Dunn's test was performed to determine statistical significance within each gender (* indicates $p \leq 0.05$, ** $p \leq 0.01$, *** $p \leq 0.001$, and **** $p \leq 0.0001$; n=8 to 22 mice per group).

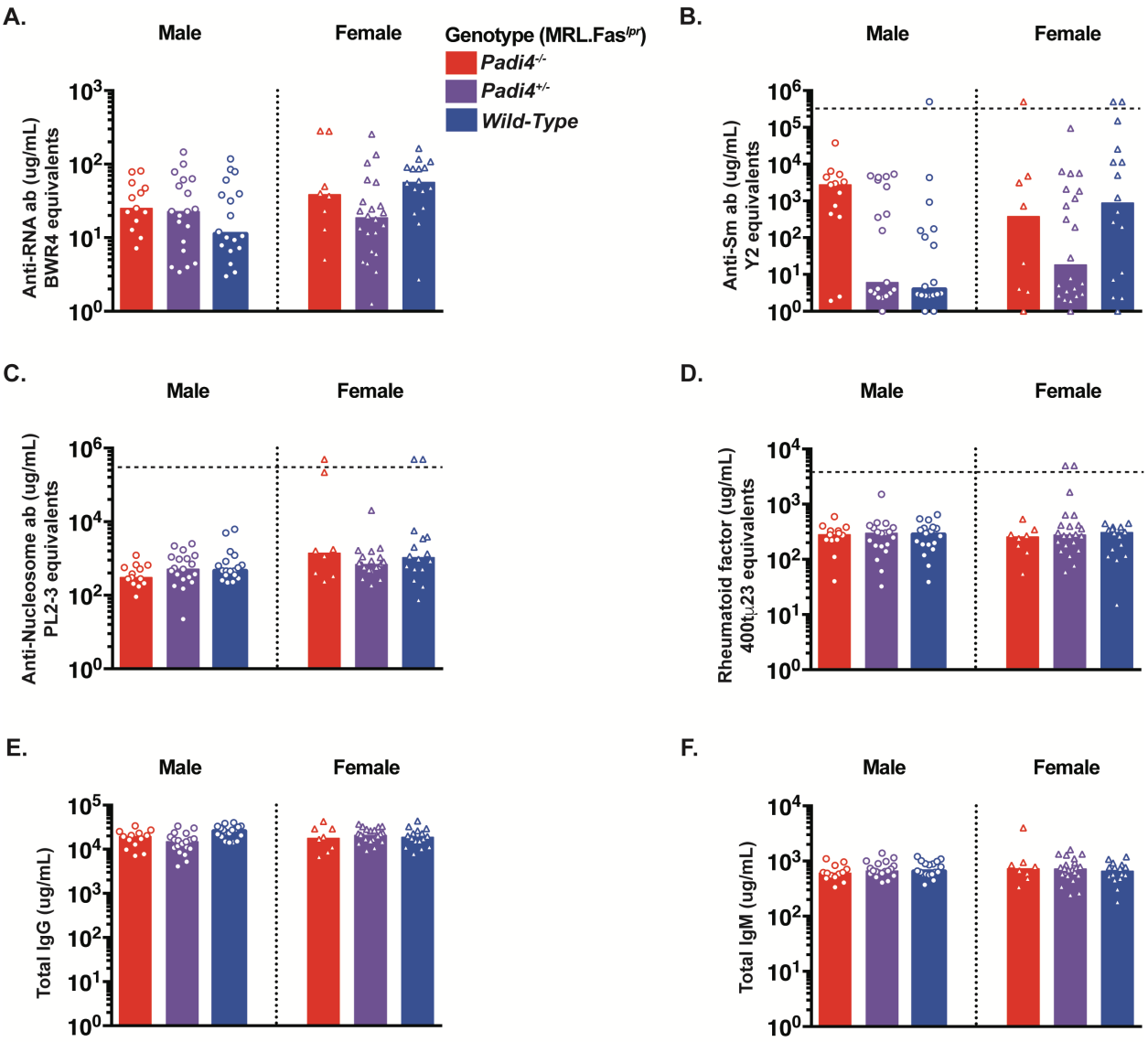

Figure 3. *Padi4*-genotype did not significantly alter the anti-self response.
(A-F) Serum anti-RNA (A), anti-Sm (B), anti-nucleosome (C), rheumatoid factor (D), and total IgM (E) and total IgG (F) antibody titers at 17 weeks of age. The dotted line denotes the upper limit of quantitation. Data representation, number of mice, and statistics are as in Figure 2.

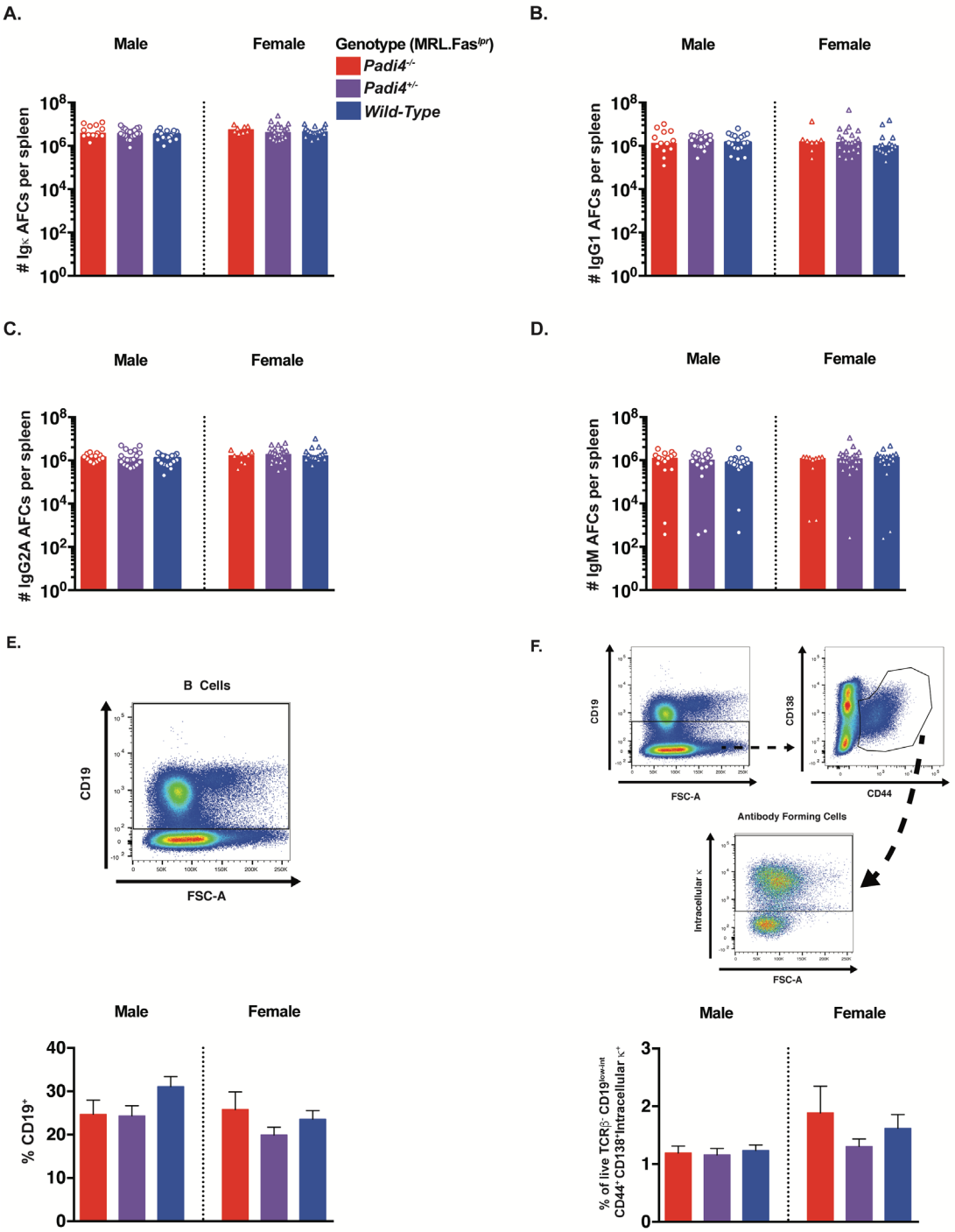

Figure 4. *Padi4* deficiency did not change the AFC compartment.
(A-D) Numbers of Igκ (A), IgG1 (B), IgG2a (C), and IgM (D) antibody forming cells (AFCs) per spleen as determined by ELISpot. **(E)** B cell gating strategy (top panel) and the percentages of live $CD19^+$ total B cells (bottom panel). **(F)** AFC gating strategy (top panel) and the percentages of live cells that are $TCR\beta^-$ $CD44^+$ $CD138^+$ intracellular κ^+ in spleens (bottom panel). Data representation, number of mice, and statistics are as in Figure 1. In panels E and F, bar graphs are represented as the mean ± SEM and a one-way ANOVA with post-hoc Holm-Sidak test was performed to determine statistical significance within each gender (* indicates $p \leq 0.05$, ** $p \leq 0.01$, *** $p \leq 0.001$, and **** $p \leq 0.0001$; n=8 to 22 mice per group).

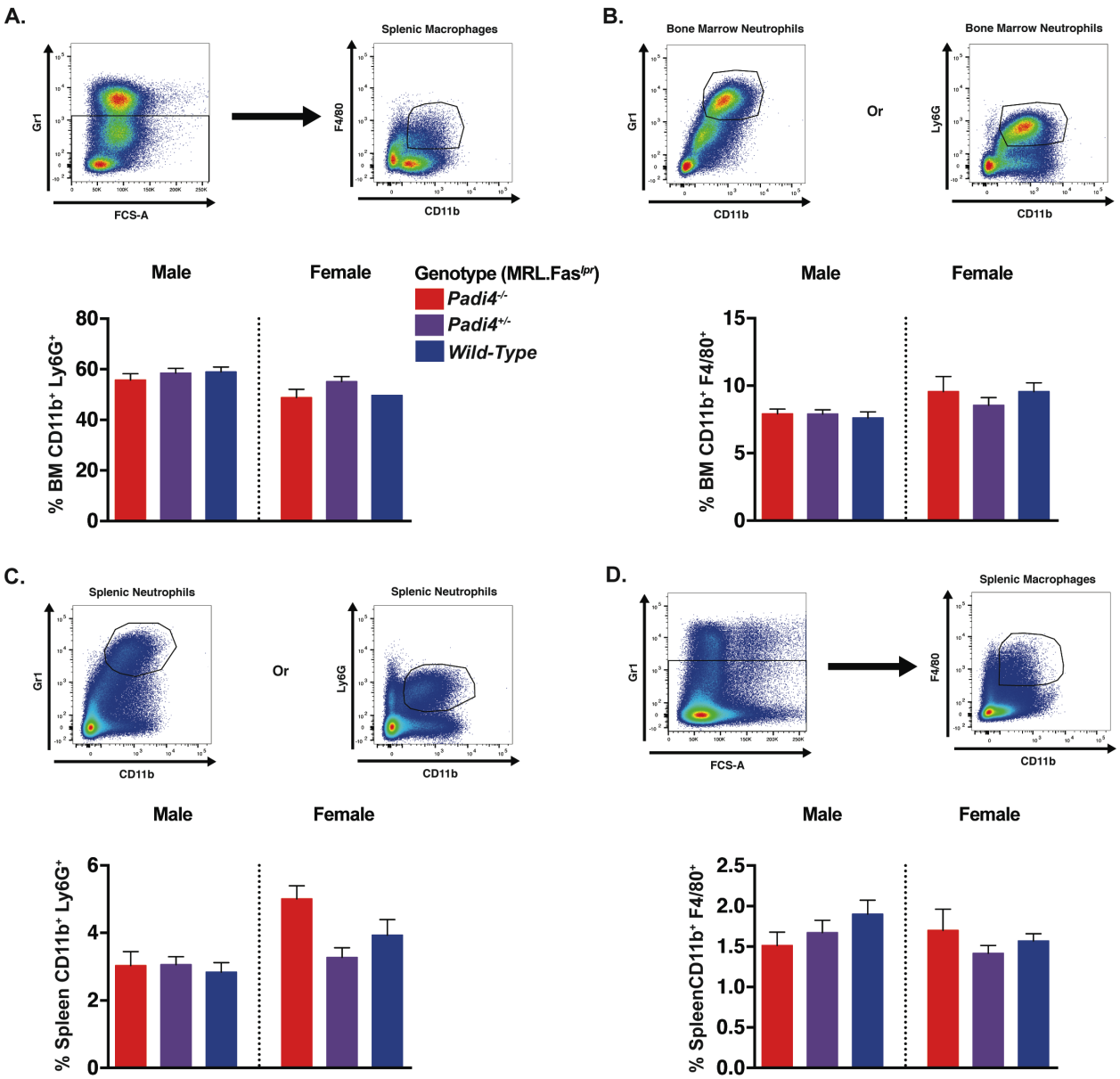

Figure 5. *Padi4*-genotype did not substantially affect the myeloid compartment.
(A) Bone marrow (BM) neutrophil gating strategy (top panel) and the percentages of live BM $CD11b^+$ $Ly6G^+$ neutrophils (bottom panel). **(B)** BM macrophage gating strategy (top panel) and the percentages of BM $CD11b^+$ $GR1^{low\text{-}int}$ $F4/80^+$ macrophages (bottom panel). **(C)** Splenic neutrophil gating strategy (top panel) and the percentages of live $CD11b^+$ $Ly6G^+$ neutrophils in the spleen (bottom panel). **(D)** Splenic macrophage gating strategy (top panel) and the percentages of splenic $CD11b^+$ $GR1^{low\text{-}int}$ $F4/80^+$ macrophages (bottom panel). Bar graphs are represented as the mean ± SEM and a one-way ANOVA with post-hoc Holm-Sidak test was performed to determine statistical significance within each gender (* indicates $p \leq 0.05$, ** $p \leq 0.01$, *** $p \leq 0.001$, and **** $p \leq 0.0001$; n=8 to 22 mice per group).

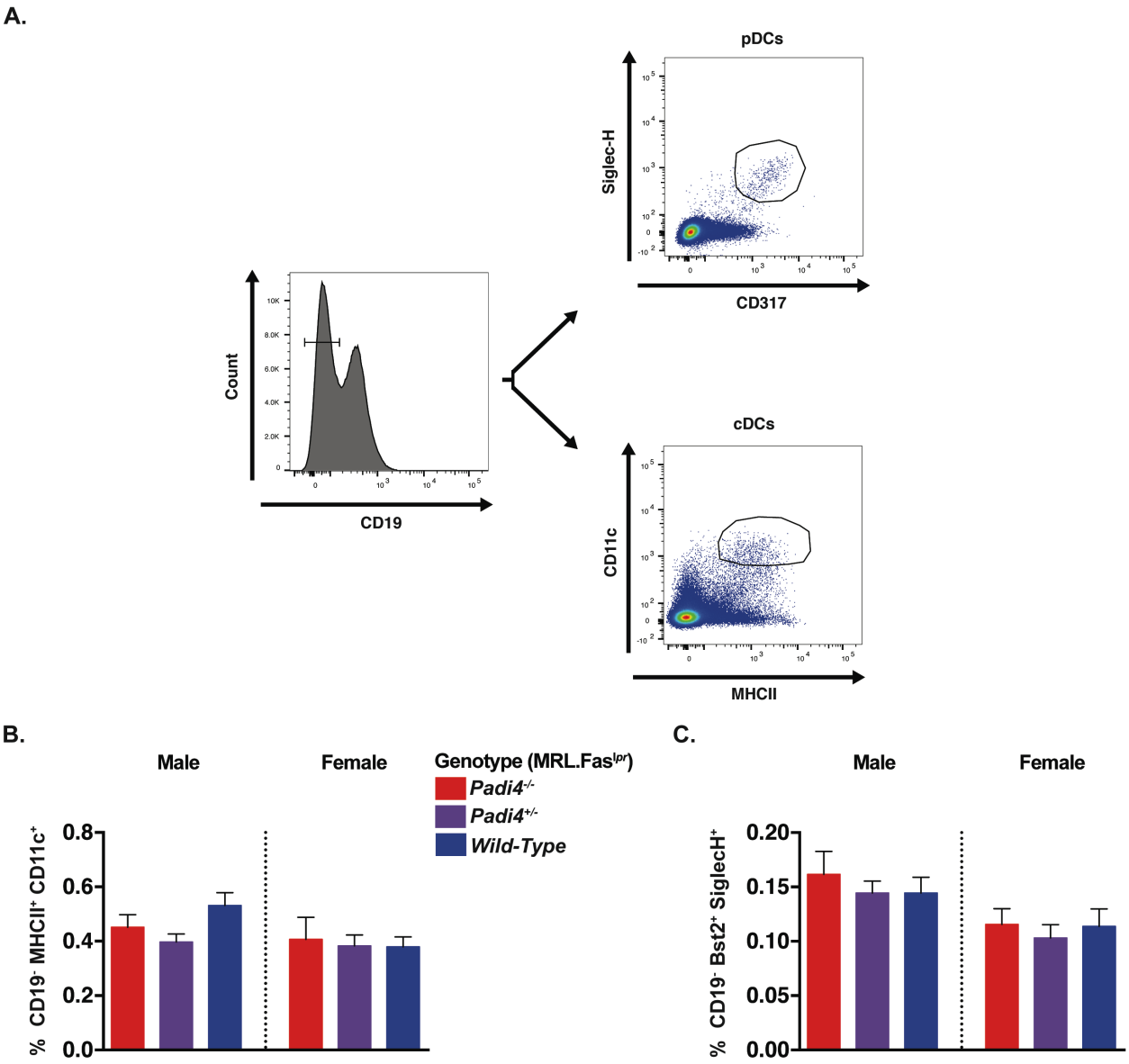

Figure 6. Dendritic cells populations were not impacted by *Padi4* deficiency.
(A) Conventional (cDC) and plasmacytoid (pDC) dendritic cell gating strategy. **(B)** Percentages of live $CD19^-$ $MHCII^+$ $CD11c^+$ cDCs and **(C)** $CD19^-$ $BST2^+$ $CD11c^+$ pDCs. Data representation, number of mice, and statistics are as in Figure 5.

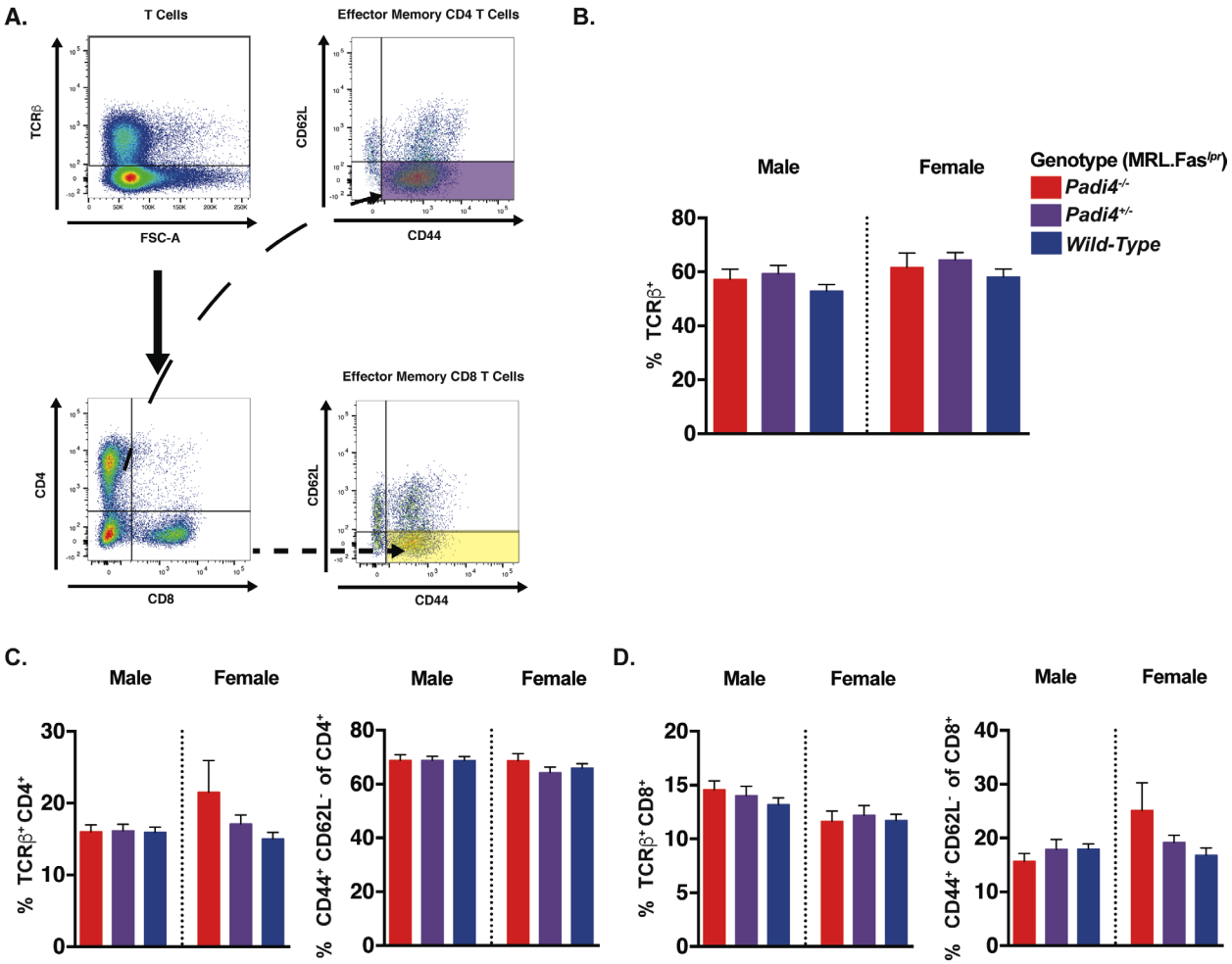

Figure 7. *Padi4* deficiency had little impact on the lymphoid compartment.
(A) T cell gating strategy. **(B)** Percentages of live TCRβ$^+$ total T cells. **(C)** Percentages of live TCRβ$^+$ CD4$^+$ T cells (left panel) and of CD4$^+$ CD44$^+$ CD62L$^-$ activated T cells (right panel). **(D)** Percentages of live TCRβ$^+$ CD8$^+$ T cells (left panel) and of CD8$^+$ CD44$^+$ CD62L$^-$ activated T cells (right panel). Data representation, number of mice, and statistics are as in Figure 5.

2.3 SYSTEMIC LUPUS ERYTHEMATOSUS IS INDEPENDENT OF ELANE IN THE MRL.FAS^{LPR} MURINE MODEL

To assess the role of *Elane*-deficiency in SLE, we utilized the *Elane-Cre* mouse. Here, a modified bacteriophage P1-derived *Cre* recombinase gene was incorporated at the ATG start codon of the *Elane* gene generating a knockin that inactivates the *Elane* locus (130). We fully backcrossed the *Elane*$^{-/-}$ allele onto crossing MRL.Fas^{lpr} background for 9 generations. Heterozygous mice were then intercrossed to produce an experimental cohort. SLE pathology was analyzed at 17 weeks of age.

2.3.1 *Elane* deficiency had no effect on nephritis or dermatitis

No differences in urine protein were detected across *Elane* genotype in both male and female cohorts (Figure 8A). *Elane* deficiency had no impact on dermatitis (Figure 8B). No statistically significant differences in glomerulonephritis or interstitial nephritis were detected among the different *Elane* genotypes in either cohort (Figure 8C and D). Similarly, *Elane* genotype did not alter splenomegaly or lymphadenopathy (Figure 8E and F).

2.3.2 *Elane* genotype has a minor impact on loss of tolerance or anti-self responses

The autoantibody response was not altered in the context of *Elane* deficiency. We did not detect any change in anti-RNA antibody (Figure 9A), anti-Sm antibody (Figure 9B), anti-nucleosome antibody (Figure 9C), and rheumatoid factor (Figure 9D) titers among the groups. Concordant with these data, there were no statistically significant differences in total kappa Ig AFC ELISpots

(Figure 10A). Wild-type female mice had a higher number of IgG1 AFCs compared to their *Elane*-deficient MRL.Fas^{lpr} counterparts (Figure 10B). This finding is unlikely to be biologically significant, as these data were not mirrored across gender. Similar AFC ELISpot results were obtained for the IgG2a and IgM isotypes (Figure 10C & D). Furthermore, *Elane*-genotype did not affect the percentages of CD19^{+} B cells (Figure 10E) or CD19$^{low\text{-}int}$ CD44^{+} CD138^{+} intracellular κ^{high} AFCs (Figure 10F).

2.3.3 *Elane* deficiency did not substantially change the myeloid compartment

Elane genotype had only a minor impact on the myeloid compartment in MRL.Fas^{lpr} mice. The percentages of CD11b^{+}Ly6G^{+} (Figure 11A) BM neutrophils and CD11b^{+}F4/80^{+}Gr1$^{low\text{-}int}$ BM macrophages (Figure 11B) were not statistically different among the groups. Additionally, no changes in CD11b^{+}Ly6G^{+} (Figure 11C) splenic neutrophils or CD11b^{+}F4/80^{+}Gr1$^{low\text{-}int}$ (Figure 11D) splenic macrophages were identified across *Elane* genotype. Female wild-type mice had a greater percentage of splenic cDCs compared to the *Elane*$^{-/-}$ group (Figure 11E). No differences in the percentages of CD19^{-}BST2^{+} SiglecH^{+} pDCs (Figure 9F) were identified among *Elane* genotypes.

2.3.4 *Elane* deficiency had a modest impact on the lymphoid compartment

Elane deficiency did not substantially impact the lymphoid compartment. All genotypes exhibited indistinguishable total percentages of TCRβ^{+} T cells (Figure 12A). The percentages of CD4^{+} T cells were elevated in female wild-type mice (Figure 12B) while CD4^{+}CD44^{+}CD62L^{-} activated T cells were elevated in male *Elane*$^{-/-}$ mice (Figure 12B). The percentages of CD8^{+} T

cells and $CD8^+CD44^+CD62L^-$ activated T cells were similar amongst wild-type and *Elane*-deficient mice (Figure 12C).

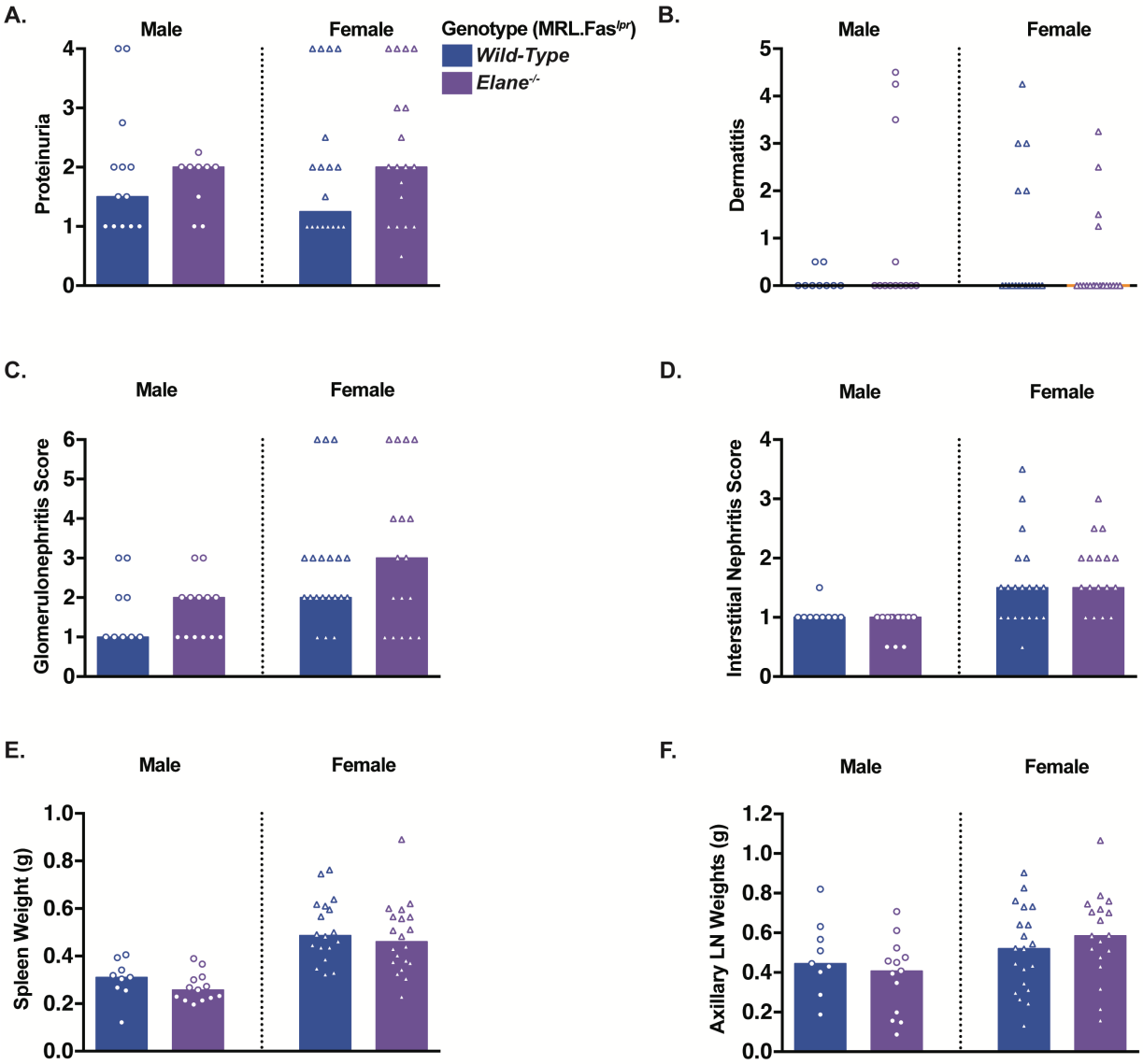

Figure 8. *Elane* genotype did not impact lupus nephritis, dermatitis, or lymphadenopathy/splenomegaly. **(A)** Proteinuria. **(B)** Dermatitis scores. **(C)** Glomerulonephritis scores. **(D)** Interstitial nephritis scores. **(E)** Spleen weight. **(F)** Axillary lymph node weights. Scores and weights are represented as a function of *Elane*-genotype and gender at 17 weeks of age. Bars represent the median and each dot represents and individual mouse. A two-tailed Mann-Whitney U test was performed to determine statistical significance within each gender (* indicates $p \leq 0.05$, ** $p \leq 0.01$, *** $p \leq 0.001$, and **** $p \leq 0.0001$; n=9 to 20 mice per group).

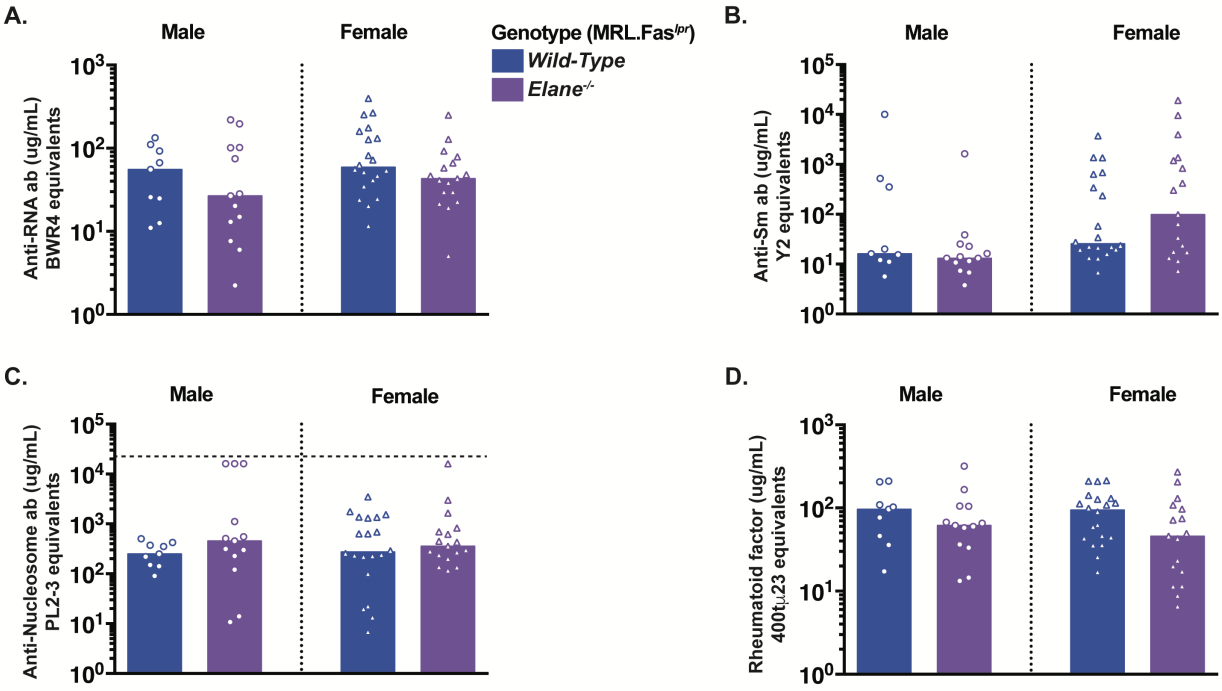

Figure 9. *Elane* genotype does not significantly alter the anti-self response.
(A-D) Serum anti-RNA (A), anti-Sm (B), anti-nucleosome (C), and rheumatoid factor (D) antibody titers at 17 weeks of age. The dotted line denotes the upper limit of quantitation. Data representation, number of mice, and statistics are as in Figure 8.

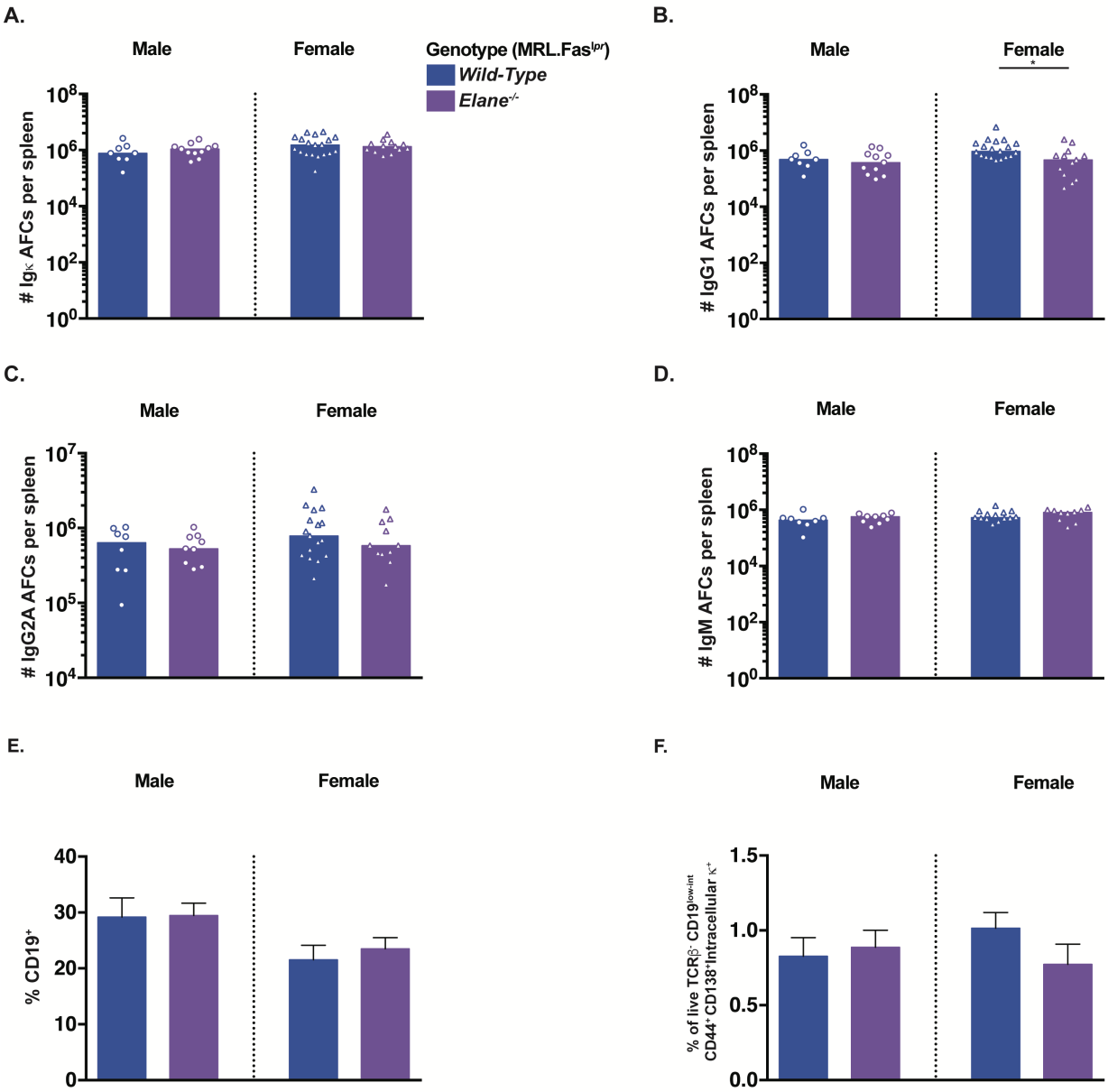

Figure 10. *Elane* deficiency did not change the AFC compartment.
(A-D) Numbers of Igκ (A), IgG1 (B), IgG2a (C), and IgM (D) antibody forming cells (AFCs) per spleen as determined by ELISpot. **(E)** Percentages of live $CD19^+$ total B cells. **(F)** Percentages of live cells that are $TCR\beta^-$ $CD44^+$ $CD138^+$ intracellular κ^+ AFCs. Data representation, number of mice, and statistics are as in Figure 8. In panel E and F, bar graphs are represented as the mean ± SEM and a two-tailed Welch's T test was performed to determine statistical significance within each gender (* indicates $p \leq 0.05$, ** $p \leq 0.01$, *** $p \leq 0.001$, and **** $p \leq 0.0001$; n=9 to 20 mice per group).

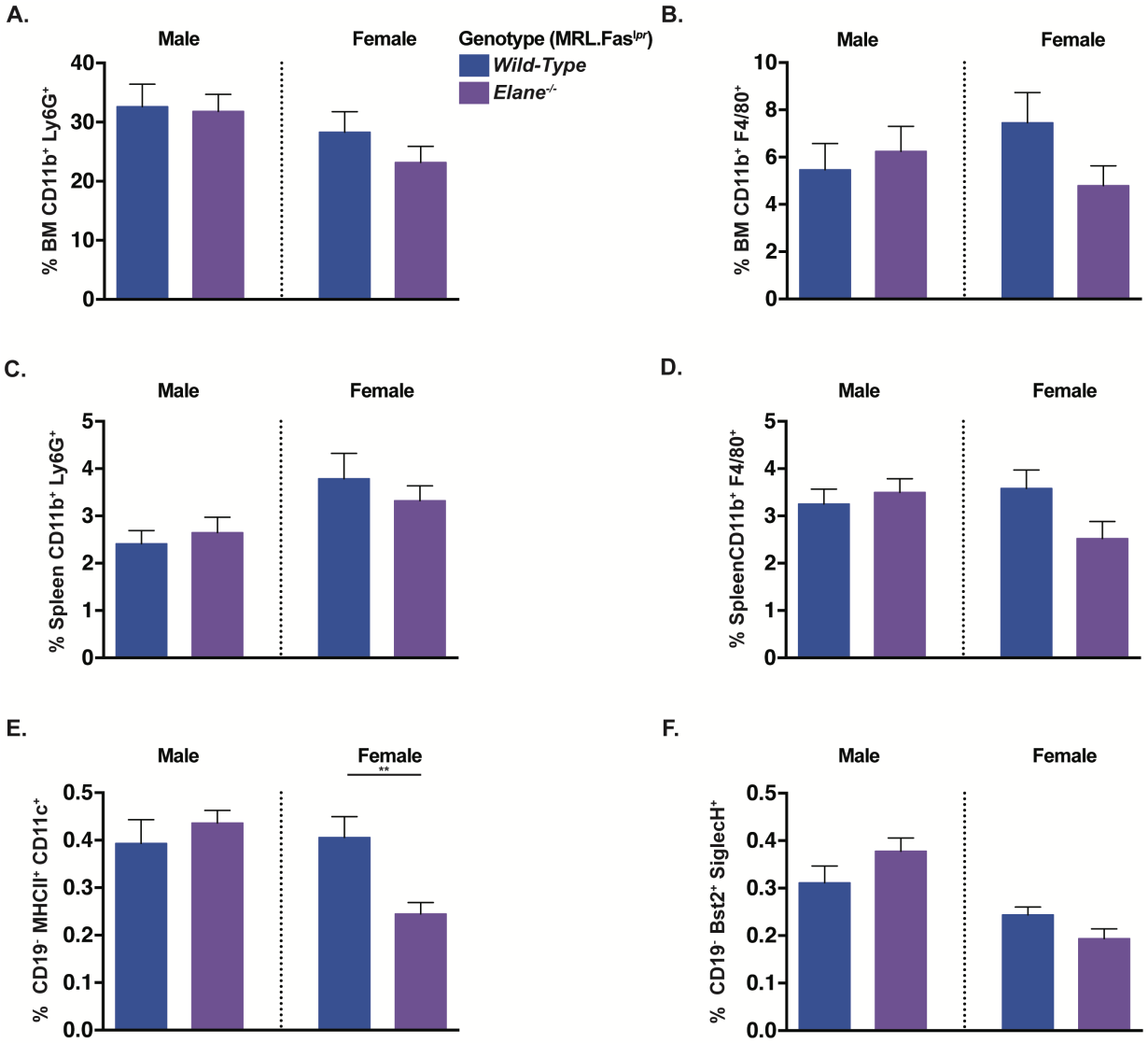

Figure 11. *Elane* genotype did not substantially affect the myeloid and DC compartments.
(A) Percentages of live bone marrow (BM) $CD11b^+$ $Ly6G^+$ neutrophils. **(B)** Percentages of BM $CD11b^+$ $GR1^{low\text{-}int}$ $F4/80^+$ macrophages. **(C)** Percentages of live $CD11b^+$ $Ly6G^+$ neutrophils in the spleen. **(D)** Percentages of splenic $CD11b^+$ $GR1^{low\text{-}int}$ $F4/80^+$ macrophages. **(E)** Percentages of live $CD19^-$ $MHCII^+$ $CD11c^+$ conventional dendritic cells and **(F)** $CD19^-$ $BST2^+$ $CD11c^+$ plasmacytoid dendritic cells. Bar graphs are represented as the mean ± SEM and two-tailed Welch's T test was performed to determine statistical significance within each gender (* indicates $p \leq 0.05$, ** $p \leq 0.01$, *** $p \leq 0.001$, and **** $p \leq 0.0001$; n=9 to 20 mice per group).

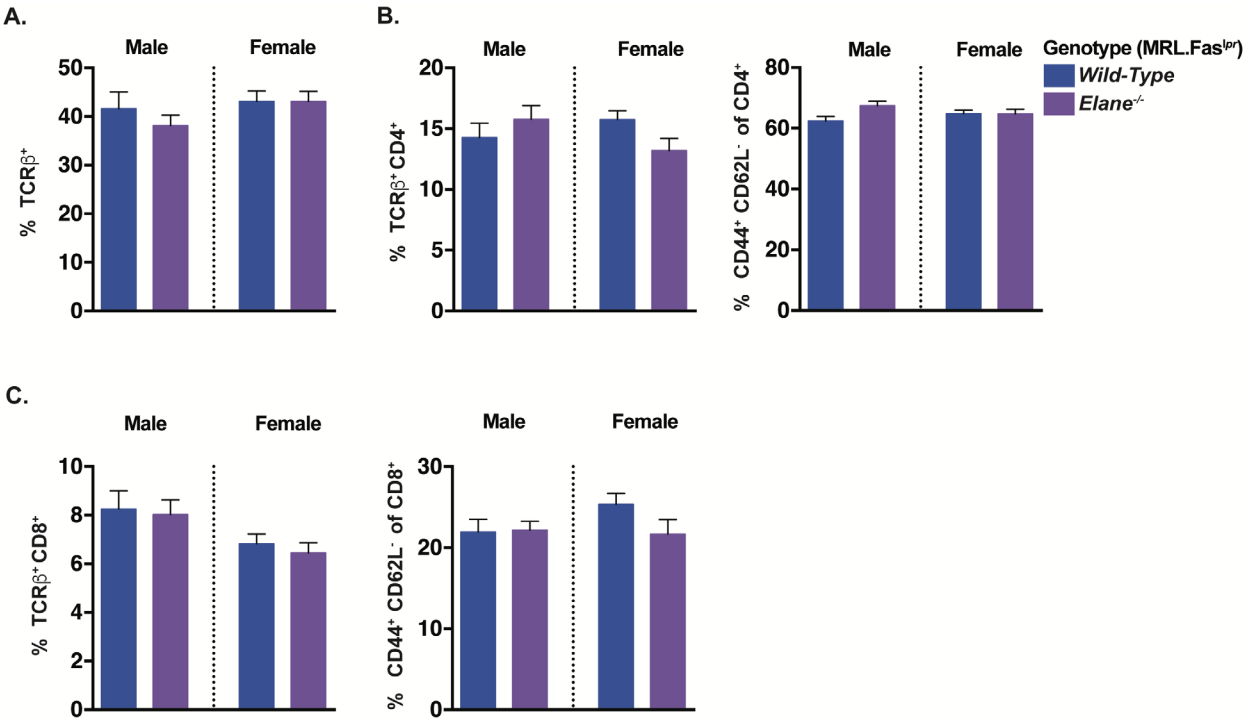

Figure 12. *Elane* deficiency had little impact on the lymphoid compartment.
(A) Percentages of live TCRβ$^+$ total T cells. **(B)** Percentages of live TCRβ$^+$ CD4$^+$ T cells (left panel) and of CD4$^+$ CD44$^+$ CD62L$^-$ activated T cells (right panel). **(C)** Percentages of live TCRβ$^+$ CD8$^+$ T cells (left panel) and of CD8$^+$ CD44$^+$ CD62L$^-$ activated T cells (right panel). Data representation, number of mice, and statistics are as in Figure 11.

2.4 DISCUSSION

Collectively, the genetic studies presented here fail to support the hypothesis that PADI4 or ELANE and by extension NET generation, alters immune system composition or pathology in SLE. We initially approached these studies by generating F2 cohorts of *Padi4*-deficient mice on the MRL.Fas^{lpr} background by crossing the *Pad4*$^{-/-}$ C57BL/6 and *Padi4*$^{+/+}$ MRL.Fas^{lpr} strains followed by intercrossing F1 progeny. Resulting *lpr* homozygotes have 50% of the SLE loci and typically develop clinical features of SLE associated with lymphoproliferation by 16–24 weeks of age. The F2 approach is an operationally reliable genetic screen to identify potential mediators of disease pathogenesis, an approach successfully used by our group and others (4, 31, 75, 131, 132). Execution of two independent genetic experiments using a mixed background F2 and a fully backcrossed Padi4-deficient MRL.Fas^{lpr} cohort, with both yielding the same results, strengthens these conclusions.

To independently confirm our genetic results that Padi4-deficiency did not affect nephritis in the MRL.Fas^{lpr} lupus model, we collaborated with Tanya Mayadas' group to test the Pan-PAD inhibitor, N-R-benzoyl-N5-(2-chloro-1-iminoethyl)-L-ornithine amide (Cl-Amidine), in a murine model of proliferative anti-glomerular basement membrane (GBM) nephritis induced by the injection of rabbit anti-GBM containing sera in mice expressing FcγRIIA selectively on neutrophils (119). In this model, antibodies directed to the glomerular basement membrane trigger an inflammatory reaction that results in severe damage of the kidney that depends on neutrophil FcγRIIA. Daily treatment of mice subjected to the anti-GBM nephritis model with Cl-Amidine did not inhibit the development of kidney damage, as measured by proteinuria and histological signs of inflammation (133). Additionally, analysis of leukocyte recruitment to the kidneys showed no reduction in Cl-Amidine versus vehicle treated animals (133).

Furthermore, FcγRs play a key role in autoimmune mediated organ damage (134, 135). To evaluate the effects of PAD inhibition specifically in the development of organ damage relevant to human disease, we partnered with the Mayadas laboratory to employ a passive human SLE-serum transfer model of nephritis (136). In this model, mice that transgenically express the human *FcγRIIA* selectively on neutrophils and additionally lack the β2 integrin *Mac-1* are susceptible to developing nephritis upon the intravenous injection of serum from patients with SLE (136). At day 10 after sera injection such mice develop proteinuria that correlates with neutrophil infiltration into the kidneys. Histological signs of disease including hypercellularity, endocapillary proliferation, and crescent formation are evident at day 14. Daily i.p. treatment with Cl-Amidine did not reduce albuminuria or histological signs of kidney damage (133). Moreover, we did not observe a reduction in neutrophil or macrophage infiltration compared with vehicle treated animals (133).

Corroborating our studies, *Padi4* deficiency does not reduce renal disease or the anti-self response in the pristane induced model of SLE (PIL) (137). In fact, *Padi4*-deficient mice subjected to PIL developed more severe proteinuria, increased auto-antibody titers, and pro-inflammatory cytokine production (137). Similarly, *Mpo*-deficient mice had more severe nephritis in the PIL model (138). Intriguingly, genetic ablation of neutrophils in the PIL model did not protect against lupus renal disease, and in fact, there are elevated levels of autoantibodies observed in this setting (137). While neutrophils were conventionally thought to play a pro-inflammatory role in autoimmunity, these data suggest an important regulatory role in SLE. We and others targeted four major mechanisms implicated in NET formation in multiple SLE and proliferative nephritis models. Taken together, these data strongly argue against the hypothesis

that NETs are a major source of autoantigen in SLE and a dominant mediator of end organ damage.

Our *Padi4*-deficient MRL.Fas^{lpr} results are discordant with previously reported PADI inhibitor studies utilizing Cl-Amidine and BB-Cl-Amidine in both MRL.Fas^{lpr} (69) and New Zealand Mixed 2328 (NZM) (70) models. One possible explanation is that the (halo) acetamidine-based PAD inhibitors could affect other PADI family members (69, 139). As with most inhibitors administered at high dose over long periods *in vivo,* it is difficult to exclude off-target effects even beyond the related PAD enzymes. Despite the fact that only PADI4 has been implicated in NET formation and its deletion demonstrates a non-redundant effect on NET assays (65, 66, 106), it can be speculated that the ability of (halo) acetamidine-based PAD inhibitors to block related enzymes could account for the differences between specific genetic deletion of *Padi4* and prior inhibitor studies. However, we believe this explanation to be less likely as Cl-Amidine pan-PAD specificity would not account for the lack of phenotype identified in the inhibitor studies using inducible models of glomerulonephritis reported here.

Moreover, our inhibitor data in IC-FcγR dependent nephritis models conflict with a recent report by Ander's group demonstrating that Cl-Amidine reduces severity of proliferative nephritis in the anti-GBM model (140). The discrepancies with published data are unlikely due to differences in treatment protocols or pharmacokinetic issues. As our studies were conducted in multiple models and in various mouse strains housed at three different animal facilities, it is unlikely that the lack of observed phenotype is due to differences in the microbiome. Furthermore, disease in MRL.Fas^{lpr} germ-free mice was not grossly altered (141), again suggesting that microbiome is not a major factor in the model.

Although Cl-Amidine has a short half-life, it is an irreversible inhibitor, allowing for prolonged inhibition of NET generation (142). We confirmed Cl-Amidine efficacy *in vivo* by visualizing NETs in the cremaster muscle following the reverse passive arthus (RPA) reaction by intravital microscopy. Immune complexes formed upon induction of the RPA in the cremaster muscle of the mouse induced NET formation that required neutrophil FcγRs (96). Cl-Amidine continued to significantly reduce NET formation to levels observed in *Padi4*-deficient mice 20 hours post administration, reinforcing the conclusion that the protocol of Cl-Amidine treatment in our nephritis model was effective in reducing PAD activity (133). Since PAD inhibition reduces NET formation to that observed in *Padi4*-deficient mice, it is unlikely that other PAD family members are serving in a compensatory capacity to generate NETs.

Recent evidence suggests that B cell tolerance to deaminated histones may be different between mice and humans (143). Patients with systemic autoimmune diseases including rheumatoid arthritis, SLE, and Felty's syndrome can develop antibodies towards citrullinated protein antigens (101-103). In contrast, sera from SLE prone mouse strains including NZB/W, B6.Sle1, B6.Sle1.Sle3, and NZM2410 preferentially bind non-deiminated histones (143). Interestingly, splenocytes from 25-week old autoimmune NZB/W mice proliferate in response to citrullinated and non-citrullinated histones without bias (143). These data suggest that autoimmune mice may maintain strong tolerance mechanisms to prevent the development of autoantibodies to deiminated histones, a finding inconsistent with the efficacy of pan-PAD inhibitors in the NZM and MRL models of SLE. Importantly, our findings and those presented by Dwivedi and colleagues highlight that systemic autoimmunity can occur in the absence of loss of tolerance to citrullinated antigens produced by NETs or by other mechanisms.

Neutrophils exposed to lupus serum and SLE associated stimuli have a greater propensity to generate NETs (68, 70, 136). However, our data disassociate the correlation between NET formation in lupus patients and mice from disease pathogenesis. Close analysis of published data in clinical settings is consistent with this dissociation. For instance, while NET degradation is impaired in some SLE patients, in fact 59-88% of SLE patients actually do degrade NETs adequately (71, 72, 144). Additionally, no statistical correlation was found between autoantibody titers, therapy, Systemic Lupus Erythematosus Disease Activity Index (SLEDAI), and *ex vivo* NET production at baseline (67). Taken together, the data reported here coupled with our previously published results in NADPH oxidase-deficient lupus prone mice, should lead the field to revisit and question whether NETs per se are critical drivers of autoimmunity or end-organ damage.

ELANE, the second most abundant protein in NETs, is critical for NET formation by modulating F-actin dynamics and degrading histones important for chromatin decondensation (111). In addition to its active role in NET formation, ELANE decorates NET structures and is proteolytically active in this setting (145). Aggregated NETs can degrade cytokines in an ELANE- dependent manner as treatment of these structures with multiple elastase inhibitors prevented the degradation of cytokines and chemokines (85). NADPH oxidase-deficient mice subjected to a monosodium urate crystal induced model of chronic neutrophilic inflammation, similar to gout, developed more severe arthritis (85). This phenotype is attributed to the inability of NADPH oxidase-deficient mice to generate aggregated NETs. Moreover, the adoptive transfer of aggregated NETs into these animals reduced disease severity (85). These data coupled with the exacerbated disease observed in *Cybb*-deficient SLE prone mice and *Padi4*-deficient mice subjected to the PIL model suggests a homeostatic function for NETs in autoimmunity. It is

conceivable that ELANE protease activity could alter self-antigen impacting its immunogenicity. As *Elane* deficiency did not impact the anti-self response nor clinical parameters of SLE in the MRL.Fas^{lpr} model, this is less likely to be a significant mechanism of loss of tolerance in autoimmunity.

While many groups implicate ELANE as a critical mediator of NET formation, several reports suggest that NETs can occur in the absence of ELANE. SLE related stimuli, such as immune complexes, can induce ELANE-independent NET formation (96). Since *Padi4* deficiency and pharmacological inhibition reduces NET formation in this setting and PADI4 pharmacological inhibition or genetic deletion does not impact SLE pathogenesis, we do not believe ELANE-independent NETs to contribute to autoimmunity. Neutrophils from *Elane*-deficient mice or wild-type neutrophils pretreated with ELANE inhibitors are reported to form NETs in response to canonical NET inducing stimuli, such as PMA and calcium ionophores (146, 147). In contrast to genetic deletion of *Padi4*, Elane-deficient mice form NETs in an experimental model of deep venous thrombosis (DVT) and *Elane* deficiency does not protect mice from DVT in this model (146). It is conceivable that other serine proteases such as Cathepsin G and Proteinase 3 serve redundant roles in mouse and humans, accounting for these differential findings in the literature. The role of ELANE in NET formation remains controversial and must be reconciled. While we cannot rule out that the lack of phenotype observed in our study is due to compensation from other serine proteases, our data demonstrate that ELANE and by extension, ELANE-dependent NET formation does not impact SLE pathology.

NETs are evolutionarily conserved, suggesting a homeostatic function (148). Consistent with the modified view favored by our results, other recent publications suggest that NETs are

not always proinflammatory and may even be immunomodulatory. Clearance of NET-like structures is an immunologically silent process and does not lead to pro-inflammatory cytokine production (149). Mice immunized with NETs do not break tolerance and show trace urinary protein levels up to 14 weeks post immunization (150). Moreover, aggregated NETs can ameliorate inflammation by inducing proteolytic cleavage of inflammatory mediators (85). NETs thus may have evolved, in part, to protect us from rather than promote autoimmunity (151).

2.5 MATERIALS AND METHODS

Mice. *Padi4*-deficient C57BL/6 mice were a kind gift from Dr. Yanming Wang (Center for Eukaryotic Gene Regulation, Department of Biochemistry and Molecular Biology, Pennsylvania State University, University Park, PA). *Elane-Cre* C57BL/6 mice were generously provided by Jürgen Roes (Department of Medicine, University College London, London, United Kingdom). Fully backcrossed mice were obtained by crossing the $Padi4^{-/-}$ or the $Elane^{Cre/wt}$ allele onto the MRL.Fas^{lpr} (The Jackson Laboratory catalogue # 000485) background for at least 9 generations. Heterozygous mice were then intercrossed to produce an experimental cohort. SLE pathology was analyzed at 16 weeks for F2 and 17 weeks for backcrossed cohorts. All mice were housed under specific-pathogen-free (SPF) conditions. Animal studies were approved by the University of Pittsburgh Institutional Animal Care Use Committee

Evaluation of SLE pathology. MRL.Fas^{lpr} SLE cohorts were analyzed as previously described (75, 80). For skin disease, mice were scored based on the extent of lesions on the dorsum of the neck and back. Macroscopic surface area was scored from 0 to 5 for an affected area up to 9.1 cm^2, with up to 1 additional point for the presence of ear (1/4 point each) and muzzle (1/2 point) dermatitis (152).

Proteinuria was screened using Albustix (Siemens). Plasma was obtained by cardiac puncture. Kidneys were removed, bisected, formalin-fixed, paraffin embedded, and H&E stained. Kidneys were scored for glomerulonephritis on a scale of 1-6 and interstitial nephritis on a scale of 1-4 in a blinded manner by a clinical pathologist (75).

Flow Cytometry. Flow cytometry was performed as previously described (75). In brief, spleens and bone marrow were homogenized and red blood cells were lysed using Ammonium-Chloride-Potassium buffer (prepared in house). Cells were resuspended in Phosphate Buffered Saline (PBS) with 3% calf serum and the FcR-blocking antibody 2.4G2. Live/dead discrimination was performed using fixable viability stain 510 (BD) or ethidium monoazide bromide (Invitrogen). Surface and intracellular staining antibodies are listed below. Cells were fixed in 1% paraformaldehyde or Cytofix/Cytoperm (BD) where appropriate. Data were obtained using a LSRII (BD) with FACS DIVA software and analyzed using FlowJo.

Antibodies used for FACS staining. Antibodies used for FACS surface and intracellular staining were as follows: IA/E-PE (Biolegend, M5/114.15.2), IA/E-APC/Cy7 (Biolegend, M5/114.15.2), Bst-2-biotin (in-house conjugated, 927), CD11c-PE/Cy7 (BD Pharmigen, HL3), CD11c-AI488 (eBioscience, N418), CD45R-APC/Cy7 (BD Pharmigen, RA3-6B2), SiglecH-Al647 (eBioscience, eBio440c), Ly6G-Al488 (in-house conjugated, 1A8), Ly6G-biotin (in-house conjugated, 1A8), Gr1-PE/Cy7 (Biolegend, RB6-8C5), Gr1-PE (Biolegend, RB6-8C5), CD11b-APC/Cy7 (Biolegend, M1/70), CD11b-PE (Biolegend, M1/70), F4/80-Al647 (in-house conjugated, BM8), F4/80-APC (Biolegend, BM8), CD44-Al488 (in-house conjugated, 1M7), CD44-APC-Cy7 (Biolegend, 1M7), TcRβ-APC/Cy7, (Biolegend, H57-597), TCRβ-PE/Cy7, (Biolegend, H57-597), TCRβ-PerCP/Cy5.5 (Biolegend, H57-597), CD62L-PE/Cy7 (Biolegend, Mel-14), CD8-Al647 (in-house conjugated, TIB 105), CD4-PE (in-house conjugated, GK1.5), CD138-PE (BD Pharmigen, 281-2), CD19-Pacblue (in-house conjugated, 1D3.2), CD19-AI647 (in-house conjugated, 1D3.2), kappa-AI488 (in-house conjugated, 187.1), kappa-Pacblue (in-house conjugated, 187.1), and GFP-FITC (Rockland, polyclonal).

ELISpot assays. AFC producing κ light chain antibodies, IgG1, IgG2a, or IgM were detected by ELISpot as previously described (11). In brief, 96-well Immulon 4 HBX plates were coated overnight at 4°C with 5 mg/ml polyclonal goat-anti mouse κ (Southern Biotech; 1050-01). Nonspecific binding was blocked with 1% bovine serum albumin in PBS and samples were incubated at 37°C. Alkaline phosphatase-conjugated secondary antibodies (Southern Biotech; Igκ [1050-04], IgG1 [1070-04], IgG2a [1080-04], or IgM [1020-04]) were detected with bromo-4-chloro-3-indolyl phosphate substrate (Southern Biotech).

ELISAs. Anti-Sm, anti-nucleosome, anti-RNA, rheumatoid factor, total IgM, and IgG ELISAs were performed as previously described (2, 4, 75, 153, 154). Specific antibodies were detected with alkaline phosphatase-conjugated goat anti-mouse IgG (Southern Biotech [1030-04]). The monoclonal antibodies Y2, BWR4, 400tμ23, PL4-2 or PL2-3 (in-house) were used as standards for the anti-Sm, anti-RNA, rheumatoid factor, and anti-nucleosome measurements respectively.

Statistics. Statistical analysis was performed using Prism 7.0 (Graphpad). A Kruskal-Wallis test with post-hoc Dunn's test, two-tailed Mann-Whitney U test, two-tailed Welch's t test, and a one-way ANOVA with post hoc Holm-Sidak test were performed where indicated and appropriate. A p value <0.05 was considered statistically significant.

3.0 INVESTIGATING THE CELL SPECIFIC ROLE OF CYBB IN THE PATHOGENESIS OF SLE

3.1 INTRODUCTION

The NADPH oxidase complex is at the nexus of numerous innate and adaptive immune signaling cascades, situated to be a central pleiotropic mediator of the host response to pathogens and to self. We and others have implicated the NADPH oxidase complex as a central regulator of autoimmunity in mice and humans (1–8).

3.1.1 The NADPH oxidase complex: structure, regulation, and function

The NOX NADPH oxidases are a family of transmembrane enzymes that oxidize intracellular NADPH, facilitating electron transport across the membrane and subsequent reduction of molecular oxygen into superoxide. There are seven NOX family members, including NOX1-5 and DUOX1-2, each with differential tissue distribution (155). NOX2 was historically referred to as the "phagocyte" NADPH oxidase as it is primarily expressed in phagocytic cells, such as, neutrophils and macrophages (155, 156). Flavocytochrome b558, located in intracellular vesicles, is the catalytic core of the phagocyte NADPH oxidase complex. Cytochrome b-245 β polypeptide (CYBB; NOX2; GP91) and cytochrome b-245 alpha (CYBA; $p22^{phox}$) constitute flavocytochrome b558 (Figure 13). The catalytic core is regulated by the cytosolic subunits

p67^{phox} (NCF2), p47^{phox} (NCF1), and p40^{phox} (NCF4). NADPH complex activity is tightly regulated under steady state conditions (155, 156) (Figure 13). In the resting state, regulatory subunits of the NADPH oxidase complex, P67^{phox}, P40^{phox}, and p47^{phox}, exist as a trimer while RAC is associated with its inhibitor GDI (155-157) (Figure 13). Little CYBB/CYBA heterodimer is located in the plasma membrane (155, 156). The negative regulator of reactive oxygen species (NRROS) can associate with the emerging CYBB monomer enabling its degradation by the endoplasmic reticulum associated degradation pathway (158). A variety of different stimuli can prime the NADPH oxidase complex including adhesion, engagement of pattern recognition receptors (PRRs), and proinflammatory cytokines (156, 159). Upon priming, the cytosolic trimer relocates to the flavocytochrome b558 complex in the plasma membrane (159). Phosphorylation of p47^{phox} enables its translocation to the plasma membrane where it can interact with the catalytic core (159) (Figure 13). The primed NADPH oxidase complex can be fully activated by similar signals to generate an oxidative burst (155, 156, 159).

In response to microorganisms and inflammatory stimuli, professional phagocytes undergo an NADPH oxidase complex-dependent oxidative burst, producing reactive oxygen (ROS) species requisite for microbial killing (155, 156, 159). Mice and humans without the functional NADPH oxidase complex are more susceptible to bacterial and fungal infections such as *Staphylococcus aureus* and *Aspergillus fumigatus* (120, 160). More recently, immunomodulatory roles for the NADPH oxidase complex within the myeloid compartment and in the lymphocytes have been characterized, as detailed below. The immune modulatory functions of the NADPH oxidase complex could represent an important checkpoint in the initiation and progression of the anti-self response.

3.1.2 The regulatory role of NADPH oxidase in the myeloid compartment

The recognition and removal of dead cells and associated debris is a critical step towards the resolution of inflammation and important to prevent immune recognition of self. The NADPH oxidase complex is important for the clearance of dead cells by macrophages. Upon apoptotic cell death, phosphatidylserine (PS) is transferred from the inner leaflet to the outer membrane where it can initiate the ingestion of the dead cell (55). Both the externalization of PS and subsequent uptake of the dying cell by macrophages is dependent on NADPH oxidase generated ROS. It has also been shown that NADPH oxidase is required for the oxidative modification of PS to lysophosphatidylserine which can be recognized by the G-protein-coupled receptor G2A on macrophages, facilitating uptake of dying cells (84, 161, 162). Engagement of the G2A receptor by lyso-PS induces prostaglandin E_2 (PGE_2) (163). PGE_2 engages the prostaglandin E_2 (EP2) receptor on the activated macrophages in an autocrine and paracrine manner to induce adenylate cyclase and protein kinase A (163). This cascade activates Rac1 which is required for the engulfment of dying cells. NADPH oxidase-deficient macrophages from humans and mice exhibit an impaired ability remove dead cells (163). Interestingly, IFNγ priming can restore ability of NADPH oxidase deficient macrophages to engulf dead cells via a TNFα and Nitric oxide-dependent mechanism (86). More recently non-conical autophagy or LAP has been implicated in the degradation of dead cell debris by macrophages (164). LAP occurs when particles that induce phagocytosis concomitantly engage cell surface receptors and recruitment of autophagy machinery, facilitating phagosome maturation and the degradation of the engulfed content (89, 164). Reports suggest that CYBB is requisite for LAP and that LAP-deficient mice develop spontaneous autoimmunity (89, 90). The role of CYBB and LAP will be detailed in

chapter 4. Taken together, these studies highlight an important role for NADPH oxidase in dead cell clearance. Dysfunctional clearance of dead cell cells and resulting debris could provide a source of autoantigen fostering the development of systemic autoimmunity.

NADPH oxidase-dependent ROS are critical for the formation of classical NETs (63, 64). While the putative role of NETs was initially thought to be proinflammatory in the context of autoimmunity, recent evidence suggests that this is not the case, and in fact, NETs may be immunomodulatory (75, 133, 137). In response to monosodium urate crystals, a murine model for gout, NADPH oxidase-dependent NETs can form aggregated structures that degrade proinflammatory cytokines (85). *Padi4*-deficient mice, which have impaired NET formation, develop exacerbated manifestations of SLE when subjected to pristane-induced lupus (137). It is thus plausible that one mechanism by which NADPH oxidase exerts its protective effects is through the formation of classical NETs, which in turn are protective rather than pathogenic. The role of NETs, NADPH oxidase, and SLE are further discussed in chapter 2.

3.1.3 NADPH oxidase has a duel stimulatory and inhibitory role in B cells

While the NADPH oxidase complex is predominantly expressed in phagocytes and best described in the myeloid compartment, it is also expressed and functional in lymphocytes. CYBB is postulated to be the primary source of H_2O_2 in B cells and is important for efficient activation and differentiation (165). In one study, H_2O_2 is transported by aquaporin 8 across the membrane to enhance B cell receptor (BCR) signaling (165). BCR signaling induces early production of ROS that is dependent on CYBB but later ROS production is a product of mitochondrial respiration (166). While *Cybb*-deficient B cells did not generate detectable early ROS upon B cell stimulation, BCR signaling and BCR-induced activation and proliferation

remained intact pointing to a critical role for mitochondrial ROS in B cell function (166). B cells are reported to have a high phagocytic capacity and can generate NADPH oxidase-dependent ROS (167). Reciprocally, NADPH oxidase deficient B cells demonstrate reduced bacterial killing capacity (167). Contrary to these reports, other groups suggest that B cell CYBB generated ROS negatively regulates BCR induced cell cycle entry, proliferation and T cell independent antibody responses (88). Patients with chronic granulomatous disease (CGD), characterized by loss of function mutations in NADPH oxidase subunits, have an impaired B cell memory compartment with reduced numbers of $CD19^{+}CD27^{+}$ and resting $CD19^{+}$ $CD27^{+}$ $CD21^{+}$ memory B cells (168). Concordantly, these patients have lower measles-specific antibody titers and antibody secreting cell numbers (168). Similar to murine studies, B cells isolated from CGD patients have a reduced capacity to respond to BCR and TLR9 stimuli (169). Taken together, these studies emphasize that the function of NADPH oxidase in B cells requires further exploration.

3.1.4 Immunomodulatory functions of NADPH oxidase in T cells

The phagocyte NADPH oxidase complex is expressed and functional in T cells but its role in immune function remains enigmatic. T cell receptor (TCR) stimulation induces sustained H_2O_2 production requiring preformed FAS and FAS ligand to induce NADPH oxidase ROS (87). NADPH oxidase-deficient T cells intrinsically skew towards the T helper (Th)1, Th2, and Th17 lineages (82, 170, 171). Concordantly, adoptive transfer of *Cybb*-deficient CD4 T cells into a RAG-deficient host increases arthritis severity, suggesting intrinsic T cell CYBB-dependent ROS production regulates T cell responses (82). More recently, it has been shown that $CD8^{+}$ T regulatory (Tregs) cell suppression requires CYBB dependent ROS production (172).

Intriguingly, $CD8^+$ Tregs suppressed $CD4^+$ T cell function by transferring CYBB to $CD4^+$ T cells via exosomes (172). Surprisingly, $CD8^+$ Tregs from older human subjects are CYBB-deficient, a finding that also extends to patients with Giant Cell Vasculitis, an autoimmune disease characterized by inflammation of medium and large blood vessels (172).

CYBB can regulate T cell responses by extrinsic mechanisms. Indoleamine 2,3-dioxygenase (IDO), suppresses T cell responses by degradation of tryptophan (173, 174). Pro-inflammatory stimuli, such as IFNγ, can induce IDO expression in dendritic cells and phagocytes (173-175). ROS are an important mediator for the oxidative cleavage of tryptophan. *Cybb*-deficient mice exhibit a blockade in tryptophan metabolism and in turn detrimental immunopathology in the setting of *Aspergillus fumigatus* infection mediated by γδ T cells, increased IL-17 production, and a reduction in Tregs (176). However, diverging from this finding in mice, CGD patients do not display a defect in IDO activity (177, 178). These studies suggest a fundamental regulatory role for NADPH oxidase in T cell function, representing a potential mechanism to restrain T cell mediated autoimmunity.

3.1.5 NADPH oxidase in SLE

A connection between X-linked CGD and systemic autoimmunity was first reported over 60 years ago (179). Male patients with X-linked CGD, characterized by loss of function mutations in *CYBB*, are at greater risk of developing SLE (120). This observation extends to carrier mothers of affected males, indicating that heterozygous dosing of the *CYBB* allele is sufficient to drive SLE susceptibility (121, 122). More recently, loss of function polymorphisms in *NCF1* and *NCF2* are reported to confer increased SLE risk across multiple ethnic groups (123-125). Mouse models of CGD, in which critical components of the NADPH oxidase complex have been

genetically deleted, recapitulate increased autoimmunity susceptibility observed in human patients. NADPH oxidase-deficient C57BL/6 non-autoimmune mice develop a spontaneous lupus-like disease (89, 180). Clinical and immunological manifestations of SLE were exacerbated in *Cybb*-deficient MRL.Fas^{lpr} mice (75). Reinforcing these findings, *Ncf2* deficiency in the NZM.2328 lupus prone mouse strain worsened renal manifestations of SLE and the anti-self response (76). Mice harboring the *Ncf1*^{m1j} loss of function mutation developed aggravated arthritis when subjected to the collagen induced arthritis model (181). Similarly, *Ncf1*^{m1j} mice develop more severe SLE when triggered by intraperitoneal injection of pristane (137). Strikingly NADPH oxidase agonists reduced pristane-induced SLE kidney disease, autoantibody titers, and the production of pro-inflammatory cytokines (137). Collectively, these studies show that the phagocyte NADPH complex is critical for the regulation of autoimmune pathology in mice and humans.

While, NADPH oxidase-dependent ROS is protective in the setting of autoimmunity, the mechanism(s) that constrain pathologic inflammation *in vivo* are unknown. Here, we aim to establish in which cell type does *Cybb* deficiency drive systemic autoimmunity by employing *in vivo* chimera and conditional knockout approaches to delete *Cybb* on specific cell subsets in the MRL.Fas^{lpr} SLE model.

3.2 ASSESSMENT OF HEMATOPOIETIC CYBB ON THE PATHOGENESIS OF SLE

While CYBB is predominantly expressed in the myeloid compartment, in recent years it has become apparent that it is also expressed in lymphocytes and the stroma, including the

endothelium, fibroblasts, muscle, and hepatocytes (155, 156). To determine whether CYBB in the hematopoietic compartment is the primary driver of the exacerbated manifestations of autoimmunity that we and others observe in global *Cybb*-deficient mice, we generated reciprocal bone marrow chimeras. Here, *Cybb*-sufficient or -deficient MRL.Fas^{lpr} SLE prone mice were irradiated at 6-7 weeks of age and reconstituted with either *Cybb*-sufficient or *Cybb*-deficient MRL.Fas^{lpr} bone marrow. SLE pathology was assessed in chimeric mice 16 weeks post irradiation unless otherwise indicated.

3.2.1 Hematopoietic *Cybb* deficiency decreased survival and exacerbated kidney disease in the MRL.Fas^{lpr} SLE mouse model

Hematopoietic *Cybb* deficiency recapitulated exacerbated clinical manifestations of SLE observed in global *Cybb*$^{-/-}$ MRL.Fas^{lpr} mice. Strikingly, hematopoietic *Cybb* deficiency decreased survival of MRL.Fas^{lpr} females (Figure 14A). Urine protein was elevated in mice receiving *Cybb*$^{-/-}$ bone marrow (Figure 14B). Concordantly, *Cybb*-deficient bone marrow reconstitution worsened glomerular and interstitial nephritis (Figure 14C and D). Spleen weight was increased in MRL.Fas^{lpr} mice with a hematopoietic *Cybb* defect (Figure 15A). However, no differences in lymphadenopathy were observed across groups (Figure 15B).

3.2.2 Hematopoietic *Cybb* deficiency altered the anti-self response in MRL.Fas^{lpr} mice

We have previously shown that *Cybb*-deficient and the heterozygous female MRL.Fas^{lpr} mice were more likely to make high-titers of antibodies to RNA and to the ribonucleoprotein SM. Here, anti-RNA titers were elevated in male mice with a hematopoietic *Cybb* defect (Figure

16A). However, this phenotype was not observed in female MRL.Fas^{lpr} mice. It is possible that as female SLE prone mice develop disease with faster kinetics compared to their male counterparts, we missed the window of difference. Hematopoietic *Cybb* deficiency did not alter anti-Sm titers (Figure 16B). Intriguingly, anti-nucleosome titers were reduced in SLE-prone mice with a hematopoietic *Cybb* defect (Figure 16C), a finding not observed in the setting of global *Cybb* deficiency. Rheumatoid factor titers were reduced in female mice reconstituted with *Cybb*-deficient bone marrow (Figure 16D). As this finding was not seen in male mice, its biological significance is unclear.

3.2.3 The B cell and AFC compartment were not altered in SLE prone mice with a hematopoietic *Cybb* defect

AFCs were expanded in the absence of global *Cybb* in the MRL.Fas^{lpr}. This finding was not recapitulated in MRL.Fas^{lpr} with a hematopoietic *Cybb* defect. There were no statistically significant differences in total kappa Ig AFC ELISpots (Figure 17A). Similar AFC ELISpot results were obtained for the IgG1, IgG2a, and IgM isotypes (Figure 17B-D). Furthermore, hematopoietic *Cybb* deficiency did not affect the percentage of CD19^{+} B cells (Figure 4E) or CD19$^{low\text{-}int}$ CD44^{+} CD138^{+} intracellular κ^{high} AFCs (Figure 4F).

3.2.4 Hematopoietic *Cybb* deficiency was sufficient to expand the myeloid compartment MRL.Fas^{lpr} mice

We previously reported that *Cybb*$^{-/-}$ MRL.Fas^{lpr} mice had an expanded myeloid compartment, characterized by increased percentages of splenic neutrophils and macrophages. Female mice

with a hematopoietic *Cybb* defect had an increased percentage of bone marrow neutrophils (Figure 18A) but not macrophages (Figure 18B). The percentages of splenic neutrophils and macrophages were increased in both female and male SLE prone recipients reconstituted with *Cybb*$^{-/-}$ bone marrow. (Figure 18C and D). No differences in the percentages of CD19^{-} CD11c^{+}MHCII^{+} cDCs (Figure 18E) and CD19^{-}BST2^{+} SiglecH^{+} pDCs (Figure 18F) were identified among the groups.

3.2.5 Hematopoietic *Cybb* deficiency did not alter the T cell compartment

Hematopoietic *Cybb* deficiency did not substantially impact the lymphoid compartment. All genotypes exhibited indistinguishable total percentages of TCRβ^{+} T cells (Figure 19A). The percentages of CD4^{+} T cells and CD4^{+}CD44^{+}CD62L^{-} activated T cells were also not significantly different across all groups (Figure 19B). Similar results were obtained for naive and activated CD8^{+} T cells (Figure 19C).

3.2.6 Stromal *Cybb* deficiency did not drive SLE kidney disease

Cybb-deficient SLE prone mice reconstituted with wild-type bone marrow did not develop exacerbated glomerulonephritis (Figure 20A). Aggravated interstitial nephritis was not observed in SLE prone *Cybb*$^{-/-}$ recipients reconstituted with wild-type bone marrow (Figure 20B). Heterozygous (*Cybb*$^{+/-}$) female SLE prone mice developed exacerbated manifestations of SLE, an observation that extends to female patients that carry one copy of the loss of function CYBB allele. To assess the threshold of *Cybb* deficiency that is required to drive SLE, we generated mixed bone marrow chimeras. Reconstitution of wild-type MRL.Fas^{lpr} recipients with 20% of

Cybb$^{-/-}$ bone marrow was not sufficient to worsen glomerulonephritis or interstitial nephritis (Figure 20C and D). The 80-20 mixed bone marrow chimeras represent an important negative control for section 3.3.

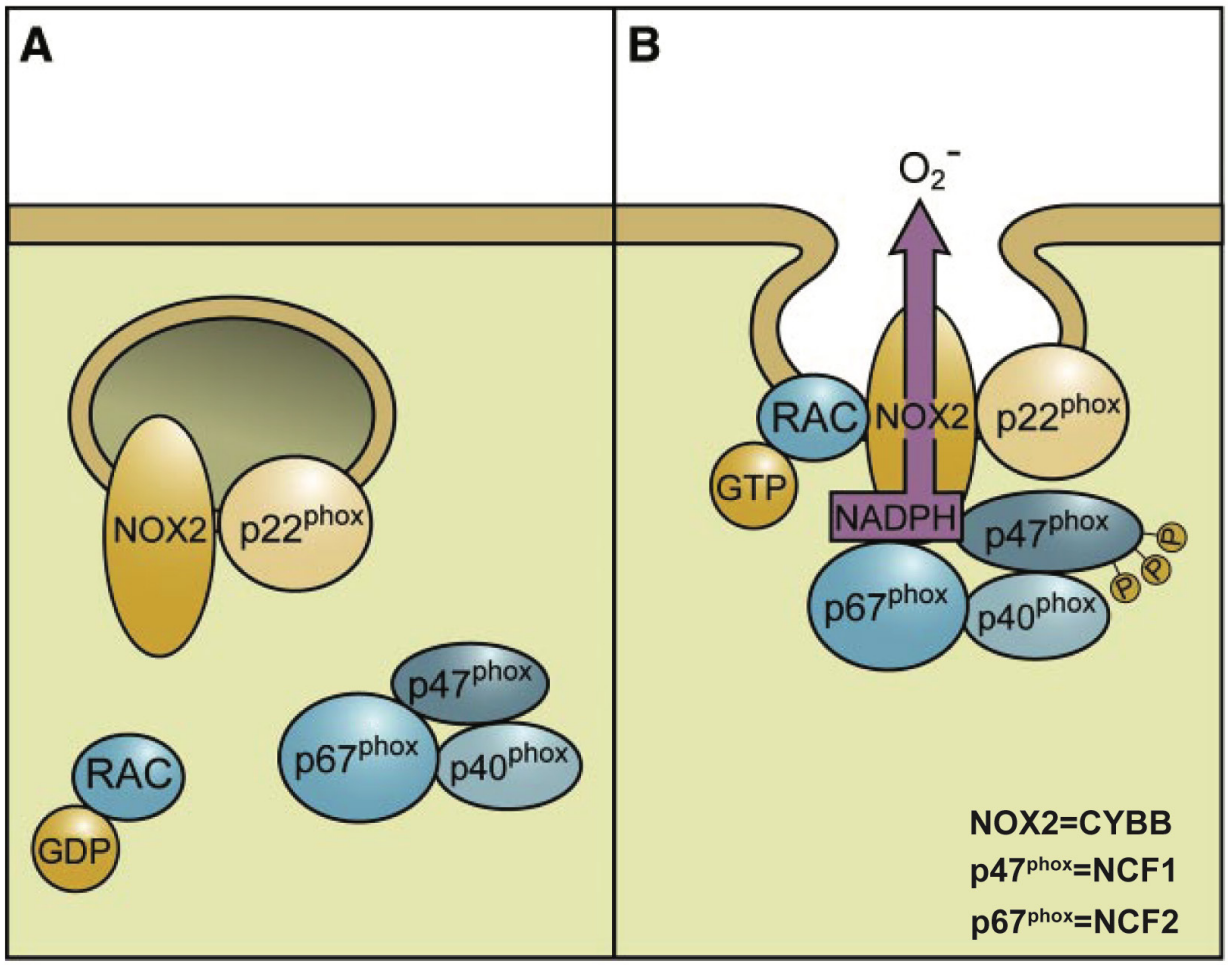

Figure 13. Assembly of the phagocyte NADPH oxidase.
The phagocyte NADPH oxidase was the first identified and is the best studied member of the NOX family. It is highly expressed in granulocytes and monocyte/macro- phages and contributes to killing of microbes. In resting neutrophil granulocytes, CYBB (NOX2) and $p22^{phox}$ are found primarily in the membrane of intracellular vesicles. They exist in close association, co-stabilizing one another. Upon activation, there is an exchange of GDP for GTP on RAC leading to its activation. Phosphorylation of the cytosolic $p47^{phox}$ (NCF1) subunit leads to conformational changes allowing interaction with $p22^{phox}$. The movement of $p47^{phox}$ brings with it the other cytoplasmic subunits, $p67^{phox}$ (NCF2) and $p40^{phox}$, to form the active CYBB enzyme complex. Once activated, there is a fusion of CYBB-containing vesicles with the plasma membrane or the phagosomal membrane. The active enzyme complex transports electrons from cytoplasmic NADPH to extracellular or phagosomal oxygen to generate superoxide (O_2^-) Adapted from: Bedard K, and Krause KH. The NOX family of ROS-generating NADPH oxidases: physiology and pathophysiology. *Physiol Rev.* 2007;87(1):245-313

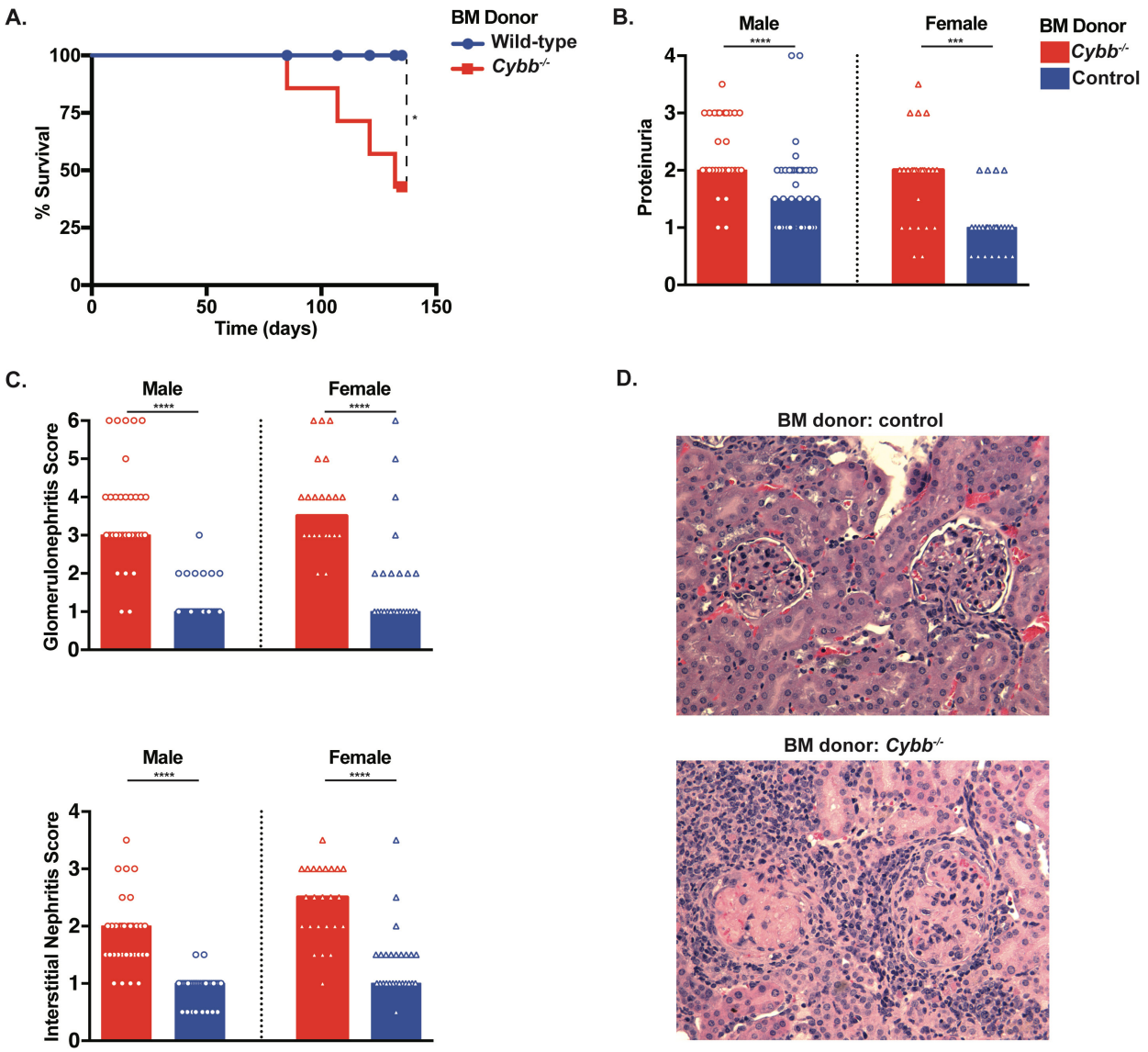

Figure 14. Hematopoietic *Cybb* deficiency decreases survival and exacerbated kidney disease in the MRL.Fas^{lpr} SLE mouse model.

(A) Kaplan-Meier survival curve of female MRL.Fas^{lpr} recipients reconstituted with *Cybb*$^{+/+}$ (n=8) or *Cybb*$^{-/-}$ (n=7) bone marrow **(B)** Proteinuria. **(C)** Glomerulonephritis scores (top panel) and interstitial nephritis scores (bottom panel). **(D)** Representative images of H&E-stained kidney sections showing glomeruli and interstitial infiltrates from MRL.Fas^{lpr} recipients receiving control (top panel) or *Cybb*$^{-/-}$ bone marrow. Weights are represented as a function of *Cybb*-genotype and gender at 16 weeks post-irradiation. Bars represent the median and each dot represents and individual mouse. A log-rank test (A) or a two-tailed Mann-Whitney test (B-D) was performed to determine statistical significance within each gender (* indicates $p \leq 0.05$, ** $p \leq 0.01$, *** $p \leq 0.001$, and **** $p \leq 0.0001$; n=24 to 40 mice per group unless otherwise indicated).

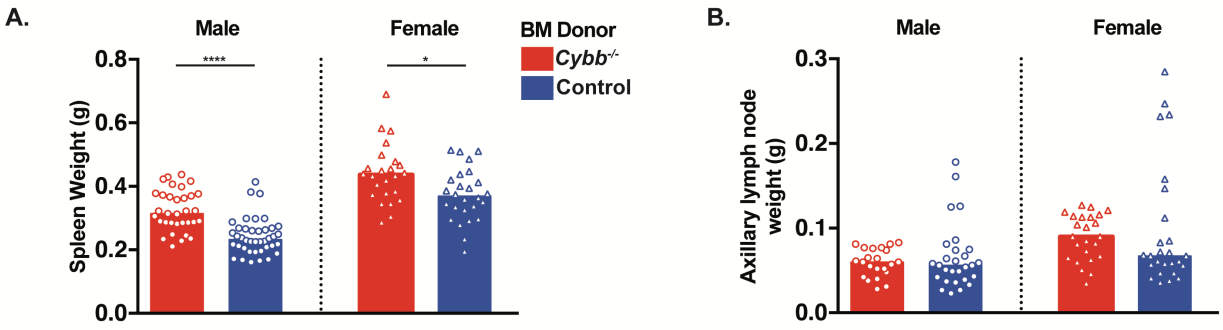

Figure 15. Increased splenomegaly in MRL.Fas^{lpr} mice with a hematopoietic *Cybb* defect.
(A) Spleen weight. **(B)** Axillary lymph node weights. Weights are represented as a function of *Cybb*-genotype and gender at 16 weeks post-irradiation. Data representation, number of mice, and statistics are as in Figure 14.

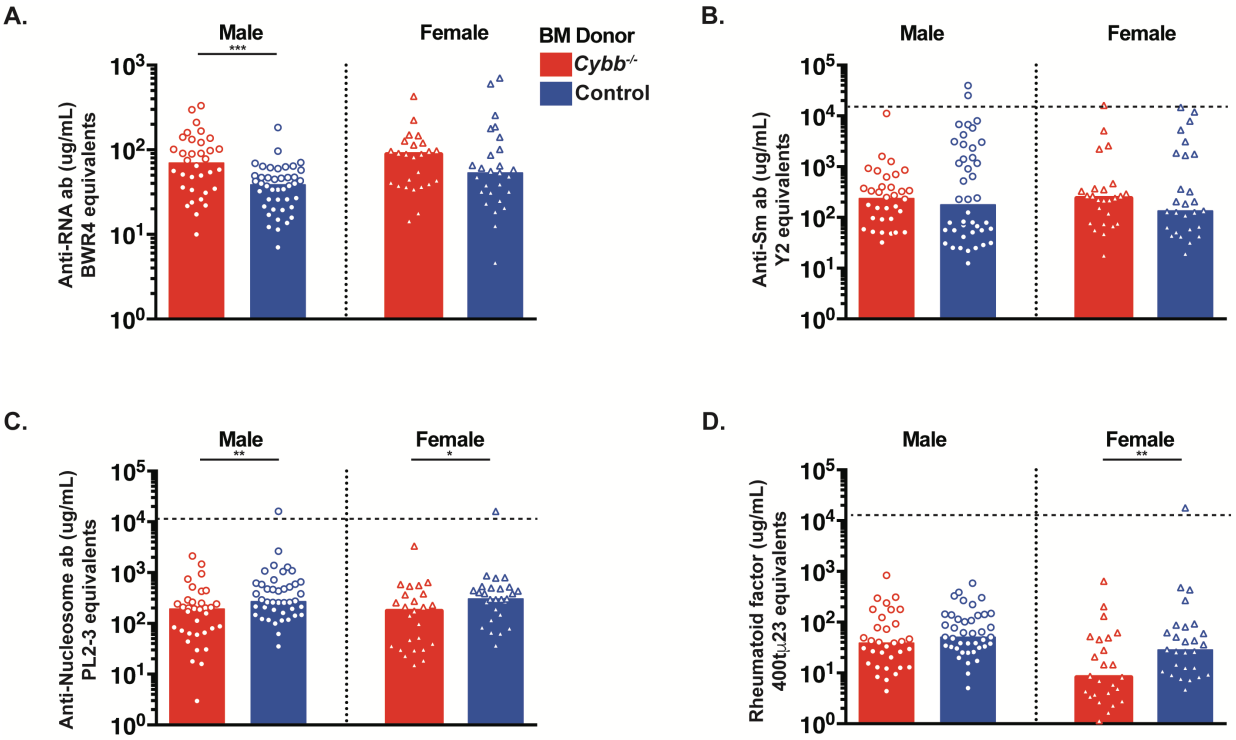

Figure 16. Increased anti-RNA but decreased anti-nucleosome titers in MRL.Fas^{lpr} mice with a hematopoietic *Cybb* defect.

(A-D) Serum anti-RNA (A), anti-Sm (B), anti-nucleosome (C), rheumatoid factor (D), antibody titers at 16 weeks post irradiation. The dotted line denotes the upper limit of quantitation. Data representation and statistics are as in Figure 14 (n=24 to 40 mice per group).

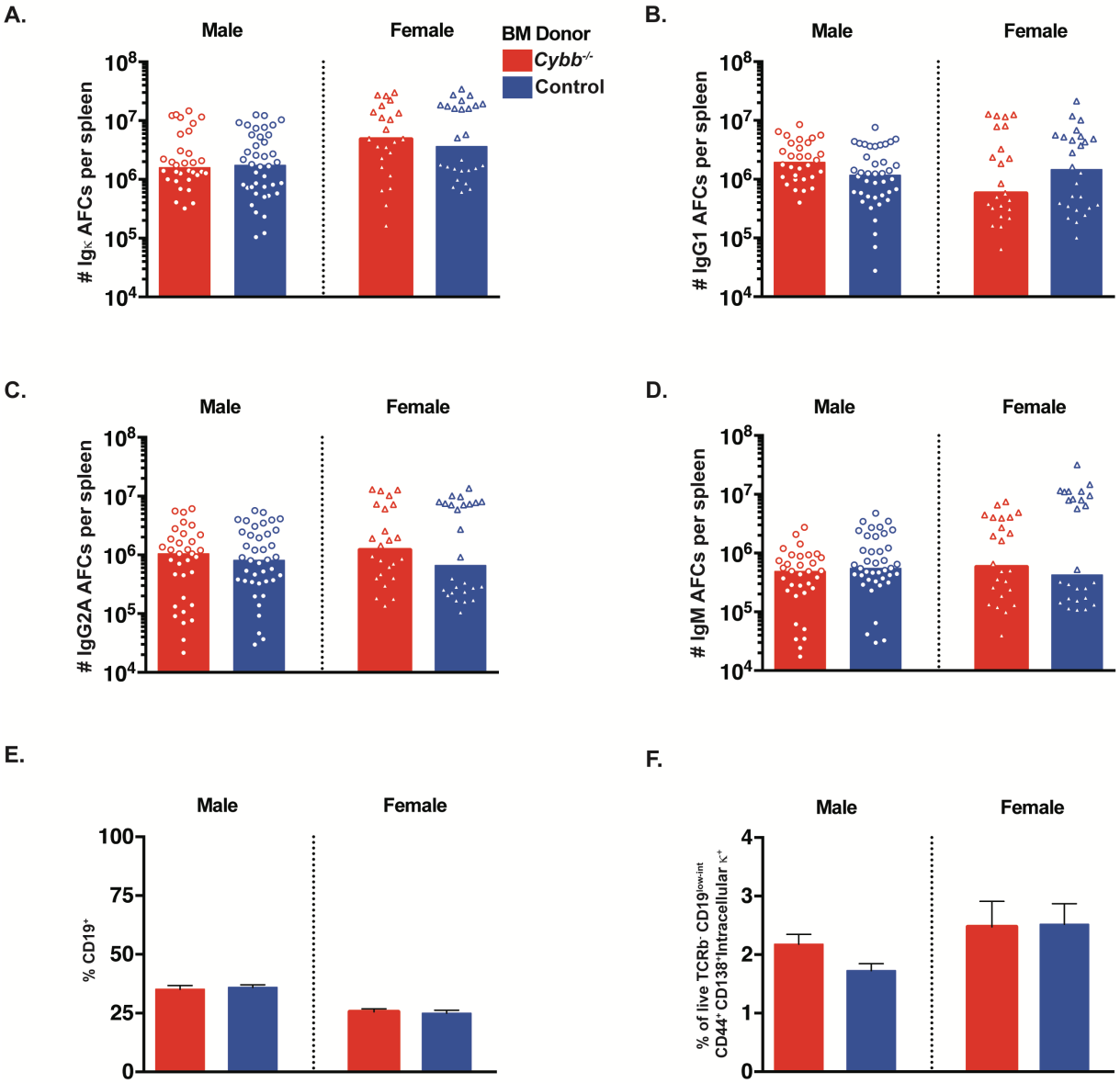

Figure 17. Hematopoietic *Cybb* deficiency did not change the B cell or AFC compartments.
(A-D) Numbers of Igκ (A), IgG1 (B), IgG2a (C), and IgM (D) antibody forming cells (AFCs) per spleen as determined by ELISpot. **(E)** Percentages of live $CD19^+$ total B cells. **(F)** Percentages of live cells that are $TCR\beta^-$ $CD44^+$ $CD138^+$ intracellular κ^+ AFCs. Data representation, number of mice, and statistics are as in Figure 13. In panels E and F, bar graphs are represented as the mean ± SEM and a two-tailed Welch's T test was performed to determine statistical significance within each gender (* indicates $p \leq 0.05$, ** $p \leq 0.01$, *** $p \leq 0.001$, and **** $p \leq 0.0001$; n=24-40 mice per group).

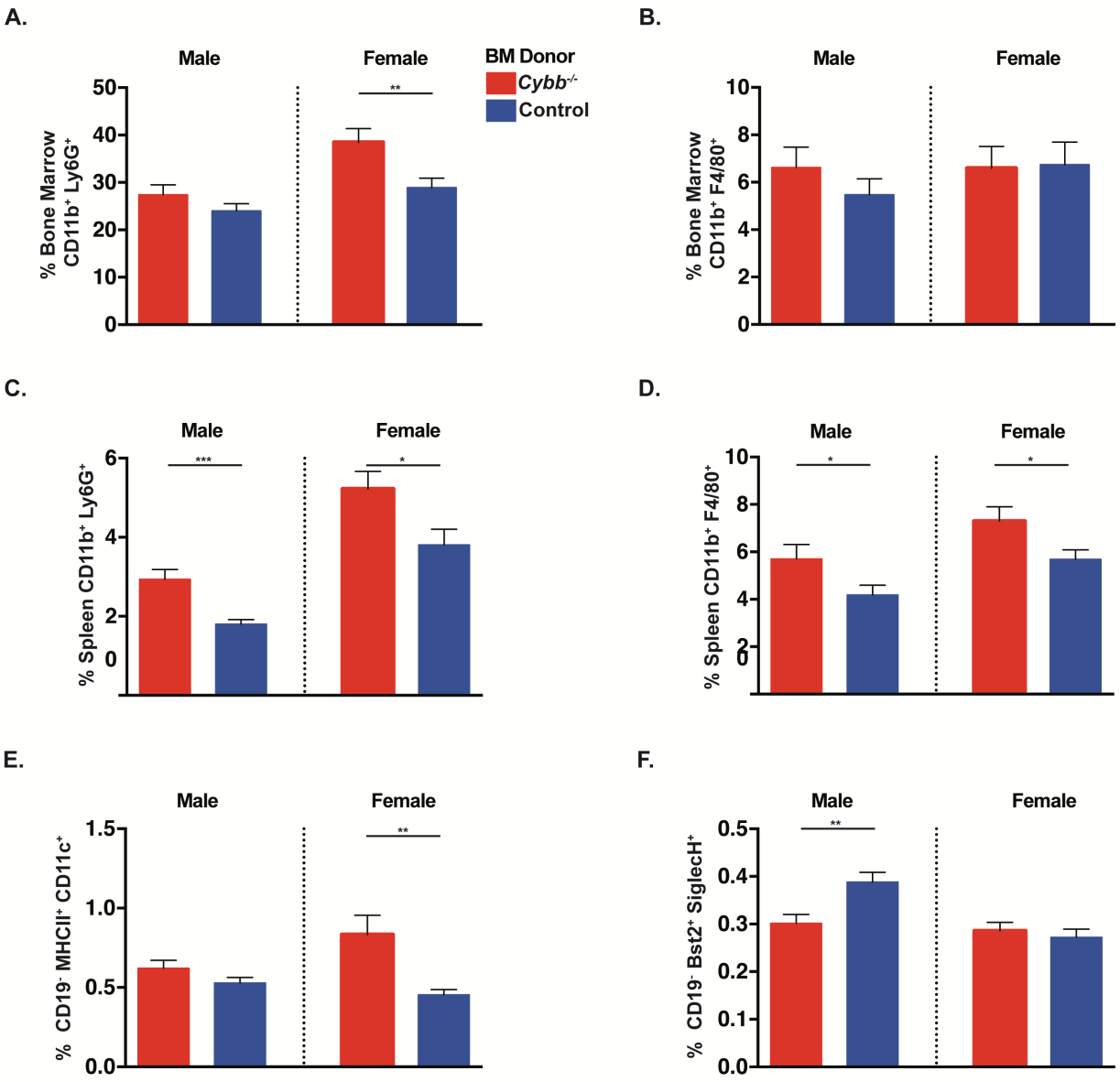

Figure 18. Expanded myeloid compartment in MRL.Fas^{lpr} mice with a hematopoietic *Cybb* defect.
(A) Percentages of live bone marrow (BM) CD11b^{+} Ly6G^{+} neutrophils. **(B)** Percentages of BM CD11b^{+} GR1$^{low\text{-}int}$ F4/80^{+} macrophages. **(C)** Percentages of live CD11b^{+} Ly6G^{+} neutrophils in the spleen. **(D)** Percentages of splenic CD11b^{+} GR1$^{low\text{-}int}$ F4/80^{+} macrophages. **(E)** Percentages of live CD19^{-} MHCII^{+} CD11c^{+} conventional dendritic cells and **(F)** CD19^{-} BST2^{+} CD11c^{+} plasmacytoid dendritic cells. Bar graphs are represented as the mean ± SEM and a two-tailed Welch's T test was performed to determine statistical significance within each gender (* indicates $p \leq 0.05$, ** $p \leq 0.01$, *** $p \leq 0.001$, and **** $p \leq 0.0001$; n=24-40 mice per group).

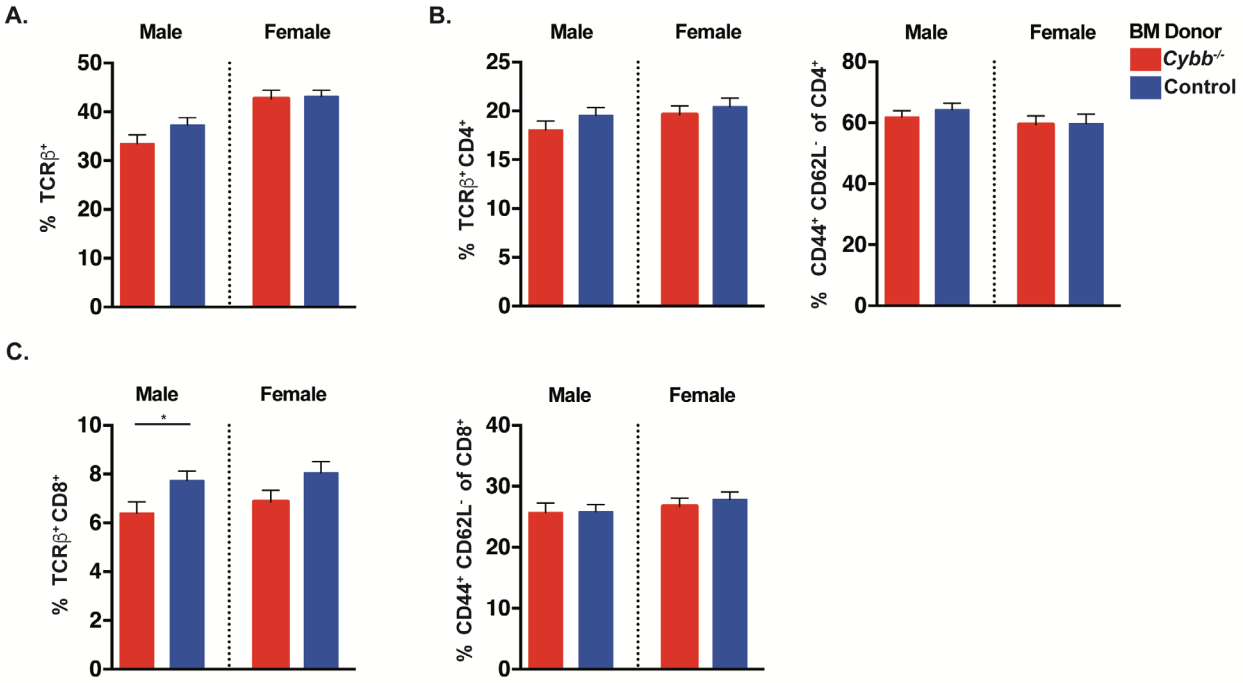

Figure 19. Hematopoietic *Cybb* deficiency had little impact on the T cell compartment.
(A) Percentages of live TCRβ$^+$ total T cells. **(B)** Percentages of live TCRβ$^+$ CD4$^+$ T cells (left panel) and of CD4$^+$ CD44$^+$ CD62L$^-$ activated T cells (right panel). **(C)** Percentages of live TCRβ$^+$ CD8$^+$ T cells (left panel) and of CD8$^+$ CD44$^+$ CD62L$^-$ activated T cells (right panel). Data representation, number of mice, and statistics are as in Figure 18.

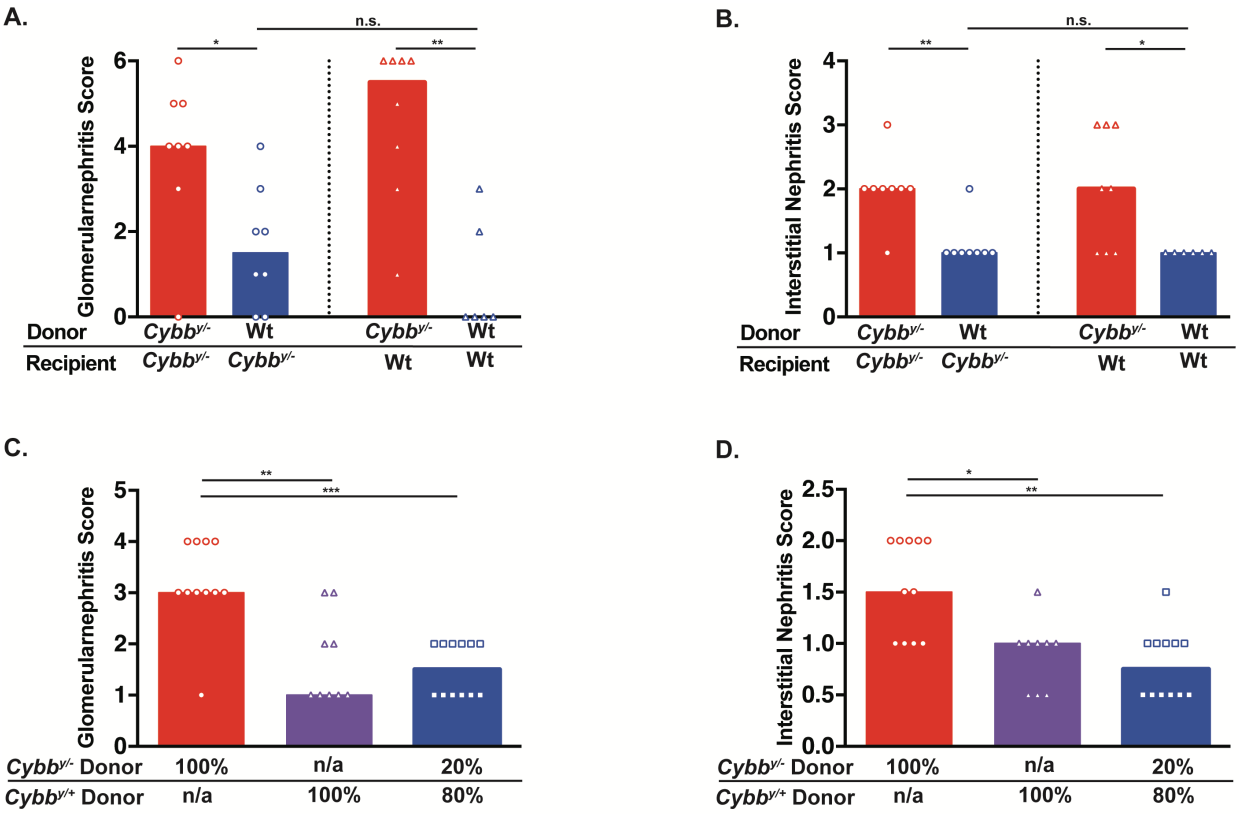

Figure 20. Stromal *Cybb* deficiency did not affect glomerulonephritis or interstitial nephritis.
(A) Glomerulonephritis scores and **(B)** interstitial nephritis scores of the reciprocal bone marrow chimera cohort (n=6 to 8 mice per group). **(C)** Glomerulonephritis scores and **(D)** interstitial nephritis scores of the 20/80 mixed bone marrow chimera cohort (n=9 to 12 mice per group). Scores are represented as a function of *Cybb*-genotype and gender at 12 weeks (A & B) and 16 weeks (C & D) post irradiation. Data representation and statistics are as in Figure 14.

3.3 DEVELOPMENT OF A NOVEL CHIMERA SYSTEM TO DELETE *CYBB* IN THE MYELOID COMPARTMENT

Our data convincingly show that hematopoietic *Cybb* deficiency was sufficient to drive SLE pathogenesis. The phenotype that we observed in our chimera system excludes a role for stromal *Cybb* deficiency as a major contributor responsible for the exacerbated lupus observed in the *Cybb* global knockout MRL.Fas^{lpr} system. Nonetheless, NADPH oxidase can constrain inflammation (82, 83) by neutrophil (84, 85), macrophage (86), and/or lymphocyte-dependent (87, 88) mechanisms. To further assess the cell specific role of *Cybb* deficiency in SLE, we generated a novel chimera strategy to delete *Cybb* selectively in the myeloid compartment, specifically in neutrophils and macrophages. We first chose to target the myeloid compartment as *Cybb* is highly expressed in phagocytes and has well characterized immunoregulatory functions in this compartment, including the modulation of neutrophil death and subsequent clearance by macrophages.

To delete *Cybb* selectively in the myeloid compartment, we crossed the *LysM-Cre* (182) to the *Rosa26-eGFP-DTA* (183) strains on the MRL.Fas^{lpr} background (*ΔLysM*). Removal of the transcriptional stop site will only occur in LysM expressing cells, such as neutrophils and macrophages, leading to expression of a diphtheria toxin subunit and selective killing of that cell. 5-7 week old MRL.Fas^{lpr} recipients were irradiated and reconstituted with an 80:20 mixture of *ΔLysM* and *Cybb*-deficient (*ΔLysM Cybb*$^{-/-}$) or *Cybb*-sufficient (*ΔLysM Cybb*$^{+/+}$) bone marrow. In the reconstituted irradiated MRL.Fas^{lpr} recipient, we expect ~100% of neutrophils, 50% of

macrophages, and 20% of the remaining hematopoietic compartment to be *Cybb*-deficient (Figure 21). Importantly, reconstitution of wild-type MRL.Fas^{lpr} recipients with 20% of *Cybb*$^{-/-}$ bone marrow was not sufficient to worsen glomerulonephritis or interstitial nephritis (Figure 20C and D). As a positive control known to develop exacerbated manifestations of SLE, *Cybb*-sufficient MRL.Fas^{lpr} SLE prone mice were irradiated and reconstituted with *Cybb*$^{-/-}$ MRL.Fas^{lpr} bone marrow (red bars). SLE pathology was assessed in chimeric mice 16 weeks post irradiation.

3.3.1 *Cybb* was effectively deleted in the myeloid compartment of *ΔLysM Cybb*$^{-/-}$ MRL.Fas^{lpr} mice

Deletion of *Cybb* was quantitated by qPCR of genomic DNA acquired from FACS-sorted cell populations. Additionally, GFP expression was used as a surrogate measure of *Cybb*-sufficient reconstitution. Cells from the *ΔLysM* donor that either do not express Cre or escape Cre mediated recombination at the *Rosa26-eGFP-DTA* locus will survive and continue to express GFP. *Cybb* was efficiently deleted in splenic CD11b^{+}Gr1^{+} neutrophils (88.09% ± 2.128) (Figure 22A). Consistent with the prior literature (184), deletion efficiency was 46.28% (± 2.026) in CD11b^{+}F4-80^{+} splenic macrophages (Figure 22B). As expected, *Cybb* was not efficiently deleted in the B cell (30.72% ± 2.427) or T cell (16.1% ± 5.223) compartments. Of note, the deletion efficiency assessed by qPCR was different than the percentage of GFP^{+} T cells, with the latter underrepresenting the *Cybb*-sufficient contribution. It is likely that this is due to the presence of radioresistant T cells in the host, which would not express GFP.

3.3.2 *Cybb* deficiency in LysM expressing cells was sufficient to exacerbate SLE kidney disease

Proteinuria was increased in *ΔLsyM Cybb*$^{-/-}$ MRL.Fas^{lpr} female mice (Figure 23A). No differences in the incidence or severity of dermatitis were observed amongst the groups (Figure 23B). *Cybb* deficiency in LysM expressing cells exacerbated glomerular and interstitial nephritis in both male and female MRL.*Fas*^{lpr} mice (Figure 23C and D). Spleen weight was increased in male *ΔLsyM Cybb*$^{-/-}$ MRL.Fas^{lpr} mice, a finding not recapitulated in the female cohort (Figure 24 A and B). Proteinuria, glomerulonephritis and interstitial nephritis scores were elevated in the positive control MRL.Fas^{lpr} recipients reconstituted with *Cybb*$^{-/-}$ bone marrow (Figure 23A, C, and D).

3.3.3 Myeloid *Cybb* deficiency did not have a major impact on the anti-self response.

ΔLsyM Cybb genotype did not generally alter the autoantibody response. As expected, Anti-RNA antibody titers were elevated in male mice receiving 100% *Cybb*$^{-/-}$ MRL.Fas^{lpr} bone marrow (Figure 25A). We did not detect any change in anti-Sm (Figure 25B), anti-nucleosome (Figure 25C), or rheumatoid factor (Figure 25D) titers across the groups.

3.3.4 The AFC compartment was altered in SLE prone mice with a myeloid *Cybb* defect

Total kappa Ig AFC ELISpots were elevated in male *ΔLsyM Cybb*$^{-/-}$ MRL.Fas^{lpr} mice (Figure 26A). In male mice receiving 100% *Cybb*$^{-/-}$ MRL.Fas^{lpr} bone marrow, total Ig kappa and IgG1 AFCs were increased (Figure 26A and B). There were no statistically significant differences in

AFC ELISpots for the IgG2a and IgM isotypes (Figure 26C and D). Furthermore, *ΔLsyM Cybb* genotype did not affect the percentage of $CD19^+$ B cells (Figure 26E). $CD19^{low\text{-}int}$ $CD44^+$ $CD138^+$ intracellular κ^{high} AFCs were elevated in female MRL.Fas^{lpr} recipients receiving Δ*LsyM* $Cybb^{-/-}$ bone marrow as assessed by flow cytometry, a finding not observed in the male cohort (Figure 26F).

3.3.5 *Cybb* deficiency in LysM expressing cells did not alter the composition of the myeloid compartment in MRL.Fas^{lpr} mice

The percentage of $CD11b^+Ly6G^+$ bone marrow neutrophils (Figure 27A) was elevated in male mice receiving 100% $Cybb^{-/-}$ bone marrow compared to *ΔLsyM* $Cybb^{+/+}$ negative controls. *ΔLsyM Cybb* genotype did not impact the percentage of bone marrow $CD11b^+F4/80^+Gr1^{low\text{-}int}$ macrophages (Figure 27B). No statistically significant difference in splenic neutrophils or macrophages was observed (Figure 27C and D). Additionally, we did not find any changes in the percentages of $CD19^-CD11c^+MHCII^+$ cDCs (Figure 27E) and $CD19^-BST2^+$ $SiglecH^+$ pDCs with the exception that female MRL.Fas^{lpr} recipients receiving 100% $Cybb^{-/-}$ bone marrow had an increased percentage of pDCs compared to *ΔLsyM* $Cybb^{+/+}$ negative controls (Figure 27F).

3.3.6 Myeloid *Cybb* deficiency did not alter the T cell compartment

Cybb deficiency in LysM expressing cells did not substantially impact the lymphoid compartment. All genotypes exhibited no statistical differences in the total percentages of $TCR\beta^+$ T cells (Figure 28A). The percentages of $CD4^+$ T cells and $CD4^+CD44^+CD62L^-$ activated T cells were also not significantly different across all groups (Figure 28B). Similar results were obtained

for naive and activated $CD8^+$ T cells (Figure 28C).

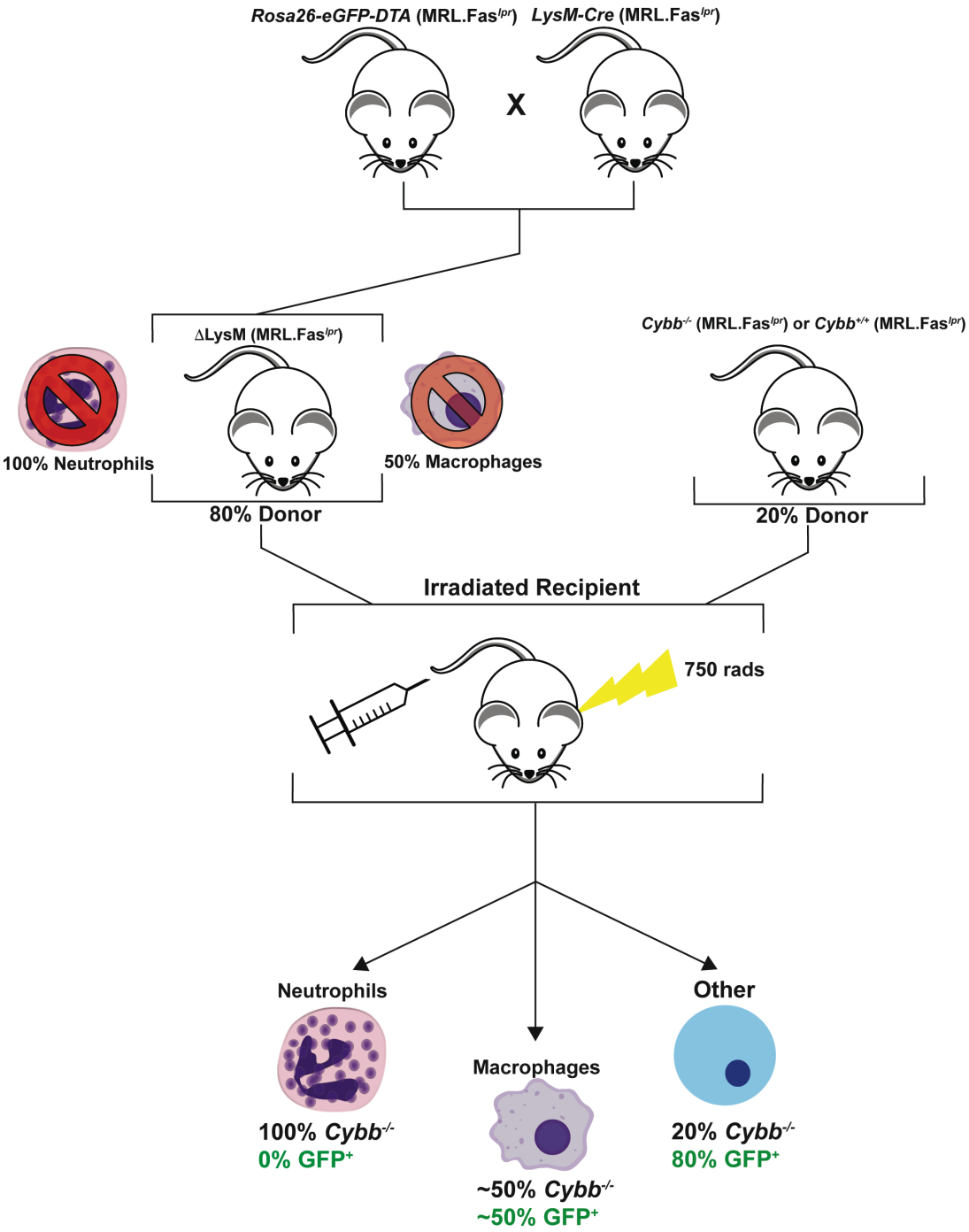

Figure 21. Chimera strategy to delete Cybb in the myeloid compartment of SLE prone mice.
To generate a neutrophil and macrophage-deficient donor we crossed the *LysM-Cre* to the Rosa26-eGFP-DTA strains on the MRL.Fas^{lpr} background (*ΔLysM*). Cre mediated removal of the transcriptional stop site will only occur in LysM expressing cells leading to expression of a diphtheria toxin subunit and cell death. 6-7 week old MRL.Fas^{lpr} recipients were irradiated and reconstituted with an 80:20 mixture of ΔLysM and cybb-deficient (*ΔLysM Cybb*$^{-/-}$) or *Cybb*-sufficient (*ΔLysM Cybb*$^{+/+}$) bone marrow. In the reconstituted irradiated MRL.Fas^{lpr} recipient, we expect ~100% of neutrophils, 50% of macrophages, and 20% of the remaining hematopoietic compartment to be *Cybb*-deficient.

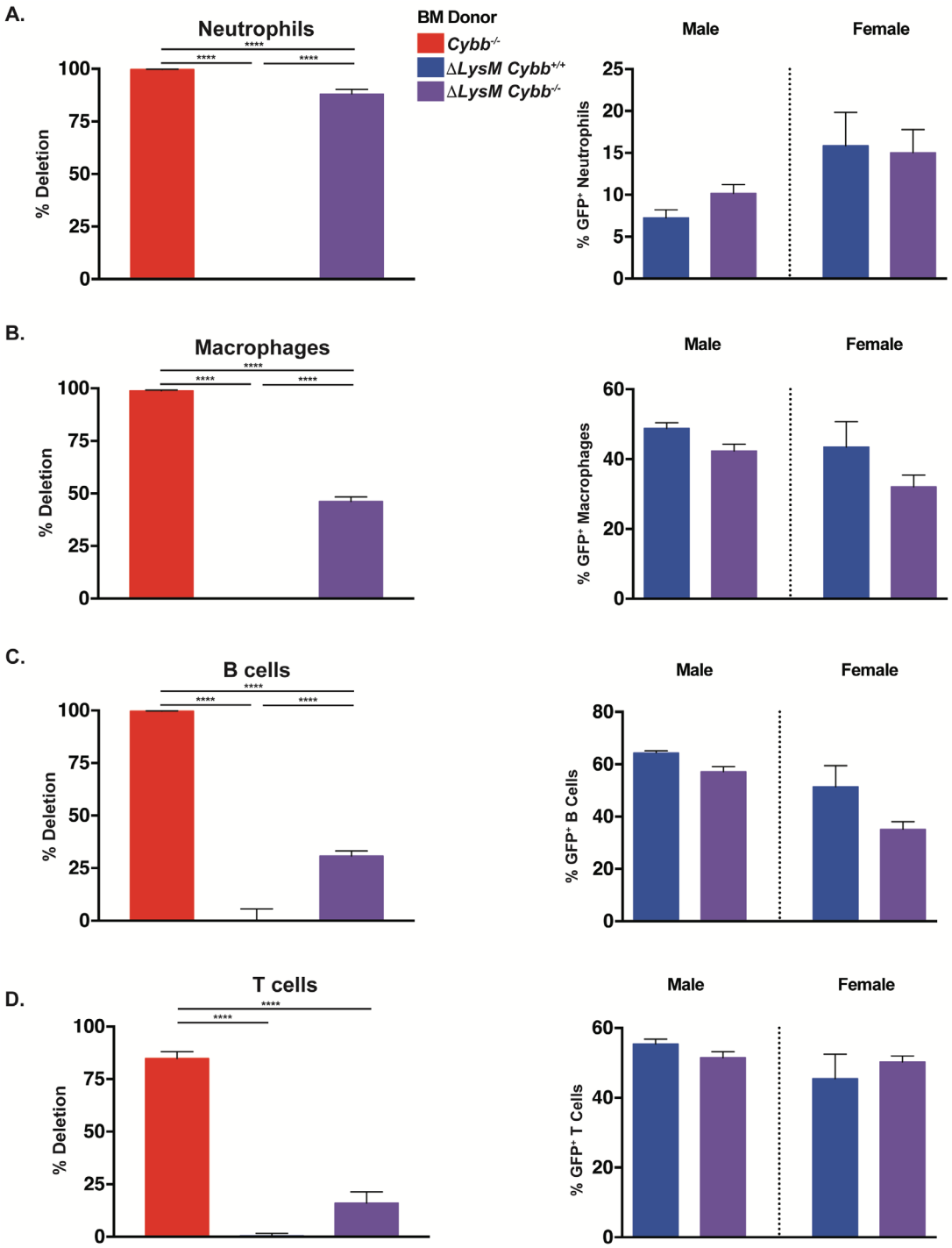

Figure 22. *Cybb* was effectively deleted in neutrophils and macrophages from *ΔLysM Cybb*$^{-/-}$ MRL.Fas^{lpr} mice. *Cybb* deletion efficiency was quantitated by qPCR of genomic DNA isolated from FACS sorted cells. GFP^{+} cells from the *ΔLysM* mice that escaped Cre mediated deletion served as a surrogate for *Cybb*-sufficient reconstitution. **(A)** *Cybb* deletion efficiency in n neutrophils (left panel) and the % GFP^{+} splenic neutrophils (right panel). **(B)** *Cybb* deletion efficiency in macrophages (left panel) and the % GFP^{+} splenic macrophages (right panel). **(C)** *Cybb* deletion efficiency in B cells (left panel) and the % GFP^{+} splenic B cells (right panel). **(D)** *Cybb* deletion efficiency in T cells (left panel) and the % GFP^{+} splenic T cells (right panel). A one-way ANOVA with post-hoc Holm-Sidak test was performed to determine statistical significance (* indicates $p \leq 0.05$, ** $p \leq 0.01$, *** $p \leq 0.001$, and **** $p \leq 0.0001$; n=4 to 12 mice per group).

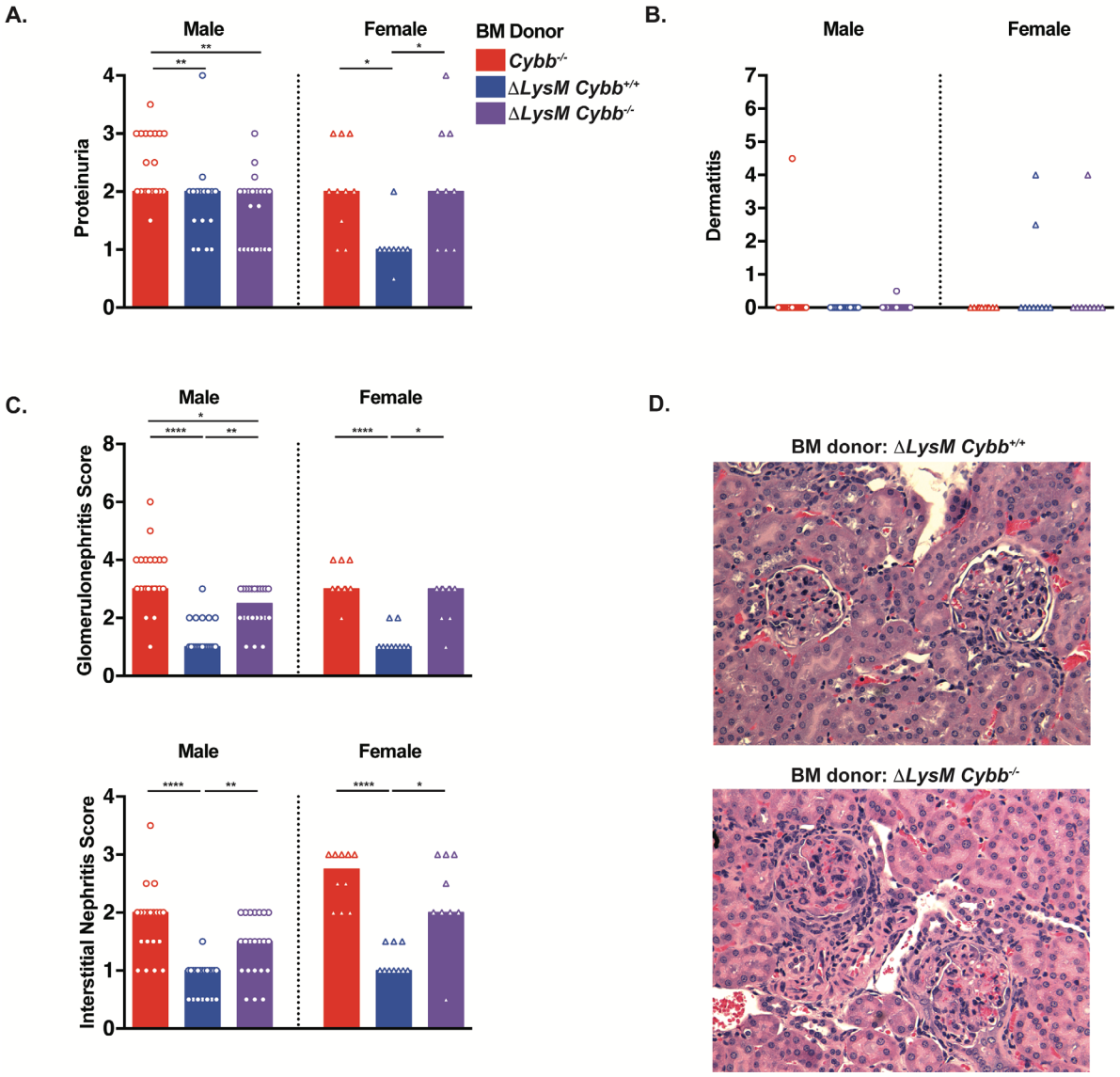

Figure 23. Myeloid *Cybb* deficiency was sufficient to exacerbate SLE kidney disease.
(A) Proteinuria. **(B)** Dermatitis. **(C)** Glomerulonephritis scores (top panel) and interstitial nephritis scores (bottom panel). **(D)** Representative images of H&E-stained kidney sections showing glomeruli and interstitial infiltrates from MRL.Fas^{lpr} recipients receiving control (top panel) or *ΔLysM cybb*$^{-/-}$ bone marrow. Scores are represented as a function of *Cybb*-genotype and gender at 16 weeks post-irradiation. Bars represent the median and each dot represents and individual mouse. A Kruskal-Wallis test with post-hoc Dunn's test was performed to determine statistical significance within each gender (* indicates $p \leq 0.05$, ** $p \leq 0.01$, *** $p \leq 0.001$, and **** $p \leq 0.0001$; n=9 to 22 mice per group).

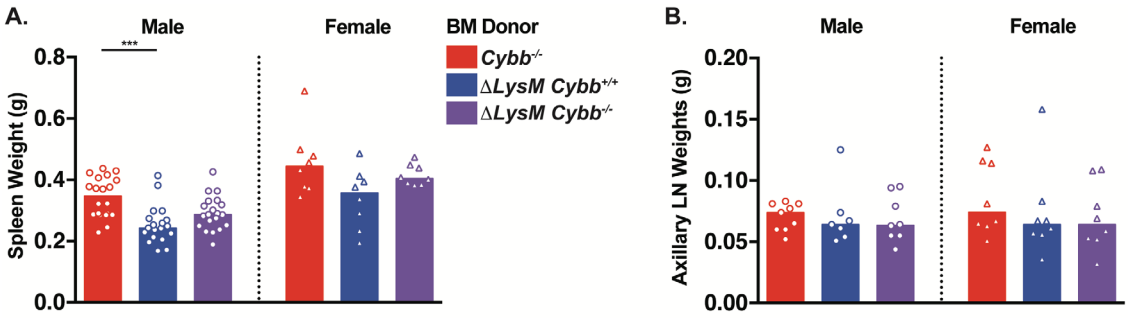

Figure 24. *Cybb* deficiency in LysM expressing cells did not impact splenomegaly or lymphadenopathy in MRL.Fas^{lpr} mice.

(A) Spleen weight. **(B)** Axillary lymph node weights. Weights are represented as a function of *Cybb*-genotype and gender at 16 weeks post-irradiation. Data representation, number of mice, and statistics are as in Figure 23.

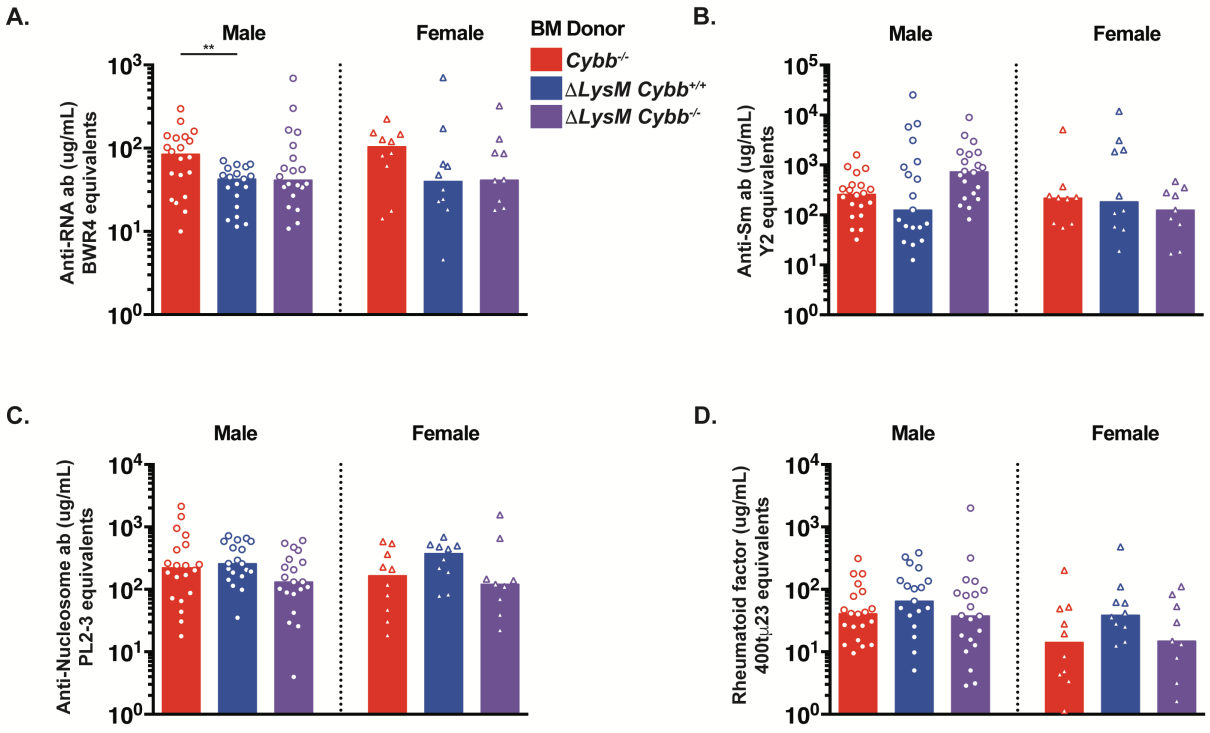

Figure 25. Myeloid *Cybb* deficiency did not alter the anti-self response.
(A-D) Serum anti-RNA (A), anti-Sm (B), anti-nucleosome (C), rheumatoid factor (D) antibody titers at 16 weeks post irradiation. Data representation and statistics are as in Figure 23.

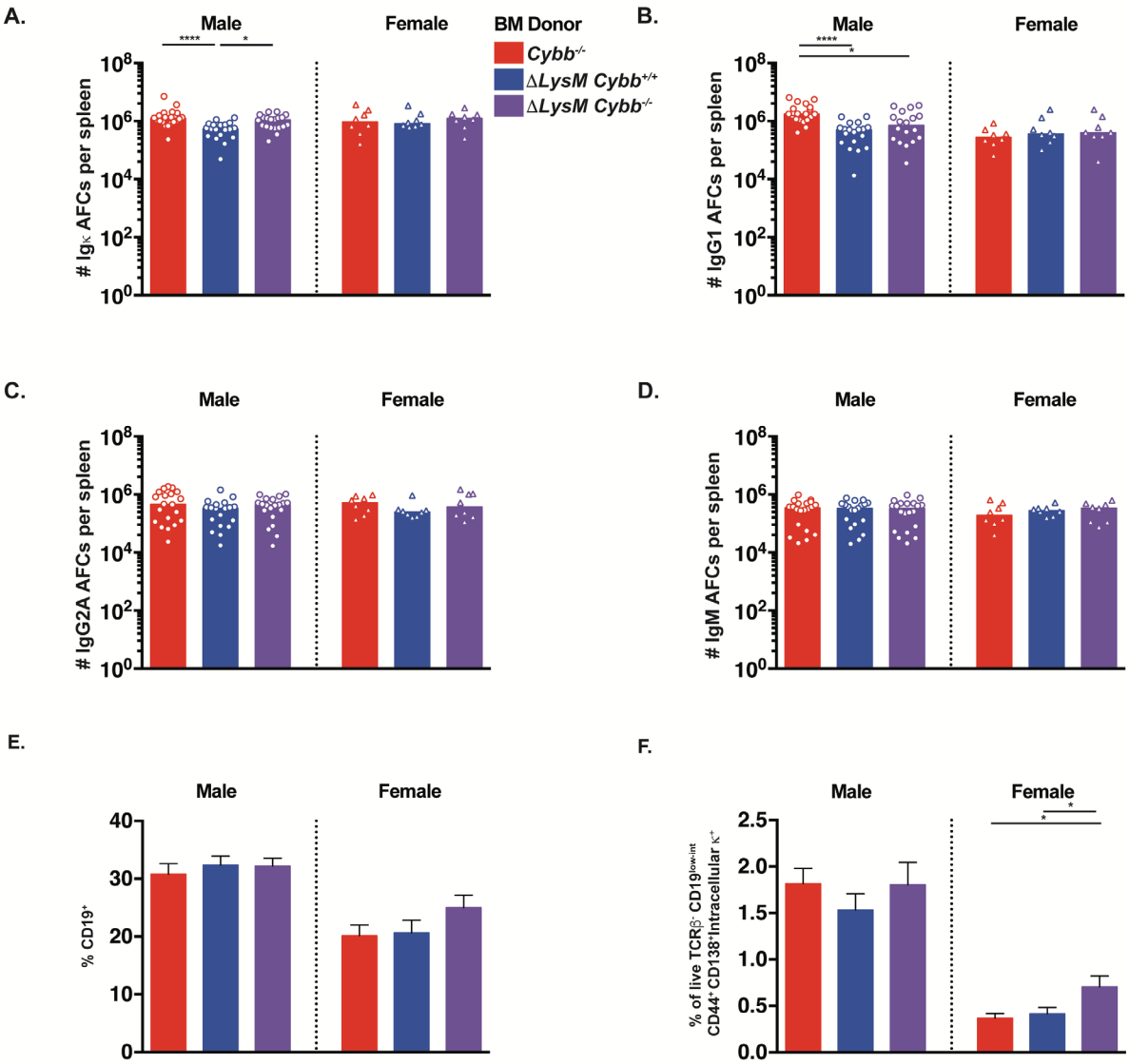

Figure 26. Igκ AFCs were increased in SLE prone mice with a myeloid *Cybb* defect
Numbers of Igκ (A), IgG1 (B), IgG2a (C), and IgM (D) antibody forming cells (AFCs) per spleen as determined by ELISpot. **(E)** Percentages of live $CD19^+$ total B cells. **(F)** Percentages of live cells that are $TCR\beta^-$ $CD44^+$ $CD138^+$ intracellular κ^+ AFCs. Data representation, number of mice, and statistics are as in Figure 23. In panels E and F, bar graphs are represented as the mean ± SEM and a two-tailed Welch's T test was performed to determine statistical significance within each gender (* indicates $p \leq 0.05$, ** $p \leq 0.01$, *** $p \leq 0.001$, and **** $p \leq 0.0001$; n=8 to 20 mice per group).

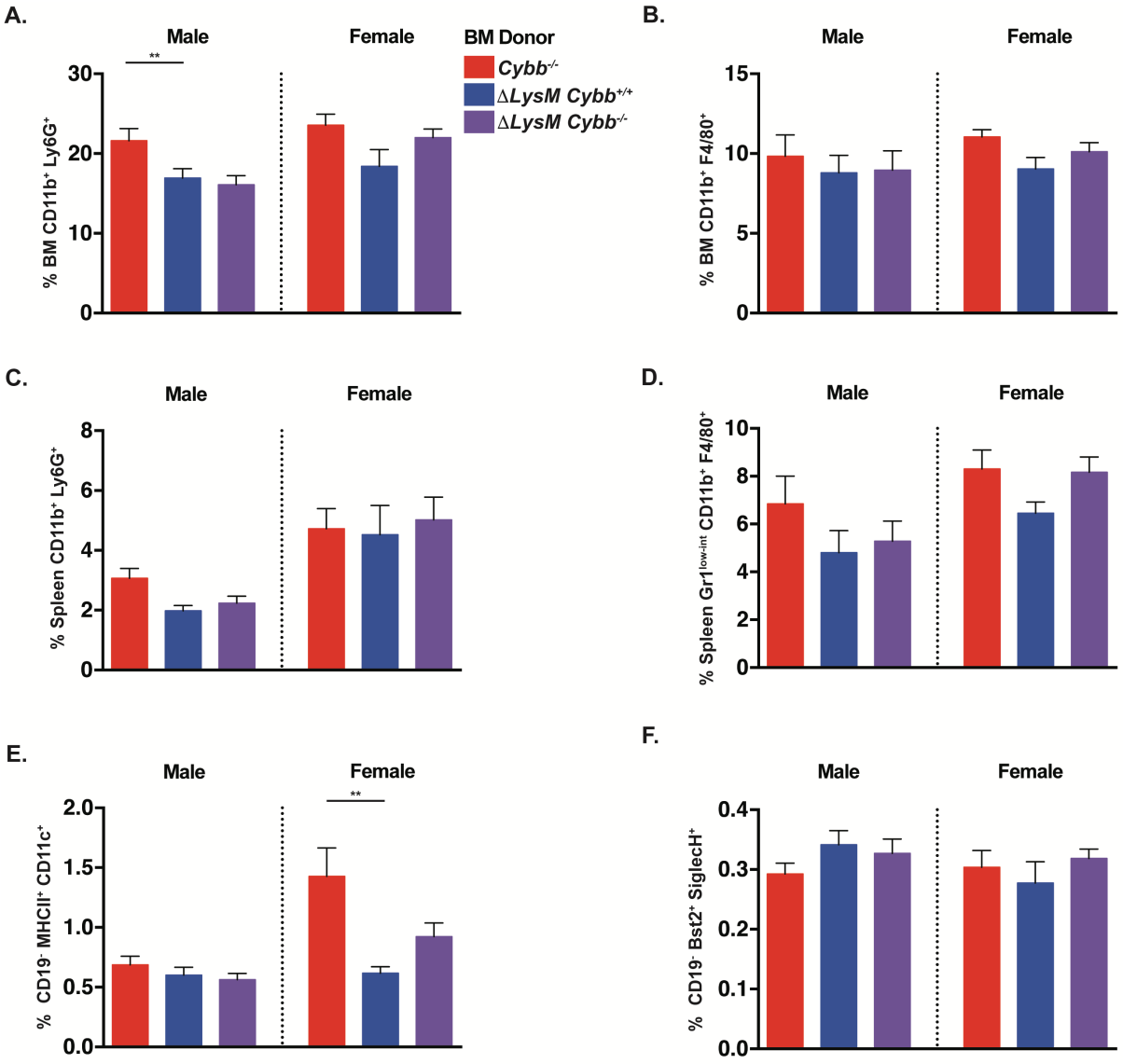

Figure 27. *Cybb* deficiency in LysM expressing cells did not alter the composition of the myeloid compartment in MRL.Fas^{lpr} mice.

(A) Percentages of live bone marrow (BM) CD11b^{+} Ly6G^{+} neutrophils. **(B)** Percentages of BM CD11b^{+} GR1$^{low\text{-}int}$ F4/80^{+} macrophages. **(C)** Percentages of live CD11b^{+} Ly6G^{+} neutrophils in the spleen. **(D)** Percentages of splenic CD11b^{+} GR1$^{low\text{-}int}$ F4/80^{+} macrophages. **(E)** Percentages of live CD19^{-} MHCII^{+} CD11c^{+} conventional dendritic cells and **(F)** CD19^{-} BST2^{+} CD11c^{+} plasmacytoid dendritic cells. Bar graphs are represented as the mean ± SEM and a two-tailed Welch's T test was performed to determine statistical significance within each gender (* indicates p≤0.05, ** p≤0.01, *** p≤0.001, and **** p≤0.0001; n=8-20 mice per group).

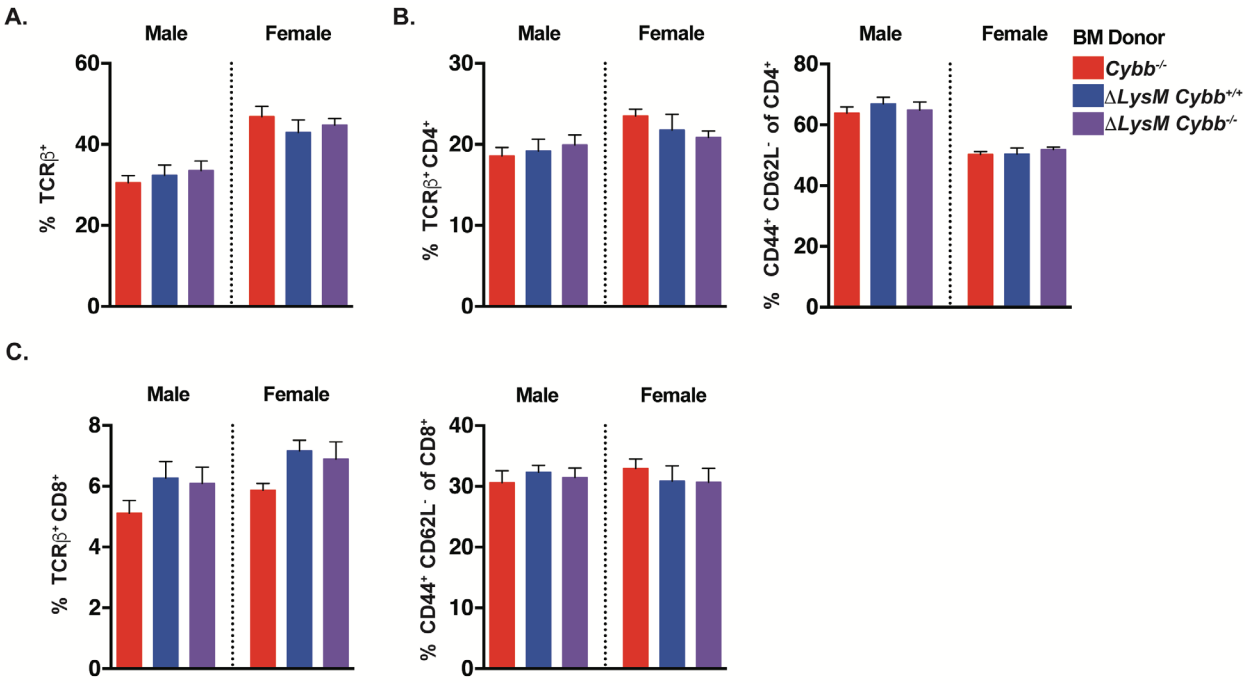

Figure 28. Myeloid *Cybb* deficiency did not alter the T cell compartment.
(A) Percentages of live TCRβ$^+$ total T cells. **(B)** Percentages of live TCRβ$^+$ CD4$^+$ T cells (left panel) and of CD4$^+$ CD44$^+$ CD62L$^-$ activated T cells (right panel). **(C)** Percentages of live TCRβ$^+$ CD8$^+$ T cells (left panel) and of CD8$^+$ CD44$^+$ CD62L$^-$ activated T cells (right panel). Data representation, number of mice, and statistics are as in Figure 27.

3.4 GENERATION OF THE *CYBB* CONDITIONAL KNOCKOUT MOUSE ON THE MRL.FAS^{LPR} BACKGROUND USING CRISPR-CAS9

The cell specific role of CYBB in SLE has significant implications as to the mechanism by which CYBB contributes to autoimmunity. To investigate the tissue-specific function of CYBB in lupus, we generated a *Cybb* conditional allele directly on the MRL.Fas^{lpr} background using CRISPR-Cas9 technology (185) coupled with *in vitro* fertilization (186) (Figure 16A). *In vitro* fertilization was used to generate single cell MRL.Fas^{lpr} embryos. Resulting embryos were injected at the pronuclear stage with single guide RNAs (sgRNA), Cas9 endonuclease, and single-stranded oligo (ssODN) repair templates to edit the murine genome.

3.4.1 CRISPR-Cas9 targeting strategy to generate the *Cybb* conditional knockout mouse on an autoimmune background

We developed a workflow (Figure 29A) to insert two loxP sites flanking exon 4 of *Cybb* (Figure 29B). We chose to target exon 4 as it codes for a critical transmembrane domain that binds p47^{phox} and heme groups. Following Cre-mediated deletion of exon 4, splicing of exon 3 into exon 5 would result in a frameshift generating a premature stop codon in exon 5. Two sgRNAs were used to generate double-stranded breaks flanking exon 4 of *Cybb*. The resulting double-stranded breaks were repaired using ssODNs harboring a loxP and an EcoR1 restriction site to facilitate screening. (Figure 29B). One founder had correct insertion of a loxP site in intron 3

(Figure 29C; upper panel) with concomitant insertion of a loxP sequence in intron 4. However, we identified a one base pair deletion in the Cre binding arm of the intron 4 loxP site (Figure 29C; lower panel). Based on *in vitro* studies showing that mutations in the loxP arms can be tolerated (187), we proceeded to test the functionality of this floxed allele *in vivo* by crossing it to the *LysM-Cre* and *Mrp8-Cre* strains as described later in this chapter.

3.4.2 A serial targeting approach to make *Cybb* conditional knockout mouse on the MRL.Fas^{lpr} strain using CRISPR-Cas9

It is possible that the mutated loxP site described above does not work as well as the wild-type version. To address this concern, we moved forward to generate a *Cybb*-floxed allele with two wild-type loxP sites. At present, we find, as do many others attempting to produce mutant mice with CRISPR-Cas9 technology, that the efficiency of accurate homology directed repair (HDR) is too low to consistently produce conditional alleles in a single step. Correct integration of two loxP sites requires the simultaneous occurrence of two unlikely events. We overcame this limitation by employing a strategy to insert loxP sites in two steps. The first round of gene editing yielded a mouse with a single intact loxP site in intron 4 but no loxP site in intron 3. We took advantage of this founder and used *in vitro* fertilization coupled with CRISPR-Cas9 to insert the second loxP site into intron 3 of *Cybb* (Figure 30). As the first round of CRISPR-Cas9 gene editing resulted in an indel at the intron 3 target site, we designed a modified sgRNA to account for the new target site sequence. One founder was identified with two wild-type loxP sites flanking exon 4 (Figure 31).

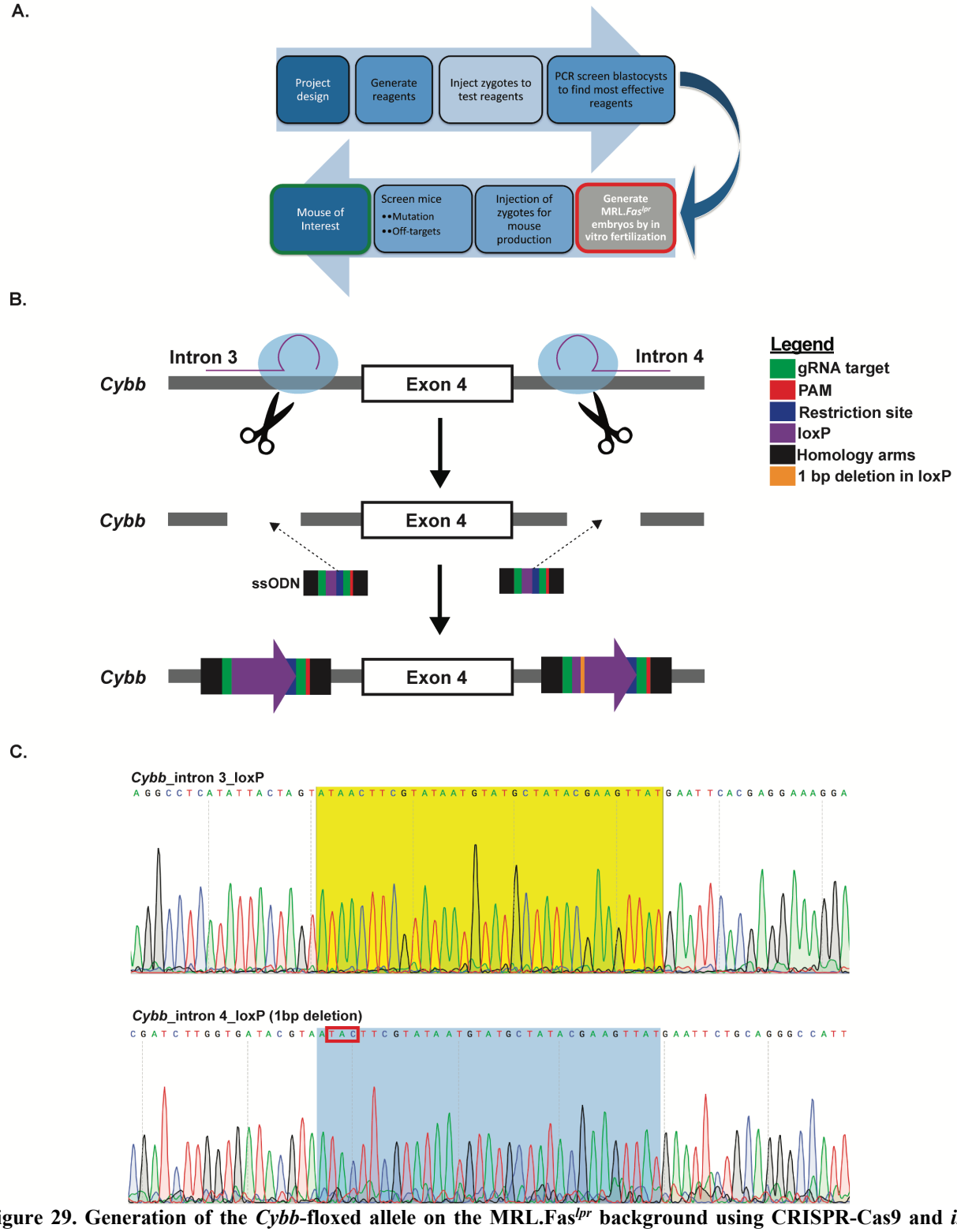

Figure 29. Generation of the *Cybb*-floxed allele on the MRL.Fas^{lpr} background using CRISPR-Cas9 and *in vitro* fertilization.

(A) Workflow to genetically modify MRL.Fas^{lpr} mice using CRISPR-Cas9. (B) CRISPR-Cas9 strategy to generate the *Cybb*-floxed allele. (C) Sequencing chromatograms of the two loxP sites flanking exon 4 in the *Cybb*-floxed MRL.Fas^{lpr} founder.

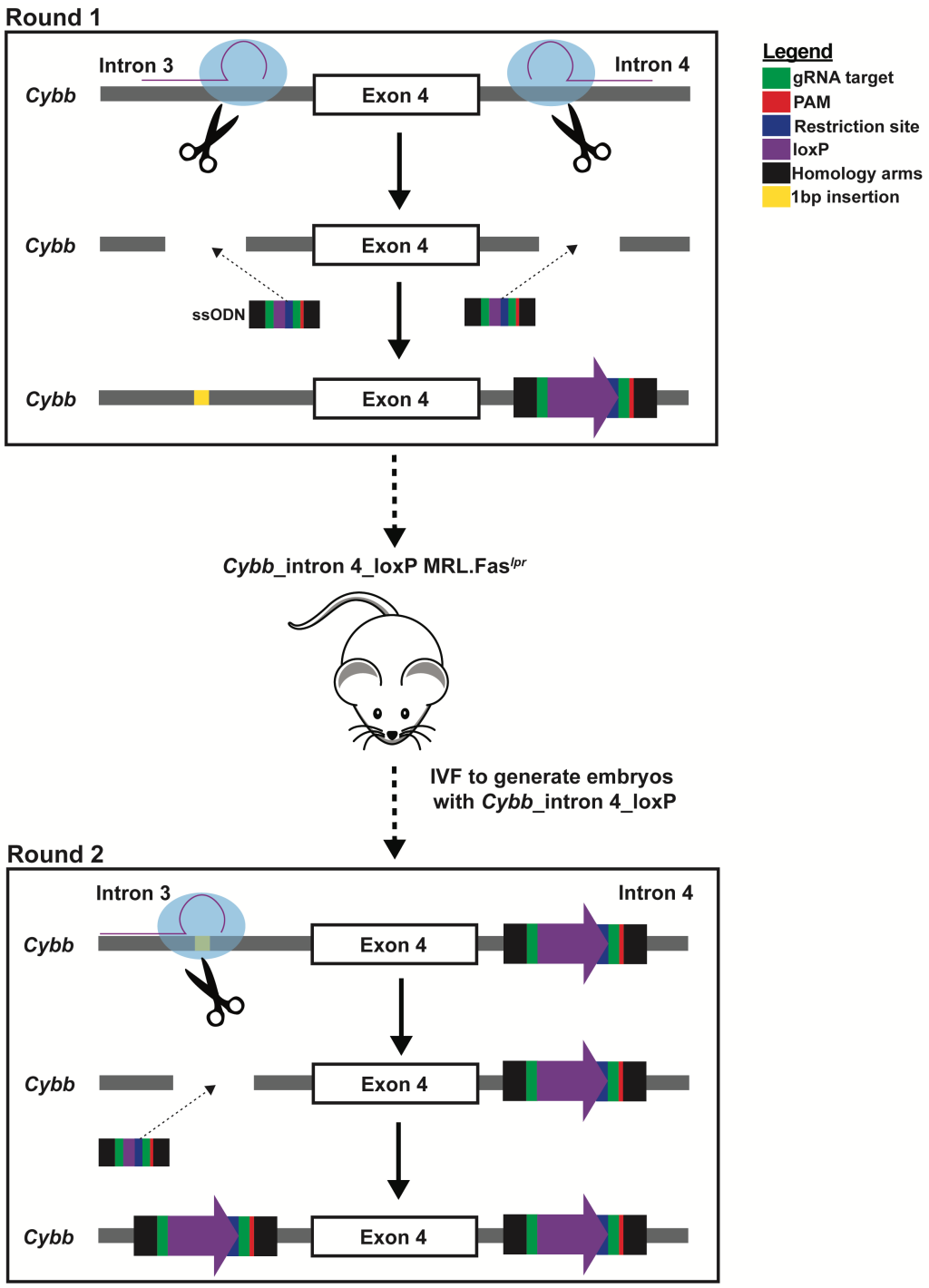

Figure 30. Schematic of a serial targeting approach to generate the *Cybb*-floxed MRL.Fas^{lpr} allele by CRISPR-Cas9 mediated gene editing.

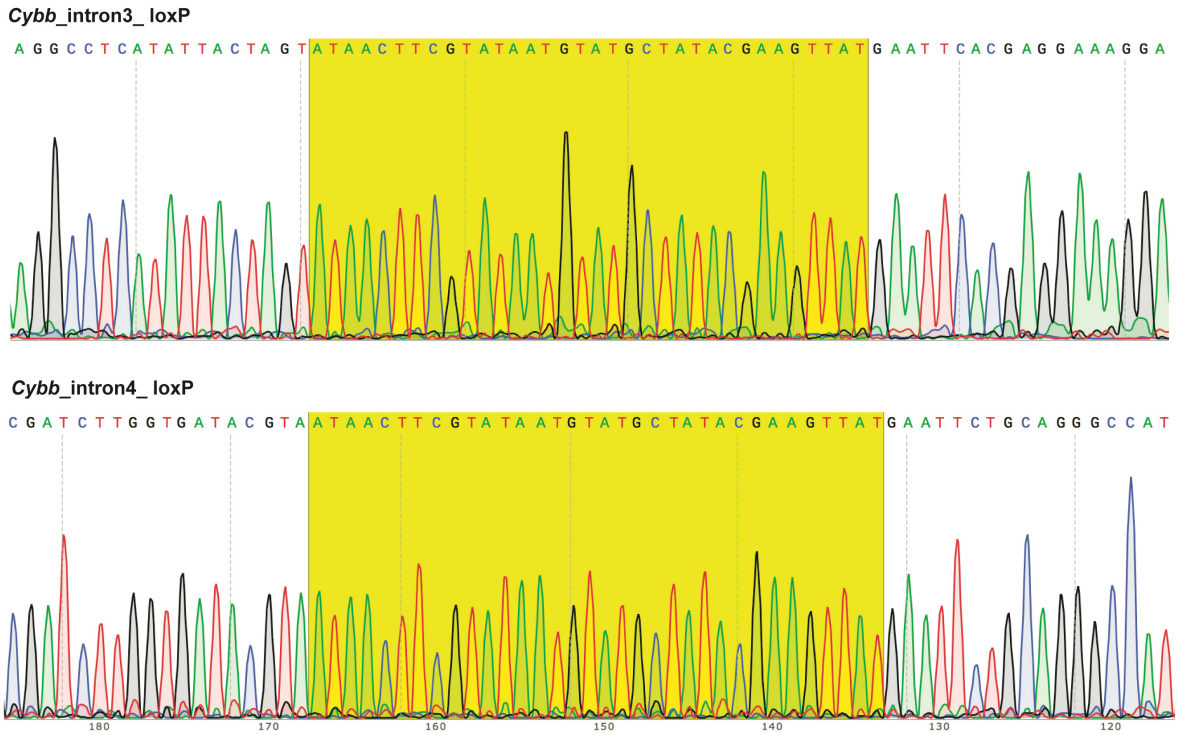

Figure 31. A serial targeting strategy successfully generated a *Cybb*-floxed allele on the MRL.Fas^{lpr} background with two wild-type loxP sites.
Sequencing chromatograms of the two loxP sites flanking exon 4 in the *Cybb*-floxed MRL.Fas^{lpr} founder mouse generated by the serial CRISPR-Cas9 targeting strategy.

3.5 ANALYSIS OF *CYBB* DELETION IN MACROPHAGES AND NEUTROPHILS IN THE INITIATION AND PROGRESSION OF SLE USING A CONDITIONAL KNOCKOUT APPROACH

To confirm the role of macrophage and neutrophil *Cybb* deletion in SLE identified by our chimera approached, we generated homozygous *Cybb*-floxed mice that were also heterozygous or homozygous for *LysM-Cre*. *LysM-Cre* negative *Cybb*-floxed littermates served as a negative control in this cohort. SLE pathology was assessed at 19-20 weeks of age.

3.5.1 *Cybb* is effectively deleted in the myeloid compartment of male *LysM-Cre* positive *Cybb*-floxed MRL.Fas^{lpr} mice but not in females

Cybb deletion was measured by qPCR of genomic DNA acquired from FACS-sorted immune cell populations. *Cybb* was efficiently deleted in splenic CD11b^{+}Gr1^{+} neutrophils isolated from male *Cybb*$^{fl/y}$ *LysM-Cre*$^{+/-}$ (%72.51 ±1.46) and *Cybb*$^{fl/y}$ *LysM-Cre*$^{+/+}$ MRL.Fas^{lpr} mice (92.47% ±1.23) (Figure 32A). *LysM-Cre* is known to be less efficient in targeting macrophages than neutrophils. Paralleling this observation, *Cybb* deletion in *Cybb*$^{fl/fl}$ *LysM-Cre*$^{+/-}$ *CD11b*$^{+}$*F4-80*$^{+}$ splenic macrophages was 31% (± 3.016). *LysM-Cre* homozygosity increased *Cybb* deletion in *Cybb*$^{fl/fl}$ *LysM-Cre*$^{+/+}$ macrophages to 53.38% (±4.517) (Figure 32B). *Cybb* deletion efficiency was significantly lower in the female cohort. In female *Cybb*$^{fl/fl}$ *LysM-Cre*$^{+/-}$ mice, the mean *Cybb* deletion in neutrophils was 46.81% (±2.59) (Figure 32A). Similar to the male cohort, *LysM-Cre* homozygosity increased *Cybb* deletion in *Cybb*$^{fl/fl}$ *LysM-Cre*$^{+/+}$ neutrophils to 79.82% (±1.69) (Figure 32A). Surprisingly, no detectible deletion of *Cybb* was measured in splenic macrophages from female *Cybb*$^{fl/fl}$ *LysM-Cre*$^{+/-}$ mice (Figure 32B). However, *Cybb*$^{fl/fl}$ *LysM-*

Cre$^{+/+}$macrophages isolated from female mice had a deletion efficiency of 24.47% (±9.82) (Figure 32B). Of note, *LysM-Cre* homozygous mice were not included in the presented downstream analyses (Figure 32B). *LysM-Cre* is a site directed knockin resulting in a non-functional allele. Therefore, homozygotes are *LysM*-deficient, potentially confounding analysis and interpretation of any observed phenotype.

3.5.2 LysM *Cybb* deficiency worsened renal disease in female MRL.Fas^{lpr} mice

There was a trend towards increased proteinuria in female *Cybb*$^{fl/fl}$ *LysM-Cre*$^{+/-}$ MRL.Fas^{lpr} mice at 14 and 20 weeks of age (Figure 33A and B). Concordantly, glomerulonephritis and initial nephritis was exacerbated in this group (Figure 33C and D). We did not observe any differences in proteinuria or histological assessment of nephritis in the male cohort (Figure 33C and D). No differences in splenomegaly or lymphadenopathy were identified among the groups (Figure 33E and F).

3.5.3 *Cybb* deficiency in the myeloid compartment had a minimal effect on the anti-self response

Autoantibody titers were not affected by conditional *Cybb* deficiency in LysM expressing cells. We did not observe any change in anti-RNA antibody (Figure 34A), anti-Sm antibody (Figure 34B), anti-nucleosome antibody (Figure 34C), or rheumatoid factor (Figure 34D) titers in *Cybb*$^{fl/fl}$ *LysM-Cre*$^{+/-}$ MRL.Fas^{lpr} mice compared to controls. Male *Cybb*$^{fl/y}$ *LysM-Cre*$^{+/-}$ MRL.Fas^{lpr} mice had an increase in the percentage of CD19^{+} B cells (Figure 34E) and a trend towards an elevated percentage of CD19$^{low\text{-}int}$ CD44^{+} CD138^{+} intracellular κ^{high} AFCs (Figure

43F; p=0.069). As this finding was not recapitulated in the female cohort, and correlates neither with altered antibody profile nor disease severity, its biological significance is unclear.

3.5.4 Bone marrow neutrophils and macrophages were reduced in female *Cybb$^{fl/fl}$ LysM-Cre$^{+/-}$* MRL.Fas^{lpr} mice

Conditional *Cybb* deficiency in LysM expressing cells altered the myeloid compartment in female MRL.Fas^{lpr} mice. The percentage of bone marrow CD11b^{+} GR1^{+} neutrophils and CD11b^{+}F4/80^{+}Gr1$^{low\text{-}int}$ macrophages were reduced in *Cybb$^{fl/fl}$ LysM-Cre$^{+/-}$* females compared to controls (Figure 35A and B). Reciprocally, the percentage of splenic neutrophils was expanded in this same group (Figure 35C). No statistically significant differences in splenic macrophages were identifed (Figure 35D). Male *Cybb$^{fl/y}$ LysM-Cre$^{+/-}$* mice exhibited an increased percentage of CD19^{-}CD11c^{+}MHCII^{+} cDCs, a finding not observed in the female cohort. We did not identify any changes in pDCs amongst the groups.

3.5.5 Conditional LysM *Cybb* deficiency did not significantly alter the T cell compartment

Similar to our chimera studies, conditional *Cybb* deficiency in macrophages and neutrophils had little impact on the lymphoid compartment. All genotypes exhibited no statistical differences in the total percentages of TCRβ^{+} T cells (Figure 36A). The percentages of CD4^{+} T cells and CD4^{+}CD44^{+}CD62L^{-} activated T cells were also not significantly different across all groups (Figure 36B). No changes in the percentages of naive and activated CD8^{+} T cells were observed (Figure 36C).

To summarize our interim findings, hematopoietic but not stromal *Cybb* deficiency exacerbated multiple manifestations of lupus in the MRL.Fas^{lpr} model. Moreover, employing a chimera approach to delete *Cybb* in the myeloid compartment was sufficient to exacerbate SLE renal disease. Taken together, our data convincingly highlights neutrophil and/or macrophage CYBB as a critical regulator of autoimmunity.

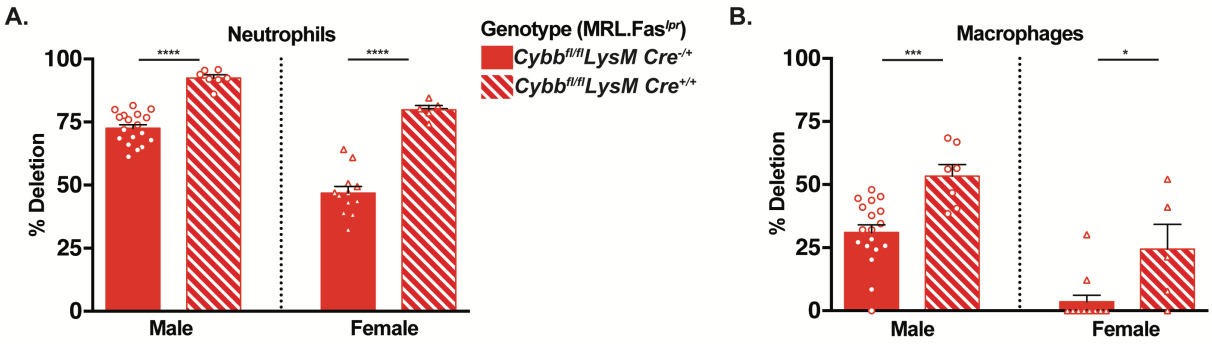

Figure 32. *Cybb* was effectively deleted in the myeloid compartment of male *LysM-Cre* positive *Cybb*-floxed MRL.Fas^{lpr} mice but not in females.

Cybb deletion efficiency in n neutrophils (A) and macrophages (B). A two-tailed Welch's T test was performed to determine statistical significance within each gender (* indicates $p \leq 0.05$, ** $p \leq 0.01$, *** $p \leq 0.001$, and **** $p \leq 0.0001$; n=5 to 8 mice per group).

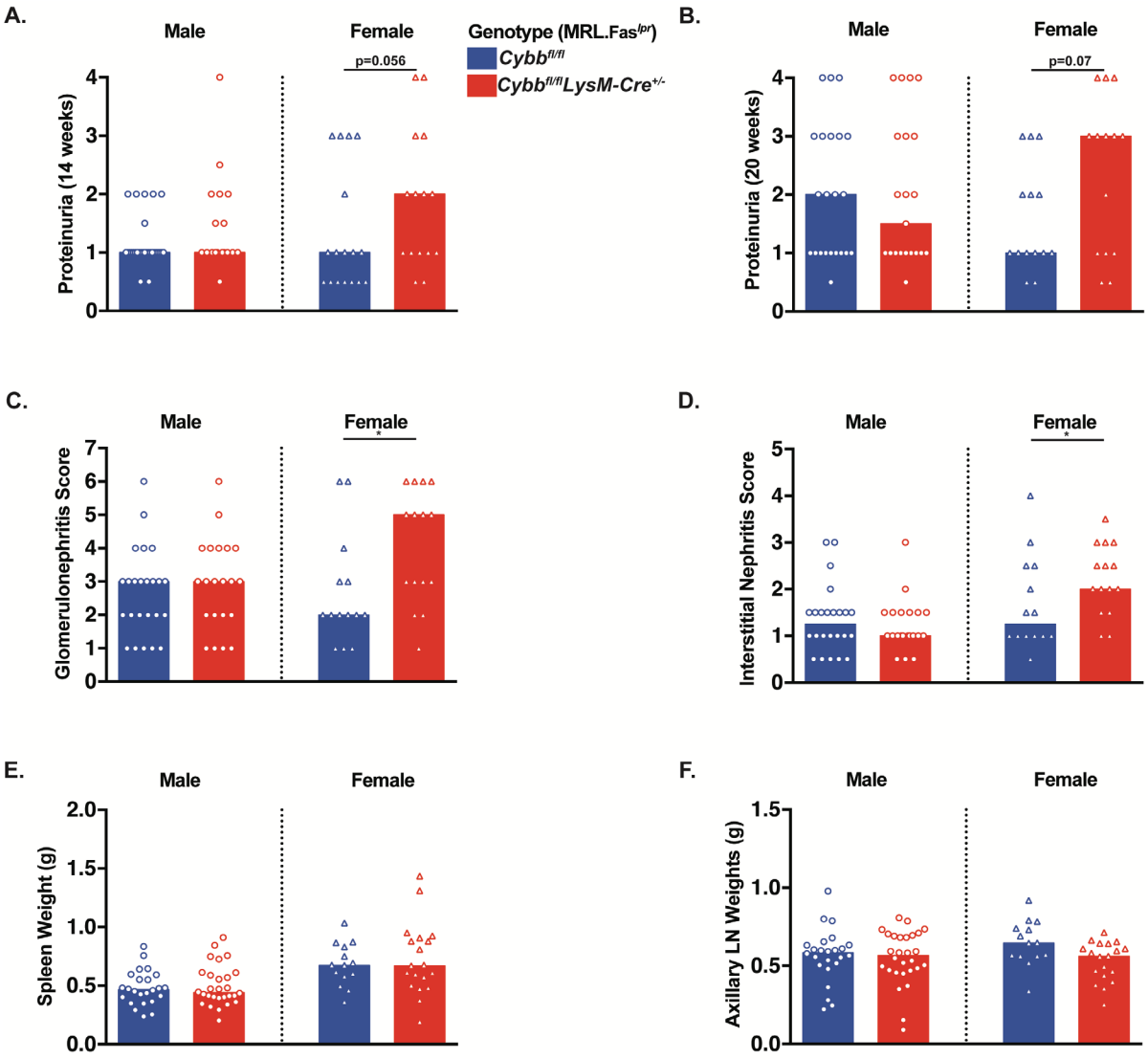

Figure 33. Conditional *Cybb* deletion in the myeloid compartment exacerbated glomerulonephritis and interstitial nephritis in female MRL.Fas^{lpr} mice.

(A) Proteinuria at 14 weeks of age. (B) Proteinuria at 20 weeks of age. **(C)** Glomerulonephritis scores and **(D)** Interstitial nephritis scores. **(E)** Spleen Weight. **(F)** Axillary lymph node weights. Scores and weights are represented as a function of *Cybb-flox LysM-Cre* genotype and gender at 20 weeks of age unless otherwise indicated. Bars represent the median and each dot represents and individual mouse. A one-tailed Mann-Whitney test was performed to determine statistical significance within each gender (* indicates $p \leq 0.05$, ** $p \leq 0.01$, *** $p \leq 0.001$, and **** $p \leq 0.0001$; n=14 to 24 mice per group unless otherwise indicated).

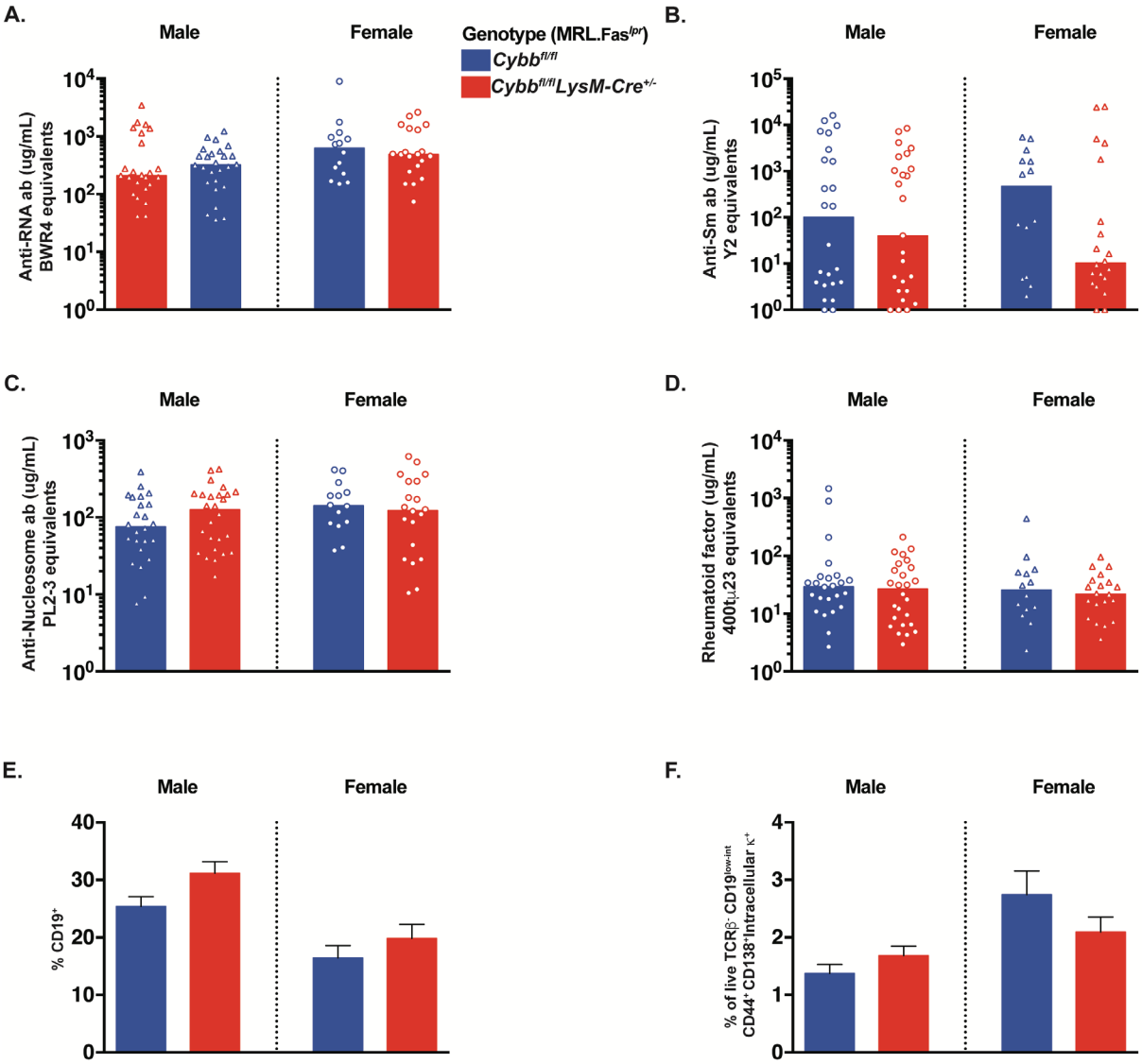

Figure 34. *Cybb* deficiency in the myeloid compartment did not substantially impact the anti-self response. **(A-D)** Serum anti-RNA (A), anti-Sm (B), anti-nucleosome (C), rheumatoid factor (D), antibody titers at 20 weeks of age **(E)** Percentages of live $CD19^+$ total B cells. **(F)** Percentages of live cells that are $TCR\beta^-$ $CD44^+$ $CD138^+$ intracellular κ^+ AFCs. Data representation, number of mice, and statistics are as in Figure 33. In panels E and F, bar graphs are represented as the mean ± SEM and a Welch's T test was performed to determine statistical significance within each gender (* indicates $p \leq 0.05$, ** $p \leq 0.01$, *** $p \leq 0.001$, and **** $p \leq 0.0001$; n=14 to 24 mice per group).

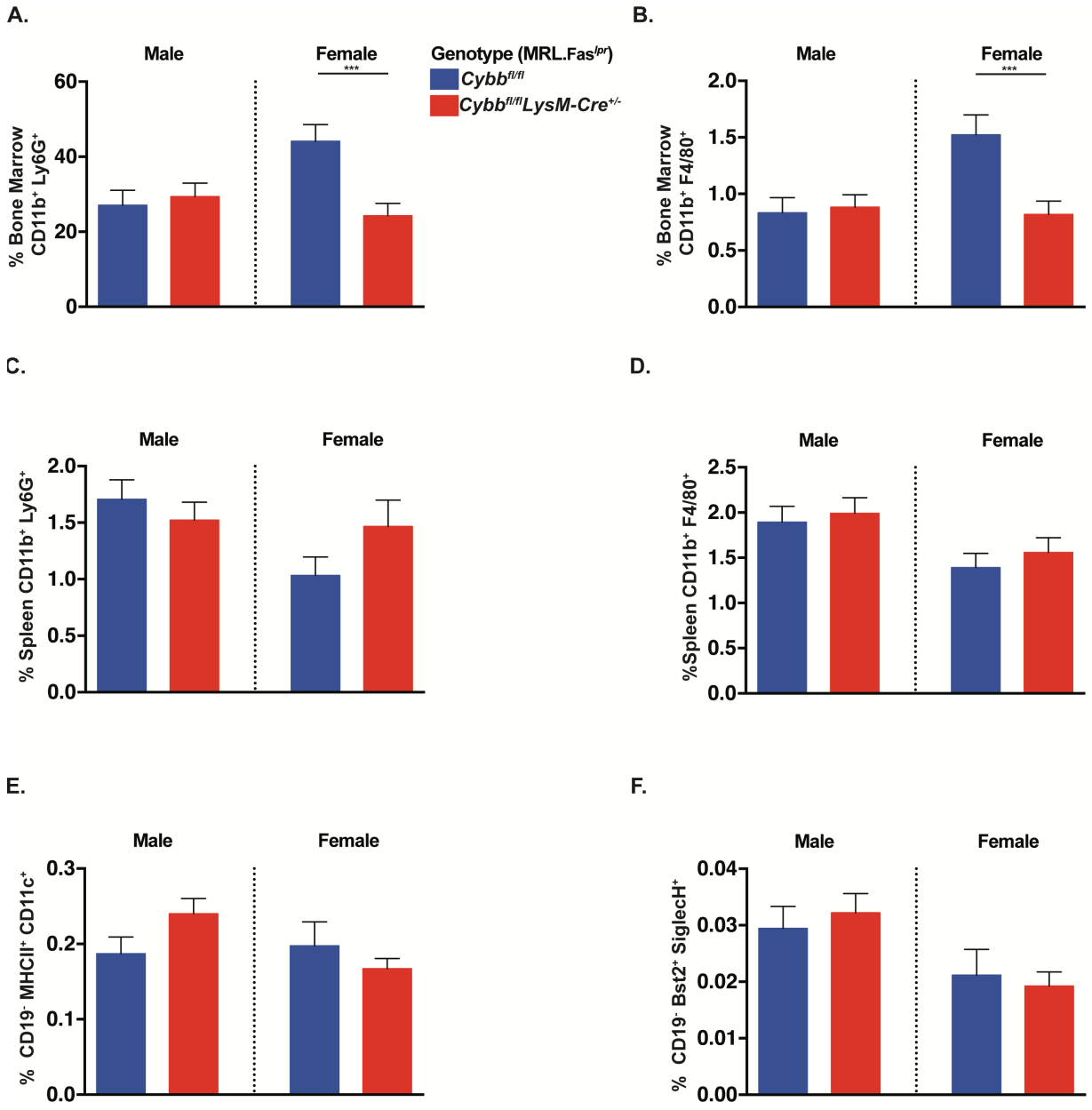

Figure 35. Reduced bone marrow neutrophils and macrophages in female *Cybb$^{fl/fl}$ LysM-Cre$^{+/-}$* MRL.Fas^{lpr} mice.

(A) Percentages of live bone marrow (BM) CD11b^{+} Ly6G^{+} neutrophils. **(B)** Percentages of BM CD11b^{+} GR1$^{low\text{-}int}$ F4/80^{+} macrophages. **(C)** Percentages of live CD11b^{+} Ly6G^{+} neutrophils in the spleen. **(D)** Percentages of splenic CD11b^{+} GR1$^{low\text{-}int}$ F4/80^{+} macrophages. **(E)** Percentages of live CD19^{-} MHCII^{+} CD11c^{+} conventional dendritic cells and **(F)** CD19^{-} BST2^{+} CD11c^{+} plasmacytoid dendritic cells. Bar graphs are represented as the mean ± SEM and a Welch's T test was performed to determine statistical significance within each gender (* indicates $p \leq 0.05$, ** $p \leq 0.01$, *** $p \leq 0.001$, and **** $p \leq 0.0001$; n=14 to 24 mice per group).

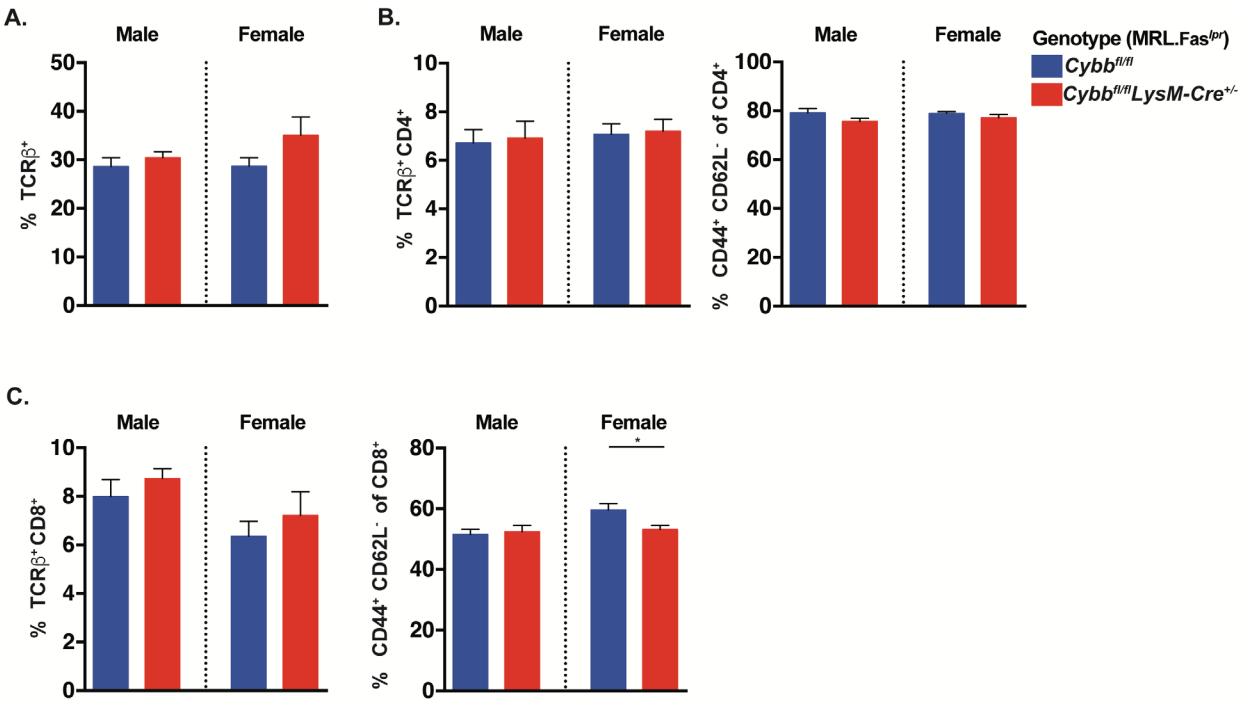

Figure 36. Conditional myeloid *Cybb* deficiency did not significantly alter the T cell compartment.
(A) Percentages of live TCRβ$^+$ total T cells. **(B)** Percentages of live TCRβ$^+$ CD4$^+$ T cells (left panel) and of CD4$^+$ CD44$^+$ CD62L$^-$ activated T cells (right panel). **(C)** Percentages of live TCRβ$^+$ CD8$^+$ T cells (left panel) and of CD8$^+$ CD44$^+$ CD62L$^-$ activated T cells (right panel). Data representation, number of mice, and statistics are as in Figure 35.

3.6 EMPLOYING A CONDITIONAL KNOCKOUT APPROACH TO ASSESS NEUTROPHIL SPECIFIC *CYBB* DELETION IN SLE PATHOGENESIS

The tools utilized thus far do not decipher the differential contribution of neutrophil versus macrophage CYBB in disease. Here, we utilize *Mrp8-Cre* (188) to specifically delete *Cybb* in neutrophils by crossing the *Cybb-floxed* allele to *Mrp8-Cre*. Taken together with our prior data, these studies will allow us to deduce the differential contribution of macrophage and neutrophil CYBB to systemic autoimmunity. SLE pathology was assessed at 18 weeks of age. Of note, the data presented here is preliminary and this line of investigation is still in progress.

3.6.1 Neutrophil *Cybb* deficiency exacerbated renal disease in male MRL.Fas^{lpr} mice

While no differences in urine protein were observed in the female cohort, male *Cybb*$^{fl/fl}$ *Mrp8-Cre*$^{+/-}$ MRL.Fas^{lpr} mice had a trend towards increased proteinuria at 18 weeks of age (Figure 37A). No differences in the incidence of dermatitis were detected amongst the groups (Figure 37B). Glomerulonephritis was more severe in *Cybb*$^{fl/y}$ *Mrp8-Cre*$^{+/-}$ male SLE prone mice but interstitial nephritis remained unaffected (Figure 37C and D). However, no differences in glomerulonephritis or interstitial nephritis were identified in female *Cybb*$^{fl/fl}$*Mrp8-Cre*$^{+/-}$ MRL.Fas^{lpr} mice (Figure 37C and D). Conditional *Cybb* deficiency in neutrophils increased spleen but not axillary lymph node weights in male SLE-prone mice (Figure 37E and F; p=0.0576).

3.6.2 Conditional *Cybb* deletion in neutrophils did not alter the anti-self response in SLE prone mice

Autoantibody titers were not affected by conditional *Cybb* deficiency in neutrophils. We did not observe any change in anti-RNA antibody (Figure 26A), anti-Sm antibody (Figure 26B), anti-nucleosome antibody (Figure 38C), or rheumatoid factor (Figure 38D) titers among the groups. No differences in in the percentages of $CD19^{+}$ B cells (Figure 38E) or $CD19^{low\text{-}int}$ $CD44^{+}$ $CD138^{+}$ intracellular κ^{high} AFCs (Figure 38F) were identified in *Cybb*$^{fl/fl}$ *Mrp8-Cre*$^{+/-}$ MRL.Fas^{lpr} mice compared to controls.

3.6.3 Neutrophil specific *Cybb* deletion did not alter the composition of the myeloid compartment in MRL.Fas^{lpr} mice

Since the myeloid compartment was expanded in the setting of hematopoietic *Cybb* deficiency, we explored whether conditional deletion of *Cybb* in neutrophils changes the myeloid compartment. The percentages of bone marrow $CD11b^{+}$ $GR1^{+}$ neutrophils and macrophages were not altered in *Cybb*$^{fl/fl}$ *Mrp8-Cre*$^{+/-}$ MRL.Fas^{lpr} mice compared to controls (Figure 39A and B). No statistically significant differences in splenic $CD11b^{+}$ $GR1^{+}$ neutrophils (Figure 39C) or $CD11b^{+}F4/80^{+}Gr1^{low\text{-}int}$ macrophages were observed (Figure 39D). *Cybb*$^{fl/fl}$ *Mrp8-Cre*$^{+/-}$ did not have any impact on the percentage of $CD19^{-}CD11c^{+}MHCII^{+}$ (Figure 39E) or $CD19^{-}BST2^{+}$ $SiglecH^{+}$ pDCs (Figure 39F).

3.6.4 Neutrophil specific *Cybb* deletion does not alter the T cell compartment in MRL.Fas^{lpr} mice

Concordant with our prior studies, conditional *Cybb* deficiency in neutrophils did not impact the lymphoid compartment. No statistical differences in the total percentages of TCRβ^{+} T cells were observed (Figure 40A). *Cybb* deletion in neutrophils did not significantly change the percentages of CD4^{+} T cells and CD4^{+}CD44^{+}CD62L^{-} activated T cells across all groups (Figure 40B). Additionally, we did not observe any differences in the percentages of naive and activated CD8^{+} T cells (Figure 40C).

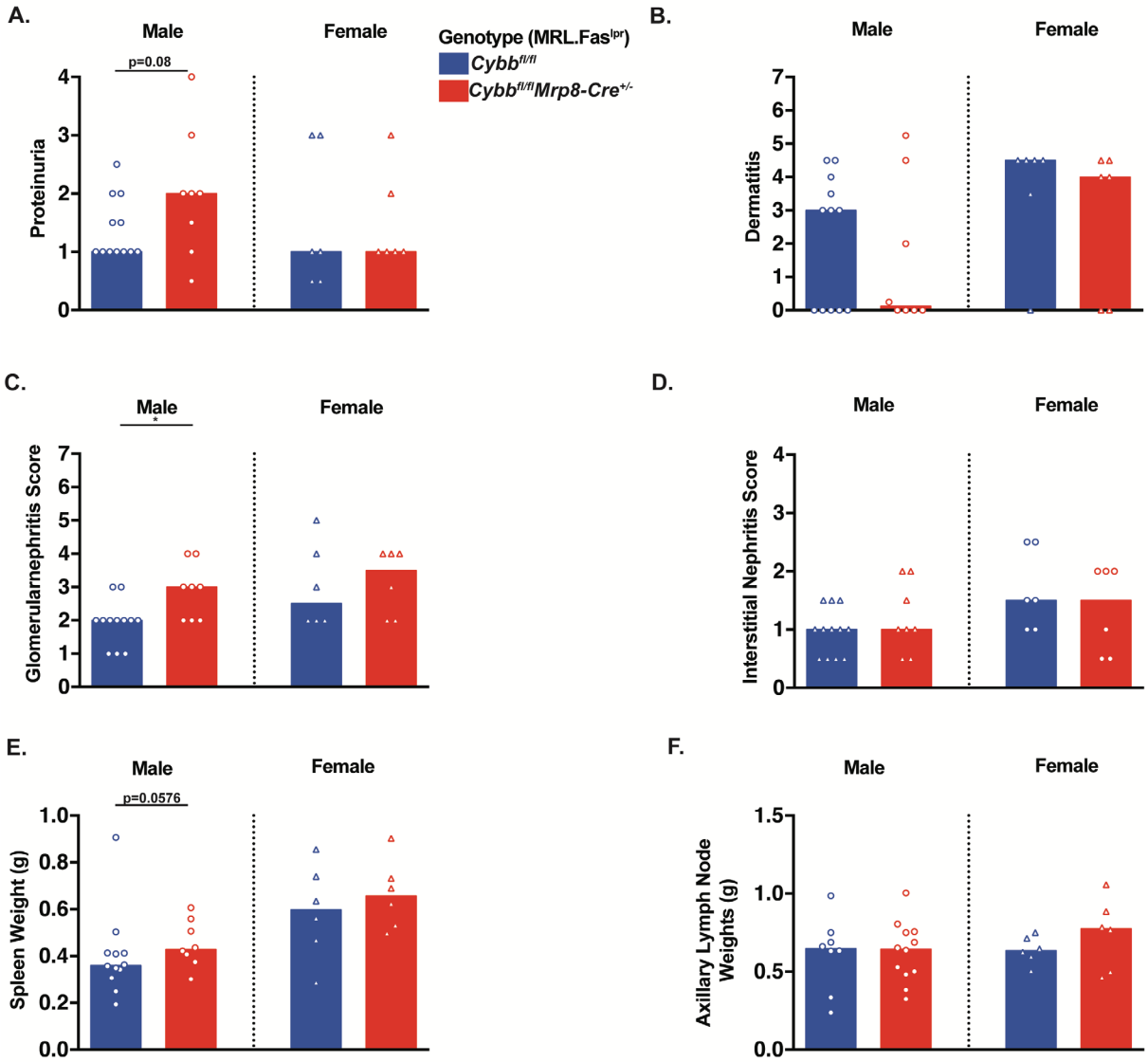

Figure 37. Neutrophil *Cybb* deficiency exacerbated glomerulonephritis and increased splenomegaly in male MRL.Fas^{lpr} mice.

(A) Proteinuria. **(B)** Dermatitis. **(C)** Glomerulonephritis scores. **(D)** Interstitial nephritis scores. **(E)** Spleen Weight. **(F)** Axillary lymph node weights. Scores and weights are represented as a function of *Cybb-flox LysM-Cre* genotype and gender at 18 weeks of age. Bars represent the median and each dot represents and individual mouse. A two-tailed Mann-Whitney test was performed to determine statistical significance within each gender (* indicates $p \leq 0.05$, ** $p \leq 0.01$, *** $p \leq 0.001$, and **** $p \leq 0.0001$; n=6 to 12 mice per group unless otherwise indicated).

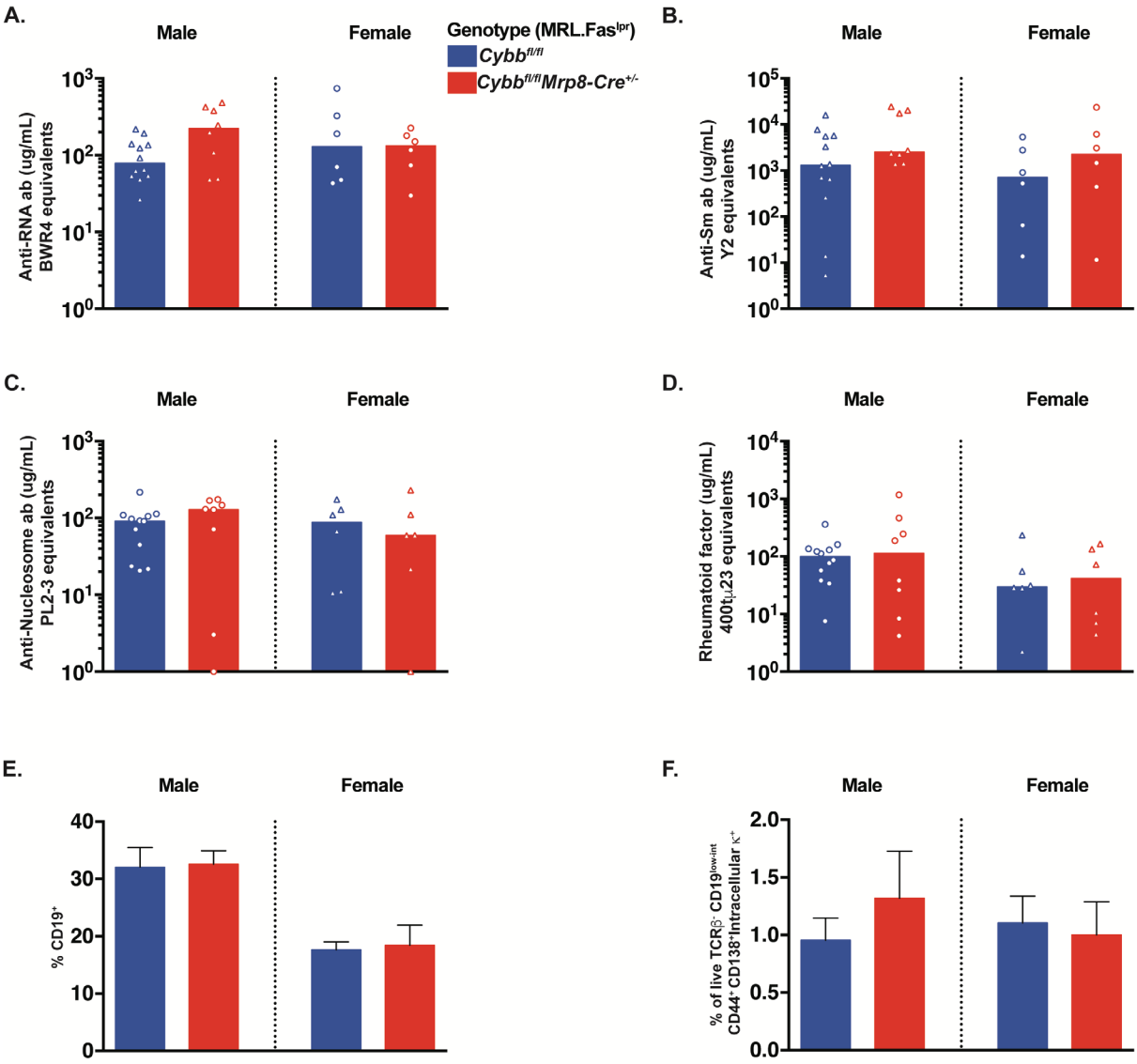

Figure 38. Conditional *Cybb* deletion in neutrophils has no impact on the anti-self response in SLE prone mice.

(A-D) Serum anti-RNA (A), anti-Sm (B), anti-nucleosome (C), rheumatoid factor (D), antibody titers at 20 weeks of age **(E)** Percentages of live $CD19^+$ total B cells. **(F)** Percentages of live cells that are $TCR\beta^-$ $CD44^+$ $CD138^+$ intracellular κ^+ AFCs. Data representation, number of mice, and statistics are as in Figure 37. In panels E and F, bar graphs are represented as the mean ± SEM and a two-tailed Welch's T test was performed to determine statistical significance within each gender (* indicates $p \leq 0.05$, ** $p \leq 0.01$, *** $p \leq 0.001$, and **** $p \leq 0.0001$; n=6 to 12 mice per group).

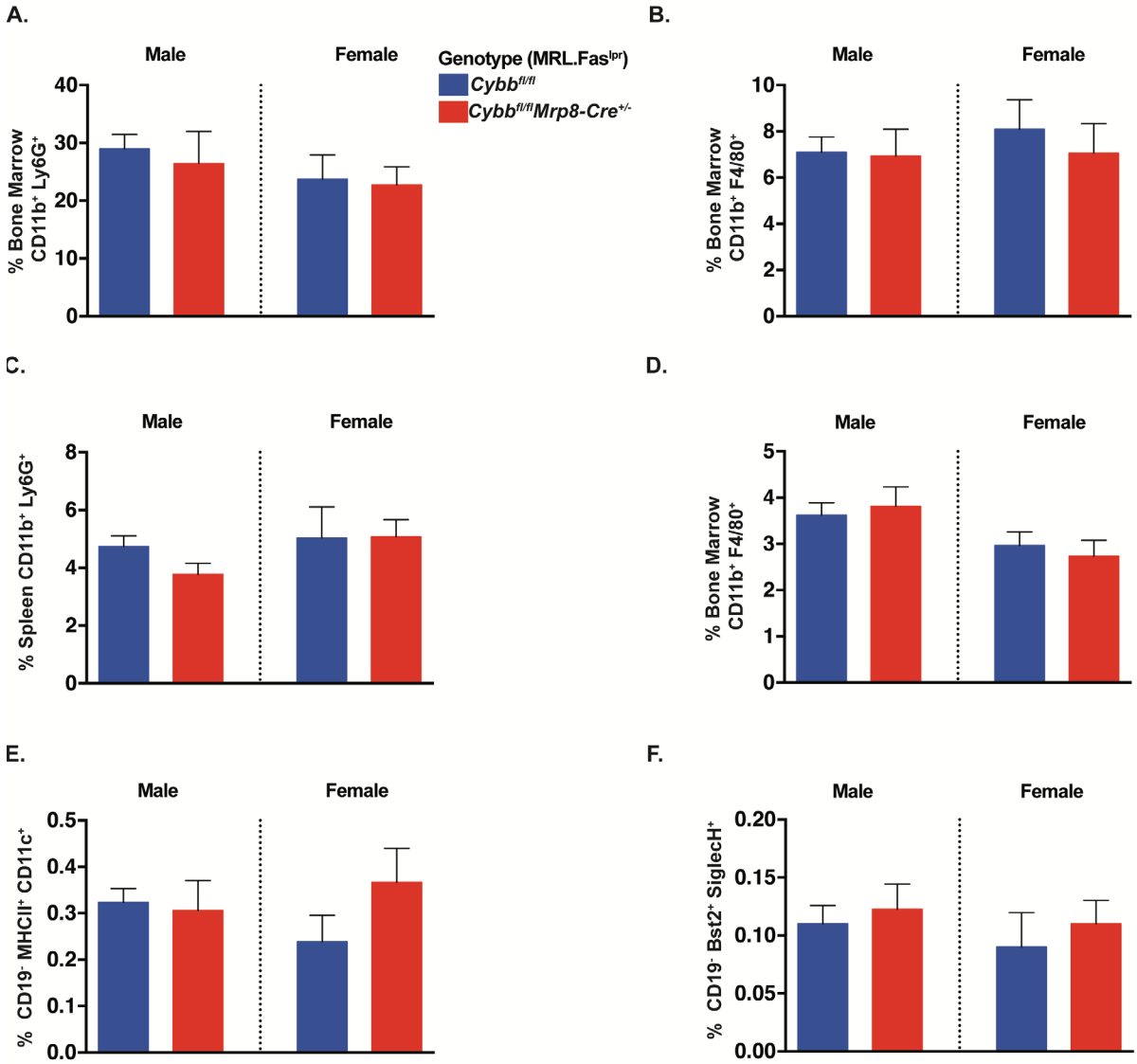

Figure 39. Neutrophil specific *Cybb* deletion did not change the percentages of neutrophils, macrophages or DCs in MRL.Fas^{lpr} mice.

(A) Percentages of live bone marrow (BM) CD11b$^+$ Ly6G$^+$ neutrophils. **(B)** Percentages of BM CD11b$^+$ GR1$^{low\text{-}int}$ F4/80$^+$ macrophages. **(C)** Percentages of live CD11b$^+$ Ly6G$^+$ neutrophils in the spleen. **(D)** Percentages of splenic CD11b$^+$ GR1$^{low\text{-}int}$ F4/80$^+$ macrophages. **(E)** Percentages of live CD19$^-$ MHCII$^+$ CD11c$^+$ conventional dendritic cells and **(F)** CD19$^-$ BST2$^+$ CD11c$^+$ plasmacytoid dendritic cells. Bar graphs are represented as the mean ± SEM and a two-tailed Welch's T test was performed to determine statistical significance within each gender (* indicates $p \leq 0.05$, ** $p \leq 0.01$, *** $p \leq 0.001$, and **** $p \leq 0.0001$; n=6 to 12 mice per group).

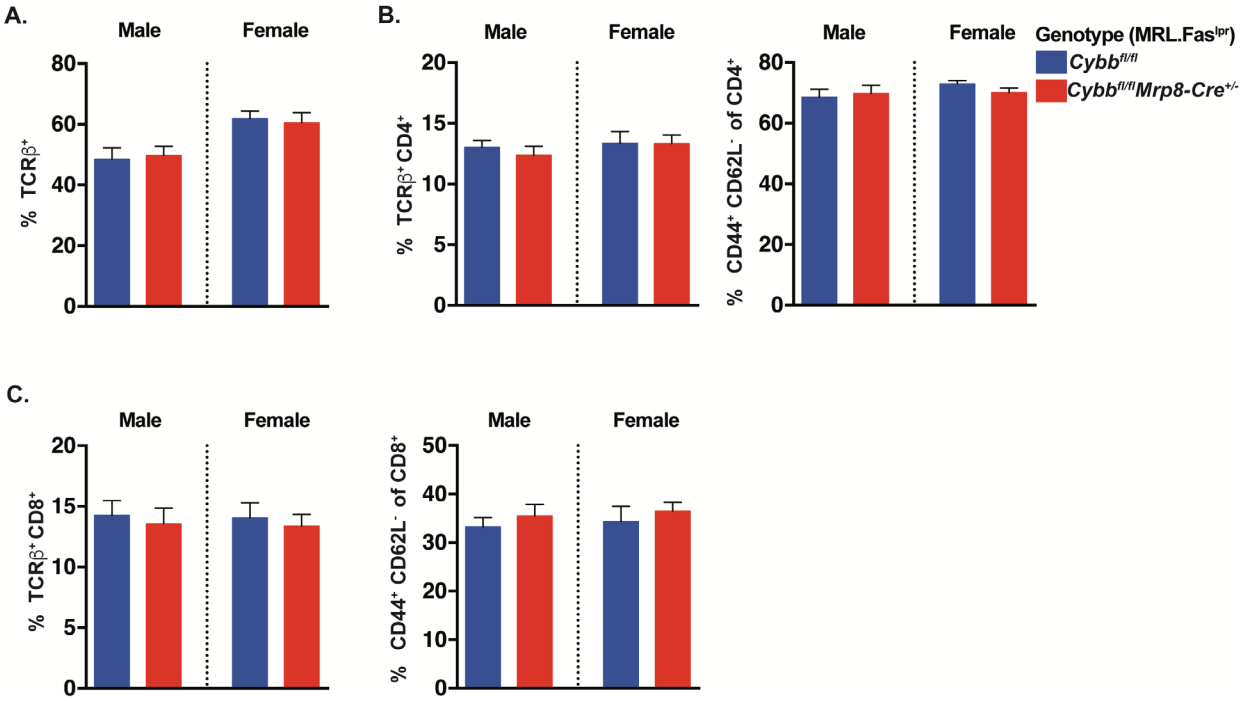

Figure 40. Neutrophil specific *Cybb* deletion did not alter the T cell compartment in MRL.Fas^{lpr} mice.
(A) Percentages of live TCRβ$^+$ total T cells. **(B)** Percentages of live TCRβ$^+$ CD4$^+$ T cells (left panel) and of CD4$^+$ CD44$^+$ CD62L$^-$ activated T cells (right panel). **(C)** Percentages of live TCRβ$^+$ CD8$^+$ T cells (left panel) and of CD8$^+$ CD44$^+$ CD62L$^-$ activated T cells (right panel). Data representation, number of mice, and statistics are as in Figure 39.

3.7 DISCUSSION

Here, we provide data that supports myeloid-expressed CYBB as a fundamental negative regulator of SLE pathogenesis. Multiple approaches employed in this study reinforce our findings. First, to identify the differential contribution of CYBB in the stromal and hematopoietic compartments, we used a reciprocal bone marrow chimera approach. Notably, we found that hematopoietic, but not stromal, *Cybb* deficiency is sufficient to exacerbate autoantibody production, lupus nephritis, and reduce survival in the MRL.Fas^{lpr} model. These findings highlight that *Cybb* deficiency in a hematopoietic cell subset was the likely driver of the observed phenotype. To home in on which compartment(s) CYBB deficiency exerts its regulatory function, we developed a novel chimera strategy to delete *Cybb* selectively in the myeloid compartment, specifically in neutrophils and macrophages. *Cybb* deletion in macrophages and neutrophils was sufficient to exacerbate glomerular and interstitial nephritis. In parallel, we generated a *Cybb* conditional allele directly on MRL.Fas^{lpr} background to enable further characterization of tissue-specific CYBB function in SLE. Conditional deletion of *Cybb* in macrophages and neutrophils using *LysM-Cre* partially recapitulated the phenotype that we observed in the chimera system. The mechanism by which myeloid *Cybb* deletion exacerbates SLE remains enigmatic but will be further explored in chapter 4.

While our data implicates myeloid CYBB deficiency as responsible for exacerbating multiple manifestations of lupus, it is still an outstanding question whether absence of CYBB in the neutrophil and/or macrophage is the primary culprit. The role of CYBB in macrophages and neutrophils may not be mutually exclusive but the answer to this question does hint at the potential mechanisms by which CYBB modulates disease. If CYBB deficiency in the neutrophil is the major driver of lupus, it is potentially due to neutrophil death. Billions of neutrophils die

each day posing a major potential antigen load (91). In the context of CYBB deficiency, the neutrophil may die by a more immunogenic manner, such as catastrophic necrosis, programmed necroptosis, pyroptosis, or ferroptosis. It is possible that in the absence of CYBB, the process of NET formation is obstructed, resulting in frustrated NET generation that could be uniquely immunogenic. Moreover, NADPH oxidase complex-dependent ROS can inhibit caspases (189) (190). In the absence of CYBB increased neutrophil apoptosis has been observed (189). Additionally, proteases, such as Cathepsins, are inhibited by CYBB generated ROS (191). As proteases are abundant in neutrophil granules and can be released upon neutrophil death into the extracellular environment, it is possible increased protease activity due to CYBB deficiency could generate neo self-antigens. A higher degree of residual protease activity following neutrophil death could also be a direct cause of increased tissue damage in the absence of neutrophil-expressed CYBB. Caspases are implicated in the processing of pro-inflammatory cytokines such as IL-1 family members. Abrogation of CYBB function can lead to increased production of functional IL-1β in CGD mice and humans (85, 90, 192, 193). If macrophage CYBB deficiency is responsible for exacerbated autoimmunity, it likely results from a failure of the macrophage to clear dead cells and resulting debris as addressed in the introduction of this chapter and further discussed in chapter 4.

To date, the efficiency and specificity of existing myeloid Cre strains limits the ability to directly assess the differential contribution of myeloid subsets in murine models. For instance, others and we have shown that *LysM-Cre* efficiently targets neutrophils but variably targets macrophages populations. Using our chimera system, we attempted to assess the role of neutrophil *Cybb* deletion using the neutrophil specific Cre strains, *Elane-Cre* and *Mrp8-Cre*, along with *LysM-Cre* to generate a neutropenic primary donor. No phenotype was observed in

the chimera cohort using the *ΔElane* (*Elane-Cre*$^{+/-}$ *Rosa26-eGFP-DTA* $^{+/-}$) mouse as the primary chimera donor (data not shown). We assessed hematopoietic reconstitution in this cohort by using GFP as a surrogate to approximate *Cybb* sufficiency. Unfortunately, over 65% of the neutrophils were wild-type in this cohort (data not shown). Though *Elane-Cre* is specific to neutrophils it is known to have a poor efficiency. As *Mrp8-Cre* is specific and efficient at targeting neutrophils, we backcrossed this allele to the MRL.Fas^{lpr} background. To generate a neutropenic donor, we crossed the *Mrp8-Cre* MRL.Fas^{lpr} to the *Rosa26-eGFP-DTA* allele. The resulting ΔMRP8 (*Mrp8-Cre*$^{+/-}$ *Rosa26-eGFP-DTA* $^{+/-}$) mice were not viable, likely due to the transient expression of *Mrp8-Cre* during embryonic development. As an alternative to the chimera strategy, we can use the *Cybb* conditional allele to specifically delete *Cybb* in neutrophils, bypassing the technical issues encountered in the chimera system. Here, we utilized *Mrp8-Cre* to specifically delete *Cybb* in neutrophils by crossing the *Cybb*-floxed allele to Mrp8-Cre. Preliminary results are reported here and these studies remain ongoing. Taken together with our prior data, these studies will allow us to deduce the differential contribution of macrophage and neutrophil CYBB to systemic autoimmunity.

Strikingly, although glomerular and interstitial nephritis was exacerbated in female mice upon conditional deletion of *Cybb* in LysM expressing cells, *Cybb* deletion in neutrophils was only ~40% and was nearly undetectable in macrophages. *Cybb* heterozygous MRL.Fas^{lpr} female mice do develop worse SLE. Importantly, 50% of cells in global *Cybb* heterozygotes are *Cybb*-deficient due to inactivation of one X chromosome in female mice. The presence of *Cybb*-sufficient cells do not confer protection in the heterozygotes, paralleling our observations in the chimera and conditional knockout system employed in this study. Preliminary data show a trend towards increased proteinuria in male mice with conditional deletion of *Cybb* solely in

neutrophils. These two findings, taken together with the phenotype observed in our chimera system, suggest that neutrophil Cybb deficiency may be the major driver of the phenotype.

Cybb deficiency in the myeloid compartment, mediated by LysM-Cre in both our chimera and conditional knockout systems, does not fully recapitulate the *Cybb* global knockout or total hematopoietic chimera phenotype. There are several explanations that could account for this discrepancy. First, *LysM-Cre* does not efficiently target macrophages. Therefore, if the exacerbated disease observed in the global and hematopoietic *Cybb* knockouts is at least in part due to a function of CYBB in macrophages, we may only observe partial penetrance of the phenotype. As CYBB is expressed in other immune cell subsets and is known to exert regulatory functions in B and T cells important in the pathogenesis of lupus, it is possible that intact lymphocyte CYBB dampens disease severity in both the myeloid chimera and conditional knockout systems.

Surprisingly, conditional deletion of *Cybb* in LysM expressing cells was lower than expected in female mice based on our previous experience and the reported literature (184). *Cybb* deletion in macrophages was nearly undetectable. It is possible that inactivation of one of the two X chromosomes prevents Cre from mediating recombination at the X-inactivated *Cybb* locus. Chromatin structure and modification can impact locus specific Cre mediated recombinase activity. Alternatively, the single base pair deletion in the intron 4 loxP site could reduce recombination efficiency, especially in the setting of an inefficient or poorly expressed Cre. Given that LysM-Cre efficiently deleted *Cybb* in the males, we believe this explanation to be less likely. Nevertheless, we will formally test this idea by repeating these experiments using the *Cybb* conditional allele with fully “wild-type” loxP sites on both sides.

CYBB deficiency in human CGD patients is associated with severe recurrent bacterial and fungal infections (120). We do not believe that an infectious process is the primary driver of the exacerbated phenotype observed here. All cohorts were housed in a specific pathogen free facility and maintained on broad spectrum antibiotics for the duration of the experiment. All mice were cohoused such that mice of different genotypes would share microbial flora. The autoantibody profiles coupled with the glomerular and interstitial nephritis observed by histology are consistent with the SLE-like disease observed in MRL.Fas^{lpr} mice. Mice and humans that are NADPH oxidase functional heterozygotes are more susceptible to autoimmunity but not to infection. Exacerbated manifestations of SLE observed here are unlikely to be due to changes in the microbiome. Autoimmunity in MRL.Fas^{lpr} mice is not mediated by the microbiome (141). *Ncf1*$^{m1j/m1J}$ mice rederived in a germ-free facility are still more susceptible to inflammatory arthritis (181). Additionally, the total hematopoietic chimeras were performed at two different intuitions. Taken together, it is unlikely that either infections processes or changes in the microbiome are responsible for the more severe disease we observed in multiple systems.

Aside from the insights into how CYBB regulates autoimmunity, we also made contributions to methods for mouse genetic engineering. We developed a workflow to employ Crispr-Cas9, in combination with *in vitro* fertilization, to generate a conditional knockout mouse directly on the MRL.Fas^{lpr} background. By conventional ES approaches it would take 1.5-2 years to generate a mouse of interest on either a mixed or C57BL/6 background and then an additional 2 years to backcross the founder to an autoimmune mouse strain at an expense of nearly $50,000. The approach we adopted here revolutionizes the study of autoimmunity as we can generate the tools needed to test a hypothesis in a causative way in less than 4 months and at a fraction of the cost. Moreover, by generating the mouse of interest directly on an autoimmune strain, we

eliminate the possibility that linked alleles carried by backcrossing contribute to the observed phenotype. This approach can be extended to the generation of conventional knockouts, point mutants, and insertion of large constructs.

Another significant finding of our work is that single base pair deletion in the Cre binding region of a loxP site can be tolerated, allowing for Cre mediated recombination *in vivo*. In male mice, the efficiency of *LysM-Cre* mediated deletion of the conditional *Cybb* allele with a single base pair deletion in the intron 4 loxp site is consistent with the reported literature (187). *In vitro* studies indicate that loxP mutations are tolerated *in vitro* (187). LoxP variants are frequently used within the scientific community. Further testing is required and ongoing to determine whether this conditional allele functions as efficiently as that with two wild-type loxP sites. This finding is important because point mutations in loxP sites are a common finding in conditional knockout animals generated by CRISPR-Cas9 and these founders could potentially still be used by the research community.

Collectively the data we present here suggests that CYBB is protective in SLE due to a fundamental regulatory activity of CYBB in macrophages and/or neutrophils, highlighting CYBB as a target for further mechanistic study and therapeutic development.

3.8 MATERIALS AND METHODS

Mice. *Cybb*-deficient (Catalogue# 002365), *LysM-Cre* (Catalogue# 004781), *Mrp8-Cre* C57BL/6 (Catalogue# 021614) mice were purchased from the Jackson Laboratories and backcrossed to the MRL.Fas^{lpr} strain for at least 9 generations. Homozygosity for the H2^{k} haplotype and the *lpr* mutation was verified by PCR. The *Cybb*-floxed MRL.Fas^{lpr} mice were

generated using CRISPR-Cas9 as detailed below. All mice were housed under specific-pathogen-free (SPF) conditions. Animal studies were approved by the University of Pittsburgh Institutional Animal Care Use Committee.

Generation of Chimeric Mice. Bone marrow cells were obtained from either *Cybb*$^{-/-}$ or wild-type MRL.Fas^{lpr} littermate control mice. Cells were incubated in *ACK* (Ammonium-Chloride-Potassium) buffer for erythroid cell lysis and resuspended in injection buffer (1 × PBS, 10 mM Hepes, 2.5% acid citrate dextrose anticoagulant, and 0.5% penicillin/streptomycin). 5-7 week old *Cybb*$^{-/-}$ or *Cybb*$^{+/+}$ MRL.Fas^{lpr} recipient mice received 750 cGy from a cesium irradiator and were reconstituted with 8X10^6 *Cybb*$^{-/-}$ or *Cybb*$^{+/+}$cells per mouse. The *Cybb*-sufficient controls used throughout chapter 3, were often the *ΔLysM Cybb*$^{+/+}$ MRL.Fas^{lpr} mice described below. For the 80:20 mixed ratio bone marrow chimeras, wild-type MRL.Fas^{lpr} recipients received 1.6X10^6 *Cybb*$^{-/-}$ and 6.4X10^6 *Cybb*$^{+/+}$ cells per mouse. SLE pathology was assessed at time points indicated in the figure legends.

To delete *Cybb* selectively in the myeloid compartment, we crossed the *LysM-Cre* to the *Rosa26-eGFP-DTA* strains on the MRL.Fas^{lpr} background (*ΔLysM*). The *Rosa26-eGFP-DTA* locus contains the gene for the diphtheria toxin fragment A (DTA) that is preceded by a loxP-flanked STOP cassette so that expression of the toxin is restricted to those cells expressing Cre recombinase. Expression of DTA leads to the death of that cell. Bone marrow cells from *Cybb*$^{-/-}$, *Cybb*$^{+/+}$, and *ΔLysM* were isolated and processed as above. 6-7 week old MRL.Fas^{lpr} recipients were irradiated and reconstituted with a 80:20 mixture of ΔLysM and *Cybb*-deficient (*ΔLysM cybb*$^{-/-}$) or *Cybb*-sufficient (*ΔLysM cybb*$^{+/+}$) bone marrow.

Mice were treated prophylactically with trimethoprim and sulfadiazine diet to prevent occult infection.

Generation of the Cybb-floxed allele on the MRL.Fas^{lpr} strain using CRISPR-Cas9. *Cybb*-floxed mice were generated using CRISPR-Cas9 technology (185). Two loxP sites were inserted flanking exon 4 of *Cybb* (Figure 29B and Table 1) using ssODNs with a loxP and an Ecor1 restriction to facilitate genotyping (Integrated DNA Technologies; Table 2).

We selected a sgRNA in intron 3 and intron 4 of *Cybb* using a python script implementing the Fuzznuc algorithm (Emboss) to identify unique N_{20}NGG sequences and their associated off-targets, allowing 0-4 mismatches (194). The output was further corroborated by the Cas-OFFinder algorithm (RGEN Tools). Potential off-targets (Supplemental Table 1) with three or fewer mismatches and those without mismatch in the seed sequence (13 bp adjacent to the PAM sequence) will be screened, by amplifying each off-target locus with a specific primer pair and sequencing the PCR product in founder mice.

The sgRNA was generated from a double strand linear DNA template by annealing a target specific primer containing a T7 promoter, the *Cybb* target sequence (without PAM), and part of the tracrRNA sequence with a common primer comprising the full tracrRNA sequence (Supplemental Table 2). The annealed template was subjected to a fill in reaction and the double stranded product was amplified using the T7-19 and sgRNA-R primers (Table 1). The resulting dsDNA template was purified with the QIAquick PCR purification kit (Qiagen) and then transcribed using the MEGAshortscript T7 kit (Invitrogen). Capped Cas9 mRNA transcripts were produced from PmeI-linearized purified pcDNA3.3topo-T7-hCas9 using the mMESSAGE mMACHINE T7 ULTRA Kit (Life Technologies). The Cas9 mRNA and the sgRNA were

purified using the MEGAclear kit (Life Technologies) and eluted in nuclease-free water. Cas9 mRNA and the gRNA integrity was confirmed using a 2100 Bioanalyzer (Agilent Technologies). MRL.Fas^{lpr} pronuclear-stage zygotes were generated by *in vitro* fertilization and microinjected with sgRNAs (50 ng/µl), Cas9 mRNA (100 ng/µl), and ssODN repair templates (0.5uM) by the Gene Targeting and Transgenic Core (University of Pittsburgh). Injected zygotes were cultured overnight and transferred to pseudopregnant CD1 recipient females to obtain potential founder mice. Mice were genotyped by PCR amplification of the target locus and Restriction Fragment Length Polymorphism (RFLP) analysis. Amplified PCR products were subsequently cloned into a sequencing vector (NEB) and sequenced to verify correct targeting.

The founders were backcrossed to wild-type MRL.Fas^{lpr} mice (The Jackson Laboratory catalogue # 000485) for 2 generations.

A serial targeting strategy to make Cybb conditional knockout mouse on the MRL.Fas^{lpr} strain using CRISPR-Cas9. The aforementioned strategy to generate a *Cybb*-floxed allele yielded one founder with an intact loxP site in intron 4. This founder mouse was backcrossed to wild-type MRL.Fas^{lpr} mice for two generations and sperm from the N2 males was used to generate MRL.Fas^{lpr} embryos, harboring the intro 4 loxP site, by *in vitro* fertilization. We used CRISRP-Cas9 to retarget intron 3 as outlined above. As a 1 base pair insertion was present in the intron 3 target sequence as a result of the first round of gene editing, we generated a modified sgRNA to account for the indel in the target sequence. CRISPR-Cas9 reagents were injected into MRL.Fas^{lpr} pronuclear-stage zygotes and resulting founders were screened as described above.

LysM-Cre MRL.Fas^{lpr} mice were intercrossed with *Cybb*$^{fl/wt}$ or *Cybb*$^{fl/y}$ MRL.Fas^{lpr} mice.

Resulting *LysM-Cre*$^{+/-}$ *Cybb*$^{fl/wt}$ or *LysM-Cre*$^{+/-}$ *Cybb*$^{fl/y}$ MRL.Fas^{lpr} mice were then crossed with MRL.Fas^{lpr} *Cybb*$^{fl/y}$ males or *Cybb*$^{fl/wt}$ females respectively. To generate mice for experimental cohorts, *LysM-Cre*$^{+/-}$*Cybb*$^{fl/fl}$ and *LysM-Cre*$^{+/-}$*Cybb*$^{fl/y}$ were intercrossed. As an alternative breeding strategy, we intercrossed *LysM-Cre*$^{+/-}$ *Cybb*$^{fl/fl}$ to *Cybb*$^{fl/y}$ and *LysM-Cre*$^{+/-}$ *Cybb*$^{fl/y}$ to *Cybb*$^{fl/fl}$. This breeding strategy generated littermate controls for each group. SLE pathology was assessed at 19-20 weeks of age. Mice were treated prophylactically with trimethoprim and sulfadiazine diet to prevent occult infection.

Strategy to conditionally delete cybb from neutrophils in MRL.Fas^{lpr} mice. *Mrp8-Cre* MRL.Fas^{lpr} mice were intercrossed with *Cybb*$^{fl/wt}$ or *Cybb*$^{fl/y}$ MRL.Fas^{lpr} mice. Resulting *Mrp8-Cre*$^{+/-}$ *Cybb*$^{fl/wt}$ or *Mrp8-Cre*$^{+/-}$ *Cybb*$^{fl/y}$ MRL.Fas^{lpr} mice were then crossed with MRL.Fas^{lpr} Cybb$^{fl/y}$ males or *Cybb*$^{fl/wt}$ females respectively. To generate mice for experimental cohorts, we intercrossed *Mrp8-Cre*$^{+/-}$ *Cybb*$^{fl/fl}$ to *Cybb*$^{fl/y}$ and *Mrp8-Cre*$^{+/-}$ *Cybb*$^{fl/y}$ to *Cybb*$^{fl/fl}$. This breeding allowed us to use littermate controls for each group. SLE pathology was assessed at 18 weeks of age. Mice were treated prophylactically with trimethoprim and sulfadiazine diet to prevent occult infection.

Quantitative PCR. For assessing deletion efficiency of *Cybb*, genomic DNA extracted from FACS sorted cells and used as template for qRT-PCR. qRT-PCR reactions were completed in triplicate using Kappa SYBR Green QPCR kit. The amount of *Cybb* in each sample was normalized to the unaffected gene *Tlr9*. Genomic DNA of the same cell type from *Cybb*$^{fl/fl}$ mice was used as undeleted control. Mice were 20 weeks old. Samples were run on a Roche Light cycler instrument.

Evaluation of SLE pathology. Refer to chapter 2

Flow cytometry. Refer to chapter 2

Autoantibody ELISAs. Refer to chapter 2

Statistics. Statistical analysis was performed using Prism 7.0 (Graphpad). A Kruskal-Wallis test with post-hoc Dunn's test, one or two-tailed Mann-Whitney U test, two-tailed Welch's t test, and a log-rank test were performed where indicated and appropriate. A p value <0.05 was considered statistically significant.

Table 1. Primers for *Cybb* sgRNA generation

Primer	Sequence
sgRNA Specific Primer (Cybb_intron 3)	TAATACGACTCACTATAGG**GGCCTCATATTACTAGTACG**GTTTTAGAGCTAG AAATAGCA Blue: T7 Promoter; Black: target specific sequence; Green: Partial TracrRNA Sequence
sgRNA Specific Primer (Cybb_intron 4)	TAATACGACTCACTATAGG**GATCTTGGTGATACGTATGC**GTTTTAGAGCTAG AAATAGCA
sgRNA Specific Primer (Cybb_intron 3_mut)	TAATACGACTCACTATAGG**GCCTCATATTACTAGTTACG**GTTTTAGAGCTAG AAATAGCA
sgRNA Common Primer	AAAAAAGCACCGACTCGGTGCCACTTTTTCAAGTTGATAACGGACTAGCCTTA TTTTAACTTGCTATTTCTAGCTCTAAAAC (complementary TracrRNA sequence)
T7-19-F	TAATACGACTCACTATAGG
sgRNA-R	AAAAGCACCGACTCGGTGC

Table 2. ssODN repair constructs to generate the *Cybb*-floxed allele

ssODN	Sequence
Cybb_intron 3_loxP ssODN	**CTAGAAATATATTTTGGCAAAATTCAAAACTTTAGATAACAGTGAAAAAT GTATTTGCAACAAGGCCTCATATTACTAGTATAACTTCGTATAATGTATG CTATACGAAGTTATGAATTCACGAGGAAAGGAAACAAATGACTTAAGCTG GCTATCTGAACTGGGAGGGATGACTATCATCCCTTGTCATCAACCAAATG**
Cybb_intron 4_loxP ssODN	**GGTAGCTTGGATGATAGCACTGCACACCGGTAAGTCTTGGAAGACATTTG AAATGCAGAGAGCGATCTTGGTGATACGTAATAACTTCGTATAATGTATG CTATACGAAGTTATGAATTCTGCAGGGCCATTAGGTTGGGATCGGTTGAG TTAAGGTTAAAGCATTCAAACTATTTCCTGATGTTAGGATTCATACCTTG** **sgRNA target site, EcoRI, LoxP, PAM**

4.0 LC3-ASSOCIATED PHAGOCYTOSIS AND SLE: AN INVESTIGATION OF CYBB, RUBICON, AND IL-10 IN LUPUS PATHOGENESIS

4.1 INTRODUCTION

4.1.1 Dead cell clearance defects and SLE

Loss of tolerance to nuclear antigens and the formation of autoantibodies to nucleic acids and nucleoproteins are hallmarks of SLE pathogenesis. While the sources of autoantigens in lupus remain enigmatic, a failure to adequately dispose of dead cells and resulting debris by macrophages is a leading possibility. Indeed, macrophages from a subset of lupus patients exhibit an impaired ability to phagocytose, a finding also observed in murine models (195-198). Paralleling these observations, SLE patients with leukemia undergoing pharmacological myeloablative therapy had greater accumulation of dead cells in the bone marrow compared non-autoimmune control subjects (195). Moreover, the LE (Lupus Erythematous) cell, a typical histologic finding in SLE patients where a neutrophil or macrophage engulfed denatured nuclear debris, could represent an inability to properly degrade phagocytosed contents (199, 200).

There are several lines of evidence that link dead cell clearance pathways to the development of systemic autoimmunity in mice and in humans. C1q, a component of the C1 complex, is critical for the classic complement pathway (201). Upon opsonization, C1q can bind

dead cells, facilitating uptake by macrophages (201). Over 90% of patients with loss of function mutations in C1q develop a SLE-like disease (202, 203). C1q deficient autoimmune and non-autoimmune mouse strains are subject to decreased survival, exacerbated renal disease, and autoantibody titers (204, 205). However, it should be noted that background genetics do alter this phenotype (204, 205). Apoptotic bodies have been identified in the glomeruli of C1q-deficient mice, further highlighting a defect in dead cell clearance in diseased animals (204).

Apoptotic cells transfer phosphatidylserine (PS) from the inner leaflet of the plasma membrane to the exterior where PS serves as a putative "eat me" signal to enhance engulfment by phagocytes. PS can be recognized by TIM (T cell immunoglobulin and mucin domain containing protein)-4, a member of the TIM family primarily expressed on antigen presenting cells, where it can bind to PS exposed on the surface of apoptotic bodies to mediate their uptake (206, 207). TIM-4 deficient macrophages cannot phagocytose apoptotic cells both *in vitro* and *in vivo* (90, 164, 201). Moreover, TIM-4-deficient mice develop antibodies to double-stranded DNA, as well, hyperactive T and B cells responses (201). Similar to TIM-4, membrane tyrosine kinase c-mer (MERTK) is implicated in dead cell clearance and autoimmune pathology (207). Growth arrest specific protein-6 (GAS6) is reported to be a ligand for MERTK that can bind to PS, mediating its role in apoptotic removal (208). Clearance of exogenous apoptotic cells is delayed in mice missing the intracellular kinase domain of MERTK (*C-Mer*^{kd}). *Mer*^{kd} C57BL/6 mice have a normal lifespan but do develop autoantibodies to DNA and mild renal disease (209).

SLE associated loss of function polymorphisms in Milk fat globule-EGF factor 8 (MFG-E8) further support a role for dead cell clearance in lupus (210). MFG-E8 is a glycoprotein abundantly expressed in lactating mammary glands and milk fat globules but also can be produced by macrophages where it can bind PS and mediate engulfment of dead cells via the

$\alpha_v\beta_3$ integrin (211). *Mfg-e8*$^{-/-}$ mice develop spontaneous autoimmunity characterized by the generation of anti-nuclear antibodies, splenomegaly, and glomerulonephritis (212). Concordantly, MFG-E8-deficient mice subjected to the pristane model of SLE develop more severe renal disease and diffuse alveolar hemorrhage (213). After pristane treatment *Mfg-e8*$^{-/-}$ mice have greater accumulation of apoptotic cells in the lung and peritoneum, a phenotype partially attributed to a failure to clear this debris (213). In this same study, MFG-E8 was elevated in the serum of lupus patients, a finding that needs to be reconciled. The authors postulate that high concentrations of MFG-E8 can inhibit engulfment of apoptotic cells (213).

CYBB is implicated in both cell death and subsequent clearance of debris by macrophages. CYBB deficiency is associated with SLE in both mouse and humans. The role of CYBB in SLE was discussed in chapter 3.

Taken together, these studies emphasize that an inadequate clearance of dead cells can result in an immune response to self and end-organ damage.

4.1.2 LC3-associated phagocytosis: A distinct process from canonical autophagy required for the clearance of dead cells

Canonical autophagy refers to a catabolic cell survival process, triggered under nutrient scarce conditions, whereby the cell can degrade and recycle component (214, 215). This process requires the assembly of a preinitiation complex comprised of ULK1, FIP200, and ATG13 that is triggered under starvation conditions by AMPK and mTOR-mediated phosphorylation of ULK1 (214-216) (217). ULK1 phosphorylates BECLIN-1, a member of the Class III PI(3)K family, resulting in the translocation of this complex to the autophagosome where it can generate phosphatidylinositol 3-phosphate (PtdIns(3)P) and mediate the activation of the ubiquitination-

like protein conjugation system (214). The ubiquitination-like protein conjugation system is responsible for the lipidation of microtubule associated protein 1A/1B–light chain 3 (LC3), which can translocate to autophagosome membrane (214).

LC3 associated phagocytosis (LAP) is a novel form of non-canonical autophagy implicated in the clearance and degradation of dead cells (164). LAP can occur in cell populations with phagocytic capacity including macrophages, dendritic cells, epithelial cells, and endothelial cells (218). Upon phagocytosis, cargo can be sensed by cell surface receptors, facilitating the recruitment of a subset of the autophagy machinery and subsequent conversion of LC3 to its lipidated form, LC3-II. LC-3II decorating the phagosomal membrane mediates lysosomal to phagosomal fusion and subsequent degradation of enclosed cargo (218). Several receptor classes are associated with the induction of LAP including: (1) pattern recognition receptors that recognize conserved moieties on pathogens, (2) immunoglobulin receptors that engage opsonized particles or cells, and (3) receptors that mediate dead cell clearance, such as, the TIM family (218). Strikingly, LAP can be induced in the context of MYD88 and TRIF deficiency, suggesting that these two critical adaptors, which are required for the signaling of all TLR family members are dispensable for LAP. The pathway that initiates LAP downstream of TLRs remains to be discovered (219).

There are several major distinctions between LAP and canonical autophagy. First, the phagosome associated with LAP or the “LAPosome” is a single membrane structure, while the autophagosome is enclosed by a double membrane (219). During LAP, the phagosome is fully sealed prior to the lipidation of LC3 and the ubiquitin conjugation system requisite for this process may still be attached to the membrane at its conclusion (219). However, LC3 is lipidated during autophagosome membrane elongation and the complex is released proximal to membrane

closure (220, 221). Autophagy requires activation of the preinitiation complex, but LAP does not require the preinitiation complex for its initiation or progression (89, 164). LAP utilizes a variant of the BECLIN1-VPS34 complex that does not require ATG14 (89). LC3 lipidation in both LAP and canonical autophagy require utilization of the ubiquitin-like conjugation system comprised of ATG7, ATG3, ATG5, ATG12, and ATG16L (89). There are two molecules required for LAP but not canonical autophagy: CYBB and RUBICON, the RUN domain as BECLIN-1 interacting and cysteine-rich containing protein. CYBB operates downstream of the Class III PI(3)K complex, producing ROS requisite for the recruitment of the conjugation system (89). The function of Rubicon in LAP will be discussed in the next section.

4.1.3 RUBICON: Structure and function in the immune system

RUBICON is a 972 amino acid (108.6 kDa) protein comprised of a RUN domain, an N-terminal serine-rich region (SR-N), a coiled-coil domain (CCD), a C-terminal serine- rich region (SR-C), a helix-coil-rich region (H-C), and a cysteine-rich region (C-R) (222). Studies report that RUBICON-GFP localizes to the late endosome/lysosome, though not to the autophagosome (89, 222, 223). Rubicon is a member of the Class III PI(3)K complex and can bind BECLIN-1 at its CCD domain (222, 223). Multiple groups demonstrated that knockdown or genetic deletion of *Rubicon* increases the number of autophagosomes, identifying RUBICON as a negatively regulator of canonical autophagy (89, 222, 223). It is postulated that RUBICON blocks autophagy at the maturation step where the autophagosome fuses to the endosome/lysosome (222, 223). More recently, Martinez and colleagues reported that RUBICON is required for LAP, by associating with the LAPasome but not conventional phagosomes (89). RUBICON has opposing roles in regulating VPS34, the phosphatidylinositol 3-kinase in the Class III PI(3)K complex, during autophagy and LAP. While RUBICON reduces the activity of VPS34 during autophagy (222), it is required for VPS34 function during LAP sustaining PtdIns(3)P presence on the LAPosome (89). Therefore, RUBICON may not only serve as a negative regulator of autophagy but as a switch between these two related processes.

RUBICON is also important for the regulation of the NADPH oxidase complex by both direct and indirect mechanisms. Upon initiation of LAP, Rubicon activates the class III PI3K complex to generate PtdIns(3)P which is important for the recruitment of the soluble oxidase component $p40^{phox}$ (89). Additionally, Rubicon is reported to directly bind to $p22^{phox}$, stabilizing the NADPH oxidase complex to facilitate its localization to the phagosome (89, 224). Intriguingly, BECLIN-1 and $p22^{phox}$ do not bind to the same region of RUBICON; BECLIN-1 binds to the CCD domain while $p22^{phox}$ associates with the SRC region (224). Indeed, Rubicon-deficient macrophages do not generate NADPH oxidase dependent ROS (89, 224).

The role of RUBICON in the regulation of cytokine production and signaling remains controversial and could be context dependent. There are several lines of evidence to suggest that Rubicon negatively regulates cytokine production and signaling. In one study, RUBICON was implicated in mediating immune responses downstream of the CARD9 dependent pathways, RIG-I and Dectin-1(224). Under homeostatic conditions RUBICON binds 14-3-3β. However, upon engagement of CARD9-dependent pattern recognition receptors (PRR), RUBICON is phosphorylated and disassociates from 14-3-3β, allowing it to bind to CARD9 (224). Interestingly, CARD9 and 14-3-3β bind Rubicon at distinct domains, the H-C region and the SR-N region respectively (224). This swap of binding partners leads to the disassembly of the CARD11-BCL10-MALT1 (CBM) signalosome complex and subsequent reduction of CBM dependent pro-inflammatory cytokine production (224). Recent reports suggest that RUBICON is a negative regulator of virus induced type I IFN signaling by binding IRF3 and preventing its dimerization (225). Discordant with these observations, shRNA mediated knockdown of RUBICON in bone marrow derived macrophages (BMDMs) and in RAW264.7 cells reduce proinflammatory cytokine production induced by zymosan, *Listeria monocytogenes*, and

Mycobacterium bovis BCG (224). Proinflammatory cytokine production requires Rubicon to associate with $P22^{phox}$, indicating Rubicon is likely promoting proinflammatory cytokine production via stabilization and activation of the NADPH oxidase complex (224). More recently, it was reported that the anti-inflammatory response to apoptotic cell engulfment requires RUBICON and LAP (90). *Rubicon*-deficient macrophages generate proinflammatory cytokines in response to phagocytosis of apoptotic cells (90). Moreover, *Rubicon*-deficient mice have elevated levels of IL-1β, IL-6, IL-12p40, IP10 by 24 weeks of age (90). These discordant observations emphasize that the function of Rubicon in cytokine production is unclear and requires further investigation.

RUBICON has divergent roles in host defense. Clearance of *Aspergillus fumigatus* is impaired in the context of *Rubicon* deficiency (89). The authors attribute this phenotype to a failure in LAP as genetic deletion of other LAP mediators recapitulated this finding (89). Similarly, in *Listeria monocytogenes* infection, shRNA-mediated knockdown of RUBICON *in vivo* was deleterious to the host, resulting in decreased proinflammatory cytokine production, increased pathogen burden, and decreased survival (224). However, knockdown of RUBICON in the setting of *Candida albicans* infection and influenza had the opposite effect and protected the host, increasing survival. In these contexts, proinflammatory cytokine production was elevated and pathogen burden reduced upon shRNA mediated knockdown of RUBICON *in vivo (224)*. Taken together, the structure of RUBICON positions it to be a pleiotropic modulator of cytokine regulation able to adapt to the context of the pathogen assault.

4.1.4 LAP and autophagy in SLE

Genetic variations of several components shared by LAP and canonical autophagy are associated with systemic autoimmunity in human patients and in mice. Genome wide association studies (GWAS) suggest that the PRDM1-ATG5 gene region is associated with SLE in both Caucasian and Chinese populations (226). Interestingly, one study suggested that the risk associated with ATG5 mutations is dependent on IL-10 genotype (227). SLE patients homozygous for the rs573775 (C to T) SNP in the ATG5 gene had higher levels of serum IL-10 but lower levels of IFNα (227). Further analysis revealed that the rs573775 T allele was only a risk factor for SLE in people who were also carriers of a polymorphism in IL-10 that conferred increased IL-10 production (227). SLE patients who were concomitant high IL-10 producers and carriers of the rs573775 T allele had a significantly lower prevalence of cytopenia and a trend of reduced renal manifestations of disease (227). More recently, gain of function polymorphisms in LC3 were associated with SLE in Chinese populations. LC3 gene expression was increased in peripheral blood mononuclear cells (PBMCs) from SLE patients compared to healthy controls (208). Moreover, LC3-II protein was elevated in lymph nodes from MRL.Fas^{lpr} SLE prone mice (208).

Recently, Martinez and colleagues showed that genetic deletion of components implicated in LAP only (*Rubicon* and *Cybb*) or LAP and canonical autophagy (*Beclin1*, *Atg5*, and *Atg7*) led to an autoinflammatory syndrome in non-autoimmune strains (90). LAP-deficient C57BL/6 mice spontaneously developed elevated titers of autoantibodies and renal disease (90). Interestingly, increased levels of proinflammatory cytokines were present in the serum of LAP-deficient mice but anti-inflammatory cytokines, such as, IL-10 were reduced (90). The authors postulates that in the absence of LAP, dead cells are not cleared in an immunologically silent way as cell corpse degradation is impaired and that the inability to generate IL-10 downstream of

LAP is a major driver of the disease phenotype (90). However, one cannot exclude the possibility that an inability to degrade cell corpses could frustrate further clearance of dead cells, leading to the accumulation of self antigen. Strikingly, mice deficient in components only implicated in canonical autophagy (ULK1 and FIP200) did not develop systemic autoimmunity with age, suggesting that LAP but not canonical autophagy is required to prevent autoimmunity (90).

4.1.5 IL-10 and SLE

IL-10 is pleotropic cytokine that signals through a heterodimeric receptor composed of inducible IL-10R1 and constitutively expressed IL-10R2 (228). Upon receptor engagement, JAK1 and TYK2 are recruited to the IL-10 receptor where they can facilitate STAT3 homo/hetero dimer activation and translocation to the nucleus where STATs can serve as transcription factors (228). IL-10 is expressed in most immune cells including T cells, B cells, NK cells, DCs, macrophages, and granulocytes (228). Multiple immunosuppressive mechanisms have been ascribed to IL-10 including repression of cell proliferation, suppression of proinflammatory cytokine production, reduction in antigen presentation and expression of co-stimulatory molecules, and prevention of class switching by B cells (228).

While IL-10 is generally thought to suppress the immune response, there are circumstances, especially in the context of inflammation, where it can take on pro-inflammatory properties. One study suggests that IFNγ can reprogram IL-10 activity and signaling conferring proinflammatory function (229). This study reported that IFNγ switches the balance of IL-10 STAT activation from STAT3 to STAT1, resulting in the expression of proinflammatory genes (229). Under these circumstances, IL-10 no longer prevents suppression of cytokine production

or reduction in MHCII expression (229). IL-10 was also suggested to increase proliferation and cytotoxic activity of $CD8^+$ T cells and NK cells (230-232). In B cells, IL-10 has been shown to enhance MHCII expression, promote increased antibody secretion, and increase both survival and proliferation in vitro (233-236). However, these findings have not been confirmed in vivo.

The function of IL-10 in SLE and its cellular source remains an open question. Gain of function polymorphisms in the IL-10 promoter are associated with SLE in European populations (237, 238). Elevated levels of IL-10 are observed in SLE patients and associated with disease activity (239). In this context, it is possible that increased IL-10 expression serves as a feedback mechanism to ameliorate rampant inflammation. Surprisingly, continuous administration of anti-IL10 antibodies delayed onset of autoimmunity in the NZB/W F1 spontaneous mouse model of SLE (240). This observation was also recapitulated in a small study of human lupus patients. Here, anti-IL-10 administered to six human lupus patients with active disease led to a reduction in disease activity (241). These studies implicate IL-10 as pathogenic in lupus.

In contrast, some studies support a regulatory role of IL-10 in autoimmunity. IL-10 deficient mice on a non-autoimmune background develop inflammatory bowel disease. Genetic deletion of IL-10 in the MRL.Fas^{lpr} model of SLE reduced survival and exacerbated renal manifestations of lupus (242). Supporting this finding, low dose overexpression of IL-10 in the spontaneous B6.Sle1.Sle2.Sle3 model, in which 3 SLE loci derived from the NZM2410 autoimmune prone strain were crossed onto the C57BL/6 background, delayed the formation of autoantibodies and reduced the severity of renal disease (243). B cell-produced IL-10 has been implicated in autoimmune diseases including SLE (244). The role of B cell derived IL-10 in SLE was tested by our group using a Cre-lox approach to specifically knockout IL-10 in B cells in the MRL.Fas^{lpr} model (245). However, B cell-specific IL-10 deletion did not impact clinical or

immunological manifestations of SLE (245). To determine the cellular source of IL-10 in SLE, our group crossed MRL.Fas^{lpr} mice to the *10BiT* reporter strain, where *Thy-1.1* expressed under the control of an *Il10* promoter marks cells that transcribe *Il10* (245). This study revealed that T cells and macrophages are the primary IL-10 producers in SLE prone mice (245). As noted above, IL-10 is not produced upon the engulfment of dead cells by macrophages that have a defect in LAP. IL-10 production was suggested to be requisite for prevention of autoimmune manifestations in the setting of defective LAP (90). To date, the role of IL-10 in SLE remains controversial and requires further exploration.

4.1.6 An approach to investigate whether *Cybb* deficiency exacerbates SLE by a defect in LAP

While evidence suggests that blocking non-canonical autophagy can drive an anti-self response in a non-autoimmune setting, its role in SLE remains enigmatic. As NADPH oxidase is required for LAP, it is possible that the exacerbated disease observed in the context of *Cybb* deficiency is due to inhibition of this process. Here, we aimed to determine whether *Cybb* deficiency exacerbates SLE by prevention of dead cell clearance due to a defect in LAP and subsequent inhibition of anti-inflammatory cytokine production. We addressed this question by genetically deleting another requisite component for LAP, Rubicon, in the MRL.Fas^{lpr} lupus model. To determine whether CYBB and RUBICON act in the same pathway (ie LAP), we performed an in vivo complementation experiment, analyzing *Cybb* and *Rubicon* single and double knockout mice in the setting of lupus. Furthermore, we elucidated the function of IL-10 expressed in myeloid cell in SLE using a Cre-lox approach.

4.2 EVALUATION OF THE ROLE OF RUBICON IN SLE PATHOGENESIS

To investigate the role of Rubicon in systemic autoimmunity, we generated a Rubicon-deficient mouse on the MRL.Fas^{lpr} background using CRISPR-Cas9 technology. Heterozygous knockout mice were intercrossed to produce an experimental cohort. SLE pathology was analyzed at 17 weeks of age. If *Cybb* deficiency promotes lupus by a defect in LAP, we expect that *Rubicon*$^{-/-}$ and *Rubicon*$^{-/-}$ *Cybb*$^{-/-}$ MRL.Fas^{lpr} mice to develop exacerbated manifestations of SLE.

4.2.1 Generation of the *Rubicon*$^{-/-}$ on the MRL.Fas^{lpr} background using CRISPR-Cas9

The *Rubicon* knockout allele was generated directly on the MRL.Fas^{lpr} background using *in vitro* fertilization coupled with CRISPR-Cas9 technology as previously described and detailed in the materials and methods (Figure 41A) (89, 185). In brief, a premature stop codon replacing Asp188 was introduced in exon 5 of the *Rubicon* gene by homology directed repair following injection of *in vitro* generated MRL.Fas^{lpr} pronuclear-stage zygotes with capped Cas9 mRNA, a sgRNA targeting the end of exon 5, and a 183-nucleotide-long ssODN that served as a repair template. To facilitate screening of founder mice, an EcoRI restriction site was introduced adjacent to the stop codon. 42% of the mice born had at least one sequence confirmed copy of the integrated repair construct at the cut site (Figure 41B). We confirmed that RUBICON protein was absent in the spleens and bone marrow of Rubicon-deficient mice (Figure 41C).

4.2.2 *Rubicon* deficiency reduced SLE renal disease in MRL.Fas^{lpr} mice

Rubicon-deficient male and female MRL.Fas^{lpr} mice have reduced urine protein compared to wild-type controls (Figure 42A). No differences in dermatitis were identified amongst the groups (Figure 42B). While *Rubicon* genotype did not alter glomerulonephritis (Figure 42C) in MRL.Fas^{lpr} mice, interstitial nephritis was ameliorated in *Rubicon*$^{-/-}$ males with a trend towards reduction in females (Figure 42C). Spleen weight was decreased in in *Rubicon*$^{-/-}$ male and female lupus-prone mice (Figure 43A). However, no differences in lymphadenopathy were observed across the groups (Figure 43B).

4.2.3 RUBICON regulates the anti-RNA and anti-Sm response

Rubicon deficiency reduced anti-RNA titers in both male and female MRL.Fas^{lpr} mice (Figure 44A). Strikingly, anti-Sm autoantibodies were absent from male *Rubicon*$^{-/-}$ MRL.Fas^{lpr} mice (Figure 44B and C). Only one out of 19 female *Rubicon*$^{-/-}$ MRL.Fas^{lpr} mice had positive anti-Sm titer (Figure 44B and D). Intriguingly, no differences in anti-nucleosome (Figure 44E) or RF (Figure 44F) titers were identified between the groups.

4.2.4 The percentages of plasmablasts were decreased in *Rubicon*$^{-/-}$ MRL.Fas^{lpr} mice

Rubicon-deficient mice did not have any changes to the percentage of CD19+ B cells in comparison to wild-type mice (Figure 44G). However, CD19$^{low\text{-}int}$ CD44^{+} CD138^{+} intracellular κ^{high} AFCs were reduced in *Rubicon*-deficient male and female MRL.Fas^{lpr} cohorts compared to controls (Figure 44H).

4.2.5 *Rubicon* deficiency did not impact the myeloid compartment in SLE prone mice

Rubicon genotype had only a minor impact on the myeloid compartment in MRL.Fas^{lpr} mice. The percentages of CD11b^{+}Ly6G^{+} splenic neutrophils (Figure 45A) and CD11b^{+}F4/80^{+}Gr1$^{low\text{-}int}$ splenic macrophages (Figure 45B) were not statistically different across *Rubicon* genotype. *Rubicon*-deficient MRL.Fas^{lpr} females had a greater percentage of CD19^{-}CD11c^{+}MHCII^{+} cDCs (Figure 45C). Additionally, male *Rubicon*$^{-/-}$ MRL.Fas^{lpr} mice had a lower percentage of CD19^{-} BST2^{+} SiglecH^{+} pDCs (Figure 45D) compared to Rubicon-sufficient controls.

4.2.6 RUBICON did not alter the T cell compartment in MRL.Fas^{lpr} mice

Rubicon deficiency did not substantially impact the lymphoid compartment. All genotypes exhibited indistinguishable total percentages of TCRβ^{+} T cells (Figure 46A). The percentages of CD4^{+} T cells and CD4^{+}CD44^{+}CD62L^{-} activated T cells were also not significantly different across all groups (Figure 46B). Similar results were obtained for naive and activated CD8^{+} T cells (Figure 46C).

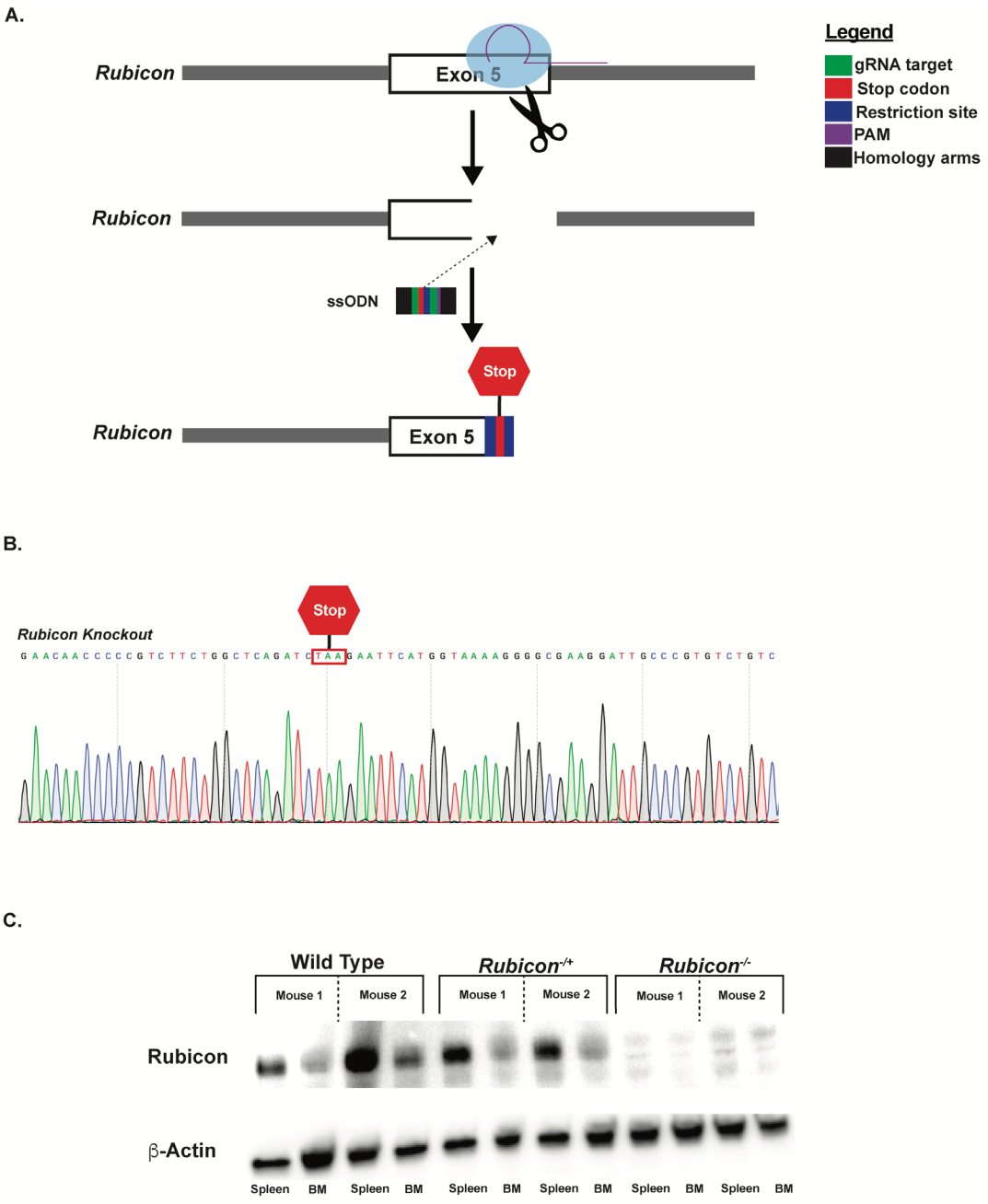

Figure 41. Generation of the *Rubicon* knockout mouse on the MRL.Fas^{lpr} background using CRISPR-Cas9 and *in vitro* fertilization.

(A) CRISPR-Cas9 strategy to generate the *Rubicon* knockout allele. (B) Sequencing chromatogram depicting the stop codon in the *Rubicon*-knockout MRL.Fas^{lpr} founder (C) Western blot analysis of spleen and bone marrow from *Rubicon*$^{+/+}$, *Rubicon*$^{+/-}$, and *Rubicon*$^{-/-}$ MRL.Fas^{lpr} mice.

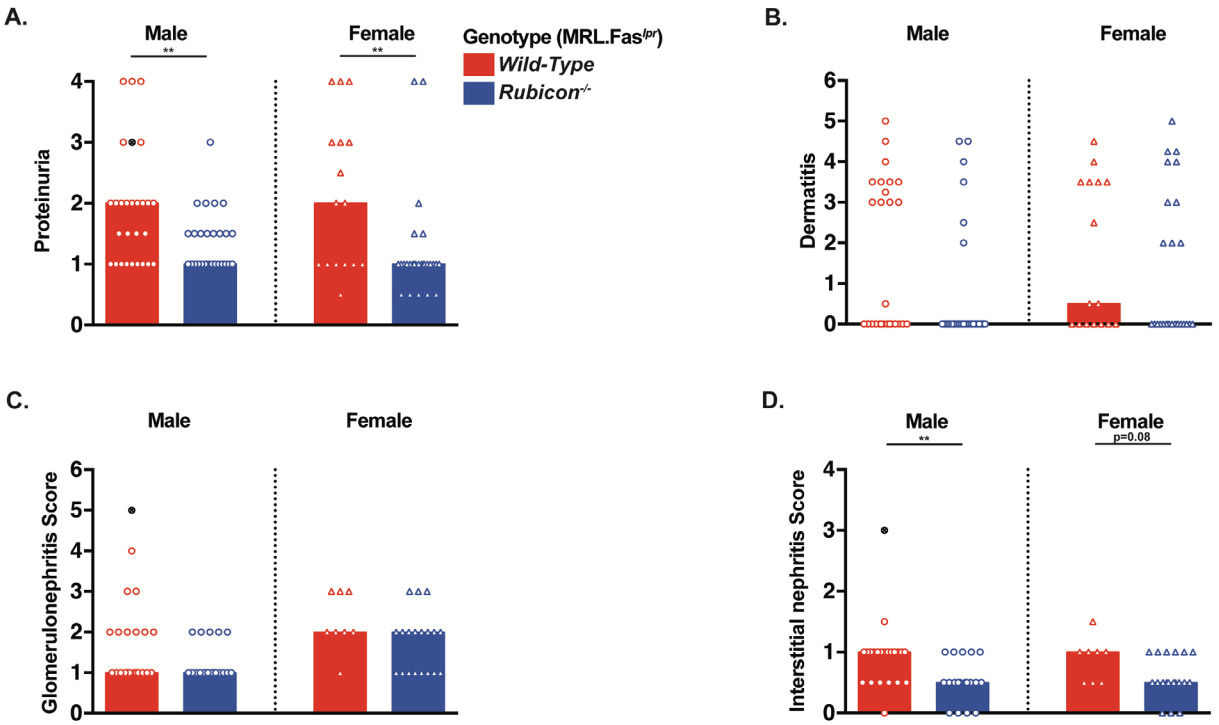

Figure 42. *Rubicon* deficiency reduced SLE renal disease in MRL.Fas^{lpr} mice.
(A) Proteinuria. **(B)** Dermatitis. **(C)** Glomerulonephritis scores. **(D)** Interstitial nephritis scores. **(E)** Spleen Weight. **(F)** Axillary lymph node weights. Scores and weights are represented as a function of *Rubicon*-genotype and gender at 18 weeks of age. Bars represent the median and each dot represents and individual mouse. A Mann-Whitney U test was performed to determine statistical significance within each gender (* indicates $p \leq 0.05$, ** $p \leq 0.01$, *** $p \leq 0.001$, and **** $p \leq 0.0001$; n=8 to 29 mice per group; ⊗ and ☒ denote deceased animals).

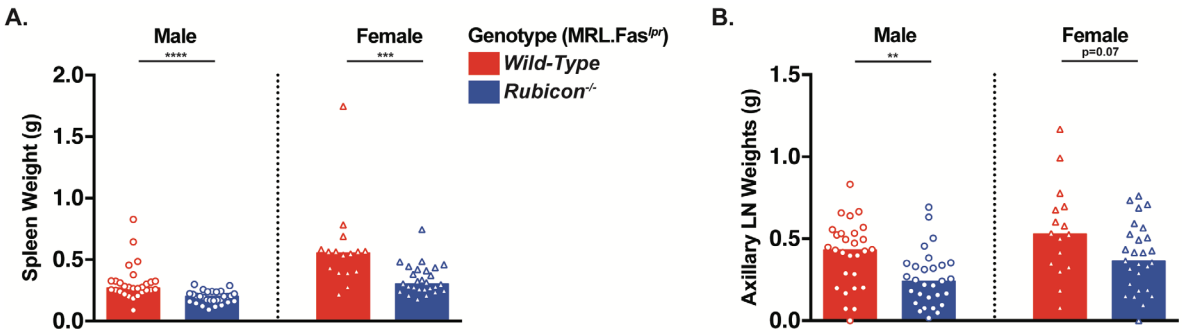

Figure 43. Decreased spleen and lymph nodes weights in *Rubicon*-deficient SLE prone mice.
(A) Spleen weight. **(B)** Axillary lymph node weights. Data representation, and statistics are as in Figure 42.

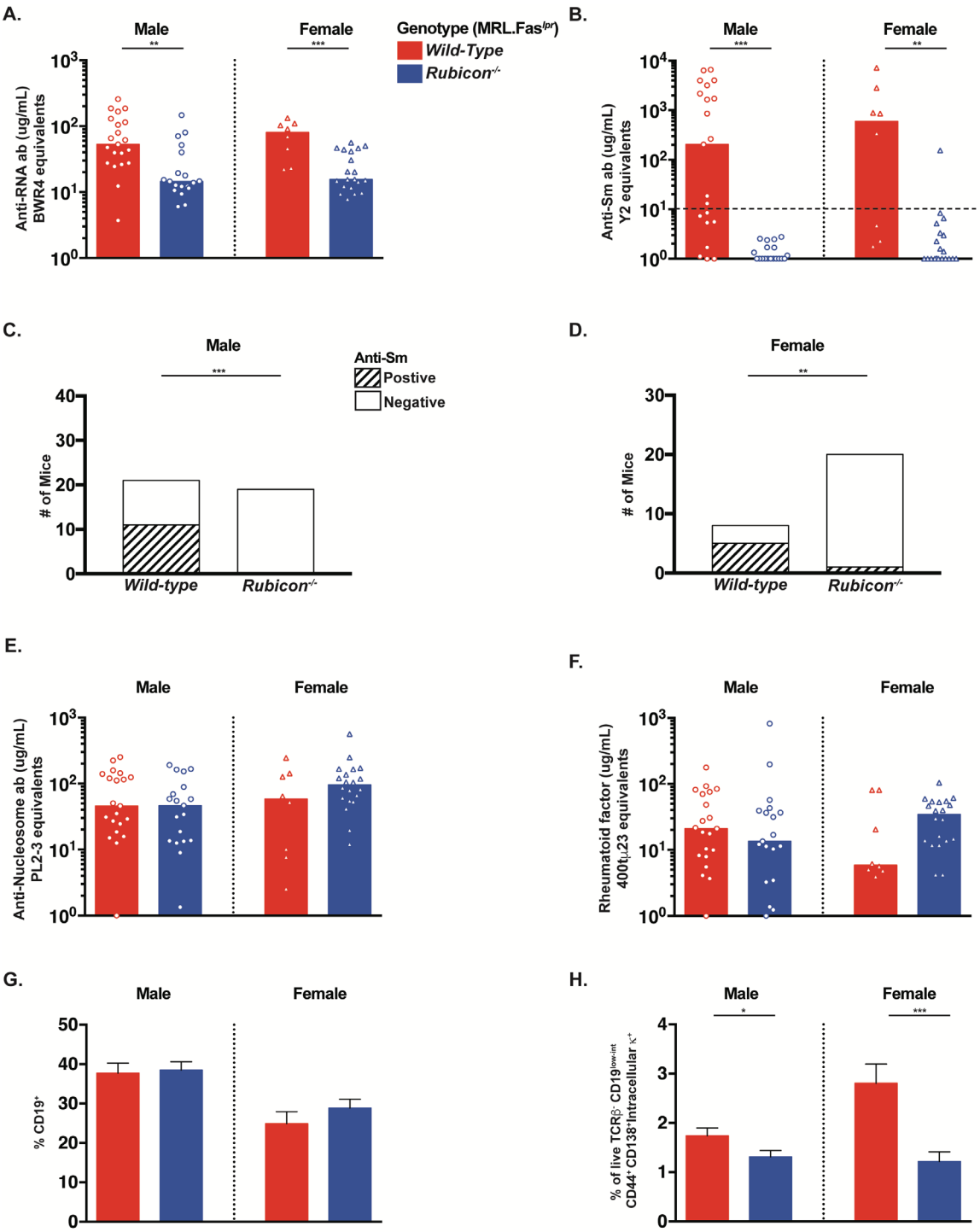

Figure 44. *Rubicon* deficiency altered the anti-self response in MRL.Fas^{lpr} mice.
(A and B) Serum anti-RNA (A), anti-Sm (B) titers. **(C and D)** Number of male (C) and female (D) mice with positive anti-Sm titers. The dotted line in B represents the positive threshold. **(E and F)** Serum anti-nucleosome antibody (E) and rheumatoid factor titers (E). **(G)** Percentages of live CD19$^+$ total B cells. **(H)** Percentages of live cells that are TCRβ$^-$ CD44$^+$ CD138$^+$ intracellular κ$^+$ antibody forming cells. FCs. Data representation, number of mice, and statistics are as in Figure 42. In panels E and F, bar graphs are represented as the mean ± SEM and a two-tailed Welch's T test was performed to determine statistical significance within each gender. In panels C and D, a Fisher's exact test was used to determine statistical significance (* indicates p≤0.05, ** p≤0.01, *** p≤0.001, and **** p≤0.0001; n=8 to 20 mice per group).

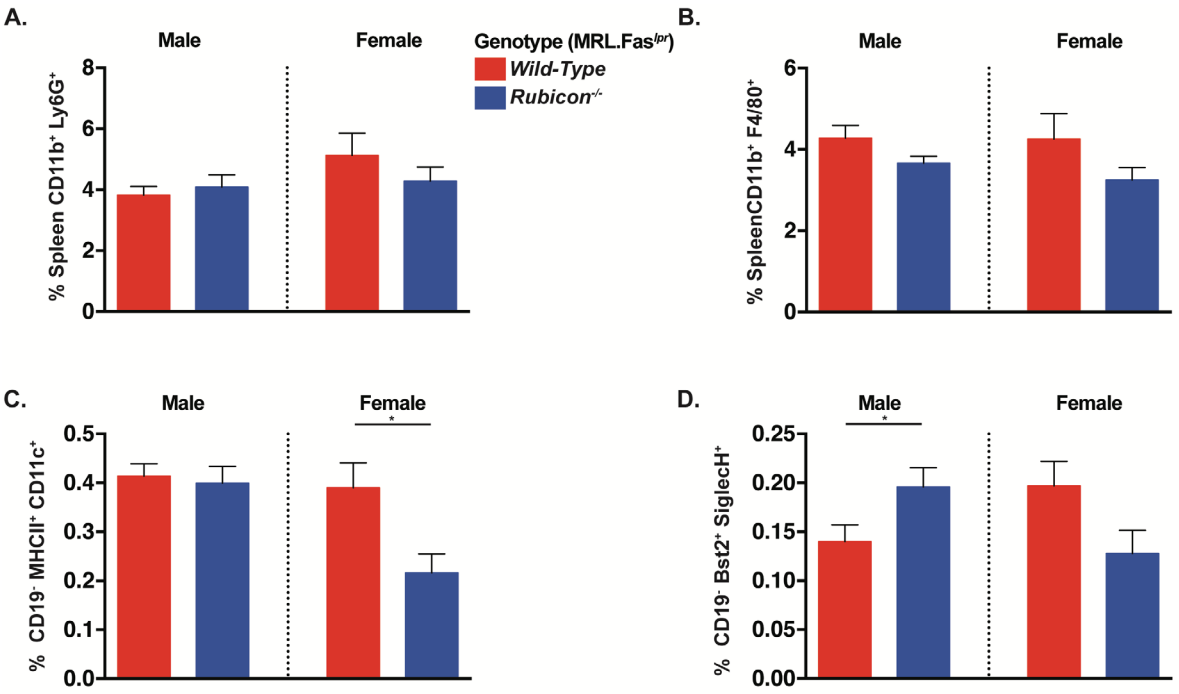

Figure 45. The composition of the myeloid compartment was not altered in *Rubicon*-deficient mice
(A) Percentages of live $CD11b^+$ $Ly6G^+$ neutrophils in the spleen. **(B)** Percentages of splenic $CD11b^+$ $GR1^{low\text{-}int}$ $F4/80^+$ macrophages. **(C)** Percentages of live $CD19^-$ $MHCII^+$ $CD11c^+$ conventional dendritic cells and **(D)** $CD19^-$ $BST2^+$ $CD11c^+$ plasmacytoid dendritic cells. Bar graphs are represented as the mean ± SEM and a two-tailed Welch's T test was performed to determine statistical significance within each gender (* indicates $p \leq 0.05$, ** $p \leq 0.01$, *** $p \leq 0.001$, and **** $p \leq 0.0001$; n=8 to 20 mice per group).

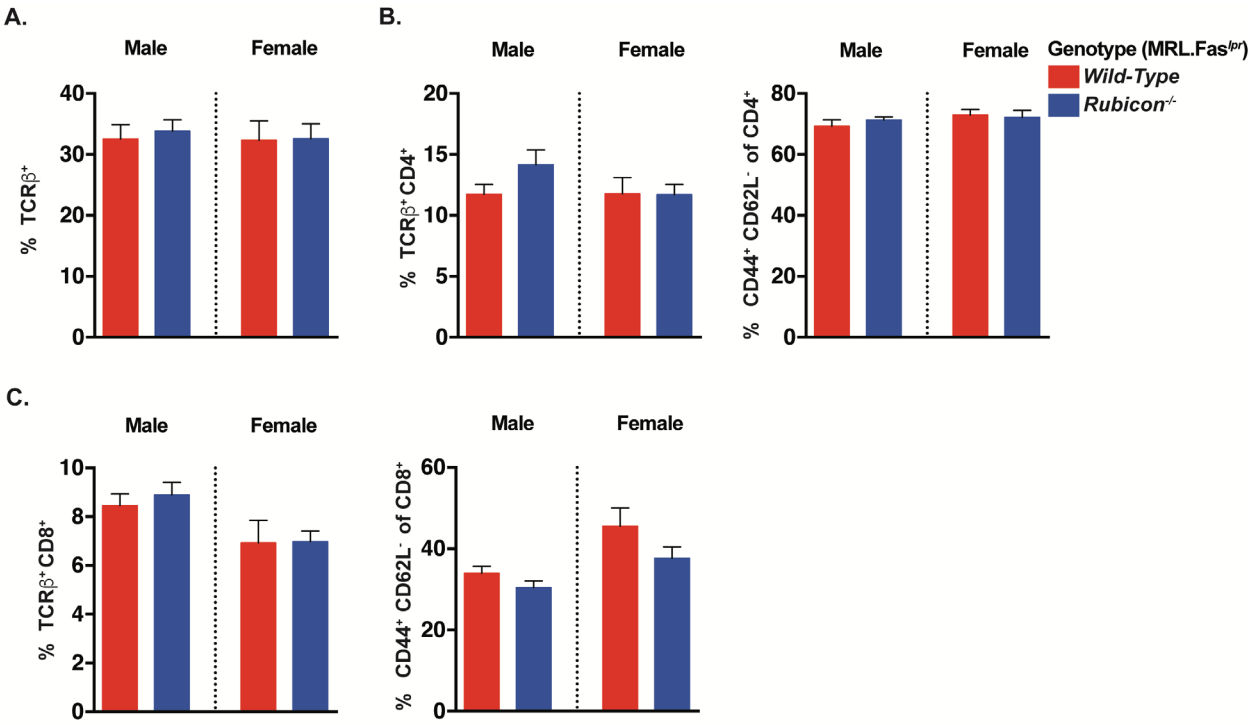

Figure 46. *Rubicon* deficiency did not alter the T cell compartment in lupus prone mice.
(A) Percentages of live TCRβ$^+$ total T cells. **(B)** Percentages of live TCRβ$^+$ CD4$^+$ T cells (left panel) and of CD4$^+$ CD44$^+$ CD62L$^-$ activated T cells (right panel). **(C)** Percentages of live TCRβ$^+$ CD8$^+$ T cells (left panel) and of CD8$^+$ CD44$^+$ CD62L$^-$ activated T cells (right panel). Data representation, number of mice, and statistics are as in Figure 45.

4.3 CHARACTERIZATION OF RUBICON IN THE SETTING OF CYBB DEFICIENCY IN SLE

Given the reported interplay between RUBICON and CYBB and their role in LAP, we sought to determine how *Rubicon*-deficiency modulates disease in the context of *Cybb* genetic deletion. We generated cohorts of *Rubicon* and *Cybb* single and double knockouts by performing the following crosses: 1. *Rubicon*$^{+/-}$ *Cybb*$^{y/-}$ X *Rubicon*$^{+/-}$*Cybb*$^{+/-}$, 2. *Rubicon*$^{+/-}$ *Cybb*$^{y/+}$ X *Rubicon*$^{+/-}$ *Cybb*$^{+/-}$, and 3. *Rubicon*$^{+/-}$ *Cybb*$^{y/+}$ X *Rubicon*$^{+/-}$*Cybb*$^{+/+}$. SLE pathology was analyzed at 17-18 weeks of age. Autoimmune-prone mice with a global defect in NADPH oxidase prematurely succumb to renal failure as the primary cause of death. This was again observed in our cohort. We nonetheless allowed the cohort to age to 17-18 weeks to better assess the effects of concomitant *Rubicon* deficiency. In order to prevent the deaths of *Cybb*$^{-/-}$ mice from artificially skewing the scores for kidney disease, we assigned these subjects the second highest proteinuria, glomerulonephritis and interstitial nephritis scores.

4.3.1 *Rubicon* deficiency reduced mortality in *Cybb*-deficient MRL.Fas^{lpr} mice

Consistent with the prior literature, in our cohort, the male and female *Cybb*-deficient MRL.Fas^{lpr} mice had a reduced lifespan compared to *Cybb*-sufficient controls. 50% or more of the experimental *Cybb*$^{-/-}$ cohort did not survive until the experimental endpoint of 17 weeks (Figure 47). Surprisingly, *Rubicon*-deficiency did not recapitulate the phenotype observed in the *Cybb*$^{-/-}$ MRL.Fas^{lpr} mice as no *Rubicon*-deficient mice died in the analyzed cohorts (Figure 47). Strikingly, Rubicon deficiency increased survival in male *Cybb*$^{-/-}$ and trended towards protection in female MRL.Fas^{lpr} mice (Figure 47; bottom panel).

4.3.2 *Rubicon* deficiency protected *Cybb*$^{-/-}$ SLE prone mice from exacerbated renal disease.

Genetic deletion of *Rubicon* reduced proteinuria in male and female *Cybb*-deficient SLE prone mice (Figure 48A). No differences in dermatitis were observed in either group (Figure 48B). Concordant with the proteinuria data, *Rubicon*-deficiency reduced both glomerulonephritis (Figure 48C and E) and interstitial nephritis (Figure 48D and E) in *Cybb*-deficient male and female MRL.Fas^{lpr} mice. Rubicon deficiency reduced spleen weight in *Cybb*$^{-/-}$ male mice MRL.Fas^{lpr} mice (Figure 49A). No changes in axillary lymph node weights were found (Figure 49B).

4.3.3 *Rubicon* deficiency abrogates the anti-Sm responses in *Cybb*-deficient MRL.Fas^{lpr} mice

We previously showed that *Cybb* deficiency increases the anti-RNA and anti-Sm response in SLE prone mice. Discordant with these observations *Rubicon*$^{-/-}$ mice have reduced responses to RNA and Sm antigen. We identify a trend towards decreased anti-RNA titers in male *Rubicon*$^{-/-}$ *Cybb*$^{-/-}$ MRL.Fas^{lpr} mice (Figure 50A). Strikingly, *Rubicon* deficiency abolishes the anti-Sm response in male *Cybb*$^{-/-}$ lupus prone mice (Figure 50B and C). Similar to what we observed in the male cohort, only 1/7 female *Rubicon*$^{-/-}$*Cybb*$^{-/-}$ female MRL.Fas^{lpr} mice had positive Anti-Sm titers (Figure 50B and D). No differences in anti-nucleosome (Figure 50E) or RF (Figure 50F) titers were identified between the *Cybb*$^{-/-}$ and *Rubicon*$^{-/-}$*Cybb*$^{-/-}$ cohorts. While no changes in the percentage of total CD19^{+} B cells (Figure 50G) was observed between groups, male *Rubicon*$^{-/-}$

Cybb$^{-/-}$ did have reduced CD19$^{low\text{-}int}$ CD44^{+} CD138^{+} intracellular κ^{high} AFCs (Figure 50H) compared to *Cybb*$^{-/-}$ SLE prone mice.

4.3.4 *Rubicon* deficiency decreased splenic macrophage expansion in female *Cybb*$^{-/-}$ SLE prone mice

Others and we have previously reported that global and hematopoietic NADPH oxidase deficiency leads to an expansion of the myeloid compartment in both autoimmune and non-autoimmune mouse strains (75, 82, 137). *Rubicon* genotype had only a minor impact on the myeloid compartment in *Cybb*-deficient MRL.Fas^{lpr} mice. All genotypes exhibited similar frequencies of CD11b^{+}Ly6G^{+} splenic neutrophils (Figure 51A) among the groups. Interestingly, Rubicon deficiency reduced the percentage of macrophages in female *Rubicon*$^{-/-}$*Cybb*$^{-/-}$ mice (Figure 51B). We did not identify and differences in the total percentage of splenic cDCs (Figure 51C) and pDCs (Figure 51D) between the groups.

4.3.5 RUBICON has a minimal impact on the T cell response in *Cybb*-deficient MRL.Fas^{lpr} mice

Rubicon deficiency did not alter the lymphoid compartment in *Cybb*$^{-/-}$ SLE prone mice. No statistically significant differences in the total percentage of TCRβ^{+} T cells (Figure 52A) were observed. The percentages of CD4^{+} T cells and CD4^{+}CD44^{+}CD62L^{-} activated T cells were also not divergent across all groups (Figure 52B). Similarly, no change in the percentage of naive and activated CD8^{+} T cells was identified between *Cybb*$^{-/-}$ and *Rubicon*$^{-/-}$*Cybb*$^{-/-}$ SLE prone mice (Figure 52C).

4.3.6 Peritoneal and bone marrow derived macrophages derived from *Rubicon*- and *Cybb*-deficient mice lipidate LC3 in response to zymosan bioparticles

Previous literature implicated RUBICON and CYBB as required for LAP and that "LAP"-deficient mice on a non-autoimmune background develop a SLE-like disease (89, 90). To confirm that LAP does not occur in *Cybb* and *Rubicon*-deficient macrophages, we generated BMDMs from 6-8 week old *Cybb*$^{-/-}$ and *Rubicon*$^{-/-}$ MRL.Fas^{lpr} mice and stimulated them with zymosan bioparticles to initiate LAP. Upon the induction of LAP, LC3 is converted to its lipidated form, LC3-II on the LAPasome membrane. This step is reported to be downstream of, and hence require, both NADPH oxidase and RUBICON. To our surprise, both *Cybb* and *Rubicon*-deficient BMDMs could lipidate LC3, a surrogate readout for LAP (Figure 53 A). These findings were recapitulated in peritoneal macrophages isolated from young Pre-autoimmune (6-8 week old) *Cybb*$^{-/-}$ and *Rubicon*$^{-/-}$ MRL.Fas^{lpr} mice (Figure 53A). Reports suggest that LC3 is elevated in autoimmune patients and in autoimmune mouse strains at disease endpoints. To further investigate this, we stimulated peritoneal macrophages isolated from 18 week old wild-type, C*ybb*$^{-/-}$, *Rubicon*$^{-/-}$, and *Cybb*$^{-/-}$ *Rubicon*$^{-/-}$ MRL.Fas^{lpr} mice (Figure 53B). We did not observe consistent increased protein expression of LC3 at baseline. Again, zymosan stimulation led to the lipidation of LC3 in all conditions. It was possible that strain differences alter the requirements for CYBB and RUBICON in LAP, as the original observations that LAP was dependent on NADPH oxidase and Rubicon were made in C57BL/6 mice. To address this issue, we stimulated BMDMs from *Cybb*$^{-/-}$ C57BL/6 mice with zymosan bioparticles. Similar to the situation in MRL.Fas^{lpr} mice, LC3 was lipidated under these conditions (Figure 53C) in cells derived from C57BL/6 mice. Of note, we used rapamycin and starvation to induce canonical

autophagy as a positive control. In our hands, these conditions led to only some weak and variable LC3 lipidation, which we attribute to significant cell death observed in these cultures.

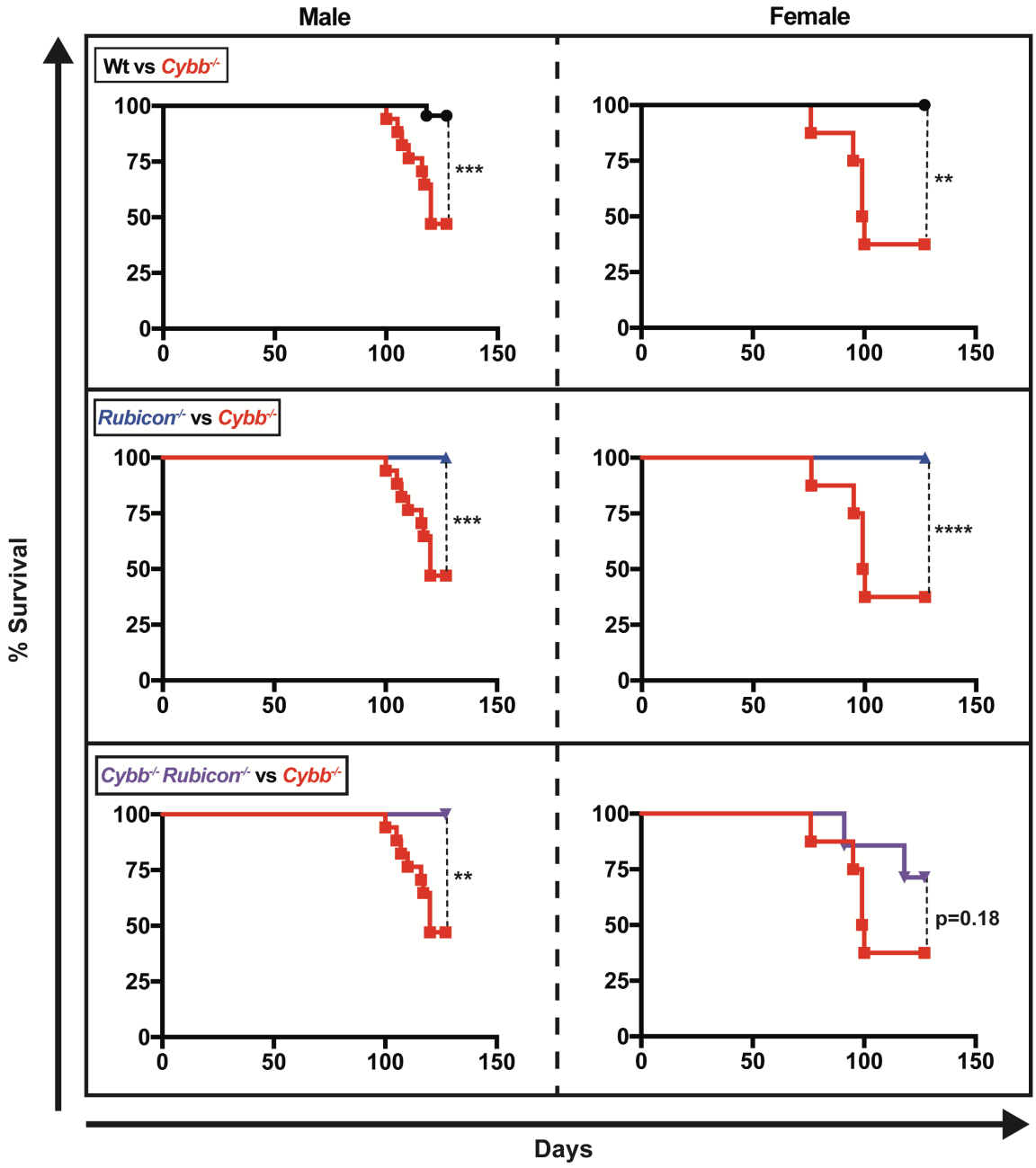

Figure 47. Rubicon deficiency conferred a survival advantage in *Cybb*-deficient MRL.Fas^{lpr} mice.
Kaplan-Meir survival curves of the following comparisons: wild-type vs. *Cybb*$^{-/-}$ (top panel), *Cybb*$^{-/-}$ vs. *Rubicon*$^{-/-}$ (middle panel), and *Cybb*$^{-/-}$ vs. *Cybb*$^{-/-}$*Rubicon*$^{-/-}$ (lower panel). Data are segregated by gender with males on the left and females on right. A log rank test was used to determine statistical significance (* indicates p≤0.05, ** p≤0.01, *** p≤0.001, and **** p≤0.0001; n=8 to 23 mice per group).

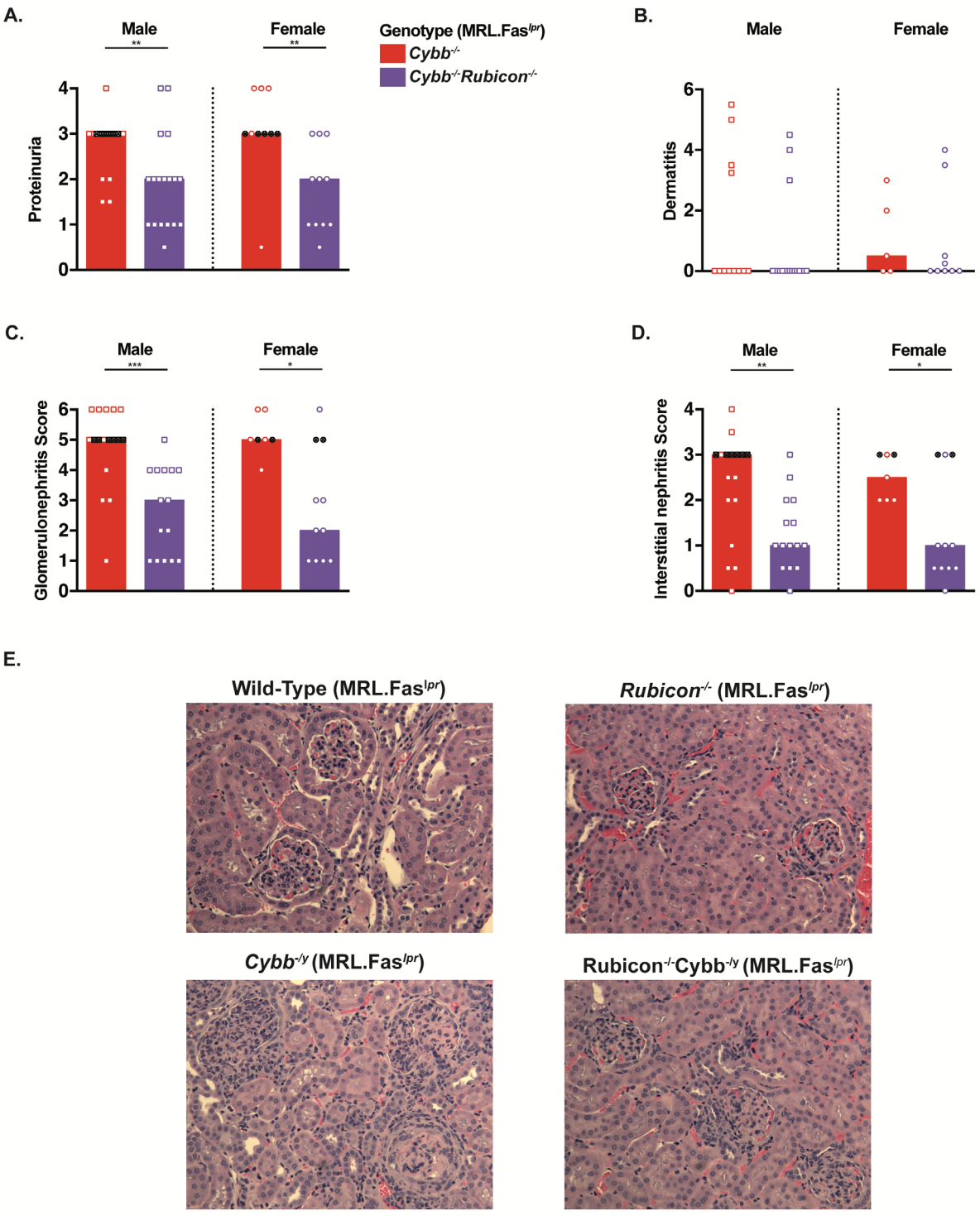

Figure 48. Rubicon deletion decreases exacerbated renal disease in *Cybb*-deficient MRL.Fas^{lpr} mice.
(A) Proteinuria. **(B)** Dermatitis. **(C)** Glomerulonephritis scores. **(D)** Interstitial nephritis scores. **(E)** Representative images of H&E-stained kidney sections showing glomeruli and interstitial infiltrates from wild-type (top left), *Rubicon*$^{-/-}$ (top right), *Cybb*$^{-/-}$ (bottom left), and *Rubicon*$^{-/-}$*Cybb*$^{-/-}$ (bottom right) MRL.Fas^{lpr} mice. Scores are represented as a function of *Rubicon*- and *Cybb*-genotype and gender at 18 weeks of age. Bars represent the median and each dot represents and individual mouse. A two-tailed Mann-Whitney U test was performed to determine statistical significance within each gender (* indicates $p \leq 0.05$, ** $p \leq 0.01$, *** $p \leq 0.001$, and **** $p \leq 0.0001$; n=7 to 29 mice per group; ⊗ and ☒ denote deceased animals).

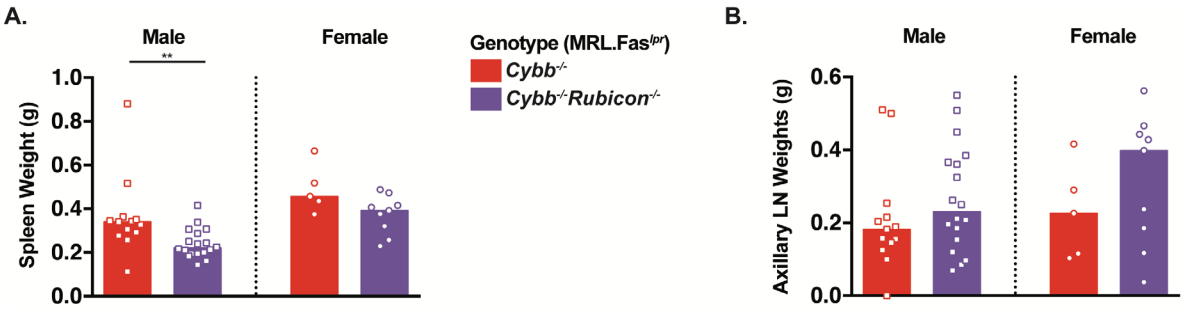

Figure 49. Decreased spleen weight in *Rubicon*$^{-/-}$*Cybb*$^{-/-}$ SLE prone mice.
(A) Spleen weight. **(B)** Axillary lymph node weights. Data representation, number of mice, and statistics are as in Figure 48.

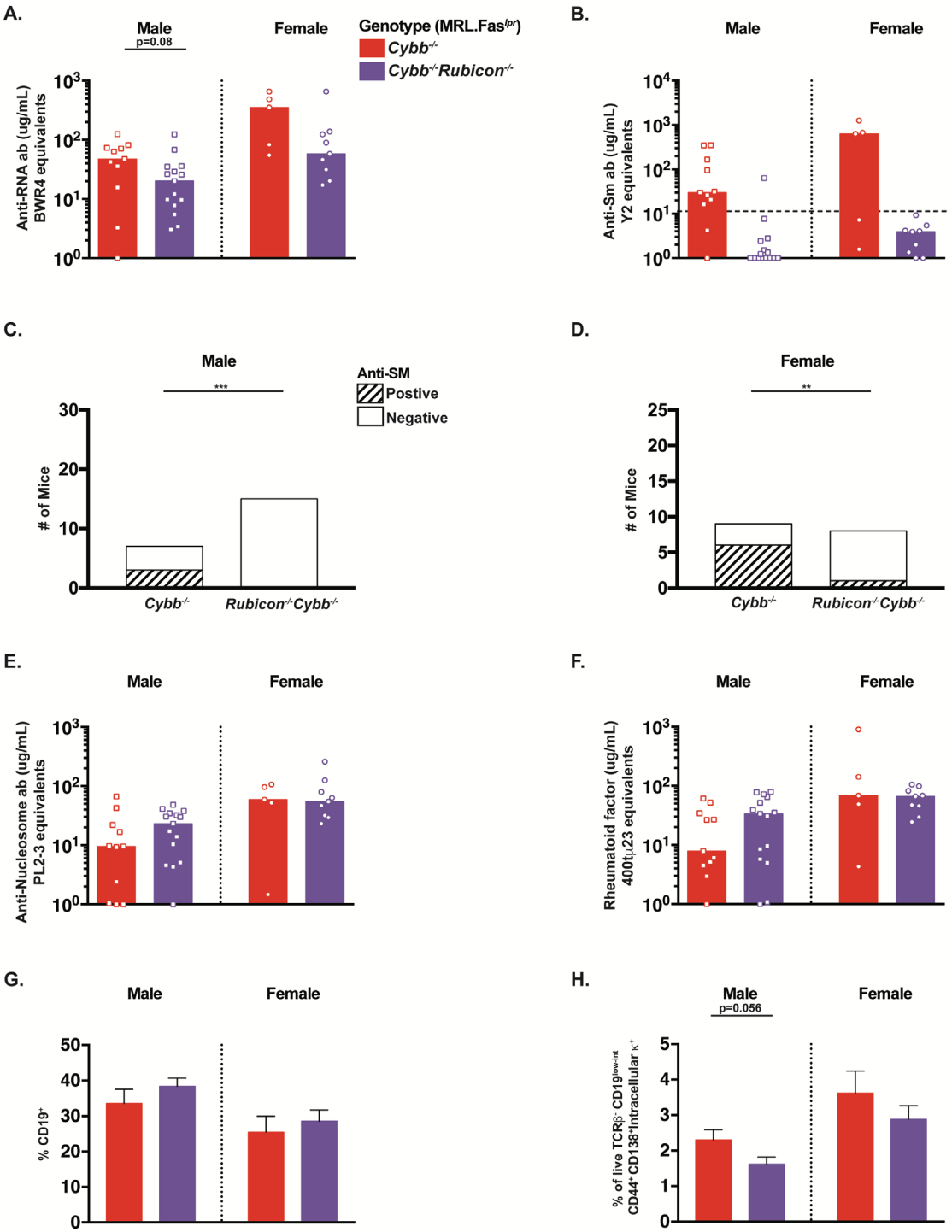

Figure 50. Rubicon deficiency abrogates the anti-Sm responses in *Cybb*-deficient MRL.Fas^{lpr} mice
(A and B) Serum anti-RNA (A), anti-Sm (B) titers at 18 weeks of age. **(C and D)** Number of male (C) and female (D) mice with positive anti-SM titers. The dotted line in B represents the positive threshold. **(E and F)** Serum anti-nucleosome antibody (E) and rheumatoid factor titers (E) at 18 weeks of age **(G)** Percentages of live CD19$^+$ total B cells. **(H)** Percentages of live cells that are TCRβ$^-$ CD44$^+$ CD138$^+$ intracellular κ$^+$ antibody forming cells. Data representation and statistics are as in Figure 48 (n=5 to 15 mice per group). In panels E and F, bar graphs are represented as the mean ± SEM and two-tailed Welch's T test was performed to determine statistical significance within each gender. In panels C and D, a Fisher's exact test was used to determine statistical significance (* indicates p≤0.05, ** p≤0.01, *** p≤0.001, and **** p≤0.0001; n=5 to 14 mice per group).

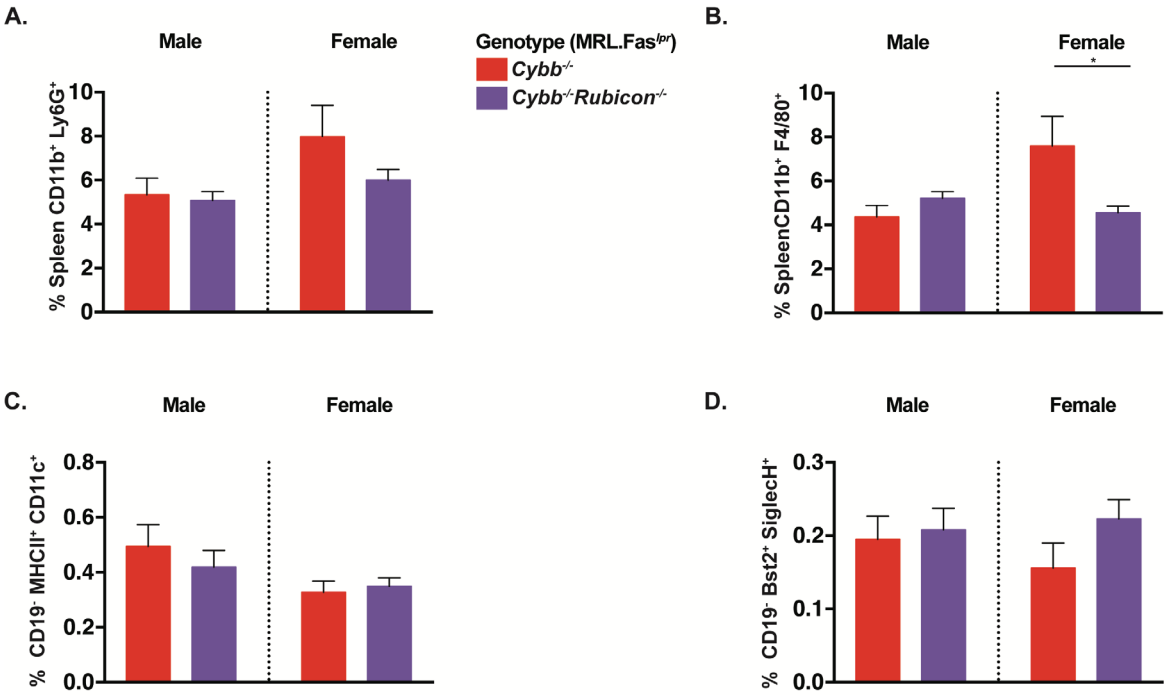

Figure 51. Rubicon deletion decreased splenic macrophage expansion in female *Cybb*-deficient SLE prone mice.

(A) Percentages of live $CD11b^+$ $Ly6G^+$ neutrophils in the spleen. **(B)** Percentages of splenic $CD11b^+$ $GR1^{low\text{-}int}$ $F4/80^+$ macrophages. **(C)** Percentages of live $CD19^-$ $MHCII^+$ $CD11c^+$ conventional dendritic cells and **(D)** $CD19^-$ $BST2^+$ $CD11c^+$ plasmacytoid dendritic cells. Bar graphs are represented as the mean ± SEM and a two-tailed Welch's T test was performed to determine statistical significance within each gender (* indicates $p \leq 0.05$, ** $p \leq 0.01$, *** $p \leq 0.001$, and **** $p \leq 0.0001$; n=5 to 14 mice per group).

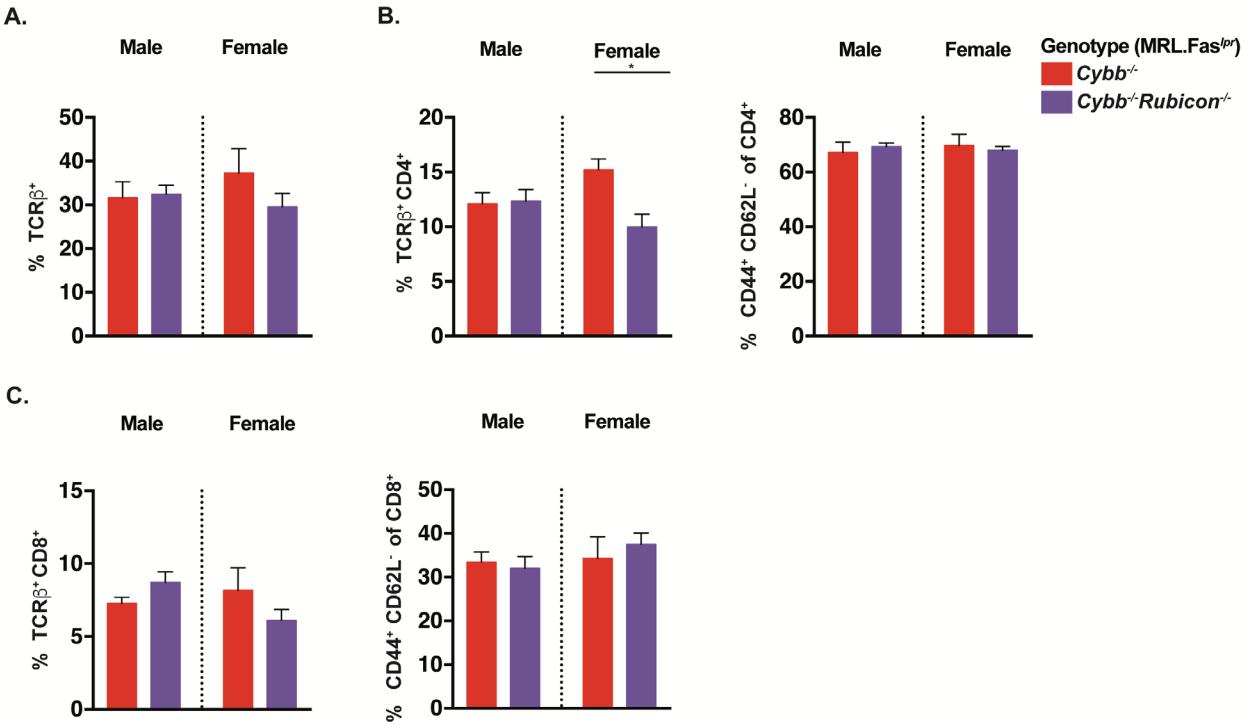

Figure 52. Rubicon deficiency did not alter the T cell compartment in *Cybb*-deficient MRL.Fas^{lpr} mice.
(A) Percentages of live TCRβ$^+$ total T cells. **(B)** Percentages of live TCRβ$^+$ CD4$^+$ T cells (left panel) and of CD4$^+$ CD44$^+$ CD62L$^-$ activated T cells (right panel). **(C)** Percentages of live TCRβ$^+$ CD8$^+$ T cells (left panel) and of CD8$^+$ CD44$^+$ CD62L$^-$ activated T cells (right panel). Data representation, number of mice, and statistics are as in Figure 51.

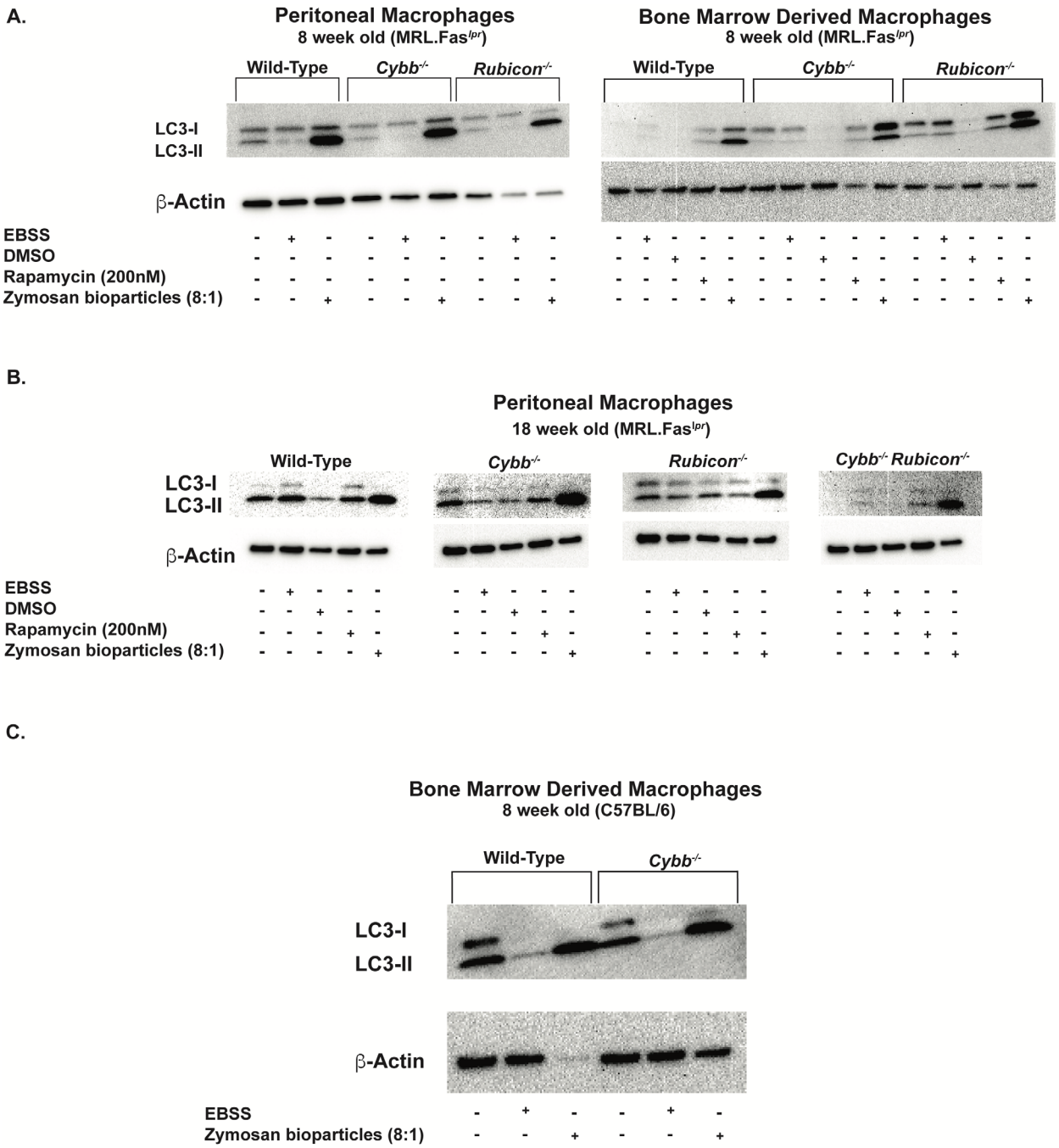

Figure 53. Zymosan bioparticles induced the lipidation of LC3 in *Rubicon*- and *Cybb*-deficient macrophages. Peritoneal macrophages or bone marrow derived macrophages (BMDMs) were subjected to starvation conditions (EBSS) or stimulated with Rapamycin (200nm) for 6 or 18 hours as indicated. LC3-associated phagocytosis was induced by feeding zymosan bioparticles (8:1 (particles/cell)) to macrophages for 6 to 18 hours as indicated. Total cell lysates were resolved using SDS-PAGE and blotted with the indicated antibodies. **(A)** Peritoneal macrophages (left) or BMDMs (right) derived from pre-diseased 8 week old wild-type, *Cybb*$^{-/-}$, or *Rubicon*$^{-/-}$ *MRL.*Fas^{lpr} *mice.* **(B)** Peritoneal macrophages isolated from 18 week old autoimmune wild-type, *Cybb*$^{-/-}$, or *Rubicon*$^{-/-}$, *Rubicon*$^{-/-}$ *Cybb*$^{-/-}$, MRL.Fas^{lpr} mice. **(C)** BMDMs derived from 8 week old C57BL/6 *Cybb*$^{-/-}$ mice.

4.4 ANALYSIS OF MYELOID *IL-10* DEFICIENCY IN SLE

To assess the role of myeloid IL-10 deficiency in SLE, we backcrossed the *IL-10*$^{fl/fl}$ and *LysM-Cre* alleles on to the MRL.Fas^{lpr} background for 10 generations. The fully backcrossed *IL-10*$^{fl/fl}$ and *LysM-Cre* MRL.Fas^{lpr} strains were intercrossed two generations to make the *IL-10*$^{fl/fl}$ allele homozygous. Resulting *IL-10*$^{fl/fl}$ *LysM Cre*$^{+/-}$ and *IL-10*$^{fl/fl}$ *LysM Cre*$^{+/-}$ were intercrossed to generate experiment cohorts. In this experiment, IL-10 should be deleted in neutrophils and macrophages of *IL-10*$^{fl/fl}$ *LysM Cre*$^{+/-}$ (*LysM ΔIL-10*) mice. SLE pathology was analyzed at 17 weeks of age.

4.4.1 *LysM Cre* efficiently deleted *IL-10* in neutrophils but only partial deletion occurs in macrophages

IL-10 deletion was measured by qPCR of genomic DNA acquired from FACS sorted immune cell populations. IL-10 was efficiently deleted in splenic CD11b^{+}Gr1^{+} neutrophils isolated from *IL-10*$^{fl/fl}$ *LysM-Cre*$^{+/-}$ mice (77.67% ±0.67; Figure 54). Paralleling our prior observation, *IL-10* deletion in *IL-10*$^{fl/fl}$ *LysM-Cre*$^{+/-}$ CD11b^{+}F4-80^{+} splenic macrophages was 43.48% (± 2.62; Figure 54). As expected, *IL-10* deletion in CD19^{+} B cells was below the limit of detection (Figure 54).

4.4.2 Renal disease was not impacted by myeloid *IL-10* deficiency in SLE prone mice

No differences in urine protein were detected in in SLE prone mice with a myeloid *IL-10* defect. (Figure 55A). The incidence of dermatitis was not different across the groups (Figure 55B). We

did not observe differences in the severity of glomerulonephritis (Figure 55C) or interstitial nephritis (Figure 55D) in *IL-10*$^{fl/fl}$ *LysM Cre*$^{+/-}$ MRL.Fas^{lpr} mice compared to myeloid IL-10 sufficient controls. No statistically significant differences in splenomegaly (Figure 55E) and lymphadenopathy were observed (Figure 55F).

4.4.3 Myeloid *IL-10* deficiency did not fundamentally alter the anti-self response

Myeloid *IL-10* genotype did not substantially alter the autoantibody response, with two notable exceptions. We did not detect any differences in anti-RNA antibody (Figure 56A) or anti-nucleosome antibody (Figure 56C) titers. Female *IL-10*$^{fl/fl}$ *LysM Cre*$^{+/-}$ *MRL.*Fas^{lpr} had lower anti-Sm titers than *IL-10*-sufficient controls (Figure 56B). Male myeloid *IL-10*-deficient mice had increased titers of RF (Figure 56D). We did not detect any change in the percentage of total CD19^{+} B cells or CD19$^{low\text{-}int}$ CD44^{+} CD138^{+} intracellular κ^{high} AFCs across groups (Figure 56E and F).

4.4.4 Myeloid *IL-10* deficiency had no impact on the composition of the myeloid compartment

Myeloid *IL-10*-genotype did not alter the percentage of CD11b^{+}Ly6G^{+} splenic neutrophils (Figure 57A) or CD11b^{+}F4/80^{+}Gr1$^{low\text{-}int}$ splenic macrophages (Figure 57B). Similarly, no differences in the percentage of splenic CD19^{-}CD11c^{+}MHCII^{+} cDCs (Figure 57C) and CD19^{-} BST2^{+} SiglecH^{+} pDCs (Figure 57D) were identified among the groups.

4.4.5 Myeloid *IL-10* deficiency had no impact on the T cell compartment

The composition of the T cell compartment was not substantially impacted by myeloid *IL-10*-deficiency in SLE prone mice. All genotypes exhibited indistinguishable total percentages of $TCR\beta^+$ T cells (Figure 58A). The percentages of $CD4^+$ T cells and $CD4^+CD44^+CD62L^-$ activated T cells were not statistically different between *IL-10*$^{fl/fl}$ *LysM Cre*$^{+/-}$ and controls (Figure 58B). Analogous findings were observed for naive and activated $CD8^+$ T cells (Figure 58C).

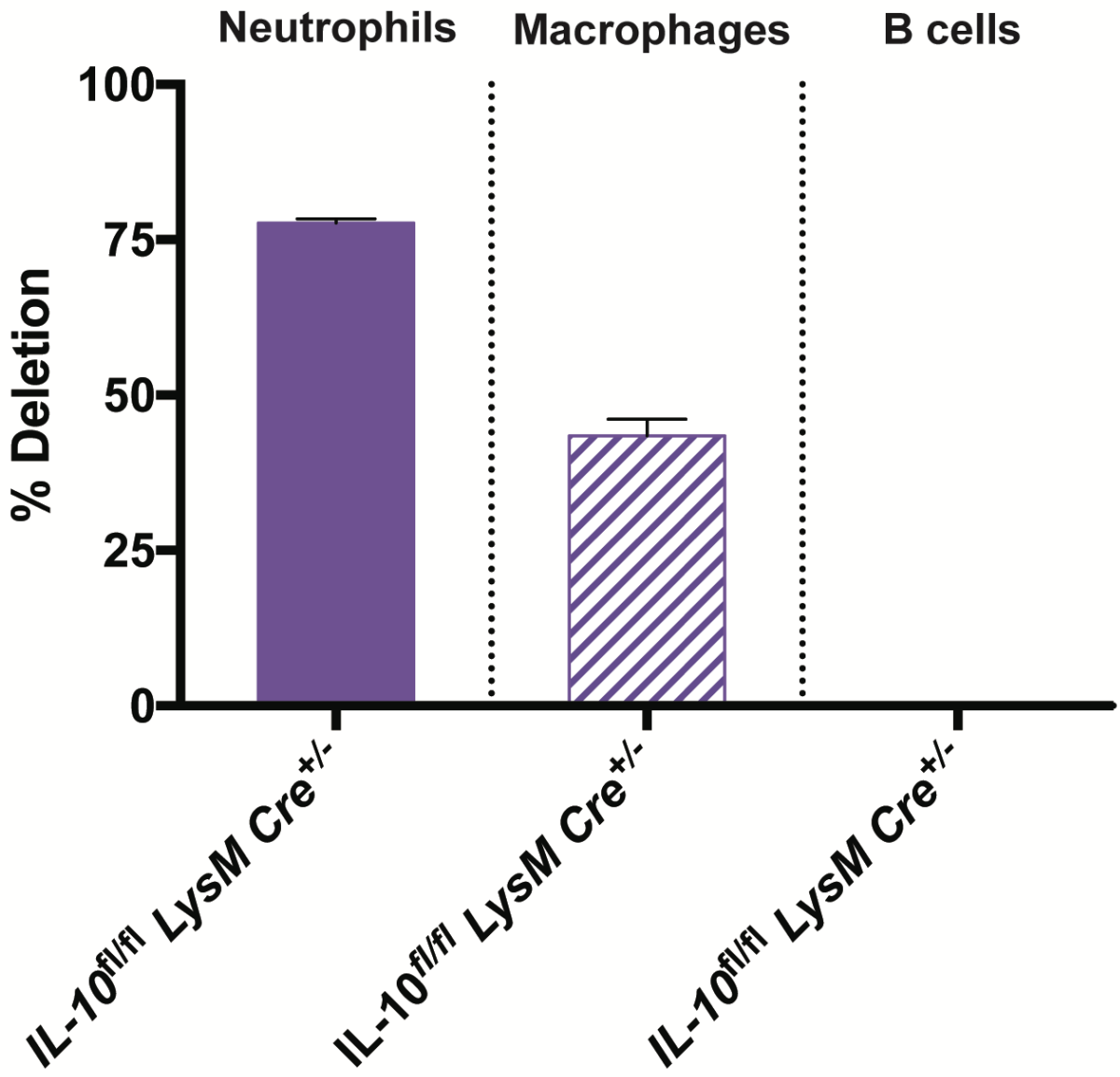

Figure 54. ***LysM Cre*** **efficiently deleted** ***IL-10*** **in neutrophils but only partial deletion occurred in macrophages.**
Cybb deletion efficiency was quantitated by qPCR of genomic DNA isolated from FACS sorted splenic neutrophil, macrophages, and B cells.

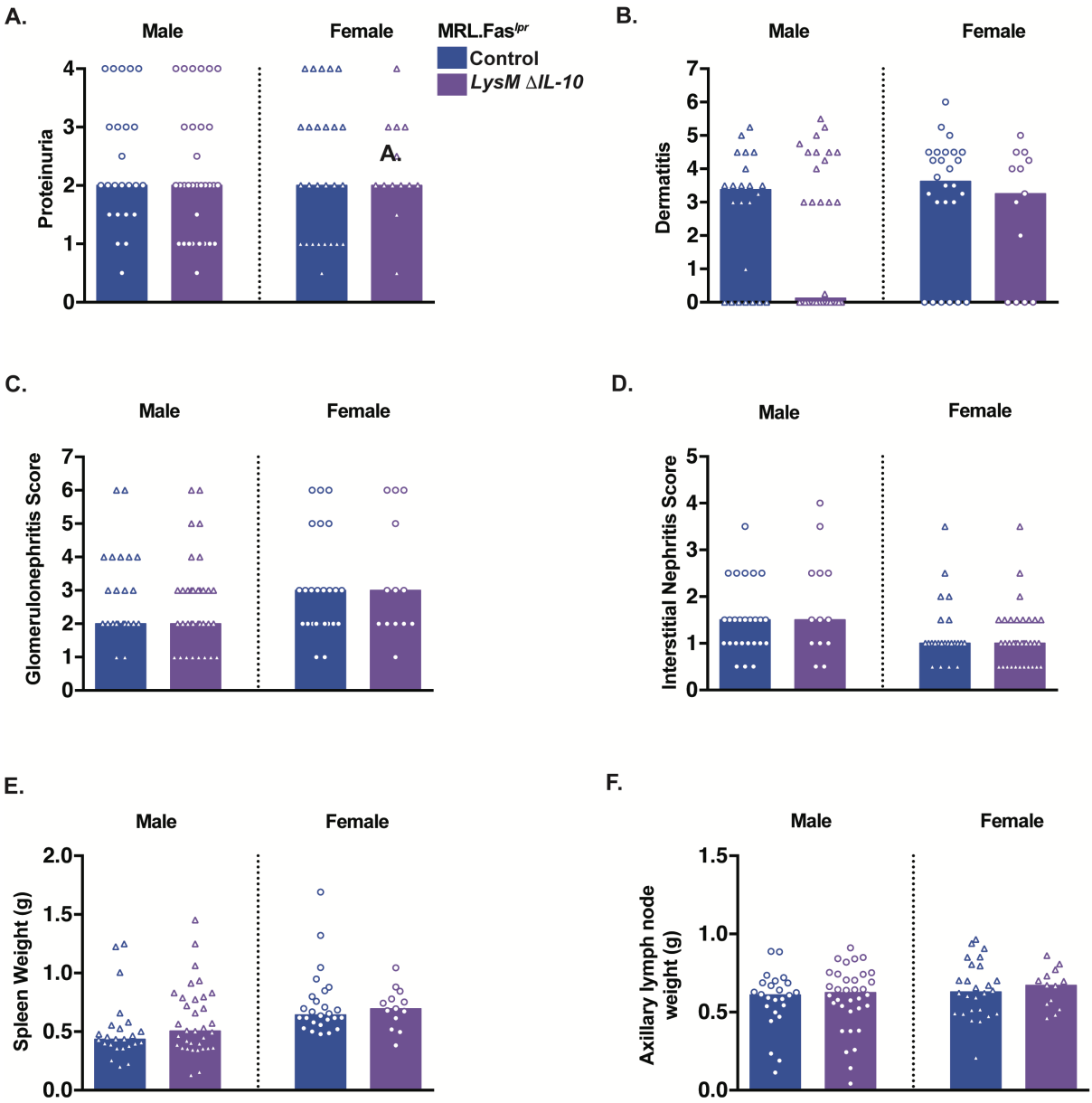

Figure 55. Myeloid *IL-10* deficiency did not impact renal disease in SLE prone mice.
(A) Proteinuria. **(B)** Dermatitis. **(C)** Glomerulonephritis scores. **(D)** Interstitial nephritis scores. **(E)** Spleen weight. **(F)** Axillary lymph node weights. Scores are represented as a function of *IL-10$^{fl/fl}$ and LysM Cre* genotype and gender at 18 weeks of age. Bars represent the median and each dot represents and individual mouse. A Mann Whitney U test was performed to determine statistical significance within each gender (* indicates $p \leq 0.05$, ** $p \leq 0.01$, *** $p \leq 0.001$, and **** $p \leq 0.0001$; n=13 to 34 mice per group).

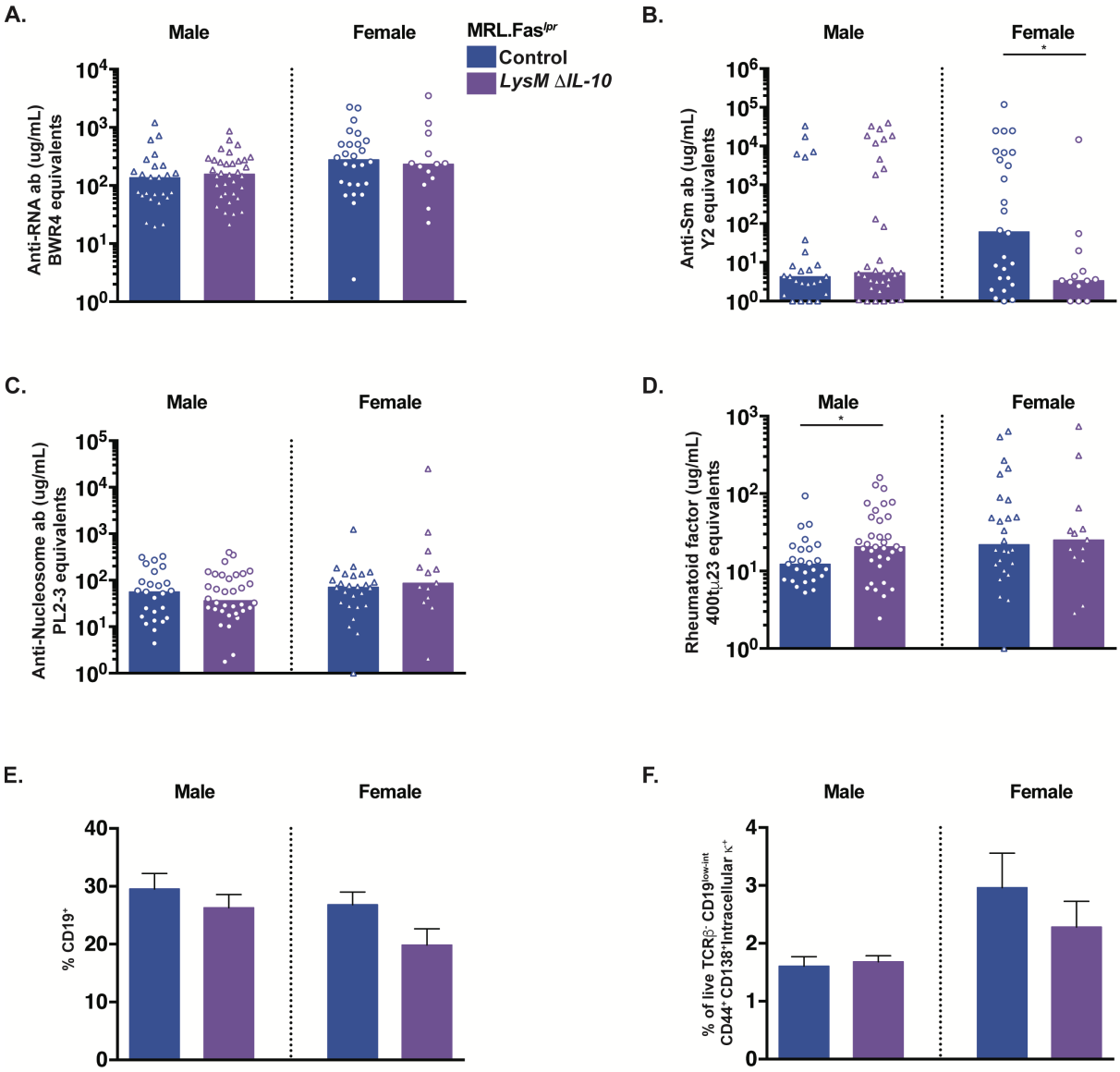

Figure 56. The anti-self response was not altered in *LysM ΔIL-10* MRL.Fas^{lpr} mice.
(A-D) Serum anti-RNA (A), anti-Sm (B), anti-nucleosome antibody (C) and rheumatoid factor titers (D) at 18 weeks of age. **(E)** Percentages of live CD19$^+$ total B cells. **(F)** Percentages of live cells that are TCRβ$^-$ CD44$^+$ CD138$^+$ intracellular κ$^+$ antibody forming cells. Data representation, number of mice, and statistics are as in Figure 55. In panels E and F, bar graphs are represented as the mean ± SEM and a two-tailed Welch's T test was performed to determine statistical significance within each gender. (* indicates p≤0.05, ** p≤0.01, *** p≤0.001, and **** p≤0.0001; n=13 to 31 mice per group).

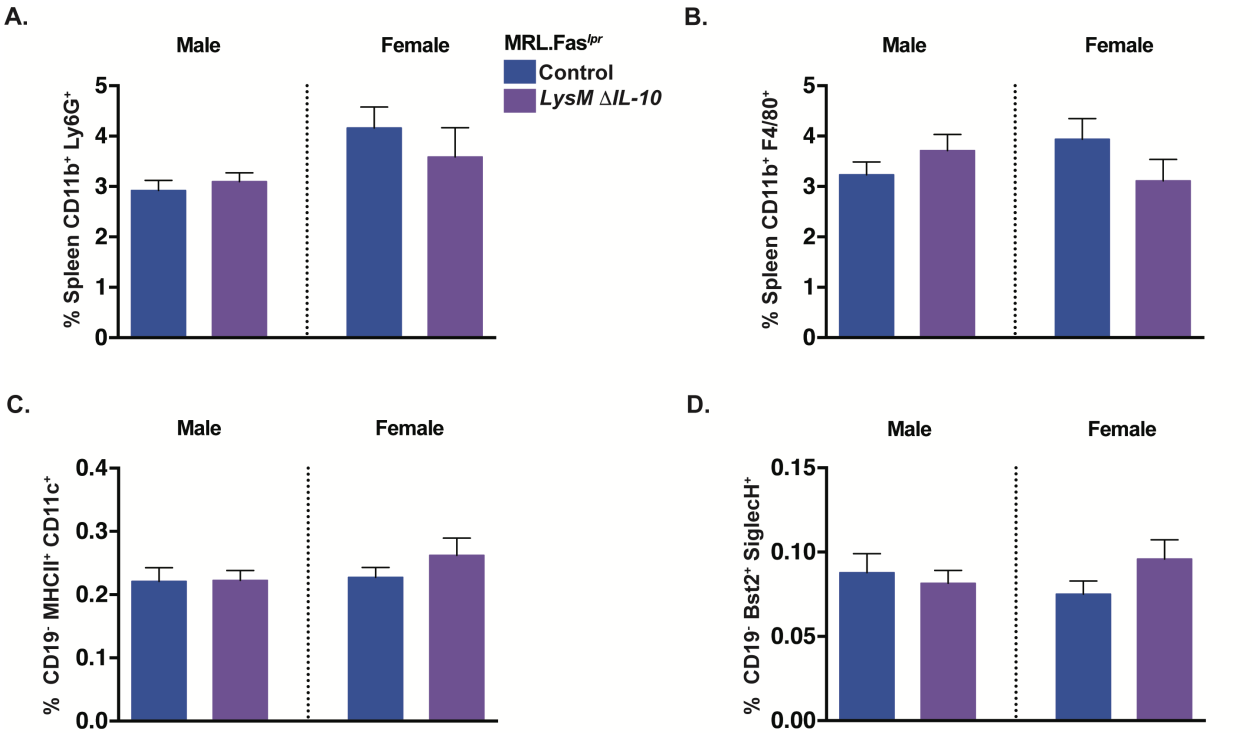

Figure 57. Myeloid *IL-10* deficiency did not change the composition of the myeloid compartment in SLE prone mice.

(A) Percentages of live $CD11b^+$ $Ly6G^+$ neutrophils in the spleen. **(B)** Percentages of splenic $CD11b^+$ $GR1^{low\text{-}int}$ $F4/80^+$ macrophages. **(C)** Percentages of live $CD19^-$ $MHCII^+$ $CD11c^+$ conventional dendritic cells and **(D)** $CD19^-$ $BST2^+$ $CD11c^+$ plasmacytoid dendritic cells. Bar graphs are represented as the mean ± SEM and a two tail Welch's T test was performed to determine statistical significance within each gender (* indicates $p \leq 0.05$, ** $p \leq 0.01$, *** $p \leq 0.001$, and **** $p \leq 0.0001$; n=13 to 31 mice per group).

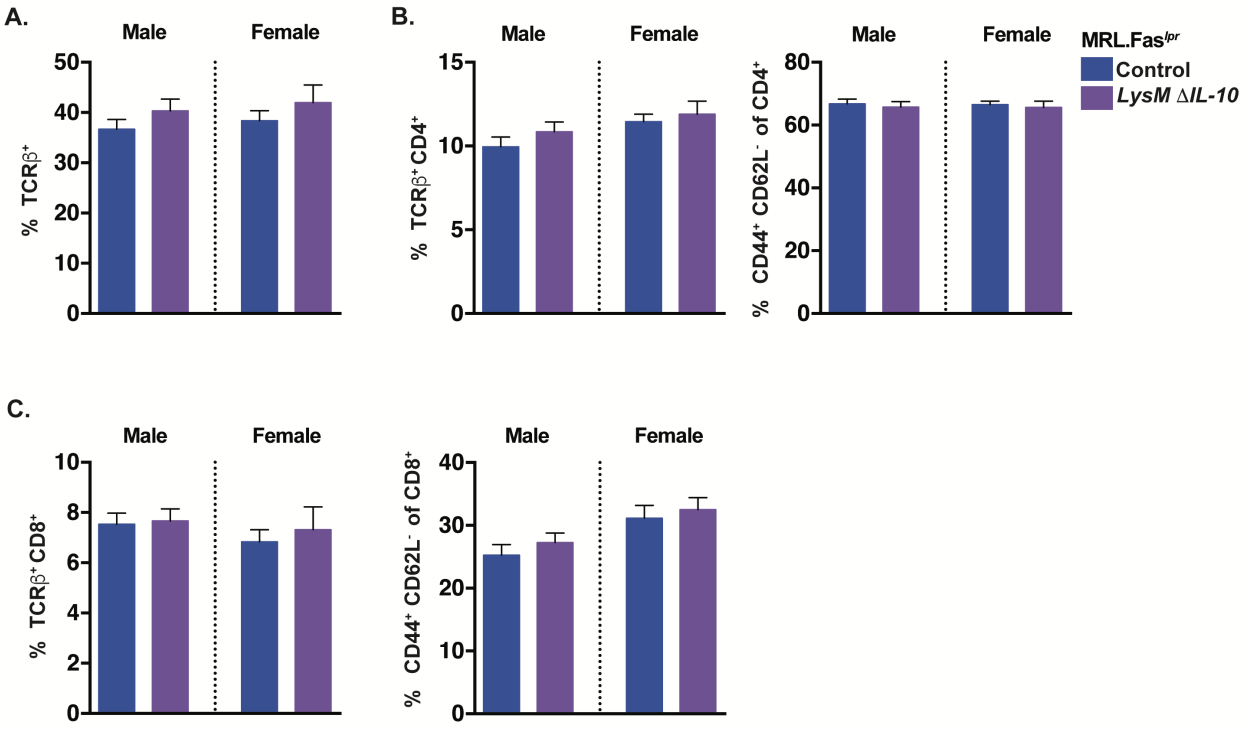

Figure 58. The T cell compartment was not impacted by myeloid *IL-10* deletion in MRL.Fas^{lpr} mice.
(A) Percentages of live TCRβ$^+$ total T cells. **(B)** Percentages of live TCRβ$^+$ CD4$^+$ T cells (left panel) and of CD4$^+$ CD44$^+$ CD62L$^-$ activated T cells (right panel). **(C)** Percentages of live TCRβ$^+$ CD8$^+$ T cells (left panel) and of CD8$^+$ CD44$^+$ CD62L$^-$ activated T cells (right panel). Data representation, number of mice, and statistics are as in Figure 57.

4.5 DISCUSSION

NADPH oxidase-deficient SLE prone mice develop exacerbated manifestations of SLE and die prematurely as a result of their disease (75, 76, 137). It has been postulated that NADPH oxidase dysfunction augments SLE by inhibiting LAP and the consequent immunologically silent degradation of dead cells. *Rubicon* and *Cybb*-deficient C57BL/6 mice develop a lupus like disease attributed to a defect in LAP (90). If these hypotheses were correct, genetic deletion of *Rubicon*, a required mediator for LAP, should phenocopy *Cybb*-deficiency in SLE prone mice. To address this question, we generated the *Rubicon* knockout mouse directly on the MRL.Fas^{lpr} SLE prone background. Unexpectedly, *Rubicon*-deficient MRL.Fas^{lpr} did not develop worsened clinical or immunological manifestations of SLE, as is the case for *Cybb*-deficient MRL.Fas^{lpr} mice. In fact, *Rubicon* deletion increases survival and ameliorates both glomerulonephritis and interstitial nephritis in *Cybb*$^{-/-}$ SLE prone mice. Production of IL-10 downstream of dead cell engulfment is thought to be a primary mechanism by which LAP protects against the immune response to self. Additionally, our group and others have identified macrophages as major producers of IL-10 in murine and human lupus. To determine the role of myeloid IL-10 in the *in vivo* disease setting, we genetically deleted *IL-10* in neutrophils and macrophages in SLE prone mice by a Cre-lox approach, crossing the *IL-10*-floxed allele with *LysM-Cre*. The *LysM Cre* allele has been previously used to conditionally knockout LAP mediators in macrophages resulting the development of a spontaneous SLE-like disease. In contrast to this observation, myeloid *IL-10* deletion did not alter SLE pathogenesis in the MRL.Fas^{lpr} model, suggesting that IL-10 production downstream of LAP is not a major regulatory mechanism augmenting systemic autoimmunity. Our complementation study demonstrates that exacerbated SLE in *Cybb*-deficient

mice is not a result of defective LAP. Taken together, the genetic studies we present here fail to support a role for defective LAP in driving SLE pathogenesis.

Martinez and colleagues implicated RUBICON and CYBB as essential for LAP (89). To confirm that *Rubicon*$^{-/-}$ and *Cybb*$^{-/-}$ MRL.Fas^{lpr} macrophages were deficient in LAP, we stimulated BMDMs with the canonical LAP inducer, zymosan coated beads. Upon LAP initiation, LC3-I is lipidated to form LC3-II and translocates to the LAPsome membrane. We measured LC3-II as a molecular readout for the initiation of LAP. To our surprise, zymosan bioparticles induced the lipidation of LC3-I to form LC3-II in macrophages from both young pre-diseased and aged *Rubicon*$^{-/}$, *Cybb*$^{-/-}$, and *Rubicon*$^{-/-}$*Cybb*$^{-/}$ MRL.Fas^{lpr} mice. Moreover, we did not observe consistent elevated expression of either LC3-I or LC3-II in macrophages from diseased animals, discordant with previous observations reporting elevated LC3 protein in the lymph nodes of autoimmune MRL.Fas^{lpr} mice (228). It is conceivable that the MRL background, or the *lpr* mutation in the *Fas* gene that serves as disease accelerator, alters the requirements for CYBB and RUBICON in LAP. To address this concern, we repeated these studies in BMDMs generated from *Cybb*$^{-/-}$ C57BL/6 mice. We found that *Cybb*$^{-/-}$ C57BL/6 BMDMs do form LC3-II in response to zymosan coated beads, contrary to expectations. Importantly, the time points used in our study were different from those used by Martinez *et al*., as we assessed LC3 at 6 hours or 18 hours post stimulation while they did so at 1 hour. It is possible that zymosan coated beads are inducing canonical autophagy, accounting for the increase in LC-II observed in our hands. To further address this issue, we will conduct experiments at shorter time point and we will confirm the localization of LC3 to the LAPasome by confocal microscopy. These studies will also be repeated in macrophages derived from mice with genetic deletions in the components of the pre-initiation complex, requisite for canonical autophagy but dispensable for LAP. Taken together,

our studies highlight a potential flaw with the current view of the proteins required for LAP. Importantly, our work indicates that Rubicon may be working through a LAP-independent mechanism to augment SLE pathogenesis.

Recently, RUBICON has been ascribed several immune regulatory functions, independent of LAP. Rubicon is reported to reduce CARD9 dependent cytokine signaling (224). In the context of viral infection, RUBICON can inhibit type I IFN responses by preventing IRF3 dimerization (225). Based on these findings, it would be unexpected that *Rubicon*-deficiency is protective in the MRL.Fas^{lpr} model. Interestingly, data from our lab showed that IRF3 deficiency did not impact SLE pathogenesis in an F2 cohort. We also showed that, while genetic deletion of CARD9 reduces splenic myeloid expansion and reduces AFCs, it does not have any impact on proteinuria (F2 and fully backcrossed cohorts) or histological kidney disease (F2 cohort) (unpublished). Thus, neither IRF3 nor CARD9 pathways are likely to be major disease drivers, and therefore, the phenotype that we observe in *Rubicon*-deficient mice is inconsistent with the role of Rubicon in modulating CARD9 and IRF3 pathways.

RUBICON can bind p22^{phox}, stabilizing the NAPDH oxidase complex, requisite for NADPH oxidase dependent proinflammatory cytokine production (224). It is possible that in the absence of RUBICON, NADPH oxidase mediated proinflammatory cytokine production is reduced in MRL.Fas^{lpr} mice. This explanation is incongruent with our findings, as *Cybb*$^{-/-}$ MRL.Fas^{lpr} mice, without a functional active NADPH oxidase complex, develop exacerbated SLE. In the setting of *Cybb*-deficiency, it is possible that compensatory upregulation of another NOX complex (e.g. NOX1) could restore NADPH oxidase function. However, as others and we have shown, genetically deleting *Cybb* or cytosolic components of the NADPH oxidase complex all lead to exacerbated SLE in murine models. Hence, such a postulated compensatory

mechanism would have to uniquely rely on the ability of RUBICON to upregulate NOX family members. As *Rubicon*-deficient mice cannot generate ROS, this explanation seems unlikely (89).

Rubicon deficiency regulates the formation of antibodies towards RNA and ribonucleoproteins but not to DNA. We have previously reported that *Cybb*-deficient MRL.Fas^{lpr} mice develop elevated anti-RNA and anti-Sm titers (75). Impressively, *Rubicon* deletion abrogates the anti-Sm response in both *Cybb*-sufficient and -deficient SLE prone mice. This phenotype resembles the autoantibody response observed in *Tlr7*$^{-/-}$ MRL.Fas^{lpr} mice. *Tlr7*$^{-/-}$ MRL.Fas^{lpr} do not produce antibodies towards RNA and ribonucleoprotein but retain their ability to generate antibodies to DNA and chromatin (2, 3). Similar to Rubicon-deficient SLE prone mice, TLR7$^{-/-}$ MRL.Fas^{lpr} mice are protected from renal manifestations of SLE (2, 3). To address whether Rubicon regulates TLR7 expression, we assessed TLR7 protein levels on total splenocytes by flow cytometry. We did not find any substantial differences in TLR7 protein expression in total B cells or the myeloid compartment (data not shown). These preliminary expression studies do not preclude Rubicon from altering TLR7 expression in specific B cell subsets. Furthermore, TLR7 and Rubicon both localize to the endosome and it is plausible that Rubicon could regulate TLR7 trafficking or signaling in B cells (89, 222, 223, 246). The interplay between Rubicon and TLR7 remains to be explored and is an active area of investigation by our laboratory.

RNA must traffic to the endosome to be detected by endosomal TLR receptors, such as TLR7. One mechanism by which Rubicon could modulate SLE pathogenesis is through trafficking of RNA cargo. Indeed, ATG5, an E3 ligase required for both autophagy and LAP, has been implicated in RNA trafficking to TLR containing endosomes in DCs (247). A similar mechanism could deliver RNA cargo to endosomal TLR7s in B cells with significant

implications for the development of TLR7-dependent antibodies in SLE. Supporting this idea, B-cell specific deletion of *Atg5*, improves both survival renal disease in the TLR7 transgenic model (TLR7.1 Tg) of SLE (248). The role of Rubicon in RNA trafficking and how that relates to SLE pathogenesis is intriguing and worthy of further study.

The *Rubicon* knockout allele generated in this study is likely a true knockout and does not produce a dominant negative product. We inserted a stop codon at position Asp188, located at the end of the RUN domain. The stop codon is situated upstream of regions known to code protein domains that bind BECLIN1, p22phox, and 14-3-3β important for RUBICON's biological function (224). We did not observe any evidence that a truncated protein product is produced in the *Rubicon* knockout mice that we generated (data not shown). Moreover, heterozygous mice do not recapitulate the phenotype of *Rubicon*-deficient SLE prone mice, as might have been expected had we generated a dominant negative allele. *Rubicon*$^{+/-}$ MRL.Fas^{lpr} mice can produce antibodies to Sm antigen. In the setting of *Cybb*-deficiency, Rubicon heterozygosity did not ameliorate SLE renal disease. Therefore, it is unlikely that the CRISPR-Cas9 strategy employed to make a Rubicon knockout mouse resulted in a dominant negative allele.

Another significant finding is that myeloid *IL-10* deficiency does not impact SLE pathogenesis in our system. As discussed in chapter 3, *LysM-Cre* has a mediocre efficiency in macrophages. It is possible that partial deletion of *IL-10* in the myeloid compartment is not sufficient to modulate SLE. However, *IL10*$^{+/-}$ MRL.Fas^{lpr} mice developed more severe renal disease and dermatitis compared to their *IL-10* intact counterparts, making this explanation less likely (242). Therefore, IL-10 production downstream of LAP in macrophages is unlikely to be a dominant immune regulatory mechanism in MRL.Fas^{lpr} mice. While macrophages do produce

IL-10 in murine lupus, the myeloid compartment is not the only cellular source of IL-10 in this setting. In addition to macrophages, T cells are major IL-10 producers in SLE prone mice (245). More specifically, IL-10 is predominantly generated by T regulatory cells and $CD4^{+}FoxP3^{-}$ T cells (245). Taken together, it is thus likely that T cell derived IL-10 plays a more critical role in regulating SLE pathogenesis.

The studies that we collectively present suggest that defective LAP is not the mechanism by which *Cybb* deficiency promotes autoimmunity. The lack of phenotype observed in SLE prone mice with myeloid specific *IL-10* deficiency strengthens this conclusion. Importantly, and unexpectedly, our data implicate RUBICON as a novel mediator of systemic autoimmunity, a finding that requires further mechanistic study and may have therapeutic implications for SLE patients.

4.6 MATERIALS AND METHODS

Mice. *IL-10*$^{fl/fl}$ C57BL/6 mice (249) were backcrossed to the MRL.Fas^{lpr} strain for at least 9 generations (245). Homozygosity for the *lpr* mutation was verified by PCR. *LysM-Cre* MRL.Fas^{lpr} mice were intercrossed with *IL-10*$^{fl/wt}$ MRL.Fas^{lpr} mice. Resulting *LysM-Cre*$^{+/-}$ *IL-10*$^{fl/wt}$ MRL.Fas^{lpr} mice were then crossed with MRL.Fas^{lpr} *IL-10*$^{fl/wt}$. To generate mice for experimental cohorts, we intercrossed *LysM-Cre*$^{+/-}$ *IL-10*$^{fl/fl}$ to *IL-10*$^{fl/fl}$. This breeding allowed us to use littermate controls for each group. SLE pathology was assessed at 18 weeks of age.

Generation of the Rubicon knockout mouse on the MRL.Fas^{lpr} background. *Rubicon*-deficient *Rubicon*-deficient MRL.Fas^{lpr} mice were generated by *in vitro* fertilization and CRISPR-Cas9

technology as previously described by replacing Asp188 with a premature stop codon (89). In brief, a sgRNA targeting exon 5 of Rubicon was selected and generated as described in chapter 3. MRL.Fas^{lpr} pronuclear-stage zygotes were injected with capped Cas9 mRNA, a gRNA targeting the end of exon 5 and a 183-nucleotide-long ssODN that served as a repair template. Mice were genotyped by PCR amplification and RFLP analysis of the target locus. Amplified PCR products were subsequently cloned into a sequencing vector (NEB) and sequenced to verify correct targeting.

To generate mice for experimental cohorts, we intercrossed: (1) *Rubicon*$^{-/+}$*Cybb*$^{y/-}$ X *Rubicon*$^{-/+}$*Cybb*$^{+/-}$, (2) *Rubicon*$^{-/+}$*Cybb*$^{y+-}$ X *Rubicon*$^{-/+}$*Cybb*$^{+/-}$, and (3) *Rubicon*$^{-/+}$ X *Rubicon*$^{-/+}$. This breeding produced littermate controls for each group. SLE pathology was assessed at 18 weeks of age.

Quantitative PCR. qPCR was used to measure *IL-10* deletion efficiency as described in chapter 3.

Evaluation of SLE pathology. Refer to chapter 1

Flow cytometry. Refer to chapter 1

Autoantibody ELISAs. Refer to chapter 1

Generation of bone marrow derived macrophages (BMDMs). Femurs, tibias, and iliac crests were harvested from MRL.Fas^{lpr} mice of indicated genotypes and bone marrow was isolated by

mortar and pestle. Cells were incubated in *ACK* (Ammonium-Chloride-Potassium) buffer for erythroid cell lysis. $10X10^6$ bone marrow cells were plated on 100mm petri dishes in 10mL of complete DMEM (Gibco) media supplemented with 10% fetal calf serum and 30% L929 macrophage colony stimulating factor (MCSF) conditioned media. Media was replaced after 3 day of culture. On day 7, adherent macrophages were harvested, replated, and rested for 24 hours prior to experimental use.

Induction of LAP and canonical autophagy. *To induce canonical autophagy, peritoneal macrophages or BMDMs were subjected to starvation conditions (*Earle's Balanced Salt Solution (EBSS)) or stimulated with Rapamycin (200nm) for 6 to 18 hours. Zymosan bioparticles (thermofisher) were added to macrophages cultures for 6 to 18 hours at a ratio of 8:1 (particles/cell) to induce LAP.

Immunoblotting. Cells were lysed in 2X llamelli's buffer (Bio-Rad) supplemented with 5% beta-mercaptoethanol and heated to 95 degrees for 5 min. Lysates analyzed by SDS-PAGE. Immunodetection was achieved using the following antibodies: LC3B (Cell Signaling; D11, 1:1000), RUBICON (Cell Signaling; D9F7,1:1000), β-Actin HRP (Cell signaling; 8H10D10, 1:10,000), Anti-Rabbit IgG HRP (Cell signaling, 1:10,000). Proteins were visualized by an ECL chemiluminescence reagent and imaged by a Protein Simple imager.

Statistics. Refer to chapter 1

5.0 CONCLUSIONS AND FUTURE STUDIES

5.1 SLE PATHOLOGY IS INDEPENDENT OF PADI4 AND ELANE

In our studies, we used an *in vivo* genetic approach to assess the causative role for NETs in SLE. We targeted two distal conserved mediators required for NET formation, *Padi4* and *Elane* in the MRL.Fas^{lpr} model. Neither *Padi4* nor *Elane* deficiency improved SLE pathology, a finding also recently recapitulated in the pristane model of lupus (77). Moreover, pharmacological inhibition of PADs using Cl-Amidine had no effect in neutrophil recruitment or glomerular injury in two independent models of IC-FcγR mediated glomerulonephritis (133). Taken together with the reproducible finding that NADPH oxidase deficiency promotes SLE in humans (120-125, 179) and in multiple murine models (75, 89, 180, 250), the work that we present here do not support the hypothesis that NETs are the primary antigen source nor directly instrumental in mediating end-organ damage in lupus. Moreover, our findings have ramifications for the development of the Padi4 inhibitors that will soon enter clinical trials to treat patients with autoimmune diseases.

Further, an important contribution of the current work is that it reveals a distinction between *Padi4*, *Elane* and *Cybb*-deficient lupus-prone mice, in that only the latter get exacerbated disease. As CYBB, ELANE, and PADI4 operate at distinct phases of NET formation, it remains possible that the aberrant products of presumably "frustrated" NET generation that would occur in the absence of each required protein might differ, in turn

accounting for the disparate disease phenotypes. As *Cybb*-deficiency leads to markedly exacerbated disease, the products of neutrophil death in the absence of CYBB could be uniquely immunogenic. Alternatively, though not exclusively, *Cybb*-deficiency might promote disease due to lack of a fundamental regulatory activity of CYBB in neutrophils (84, 85), macrophages (86), or another cell in the immune system (87, 88). This hypothesis was directly tested in chapters 3 and 4.

5.2 INHERENT DIFFICULTIES IN STUDYING NETS *IN VITRO* AND *IN VIVO*

While there is a growing body of literature that links NET formation to SLE, much of this work was conducted *in vitro* and does not necessarily reflect *in vivo* disease. Part of the confusion may stem from technical issues: it is difficult to prove presence of *in vivo* and *in vitro* NETs as no specific markers for NETs have been identified and NET-like structures can be generated by physical force (251). Moreover, antibodies used to assess histone citrullination are not necessarily specific (252). Exemplifying these issues, two recent concurrent publications by Ander's and Yousefi's groups (253, 254) describe contradictory roles for the receptor-interacting protein kinases in NET generation. We have had difficulty recapitulating robust NET formation *in vitro* by canonical NET inducing in mouse neutrophils, an issue also encountered by others groups (96). Employing a high throughput fixed cell and live cell imaging protocol, we had hoped to better define NETs and their unique features in SLE. Unfortunately, due to the aforementioned technical issues, we paused this line of investigation. In the future, we could employ *in vivo* imaging modalities in MRL.Fas^{lpr} mice with genetic deletions in the NET pathway, such as *Cybb*, to determine whether "frustrated" NET formation occurs in this setting.

Therefore, the genetic and pharmacologic *in vivo* model approach we report here, along with the consistent results obtained by targeting multiple genes in the NET pathway, provide evidence to seriously question the hypothesis that NETs promote SLE.

5.3 THE CELL SPECIFIC ROLE OF CYBB IN SLE: PRELIMINARY CONCLUSIONS

The studies that we present here, employing both a conventional bone marrow chimera approach and a novel chimera strategy to specifically delete *Cybb* in macrophages and neutrophils, demonstrate that myeloid *Cybb* deficiency is sufficient to exacerbate SLE pathogenesis. It is still unknown whether *Cybb* deficiency in the neutrophil or macrophage is the primary driver of lupus pathogenesis. This piece of the puzzle will point to the mechanism by which CYBB modulates lupus as discussed in chapter 3. We hypothesize: (1) The absence of CYBB in neutrophils may alter the way in which the neutrophil dies resulting in a more immunogenic form of cell death and (2) CYBB is critical for macrophages to engulf and degrade dying cells. These two hypotheses are not mutually exclusively and would both lead to the aberrant accumulation of autoantigen. To tackle this question, we employed the *LysM-Cre* and *Mrp8-Cre* MRL.Fas^{lpr} strains to delete the *Cybb*-floxed allele in macrophages and neutrophils or neutrophils only respectively. SLE was aggravated in both cohorts, albeit not to the degree of the global knockouts or the hematopoietic chimeras. Taken together, our preliminary studies indicate that a regulatory function of CYBB in the neutrophil is important for limiting systemic autoimmunity. The mechanism by which Cybb deficiency in neutrophils drives SLE remains to be elucidated and is an active area of investigation by our laboratory.

There are two explanations as to why conditional deletion of *Cybb* mediated by *LysM-Cre* and *Mrp8-Cre* did not recapitulate the phenotype observed in either the *Cybb* global knockouts or the Cybb hematopoietic chimeras. First, *LysM-Cre* does not efficiently target macrophages (184), and therefore, we cannot rule out a contribution for macrophage CYBB SLE. The limitations of *LysM-Cre* observed by our group and others highlights the need to develop a Cre strain that is both efficient and specific at targeting macrophage populations. It is also possible that CYBB is exerting a regulatory function in another cell type of the immune system such as B cells and T cells. To address this possibility, we are investigating the role of B cell *Cybb* in lupus by harnessing a Cre-lox approach to specifically delete *Cybb* in B cells in the MRL.Fas^{lpr} model.

5.4 *RUBICON* DEFICIENCY AMELIORATES SLE PATHOGENESIS

To test the hypothesis that absence of CYBB drives SLE pathogenesis by preventing macrophages from degrading dead cell debris via a defect in LAP, we genetically deleted another molecule in the LAP pathway, *Rubicon*, in the MRL.Fas^{lpr} SLE model. Strikingly, *Rubicon* deletion in *Cybb*-deficient MRL.Fas^{lpr} mice reduced renal disease and increased the life-span of the cohort. Moreover, Rubicon deficiency reduced autoantibodies to RNA but not DNA related autoantigens. These findings mimic the phenotype observed in *Tlr7*-deficient SLE prone mice (2, 3). It is a compelling hypothesis that Rubicon mediates lupus pathogenesis by augmenting TLR7 function or trafficking of its ligands in B cells. We can determine whether Rubicon augments TLR7 function by assessing the responses of Rubicon-deficient B cells to TLR7 ligands *in vitro*. In the *in vivo* disease setting, we can test whether *Rubicon* deficiency protects *Tlr9*$^{-/-}$ MRL.Fas^{lpr}

mice that develop exacerbated lupus which is known to be dependent on TLR7 (2, 3). Similarly, we can take advantage of murine SLE models that are driven by *Tlr7* overexpression, such as, *Yaa* mice. The relationship between RUBICON and TLR7 remains enigmatic and requires further investigation.

It is still unknown in which cell type does *Rubicon* deficiency exert its protective effect(s) in SLE pathogenesis. The differential regulation of RNA and DNA autoantibody responses point to a B cell intrinsic mechanism. The cell specific role of RUBICON in SLE can be assessed by generating the *Rubicon*-floxed allele and crossing it to tissue specific Cre strains that are already backcrossed to the MRL.Fas^{lpr} background. *CD19 Cre* can be employed to specifically delete *Rubicon* on B cells in SLE prone mice, allowing us to assess B cell specific Rubicon deletion on autoantibody responses and clinical manifestations of lupus.

Moreover, the studies presented here do not implicate LAP as a driver of SLE pathogenesis. Production of the immunoregulatory cytokine IL-10 by macrophages undergoing LAP is postulated to be a dominant mechanism constraining the anti-self response. IL-10 deficiency did not alter the disease course in the MRL.Fas^{lpr} SLE model reinforcing our conclusions. Our findings are incongruous with prior observations in non-autoimmune prone C57BL/6 mice that develop a SLE-like disease with age in the absence of LAP components, including CYBB and RUBICON. It is possible that the opposing phenotypes observed in our two studies are a result of model systems employed. The SLE-like disease identified in LAP-defective C57BL/6 mice may resemble an autoinflammatory syndrome as opposed to bonafide autoimmunity since histological SLE kidney disease was mild in these cohorts (90). It is imperative that the discrepancies between these two studies be resolved. Assessment of LAP components in additional murine models of SLE may be helpful in this regard. Importantly, our

work highlights RUBICON as a novel mediator of systemic autoimmunity. The mechanism by which RUBICON is protective in the setting of SLE remains to be explored and could represent a new druggable target for the treatment of lupus patients.

SELECTED LIST OF ABBREVIATIONS

AFC Antibody forming cell

APC Antigen presenting cell

BMDM Bone marrow derived macrophages

CARD Caspase activation and recruitment domains

CGD Chronic granulomatous disease

Cl-Amidine N-R-benzoyl-N5-(2-chloro-1-iminoethyl)-L-ornithine amide

Cybb (nox2, gp91) Cytochrome b-245, β polypeptide

DAMP danger associated molecular patterns

DC Dendritic cell

DTA Diphtheria toxin fragment A

Elane Neutrophil elastase

FcγR Fcγ receptor

GBM Glomerular basement membrane

IFN Interferon

IFNAR Interferon-α/β receptor

IL Interleukin

Interferon regulatory factorIRF

LAP LC3-associated phagocytosis

LC3	Microtubule-associated proteins 1A/1B light chain 3
lyso-PS	Lysophosphatidylserine
MPO	Myeloperoxidase
NADPH	Nicotinamide adenine dinucleotide phosphate
NCF	Neutrophil cytosolic factor
NET	Neutrophil extracellular trap
NFκB	Nuclear factor kappa-light-chain-enhancer of activated B cells
Padi4	Peptidyl arginine deiminase 4
PIL	Pristane induced lupus
PRR	Pattern recognition receptors
PS	Phosphatidylserine
ROS	Reactive oxygen species
RPA	Reverse passive Arthus reaction
Rubicon	RUN and cysteine rich domain containing beclin 1 interacting protein
sgRNA	Single guide RNA
SLE	Systemic Lupus Erythematosus
SLEDAI	Systemic Lupus Erythematosus Disease Activity Index
SM	Smith antigen
ssODN	Single stranded oligodeoxynucleotides
TLR	Toll like receptor

BIBLIOGRAPHY

1. Crowl JT, Gray EE, Pestal K, Volkman HE, and Stetson DB. Intracellular Nucleic Acid Detection in Autoimmunity. *Annual Review of Immunology.* 2017;35(1):313-36.

2. Nickerson KM, Christensen SR, Shupe J, Kashgarian M, Kim D, Elkon K, et al. TLR9 regulates TLR7- and MyD88-dependent autoantibody production and disease in a murine model of lupus. *J Immunol.* 2010;184(4):1840-8.

3. Christensen SR, Shupe J, Nickerson K, Kashgarian M, Flavell RA, and Shlomchik MJ. Toll-like receptor 7 and TLR9 dictate autoantibody specificity and have opposing inflammatory and regulatory roles in a murine model of lupus. *Immunity.* 2006;25(3):417-28.

4. Christensen SR, Kashgarian M, Alexopoulou L, Flavell RA, Akira S, and Shlomchik MJ. Toll-like receptor 9 controls anti-DNA autoantibody production in murine lupus. *J Exp Med.* 2005;202(2):321-31.

5. Subramanian S, Tus K, Li QZ, Wang A, Tian XH, Zhou J, et al. A Tlr7 translocation accelerates systemic autoimmunity in murine lupus. *Proc Natl Acad Sci U S A.* 2006;103(26):9970-5.

6. Deane JA, Pisitkun P, Barrett RS, Feigenbaum L, Town T, Ward JM, et al. Control of toll-like receptor 7 expression is essential to restrict autoimmunity and dendritic cell proliferation. *Immunity.* 2007;27(5):801-10.

7. Nickerson KM, Wang Y, Bastacky S, and Shlomchik MJ. Toll-like receptor 9 suppresses lupus disease in Fas-sufficient MRL Mice. *PLoS ONE.* 2017;12(3):1-15.

8. Santiago-Raber ML, Dunand-Sauthier I, Wu T, Li QZ, Uematsu S, Akira S, et al. Critical role of TLR7 in the acceleration of systemic lupus erythematosus in TLR9-deficient mice. *J Autoimmun.* 2010;34(4):339-48.

9. Bossaller L, Christ A, Pelka K, Nündel K, Chiang P-I, Pang C, et al. TLR9 Deficiency Leads to Accelerated Renal Disease and Myeloid Lineage Abnormalities in Pristane-Induced Murine Lupus. *The Journal of Immunology.* 2016;197(4):1044-53.

10. Lartigue A, Courville P, Auquit I, Francois A, Arnoult C, Tron F, et al. Role of TLR9 in Anti-Nucleosome and Anti-DNA Antibody Production in lpr Mutation-Induced Murine Lupus. *The Journal of Immunology.* 2006;177(2):1349-54.

11. Teichmann LL, Schenten D, Medzhitov R, Kashgarian M, and Shlomchik MJ. Signals via the adaptor MyD88 in B cells and DCs make distinct and synergistic contributions to immune activation and tissue damage in lupus. *Immunity.* 2013;38(3):528-40.

12. Yoneyama M, Kikuchi M, Natsukawa T, Shinobu N, Imaizumi T, Miyagishi M, et al. The RNA helicase RIG-I has an essential function in double-stranded RNA-induced innate antiviral responses. *Nat Immunol.* 2004;5(7):730-7.

13. Kang DC, Gopalkrishnan RV, Wu Q, Jankowsky E, Pyle AM, and Fisher PB. mda-5: An interferon-inducible putative RNA helicase with double-stranded RNA-dependent ATPase activity and melanoma growth-suppressive properties. *Proc Natl Acad Sci U S A.* 2002;99(2):637-42.

14. Satoh T, Kato H, Kumagai Y, Yoneyama M, Sato S, Matsushita K, et al. LGP2 is a positive regulator of RIG-I- and MDA5-mediated antiviral responses. *Proc Natl Acad Sci U S A.* 2010;107(4):1512-7.

15. Pichlmair A, Schulz O, Tan CP, Naslund TI, Liljestrom P, Weber F, et al. RIG-I-mediated antiviral responses to single-stranded RNA bearing 5'-phosphates. *Science.* 2006;314(5801):997-1001.

16. Yoneyama M, and Fujita T. RNA recognition and signal transduction by RIG-I-like receptors. *Immunological Reviews.* 2009;227(1):54-65.

17. Hornung V, Ellegast J, Kim S, Brzozka K, Jung A, Kato H, et al. 5'-Triphosphate RNA is the ligand for RIG-I. *Science.* 2006;314(5801):994-7.

18. Goubau D, Schlee M, Deddouche S, Pruijssers AJ, Zillinger T, Goldeck M, et al. Antiviral immunity via RIG-I-mediated recognition of RNA bearing 5'-diphosphates. *Nature.* 2014;514(7522):372-5.

19. Yoneyama M, Kikuchi M, Matsumoto K, Imaizumi T, Miyagishi M, Taira K, et al. Shared and Unique Functions of the DExD/H-Box Helicases RIG-I, MDA5, and LGP2 in Antiviral Innate Immunity. *The Journal of Immunology.* 2005;175(5):2851-8.

20. Kawai T, Takahashi K, Sato S, Coban C, Kumar H, Kato H, et al. IPS-1, an adaptor triggering RIG-I- and Mda5-mediated type I interferon induction. *Nat Immunol.* 2005;6(10):981-8.

21. Stetson DB, and Medzhitov R. Recognition of cytosolic DNA activates an IRF3-dependent innate immune response. *Immunity.* 2006;24(1):93-103.

22. Sharma S, DeOliveira RB, Kalantari P, Parroche P, Goutagny N, Jiang Z, et al. Innate immune recognition of an AT-rich stem-loop DNA motif in the Plasmodium falciparum genome. *Immunity.* 2011;35(2):194-207.

23. Seth RB, Sun L, Ea CK, and Chen ZJ. Identification and characterization of MAVS, a mitochondrial antiviral signaling protein that activates NF-kappaB and IRF 3. *Cell.* 2005;122(5):669-82.

24. Ishikawa H, Ma Z, and Barber GN. STING regulates intracellular DNA-mediated, type I interferon-dependent innate immunity. *Nature.* 2009;461(7265):788-92.

25. Buskiewicz IA, Montgomery T, Yasewicz EC, Huber SA, Murphy MP, Hartley RC, et al. Reactive oxygen species induce virus-independent MAVS oligomerization in systemic lupus erythematosus. *Sci Signal.* 2016;9(456):ra115.

26. International Consortium for Systemic Lupus Erythematosus G, Harley JB, Alarcon-Riquelme ME, Criswell LA, Jacob CO, Kimberly RP, et al. Genome-wide association scan in women with systemic lupus erythematosus identifies susceptibility variants in ITGAM, PXK, KIAA1542 and other loci. *Nat Genet.* 2008;40(2):204-10.

27. Gateva V, Sandling JK, Hom G, Taylor KE, Chung SA, Sun X, et al. JAZF1 , UHRF1BP1 and IL10 as risk loci for systemic lupus erythematosus. *Nature Genetics.* 2009;41(11):1228-33.

28. Molineros JE, Maiti AK, Sun C, Looger LL, Han S, Kim-Howard X, et al. Admixture mapping in lupus identifies multiple functional variants within IFIH1 associated with apoptosis, inflammation, and autoantibody production. *PLoS Genet.* 2013;9(2):e1003222.

29. Robinson T, Kariuki SN, Franek BS, Kumabe M, Kumar AA, Badaracco M, et al. Autoimmune disease risk variant of IFIH1 is associated with increased sensitivity to IFN-alpha and serologic autoimmunity in lupus patients. *J Immunol.* 2011;187(3):1298-303.

30. Akahoshi M, Nakashima H, Sadanaga A, Miyake K, Obara K, Tamari M, et al. Promoter polymorphisms in the IRF3 gene confer protection against systemic lupus erythematosus. *Lupus.* 2008;17(6):568-74.

31. Sharma S, Campbell AM, Chan J, Schattgen SA, Orlowski GM, Nayar R, et al. Suppression of systemic autoimmunity by the innate immune adaptor STING. *Proc Natl Acad Sci U S A.* 2015;112(7):E710-7.

32. Takaoka A, Wang Z, Choi MK, Yanai H, Negishi H, Ban T, et al. DAI (DLM-1/ZBP1) is a cytosolic DNA sensor and an activator of innate immune response. *Nature.* 2007;448(7152):501-5.

33. Ishii KJ, Kawagoe T, Koyama S, Matsui K, Kumar H, Kawai T, et al. TANK-binding kinase-1 delineates innate and adaptive immune responses to DNA vaccines. *Nature.* 2008;451(7179):725-9.

34. Unterholzner L, Keating SE, Baran M, Horan KA, Jensen SB, Sharma S, et al. IFI16 is an innate immune sensor for intracellular DNA. *Nat Immunol.* 2010;11(11):997-1004.

35. Zhang Z, Yuan B, Bao M, Lu N, Kim T, and Liu YJ. The helicase DDX41 senses intracellular DNA mediated by the adaptor STING in dendritic cells. *Nat Immunol.* 2011;12(10):959-65.

36. Sun L, Wu J, Du F, Chen X, and Chen ZJ. Cyclic GMP-AMP synthase is a cytosolic DNA sensor that activates the type I interferon pathway. *Science.* 2013;339(6121):786-91.

37. Chiu YH, Macmillan JB, and Chen ZJ. RNA polymerase III detects cytosolic DNA and induces type I interferons through the RIG-I pathway. *Cell.* 2009;138(3):576-91.

38. Ablasser A, Bauernfeind F, Hartmann G, Latz E, Fitzgerald KA, and Hornung V. RIG-I-dependent sensing of poly(dA:dT) through the induction of an RNA polymerase III-transcribed RNA intermediate. *Nat Immunol.* 2009;10(10):1065-72.

39. Stetson DB, Ko JS, Heidmann T, and Medzhitov R. Trex1 prevents cell-intrinsic initiation of autoimmunity. *Cell.* 2008;134(4):587-98.

40. Kawane K, Ohtani M, Miwa K, Kizawa T, Kanbara Y, Yoshioka Y, et al. Chronic polyarthritis caused by mammalian DNA that escapes from degradation in macrophages. *Nature.* 2006;443(7114):998-1002.

41. Shin HD, Park BL, Cheong HS, Lee HS, Jun JB, and Bae SC. DNase II polymorphisms associated with risk of renal disorder among systemic lupus erythematosus patients. *J Hum Genet.* 2005;50(3):107-11.

42. Crow YJ, Hayward BE, Parmar R, Robins P, Leitch A, Ali M, et al. Mutations in the gene encoding the 3'-5' DNA exonuclease TREX1 cause Aicardi-Goutieres syndrome at the AGS1 locus. *Nat Genet.* 2006;38(8):917-20.

43. Hur JW, Sung YK, Shin HD, Park BL, Cheong HS, and Bae SC. TREX1 polymorphisms associated with autoantibodies in patients with systemic lupus erythematosus. *Rheumatol Int.* 2008;28(8):783-9.

44. Baum R, Sharma S, Carpenter S, Li QZ, Busto P, Fitzgerald KA, et al. Cutting edge: AIM2 and endosomal TLRs differentially regulate arthritis and autoantibody production in DNase II-deficient mice. *J Immunol.* 2015;194(3):873-7.

45. Jakobs C, Perner S, and Hornung V. AIM2 Drives Joint Inflammation in a Self-DNA Triggered Model of Chronic Polyarthritis. *PLoS ONE.* 2015;10(6):e0131702.

46. Jeremiah N, Neven B, Gentili M, Callebaut I, Maschalidi S, Stolzenberg MC, et al. Inherited STING-activating mutation underlies a familial inflammatory syndrome with lupus-like manifestations. *J Clin Invest.* 2014;124(12):5516-20.

47. Liu Y, Jesus AA, Marrero B, Yang D, Ramsey SE, Sanchez GAM, et al. Activated STING in a vascular and pulmonary syndrome. *N Engl J Med.* 2014;371(6):507-18.

48. Muruve DA, Petrilli V, Zaiss AK, White LR, Clark SA, Ross PJ, et al. The inflammasome recognizes cytosolic microbial and host DNA and triggers an innate immune response. *Nature.* 2008;452(7183):103-7.

49. Hornung V, Ablasser A, Charrel-Dennis M, Bauernfeind F, Horvath G, Caffrey DR, et al. AIM2 recognizes cytosolic dsDNA and forms a caspase-1-activating inflammasome with ASC. *Nature.* 2009;458(7237):514-8.

50. Burckstummer T, Baumann C, Bluml S, Dixit E, Durnberger G, Jahn H, et al. An orthogonal proteomic-genomic screen identifies AIM2 as a cytoplasmic DNA sensor for the inflammasome. *Nat Immunol.* 2009;10(3):266-72.

51. Fernandes-Alnemri T, Yu JW, Datta P, Wu J, and Alnemri ES. AIM2 activates the inflammasome and cell death in response to cytoplasmic DNA. *Nature.* 2009;458(7237):509-13.

52. Choubey D, and Panchanathan R. Interferon-inducible Ifi200-family genes in systemic lupus erythematosus. *Immunol Lett.* 2008;119(1-2):32-41.

53. Yang CA, Huang ST, and Chiang BL. Sex-dependent differential activation of NLRP3 and AIM2 inflammasomes in SLE macrophages. *Rheumatology (Oxford).* 2015;54(2):324-31.

54. Campbell AM. *The role of NADPH oxidase in the pathogenesis of systemic lupus erythematosus.* [Order No. 3572053]. Yale University; 2013

55. Bratton DL, and Henson PM. Neutrophil clearance: when the party is over, clean-up begins. *Trends Immunol.* 2011;32(8):350-7.

56. Ravichandran KS. Beginnings of a good apoptotic meal: the find-me and eat-me signaling pathways. *Immunity.* 2011;35(4):445-55.

57. Silva MT, do Vale A, and dos Santos NM. Secondary necrosis in multicellular animals: an outcome of apoptosis with pathogenic implications. *Apoptosis.* 2008;13(4):463-82.

58. Cho YS, Challa S, Moquin D, Genga R, Ray TD, Guildford M, et al. Phosphorylation-driven assembly of the RIP1-RIP3 complex regulates programmed necrosis and virus-induced inflammation. *Cell.* 2009;137(6):1112-23.

59. Linkermann A, and Green DR. Necroptosis. *N Engl J Med.* 2014;370(5):455-65.

60. Lau A, Wang S, Jiang J, Haig A, Pavlosky A, Linkermann A, et al. RIPK3-mediated necroptosis promotes donor kidney inflammatory injury and reduces allograft survival. *Am J Transplant.* 2013;13(11):2805-18.

61. Stockwell BR, Friedmann Angeli JP, Bayir H, Bush AI, Conrad M, Dixon SJ, et al. Ferroptosis: A Regulated Cell Death Nexus Linking Metabolism, Redox Biology, and Disease. *Cell.* 2017;171(2):273-85.

62. Brinkmann V, Reichard U, Goosmann C, Fauler B, Uhlemann Y, Weiss DS, et al. Neutrophil extracellular traps kill bacteria. *Science.* 2004;303(5663):1532-5.

63. Remijsen Q, Vanden Berghe T, Wirawan E, Asselbergh B, Parthoens E, De Rycke R, et al. Neutrophil extracellular trap cell death requires both autophagy and superoxide generation. *Cell Res.* 2011;21(2):290-304.

64. Fuchs TA, Abed U, Goosmann C, Hurwitz R, Schulze I, Wahn V, et al. Novel cell death program leads to neutrophil extracellular traps. *J Cell Biol.* 2007;176(2):231-41.

65. Li P, Li M, Lindberg MR, Kennett MJ, Xiong N, and Wang Y. PAD4 is essential for antibacterial innate immunity mediated by neutrophil extracellular traps. *J Exp Med.* 2010;207(9):1853-62.

66. Hemmers S, Teijaro JR, Arandjelovic S, and Mowen KA. PAD4-mediated neutrophil extracellular trap formation is not required for immunity against influenza infection. *PLoS One.* 2011;6(7):e22043.

67. Villanueva E, Yalavarthi S, Berthier CC, Hodgin JB, Khandpur R, Lin AM, et al. Netting neutrophils induce endothelial damage, infiltrate tissues, and expose immunostimulatory molecules in systemic lupus erythematosus. *J Immunol.* 2011;187(1):538-52.

68. Garcia-Romo GS, Caielli S, Vega B, Connolly J, Allantaz F, Xu Z, et al. Netting neutrophils are major inducers of type I IFN production in pediatric systemic lupus erythematosus. *Sci Transl Med.* 2011;3(73):73ra20.

69. Knight JS, Subramanian V, O'Dell AA, Yalavarthi S, Zhao W, Smith CK, et al. Peptidylarginine deiminase inhibition disrupts NET formation and protects against kidney, skin and vascular disease in lupus-prone MRL/lpr mice. *Ann Rheum Dis.* 2015;74(12):2199-206.

70. Knight JS, Zhao W, Luo W, Subramanian V, O'Dell AA, Yalavarthi S, et al. Peptidylarginine deiminase inhibition is immunomodulatory and vasculoprotective in murine lupus. *J Clin Invest.* 2013;123(7):2981-93.

71. Hakkim A, Furnrohr BG, Amann K, Laube B, Abed UA, Brinkmann V, et al. Impairment of neutrophil extracellular trap degradation is associated with lupus nephritis. *Proc Natl Acad Sci U S A.* 2010;107(21):9813-8.

72. Leffler J, Martin M, Gullstrand B, Tyden H, Lood C, Truedsson L, et al. Neutrophil extracellular traps that are not degraded in systemic lupus erythematosus activate complement exacerbating the disease. *J Immunol.* 2012;188(7):3522-31.

73. Denny MF, Yalavarthi S, Zhao W, Thacker SG, Anderson M, Sandy AR, et al. A distinct subset of proinflammatory neutrophils isolated from patients with systemic lupus erythematosus induces vascular damage and synthesizes type I IFNs. *J Immunol.* 2010;184(6):3284-97.

74. Lande R, Ganguly D, Facchinetti V, Frasca L, Conrad C, Gregorio J, et al. Neutrophils activate plasmacytoid dendritic cells by releasing self-DNA-peptide complexes in systemic lupus erythematosus. *Sci Transl Med.* 2011;3(73):73ra19.

75. Campbell AM, Kashgarian M, and Shlomchik MJ. NADPH oxidase inhibits the pathogenesis of systemic lupus erythematosus. *Sci Transl Med.* 2012;4(157):157ra41.

76. Jacob CO, Yu N, Yoo DG, Perez-Zapata LJ, Barbu EA, Kaplan MJ, et al. Haploinsufficiency of NADPH oxidase subunit NCF2 is sufficient to accelerate full-blown lupus in NZM.2328 mice. *Arthritis Rheumatol.* 2017.

77. Kienföfer D, Hahn, Jonas, Stoof, Julia, Csepregi, Janka, Reinwald, Christiane, Johnsson, Caroline, Maueröder, Christian, Podolska, Malgorzata, Biermann, Mona, Leppkes, Moritz, Harrer, Thomas, Hultqvist, Malin, Olofsson, Peter, Munoz, Luis,Mocsai, Mocsai, Attil, Herrmann, Martin, Schett, Georg, Holmdahl, Rikard, Hoffmann, Markus. In: Shlomchik M ed.; 2017.

78. Nickerson KM, and Shlomchik MJ. *Encyclopedia of Immunobiology*. Oxford: Academic Press; 2016:227-40.

79. Hochberg MC. Updating the American College of Rheumatology revised criteria for the classification of systemic lupus erythematosus. *Arthritis Rheum.* 1997;40(9):1725.

80. Nickerson KM, Cullen JL, Kashgarian M, and Shlomchik MJ. Exacerbated autoimmunity in the absence of TLR9 in MRL.Fas(lpr) mice depends on Ifnar1. *J Immunol.* 2013;190(8):3889-94.

81. Peng SL, Moslehi J, and Craft J. Roles of interferon-gamma and interleukin-4 in murine lupus. *J Clin Invest.* 1997;99(8):1936-46.

82. Lee K, Won HY, Bae MA, Hong JH, and Hwang ES. Spontaneous and aging-dependent development of arthritis in NADPH oxidase 2 deficiency through altered differentiation of CD11b+ and Th/Treg cells. *Proc Natl Acad Sci U S A.* 2011;108(23):9548-53.

83. Hultqvist M, Olofsson P, Holmberg J, Backstrom BT, Tordsson J, and Holmdahl R. Enhanced autoimmunity, arthritis, and encephalomyelitis in mice with a reduced oxidative burst due to a mutation in the Ncf1 gene. *Proc Natl Acad Sci U S A.* 2004;101(34):12646-51.

84. Frasch SC, Berry KZ, Fernandez-Boyanapalli R, Jin HS, Leslie C, Henson PM, et al. NADPH oxidase-dependent generation of lysophosphatidylserine enhances clearance of activated and dying neutrophils via G2A. *J Biol Chem.* 2008;283(48):33736-49.

85. Schauer C, Janko C, Munoz LE, Zhao Y, Kienhofer D, Frey B, et al. Aggregated neutrophil extracellular traps limit inflammation by degrading cytokines and chemokines. *Nat Med.* 2014;20(5):511-7.

86. Fernandez-Boyanapalli R, McPhillips KA, Frasch SC, Janssen WJ, Dinauer MC, Riches DW, et al. Impaired phagocytosis of apoptotic cells by macrophages in chronic granulomatous disease is reversed by IFN-gamma in a nitric oxide-dependent manner. *J Immunol.* 2010;185(7):4030-41.

87. Jackson SH, Devadas S, Kwon J, Pinto LA, and Williams MS. T cells express a phagocyte-type NADPH oxidase that is activated after T cell receptor stimulation. *Nat Immunol.* 2004;5(8):818-27.

88. Richards SM, and Clark EA. BCR-induced superoxide negatively regulates B-cell proliferation and T-cell-independent type 2 Ab responses. *Eur J Immunol.* 2009;39(12):3395-403.

89. Martinez J, Malireddi RK, Lu Q, Cunha LD, Pelletier S, Gingras S, et al. Molecular characterization of LC3-associated phagocytosis reveals distinct roles for Rubicon, NOX2 and autophagy proteins. *Nat Cell Biol.* 2015;17(7):893-906.

90. Martinez J, Cunha LD, Park S, Yang M, Lu Q, Orchard R, et al. Noncanonical autophagy inhibits the autoinflammatory, lupus-like response to dying cells. *Nature.* 2016;533(7601):115-9.

91. Athens JW, Haab OP, Raab SO, Mauer AM, Ashenbrucker H, Cartwright GE, et al. Leukokinetic studies. IV. The total blood, circulating and marginal granulocyte pools and the granulocyte turnover rate in normal subjects. *J Clin Invest.* 1961;40:989-95.

92. Yipp BG, and Kubes P. NETosis: how vital is it? *Blood.* 2013;122(16):2784-94.

93. Yousefi S, Mihalache C, Kozlowski E, Schmid I, and Simon HU. Viable neutrophils release mitochondrial DNA to form neutrophil extracellular traps. *Cell Death Differ.* 2009;16(11):1438-44.

94. Caielli S, Athale S, Domic B, Murat E, Chandra M, Banchereau R, et al. Oxidized mitochondrial nucleoids released by neutrophils drive type I interferon production in human lupus. *J Exp Med.* 2016;213(5):697-713.

95. Lood C, Blanco LP, Purmalek MM, Carmona-Rivera C, De Ravin SS, Smith CK, et al. Neutrophil extracellular traps enriched in oxidized mitochondrial DNA are interferogenic and contribute to lupus-like disease. *Nat Med.* 2016;22(2):146-53.

96. Chen K, Nishi H, Travers R, Tsuboi N, Martinod K, Wagner DD, et al. Endocytosis of soluble immune complexes leads to their clearance by FcgammaRIIIB but induces neutrophil extracellular traps via FcgammaRIIA in vivo. *Blood.* 2012;120(22):4421-31.

97. Vossenaar ER, Zendman AJ, van Venrooij WJ, and Pruijn GJ. PAD, a growing family of citrullinating enzymes: genes, features and involvement in disease. *Bioessays.* 2003;25(11):1106-18.

98. Nakashima K, Hagiwara T, and Yamada M. Nuclear localization of peptidylarginine deiminase V and histone deimination in granulocytes. *Journal of Biological Chemistry.* 2002;277(51):49562-8.

99. Fuhrmann J, and Thompson PR. Protein Arginine Methylation and Citrullination in Epigenetic Regulation. *ACS Chem Biol.* 2016;11(3):654-68.

100. Li P, Yao H, Zhang Z, Li M, Luo Y, Thompson PR, et al. Regulation of p53 target gene expression by peptidylarginine deiminase 4. *Mol Cell Biol.* 2008;28(15):4745-58.

101. Whiting PF, Smidt N, Sterne JA, Harbord R, Burton A, Burke M, et al. Systematic review: accuracy of anti-citrullinated Peptide antibodies for diagnosing rheumatoid arthritis. *Ann Intern Med.* 2010;152(7):456-64; w155-66.

102. Singh U, Singh S, Singh NK, Verma PK, and Singh S. Anticyclic citrullinated peptide autoantibodies in systemic lupus erythematosus. *Rheumatol Int.* 2011;31(6):765-7.

103. Budhram A, Chu R, Rusta-Sallehy S, Ioannidis G, Denburg JA, Adachi JD, et al. Anti-cyclic citrullinated peptide antibody as a marker of erosive arthritis in patients with systemic lupus erythematosus: a systematic review and meta-analysis. *Lupus.* 2014;23(11):1156-63.

104. Wang Y, Li M, Stadler S, Correll S, Li P, Wang D, et al. Histone hypercitrullination mediates chromatin decondensation and neutrophil extracellular trap formation. *J Cell Biol.* 2009;184(2):205-13.

105. Martinod K, Demers M, Fuchs TA, Wong SL, Brill A, Gallant M, et al. Neutrophil histone modification by peptidylarginine deiminase 4 is critical for deep vein thrombosis in mice. *Proc Natl Acad Sci U S A.* 2013;110(21):8674-9.

106. Lewis HD, Liddle J, Coote JE, Atkinson SJ, Barker MD, Bax BD, et al. Inhibition of PAD4 activity is sufficient to disrupt mouse and human NET formation. *Nat Chem Biol.* 2015;11(3):189-91.

107. Kolaczkowska E, Jenne CN, Surewaard BG, Thanabalasuriar A, Lee WY, Sanz MJ, et al. Molecular mechanisms of NET formation and degradation revealed by intravital imaging in the liver vasculature. *Nat Commun.* 2015;6:6673.

108. Urban CF, Ermert D, Schmid M, Abu-Abed U, Goosmann C, Nacken W, et al. Neutrophil extracellular traps contain calprotectin, a cytosolic protein complex involved in host defense against Candida albicans. *PLoS Pathog.* 2009;5(10):e1000639.

109. O'Donoghue AJ, Jin Y, Knudsen GM, Perera NC, Jenne DE, Murphy JE, et al. Global Substrate Profiling of Proteases in Human Neutrophil Extracellular Traps Reveals Consensus Motif Predominantly Contributed by Elastase. *PLoS ONE.* 2013;8(9):1-12.

110. Thanarajasingam U, Jensen MA, Dorschner JM, Wampler Muskardin T, Ghodke-Puranik Y, Purmalek M, et al. A Novel ELANE Mutation Associated With Inflammatory Arthritis, Defective NETosis, and Recurrent Parvovirus Infection. *Arthritis Rheumatol.* 2017.

111. Metzler KD, Goosmann C, Lubojemska A, Zychlinsky A, and Papayannopoulos V. A myeloperoxidase-containing complex regulates neutrophil elastase release and actin dynamics during NETosis. *Cell Rep.* 2014;8(3):883-96.

112. Papayannopoulos V, Metzler KD, Hakkim A, and Zychlinsky A. Neutrophil elastase and myeloperoxidase regulate the formation of neutrophil extracellular traps. *J Cell Biol.* 2010;191(3):677-91.

113. Rochael NC, Guimaraes-Costa AB, Nascimento MT, DeSouza-Vieira TS, Oliveira MP, Garcia e Souza LF, et al. Classical ROS-dependent and early/rapid ROS-independent release of Neutrophil Extracellular Traps triggered by Leishmania parasites. *Sci Rep.* 2015;5:18302.

114. Farley K, Stolley JM, Zhao P, Cooley J, and Remold-O'Donnell E. A SerpinB1 Regulatory Mechanism Is Essential for Restricting Neutrophil Extracellular Trap Generation. *The Journal of Immunology.* 2012;189(9):4574-81.

115. Zabieglo K, Majewski P, Majchrzak-Gorecka M, Wlodarczyk A, Grygier B, Zegar A, et al. The inhibitory effect of secretory leukocyte protease inhibitor (SLPI) on formation of neutrophil extracellular traps. *Journal of Leukocyte Biology.* 2015;98(1):99-106.

116. Roberts H, White P, Dias I, McKaig S, Veeramachaneni R, Thakker N, et al. Characterization of neutrophil function in Papillon-Lefevre syndrome. *J Leukoc Biol.* 2016;100(2):433-44.

117. Sorensen OE, Clemmensen SN, Dahl SL, Ostergaard O, Heegaard NH, Glenthoj A, et al. Papillon-Lefevre syndrome patient reveals species-dependent requirements for neutrophil defenses. *J Clin Invest.* 2014;124(10):4539-48.

118. Clynes R, Dumitru C, and Ravetch JV. Uncoupling of immune complex formation and kidney damage in autoimmune glomerulonephritis. *Science.* 1998;279(5353):1052-4.

119. Tsuboi N, Asano K, Lauterbach M, and Mayadas TN. Human Neutrophil Fcγ Receptors Initiate and Play Specialized Nonredundant Roles in Antibody-Mediated Inflammatory Diseases. *Immunity.* 2008;28(6):833-46.

120. Winkelstein JA, Marino MC, Johnston RB, Jr., Boyle J, Curnutte J, Gallin JI, et al. Chronic granulomatous disease. Report on a national registry of 368 patients. *Medicine (Baltimore).* 2000;79(3):155-69.

121. Schaller J. Illness resembling lupus erythematosus in mothers of boys with chronic granulomatous disease. *Ann Intern Med.* 1972;76(5):747-50.

122. Cale CM, Morton L, and Goldblatt D. Cutaneous and other lupus-like symptoms in carriers of X-linked chronic granulomatous disease: incidence and autoimmune serology. *Clin Exp Immunol.* 2007;148(1):79-84.

123. Jacob CO, Eisenstein M, Dinauer MC, Ming W, Liu Q, John S, et al. Lupus-associated causal mutation in neutrophil cytosolic factor 2 (NCF2) brings unique insights to the structure and function of NADPH oxidase. *Proc Natl Acad Sci U S A.* 2012;109(2):E59-67.

124. Kim-Howard X, Sun C, Molineros JE, Maiti AK, Chandru H, Adler A, et al. Allelic heterogeneity in NCF2 associated with systemic lupus erythematosus (SLE) susceptibility across four ethnic populations. *Hum Mol Genet.* 2013.

125. Zhao J, Ma J, Deng Y, Kelly JA, Kim K, Bang SY, et al. A missense variant in NCF1 is associated with susceptibility to multiple autoimmune diseases. *Nat Genet.* 2017;49(3):433-7.

126. Rohrbach AS, Slade DJ, Thompson PR, and Mowen KA. Activation of PAD4 in NET formation. *Front Immunol.* 2012;3:360.

127. Bianchi M, Hakkim A, Brinkmann V, Siler U, Seger RA, Zychlinsky A, et al. Restoration of NET formation by gene therapy in CGD controls aspergillosis. *Blood.* 2009;114(13):2619-22.

128. Hakkim A, Fuchs TA, Martinez NE, Hess S, Prinz H, Zychlinsky A, et al. Activation of the Raf-MEK-ERK pathway is required for neutrophil extracellular trap formation. *Nat Chem Biol.* 2011;7(2):75-7.

129. Almyroudis NG, Grimm MJ, Davidson BA, Rohm M, Urban CF, and Segal BH. NETosis and NADPH oxidase: at the intersection of host defense, inflammation, and injury. *Front Immunol.* 2013;4:45.

130. Tkalcevic J, Novelli M, Phylactides M, Iredale JP, Segal AW, and Roes J. Impaired immunity and enhanced resistance to endotoxin in the absence of neutrophil elastase and cathepsin G. *Immunity.* 2000;12(2):201-10.

131. Shlomchik MJ, Madaio MP, Ni D, Trounstein M, and Huszar D. The role of B cells in lpr/lpr-induced autoimmunity. *J Exp Med.* 1994;180(4):1295-306.

132. Ma J, Xu J, Madaio MP, Peng Q, Zhang J, Grewal IS, et al. Autoimmune lpr/lpr mice deficient in CD40 ligand: spontaneous Ig class switching with dichotomy of autoantibody responses. *J Immunol.* 1996;157(1):417-26.

133. Gordon RA, Herter JM, Rosetti F, Campbell AM, Nishi H, Kashgarian M, et al. Lupus and proliferative nephritis are PAD4 independent in murine models. *JCI Insight.* 2017;2(10).

134. Hargreaves CE, Rose-Zerilli MJ, Machado LR, Iriyama C, Hollox EJ, Cragg MS, et al. Fcgamma receptors: genetic variation, function, and disease. *Immunol Rev.* 2015;268(1):6-24.

135. Takai T. Fc receptors and their role in immune regulation and autoimmunity. *J Clin Immunol.* 2005;25(1):1-18.

136. Rosetti F, Tsuboi N, Chen K, Nishi H, Ernandez T, Sethi S, et al. Human lupus serum induces neutrophil-mediated organ damage in mice that is enabled by Mac-1 deficiency. *J Immunol.* 2012;189(7):3714-23.

137. Kienhofer D, Hahn J, Stoof J, Csepregi JZ, Reinwald C, Urbonaviciute V, et al. Experimental lupus is aggravated in mouse strains with impaired induction of neutrophil extracellular traps. *JCI Insight.* 2017;2(10).

138. Odobasic D, Muljadi RC, O'Sullivan KM, Kettle AJ, Dickerhof N, Summers SA, et al. Suppression of Autoimmunity and Renal Disease in Pristane-Induced Lupus by Myeloperoxidase. *Arthritis Rheumatol.* 2015;67(7):1868-80.

139. Knuckley B, Causey CP, Jones JE, Bhatia M, Dreyton CJ, Osborne TC, et al. Substrate specificity and kinetic studies of PADs 1, 3, and 4 identify potent and selective inhibitors of protein arginine deiminase 3. *Biochemistry.* 2010;49(23):4852-63.

140. Kumar SV, Kulkarni OP, Mulay SR, Darisipudi MN, Romoli S, Thomasova D, et al. Neutrophil Extracellular Trap-Related Extracellular Histones Cause Vascular Necrosis in Severe GN. *J Am Soc Nephrol.* 2015;26(10):2399-413.

141. Maldonado MA, Kakkanaiah V, MacDonald GC, Chen F, Reap EA, Balish E, et al. The role of environmental antigens in the spontaneous development of autoimmunity in MRL-lpr mice. *J Immunol.* 1999;162(11):6322-30.

142. Luo Y, Arita K, Bhatia M, Knuckley B, Lee YH, Stallcup MR, et al. Inhibitors and inactivators of protein arginine deiminase 4: functional and structural characterization. *Biochemistry.* 2006;45(39):11727-36.

143. Dwivedi N, Hedberg A, Zheng YY, Neeli I, Satoh M, Morel L, et al. B Cell Tolerance to Deiminated Histones in BALB/c, C57BL/6, and Autoimmune-Prone Mouse Strains. *Front Immunol.* 2017;8:362.

144. Leffler J, Gullstrand B, Jonsen A, Nilsson JA, Martin M, Blom AM, et al. Degradation of neutrophil extracellular traps co-varies with disease activity in patients with systemic lupus erythematosus. *Arthritis Res Ther.* 2013;15(4):R84.

145. Majewski P, Majchrzak-Gorecka M, Grygier B, Skrzeczynska-Moncznik J, Osiecka O, and Cichy J. Inhibitors of serine proteases in regulating the production and function of neutrophil extracellular traps. *Frontiers in Immunology.* 2016;7(JUN):1-10.

146. Martinod K, Witsch T, Farley K, Gallant M, Remold-O'Donnell E, and Wagner DD. Neutrophil elastase-deficient mice form neutrophil extracellular traps in an experimental model of deep vein thrombosis. *Journal of Thrombosis and Haemostasis.* 2016;14(3):551-8.

147. Kenny EF, Herzig A, Kruger R, Muth A, Mondal S, Thompson PR, et al. Diverse stimuli engage different neutrophil extracellular trap pathways. *Elife.* 2017;6.

148. Brinkmann V, and Zychlinsky A. Beneficial suicide: why neutrophils die to make NETs. *Nat Rev Microbiol.* 2007;5(8):577-82.

149. Farrera C, and Fadeel B. Macrophage clearance of neutrophil extracellular traps is a silent process. *J Immunol.* 2013;191(5):2647-56.

150. Liu CL, Tangsombatvisit S, Rosenberg JM, Mandelbaum G, Gillespie EC, Gozani OP, et al. Specific post-translational histone modifications of neutrophil extracellular traps as immunogens and potential targets of lupus autoantibodies. *Arthritis Res Ther.* 2012;14(1):R25.

151. Konig MF, and Andrade F. A Critical Reappraisal of Neutrophil Extracellular Traps and NETosis Mimics Based on Differential Requirements for Protein Citrullination. *Front Immunol.* 2016;7(461):461.

152. Berland R, Fernandez L, Kari E, Han JH, Lomakin I, Akira S, et al. Toll-like receptor 7-dependent loss of B cell tolerance in pathogenic autoantibody knockin mice. *Immunity.* 2006;25(3):429-40.

153. Monestier M, and Novick KE. Specificities and genetic characteristics of nucleosome-reactive antibodies from autoimmune mice. *Mol Immunol.* 1996;33(1):89-99.

154. Blanco F, Kalsi J, and Isenberg DA. Analysis of antibodies to RNA in patients with systemic lupus erythematosus and other autoimmune rheumatic diseases. *Clin Exp Immunol.* 1991;86(1):66-70.

155. Bedard K, and Krause KH. The NOX family of ROS-generating NADPH oxidases: physiology and pathophysiology. *Physiol Rev.* 2007;87(1):245-313.

156. Lam GY, Huang J, and Brumell JH. The many roles of NOX2 NADPH oxidase-derived ROS in immunity. *Semin Immunopathol.* 2010;32(4):415-30.

157. Mizuno T, Kaibuchi K, Ando S, Musha T, Hiraoka K, Takaishi K, et al. Regulation of the superoxide-generating NADPH oxidase by a small GTP-binding protein and its stimulatory and inhibitory GDP/GTP exchange proteins. *J Biol Chem.* 1992;267(15):10215-8.

158. Noubade R, Wong K, Ota N, Rutz S, Eidenschenk C, Valdez PA, et al. NRROS negatively regulates reactive oxygen species during host defence and autoimmunity. *Nature.* 2014;509(7499):235-9.

159. El-Benna J, Dang PM, and Gougerot-Pocidalo MA. Priming of the neutrophil NADPH oxidase activation: role of p47phox phosphorylation and NOX2 mobilization to the plasma membrane. *Semin Immunopathol.* 2008;30(3):279-89.

160. Pollock JD, Williams DA, Gifford MA, Li LL, Du X, Fisherman J, et al. Mouse model of X-linked chronic granulomatous disease, an inherited defect in phagocyte superoxide production. *Nat Genet.* 1995;9(2):202-9.

161. Arroyo A, Modriansky M, Serinkan FB, Bello RI, Matsura T, Jiang J, et al. NADPH oxidase-dependent oxidation and externalization of phosphatidylserine during apoptosis in Me2SO-differentiated HL-60 cells. Role in phagocytic clearance. *J Biol Chem.* 2002;277(51):49965-75.

162. Hampton MB, Vissers MC, Keenan JI, and Winterbourn CC. Oxidant-mediated phosphatidylserine exposure and macrophage uptake of activated neutrophils: possible impairment in chronic granulomatous disease. *J Leukoc Biol.* 2002;71(5):775-81.

163. Frasch SC, Fernandez-Boyanapalli RF, Berry KZ, Leslie CC, Bonventre JV, Murphy RC, et al. Signaling via macrophage G2A enhances efferocytosis of dying neutrophils by augmentation of Rac activity. *J Biol Chem.* 2011;286(14):12108-22.

164. Martinez J, Almendinger J, Oberst A, Ness R, Dillon CP, Fitzgerald P, et al. Microtubule-associated protein 1 light chain 3 alpha (LC3)-associated phagocytosis is required for the efficient clearance of dead cells. *Proc Natl Acad Sci U S A.* 2011;108(42):17396-401.

165. Bertolotti M, Farinelli G, Galli M, Aiuti A, and Sitia R. AQP8 transports NOX2-generated H2O2 across the plasma membrane to promote signaling in B cells. *J Leukoc Biol.* 2016;100(5):1071-9.

166. Wheeler ML, and DeFranco AL. Prolonged Production of Reactive Oxygen Species in Response to B Cell Receptor Stimulation Promotes B Cell Activation and Proliferation. *The Journal of Immunology.* 2012;189(9):4405-16.

167. Kovacs I, Horvath M, Lanyi A, Petheo GL, and Geiszt M. Reactive oxygen species-mediated bacterial killing by B lymphocytes. *J Leukoc Biol.* 2015;97(6):1133-7.

168. Cotugno N, Finocchi A, Cagigi A, Di Matteo G, Chiriaco M, Di Cesare S, et al. Defective B-cell proliferation and maintenance of long-term memory in patients with chronic granulomatous disease. *Journal of Allergy and Clinical Immunology.* 2015;135(3):753-61.e2.

169. McLetchie S, Volpp BD, Dinauer MC, and Blum JS. Hyper-responsive Toll-like receptor 7 and 9 activation in NADPH oxidase-deficient B lymphoblasts. *Immunology.* 2015;146(4):595-606.

170. Tse HM, Thayer TC, Steele C, Cuda CM, Morel L, Piganelli JD, et al. NADPH oxidase deficiency regulates Th lineage commitment and modulates autoimmunity. *J Immunol.* 2010;185(9):5247-58.

171. Kwon BI, Kim TW, Shin K, Kim YH, Yuk CM, Yuk JM, et al. Enhanced Th2 cell differentiation and function in the absence of Nox2. *Allergy.* 2017;72(2):252-65.

172. Wen Z, Shimojima Y, Shirai T, Li Y, Ju J, Yang Z, et al. NADPH oxidase deficiency underlies dysfunction of aged CD8 + Tregs. 2016;126(5):1953-67.

173. Mellor AL, and Munn DH. IDO expression by dendritic cells: tolerance and tryptophan catabolism. *Nat Rev Immunol.* 2004;4(10):762-74.

174. Mellor AL, Lemos H, and Huang L. Indoleamine 2,3-Dioxygenase and Tolerance: Where Are We Now? *Front Immunol.* 2017;8:1360.

175. Munn DH, Shafizadeh E, Attwood JT, Bondarev I, Pashine A, and Mellor AL. Inhibition of T cell proliferation by macrophage tryptophan catabolism. *J Exp Med.* 1999;189(9):1363-72.

176. Romani L, Fallarino F, De Luca A, Montagnoli C, D'Angelo C, Zelante T, et al. Defective tryptophan catabolism underlies inflammation in mouse chronic granulomatous disease. *Nature.* 2008;451(7175):211-5.

177. Jurgens B, Fuchs D, Reichenbach J, and Heitger A. Intact indoleamine 2,3-dioxygenase activity in human chronic granulomatous disease. *Clin Immunol.* 2010;137(1):1-4.

178. De Ravin SS, Zarember KA, Long-Priel D, Chan KC, Fox SD, Gallin JI, et al. Tryptophan/kynurenine metabolism in human leukocytes is independent of superoxide and is fully maintained in chronic granulomatous disease. *Blood.* 2010;116(10):1755-60.

179. Landing BH, and Shirkey HS. A syndrome of recurrent infection and infiltration of viscera by pigmented lipid histiocytes. *Pediatrics.* 1957;20(3):431-8.

180. Kelkka T, Kienhofer D, Hoffmann M, Linja M, Wing K, Sareila O, et al. Reactive oxygen species deficiency induces autoimmunity with type 1 interferon signature. *Antioxid Redox Signal.* 2014;21(16):2231-45.

181. Wing K, Klocke K, Samuelsson A, and Holmdahl R. Germ-free mice deficient of reactive oxygen species have increased arthritis susceptibility. *Eur J Immunol.* 2015;45(5):1348-53.

182. Clausen BE, Burkhardt C, Reith W, Renkawitz R, and Forster I. Conditional gene targeting in macrophages and granulocytes using LysMcre mice. *Transgenic Res.* 1999;8(4):265-77.

183. Voehringer D, Liang HE, and Locksley RM. Homeostasis and effector function of lymphopenia-induced "memory-like" T cells in constitutively T cell-depleted mice. *J Immunol.* 2008;180(7):4742-53.

184. Abram CL, Roberge GL, Hu Y, and Lowell CA. Comparative analysis of the efficiency and specificity of myeloid-Cre deleting strains using ROSA-EYFP reporter mice. *J Immunol Methods.* 2014;408:89-100.

185. Pelletier S, Gingras S, and Green DR. Mouse genome engineering via CRISPR-Cas9 for study of immune function. *Immunity.* 2015;42(1):18-27.

186. Li F, Cowley DO, Banner D, Holle E, Zhang L, and Su L. Efficient genetic manipulation of the NOD-Rag1-/-IL2RgammaC-null mouse by combining in vitro fertilization and CRISPR/Cas9 technology. *Sci Rep.* 2014;4:5290.

187. Sheren J, Langer SJ, and Leinwand LA. A randomized library approach to identifying functional lox site domains for the Cre recombinase. *Nucleic Acids Research.* 2007;35(16):5464-73.

188. Passegue E, Wagner EF, and Weissman IL. JunB deficiency leads to a myeloproliferative disorder arising from hematopoietic stem cells. *Cell.* 2004;119(3):431-43.

189. Fadeel B, Ahlin A, Henter JI, Orrenius S, and Hampton MB. Involvement of caspases in neutrophil apoptosis: regulation by reactive oxygen species. *Blood.* 1998;92(12):4808-18.

190. Wilkie RP, Vissers MC, Dragunow M, and Hampton MB. A functional NADPH oxidase prevents caspase involvement in the clearance of phagocytic neutrophils. *Infect Immun.* 2007;75(7):3256-63.

191. Rybicka JM, Balce DR, Khan MF, Krohn RM, and Yates RM. NADPH oxidase activity controls phagosomal proteolysis in macrophages through modulation of the lumenal redox environment of phagosomes. *Proc Natl Acad Sci U S A.* 2010;107(23):10496-501.

192. Meissner F, Seger RA, Moshous D, Fischer A, Reichenbach J, and Zychlinsky A. Inflammasome activation in NADPH oxidase defective mononuclear phagocytes from patients with chronic granulomatous disease. *Blood.* 2010;116(9):1570-3.

193. van de Veerdonk FL, Smeekens SP, Joosten LA, Kullberg BJ, Dinarello CA, van der Meer JW, et al. Reactive oxygen species-independent activation of the IL-1beta inflammasome in cells from patients with chronic granulomatous disease. *Proc Natl Acad Sci U S A.* 2010;107(7):3030-3.

194. Rice P, Longden I, and Bleasby A. EMBOSS: the European Molecular Biology Open Software Suite. *Trends Genet.* 2000;16(6):276-7.

195. Han S, Zhuang H, Shumyak S, Wu J, Li H, Yang L-J, et al. A Novel Subset of Anti-Inflammatory CD138 ⁺ Macrophages Is Deficient in Mice with Experimental Lupus. *The Journal of Immunology.* 2017;199(4):1261-74.

196. Herrmann M, Voll RE, Zoller OM, Hagenhofer M, Ponner BB, and Kalden JR. Impaired phagocytosis of apoptotic cell material by monocyte-derived macrophages from patients with systemic lupus erythematosus. *Arthritis Rheum.* 1998;41(7):1241-50.

197. Baumann I, Kolowos W, Voll RE, Manger B, Gaipl U, Neuhuber WL, et al. Impaired uptake of apoptotic cells into tingible body macrophages in germinal centers of patients with systemic lupus erythematosus. *Arthritis Rheum.* 2002;46(1):191-201.

198. Svensson BO. Serum factors causing impaired macrophage function in systemic lupus erythematosus. *Scand J Immunol.* 1975;4(2):145-50.

199. Hepburn AL. The LE cell. *Rheumatology (Oxford).* 2001;40(7):826-7.

200. Lisnevskaia L, Murphy G, and Isenberg D. Systemic lupus erythematosus. *The Lancet.* 2014;384(9957):1878-88.

201. Mevorach D. Clearance of dying cells and systemic lupus erythematosus: the role of C1q and the complement system. *Apoptosis.* 2010;15(9):1114-23.

202. Pickering MC, Botto M, Taylor PR, Lachmann PJ, and Walport MJ. Systemic lupus erythematosus, complement deficiency, and apoptosis. *Adv Immunol.* 2000;76:227-324.

203. Arason GJ, Jorgensen GH, and Ludviksson BR. Primary immunodeficiency and autoimmunity: lessons from human diseases. *Scand J Immunol.* 2010;71(5):317-28.

204. Botto M, Dell'Agnola C, Bygrave AE, Thompson EM, Cook HT, Petry F, et al. Homozygous C1q deficiency causes glomerulonephritis associated with multiple apoptotic bodies. *Nature Genetics.* 1998;19(1):56-9.

205. Mitchell Da, Pickering MC, Warren J, Fossati-Jimack L, Cortes-Hernandez J, Cook HT, et al. C1q deficiency and autoimmunity: the effects of genetic background on disease expression. *Journal of immunology (Baltimore, Md : 1950).* 2002;168(5):2538-43.

206. Miyanishi M, Tada K, Koike M, Uchiyama Y, Kitamura T, and Nagata S. Identification of Tim4 as a phosphatidylserine receptor. *Nature.* 2007;450(7168):435-9.

207. Kobayashi N, Karisola P, Pena-Cruz V, Dorfman DM, Jinushi M, Umetsu SE, et al. TIM-1 and TIM-4 glycoproteins bind phosphatidylserine and mediate uptake of apoptotic cells. *Immunity.* 2007;27(6):927-40.

208. Nagata K, Ohashi K, Nakano T, Arita H, Zong C, Hanafusa H, et al. Identification of the product of growth arrest-specific gene 6 as a common ligand for Axl, Sky, and Mer receptor tyrosine kinases. *J Biol Chem.* 1996;271(47):30022-7.

209. Cohen PL, Caricchio R, Abraham V, Camenisch TD, Jennette JC, Roubey RA, et al. Delayed apoptotic cell clearance and lupus-like autoimmunity in mice lacking the c-mer membrane tyrosine kinase. *J Exp Med.* 2002;196(1):135-40.

210. Hu CY, Wu CS, Tsai HF, Chang SK, Tsai WI, and Hsu PN. Genetic polymorphism in milk fat globule-EGF factor 8 (MFG-E8) is associated with systemic lupus erythematosus in human. *Lupus.* 2009;18(8):676-81.

211. Hanayama R, Tanaka M, Miwa K, Shinohara A, Iwamatsu A, and Nagata S. Identification of a factor that links apoptotic cells to phagocytes. *Nature.* 2002;417(6885):182-7.

212. Hanayama R, Tanaka M, Miyasaka K, Aozasa K, Koike M, Uchiyama Y, et al. Autoimmune disease and impaired uptake of apoptotic cells in MFG-E8-deficient mice. *Science.* 2004;304(5674):1147-50.

213. Huang W, Wu J, Yang H, Xiong Y, Jiang R, Cui T, et al. Milk fat globule-EGF factor 8 suppresses the aberrant immune response of systemic lupus erythematosus-derived neutrophils and associated tissue damage. *Cell Death Differ.* 2017;24(2):263-75.

214. Shibutani ST, Saitoh T, Nowag H, Munz C, and Yoshimori T. Autophagy and autophagy-related proteins in the immune system. *Nat Immunol.* 2015;16(10):1014-24.

215. Mizushima N, Ohsumi Y, and Yoshimori T. Autophagosome formation in mammalian cells. *Cell Struct Funct.* 2002;27(6):421-9.

216. Kim J, Kundu M, Viollet B, and Guan KL. AMPK and mTOR regulate autophagy through direct phosphorylation of Ulk1. *Nat Cell Biol.* 2011;13(2):132-41.

217. Jung CH, Jun CB, Ro SH, Kim YM, Otto NM, Cao J, et al. ULK-Atg13-FIP200 complexes mediate mTOR signaling to the autophagy machinery. *Mol Biol Cell.* 2009;20(7):1992-2003.

218. Heckmann BL, Boada-Romero E, Cunha LD, Magne J, and Green DR. LC3-Associated Phagocytosis and Inflammation. *J Mol Biol.* 2017;429(23):3561-76.

219. Sanjuan MA, Dillon CP, Tait SW, Moshiach S, Dorsey F, Connell S, et al. Toll-like receptor signalling in macrophages links the autophagy pathway to phagocytosis. *Nature.* 2007;450(7173):1253-7.

220. Kabeya Y, Mizushima N, Ueno T, Yamamoto A, Kirisako T, Noda T, et al. LC3, a mammalian homologue of yeast Apg8p, is localized in autophagosome membranes after processing. *Embo j.* 2000;19(21):5720-8.

221. Mizushima N, Kuma A, Kobayashi Y, Yamamoto A, Matsubae M, Takao T, et al. Mouse Apg16L, a novel WD-repeat protein, targets to the autophagic isolation membrane with the Apg12-Apg5 conjugate. *J Cell Sci.* 2003;116(Pt 9):1679-88.

222. Zhong Y, Wang QJ, Li X, Yan Y, Backer JM, Chait BT, et al. Distinct regulation of autophagic activity by Atg14L and Rubicon associated with Beclin 1-phosphatidylinositol-3-kinase complex. *Nat Cell Biol.* 2009;11(4):468-76.

223. Matsunaga K, Saitoh T, Tabata K, Omori H, Satoh T, Kurotori N, et al. Two Beclin 1-binding proteins, Atg14L and Rubicon, reciprocally regulate autophagy at different stages. *Nat Cell Biol.* 2009;11(4):385-96.

224. Yang CS, Rodgers M, Min CK, Lee JS, Kingeter L, Lee JY, et al. The autophagy regulator Rubicon is a feedback inhibitor of CARD9-mediated host innate immunity. *Cell Host and Microbe.* 2012;11(3):277-89.

225. Kim JH, Kim TH, Lee HC, Nikapitiya C, Uddin MB, Park ME, et al. Rubicon Modulates Antiviral Type I Interferon (IFN) Signaling by Targeting IFN Regulatory Factor 3 Dimerization. *J Virol.* 2017;91(14).

226. Zhou Xj, Lu Xl, Lv Jc, Yang Hz, Qin Lx, Zhao Mh, et al. Genetic association of PRDM1-ATG5 intergenic region and autophagy with systemic lupus erythematosus in a Chinese population. *Ann Rheum Dis.* 2011;70(7):1330-7.

227. López P, Alonso-pérez E, Rodríguez-carrio J, and Suárez A. Influence of Atg5 Mutation in SLE Depends on Functional IL-10 Genotype. 2013;8(10):1-10.

228. Saraiva M, and Garra AO. The regulation of IL‐10 production by immune cells. *Nature Reviews Immunology.* 2010;10(3):170-81.

229. Herrero C, Hu X, Li WP, Samuels S, Sharif MN, Kotenko S, et al. Reprogramming of IL-10 Activity and Signaling by IFN- *The Journal of Immunology.* 2003;171(10):5034-41.

230. Rowbottom AW, Lepper MA, Garland RJ, Cox CV, and Corley EG. Interleukin-10-induced CD8 cell proliferation. *Immunology.* 1999;98(1):80-9.

231. Santin AD, Hermonat PL, Ravaggi A, Bellone S, Pecorelli S, Roman JJ, et al. Interleukin-10 increases Th1 cytokine production and cytotoxic potential in human papillomavirus-specific CD8(+) cytotoxic T lymphocytes. *J Virol.* 2000;74(10):4729-37.

232. Carson WE, Lindemann MJ, Baiocchi R, Linett M, Tan JC, Chou CC, et al. The functional characterization of interleukin-10 receptor expression on human natural killer cells. *Blood.* 1995;85(12):3577-85.

233. Itoh K, and Hirohata S. The role of IL-10 in human B cell activation, proliferation, and differentiation. *J Immunol.* 1995;154(9):4341-50.

234. Rousset F, Garcia E, Defrance T, Péronne C, Vezzio N, Hsu DH, et al. Interleukin 10 is a potent growth and differentiation factor for activated human B lymphocytes. *Proc Natl Acad Sci U S A.* 1992;89(5):1890-3.

235. Levy Y, and Brouet JC. Interleukin-10 prevents spontaneous death of germinal center B cells by induction of the bcl-2 protein. *J Clin Invest.* 1994;93(1):424-8.

236. Go NF, Castle BE, Barrett R, Kastelein R, Dang W, Mosmann TR, et al. Interleukin 10, a novel B cell stimulatory factor: unresponsiveness of X chromosome-linked immunodeficiency B cells. *J Exp Med.* 1990;172(6):1625-31.

237. Lazarus M, Hajeer AH, Turner D, Sinnott P, Worthington J, Ollier WE, et al. Genetic variation in the interleukin 10 gene promoter and systemic lupus erythematosus. *J Rheumatol.* 1997;24(12):2314-7.

238. Song GG, Choi SJ, Ji JD, and Lee YH. Associations between interleukin-10 polymorphisms and susceptibility to systemic lupus erythematosus: a meta-analysis. *Hum Immunol.* 2013;74(3):364-70.

239. Peng H, Wang W, Zhou M, Li R, Pan HF, and Ye DQ. Role of interleukin-10 and interleukin-10 receptor in systemic lupus erythematosus. *Clinical Rheumatology.* 2013;32(9):1255-66.

240. Ishida BH, Muchamuel T, Sakaguchi S, and Andrade S. Continuous Administration of Anti-Interleukin 10 Antibodies Delays Onset of Autoimmunity in N Z B / W F1 Mice. 1994;179(January).

241. Llorente L, Richaud-Patin Y, Garcia-Padilla C, Claret E, Jakez-Ocampo J, Cardiel MH, et al. Clinical and biologic effects of anti-interleukin-10 monoclonal antibody administration in systemic lupus erythematosus. *Arthritis Rheum.* 2000;43(8):1790-800.

242. Yin Z, Bahtiyar G, Zhang N, Liu L, Zhu P, Robert ME, et al. IL-10 Regulates Murine Lupus. *The Journal of Immunology.* 2002;169(4):2148-55.

243. Blenman KR, Duan B, Xu Z, Wan S, Atkinson MA, Flotte TR, et al. IL-10 regulation of lupus in the NZM2410 murine model. *Lab Invest.* 2006;86(11):1136-48.

244. Kalampokis I, Yoshizaki A, and Tedder TF. IL-10-producing regulatory B cells (B10 cells) in autoimmune disease. *Arthritis Res Ther.* 2013;15 Suppl 1:S1.

245. Teichmann LL, Kashgarian M, Weaver CT, Roers A, Muller W, and Shlomchik MJ. B Cell-Derived IL-10 Does Not Regulate Spontaneous Systemic Autoimmunity in MRL.Faslpr Mice. *The Journal of Immunology.* 2012;188(2):678-85.

246. Petes C, Odoardi N, and Gee K. The Toll for Trafficking: Toll-Like Receptor 7 Delivery to the Endosome. *Front Immunol.* 2017;8:1075.

247. Lee HK, Lund JM, Ramanathan B, Mizushima N, and Iwasaki A. Autophagy-Dependent Viral Recognition by Plasmacytoid Dendritic Cells. *Science.* 2007;315(5817):1398-401.

248. Weindel CG, Richey LJ, Bolland S, Mehta AJ, Kearney JF, and Huber BT. B cell autophagy mediates TLR7-dependent autoimmunity and inflammation. *Autophagy.* 2015;11(7):1010-24.

249. Roers A, Siewe L, Strittmatter E, Deckert M, Schluter D, Stenzel W, et al. T cell-specific inactivation of the interleukin 10 gene in mice results in enhanced T cell responses but normal innate responses to lipopolysaccharide or skin irritation. *J Exp Med.* 2004;200(10):1289-97.

250. Jacob CO, Yu N, Yoo D-G, Perez-Zapata LJ, Barbu EA, Kaplan MJ, et al. Haploinsufficiency of NADPH oxidase subunit NCF2 is sufficient to accelerate full-blown lupus in NZM.2328 mice. *Arthritis Rheumatol.* 2017.

251. Naccache PH, and Fernandes MJ. Challenges in the characterization of neutrophil extracellular traps: The truth is in the details. *Eur J Immunol.* 2016;46(1):52-5.

252. Neeli I, and Radic M. Current Challenges and Limitations in Antibody-Based Detection of Citrullinated Histones. *Frontiers in Immunology.* 2016;7:528-.

253. Desai J, Kumar SV, Mulay SR, Konrad L, Romoli S, Schauer C, et al. PMA and crystal-induced neutrophil extracellular trap formation involves RIPK1-RIPK3-MLKL signaling. *Eur J Immunol.* 2016;46(1):223-9.

254. Amini P, Stojkov D, Wang X, Wicki S, Kaufmann T, Wong WW, et al. NET formation can occur independently of RIPK3 and MLKL signaling. *Eur J Immunol.* 2016;46(1):178-84.